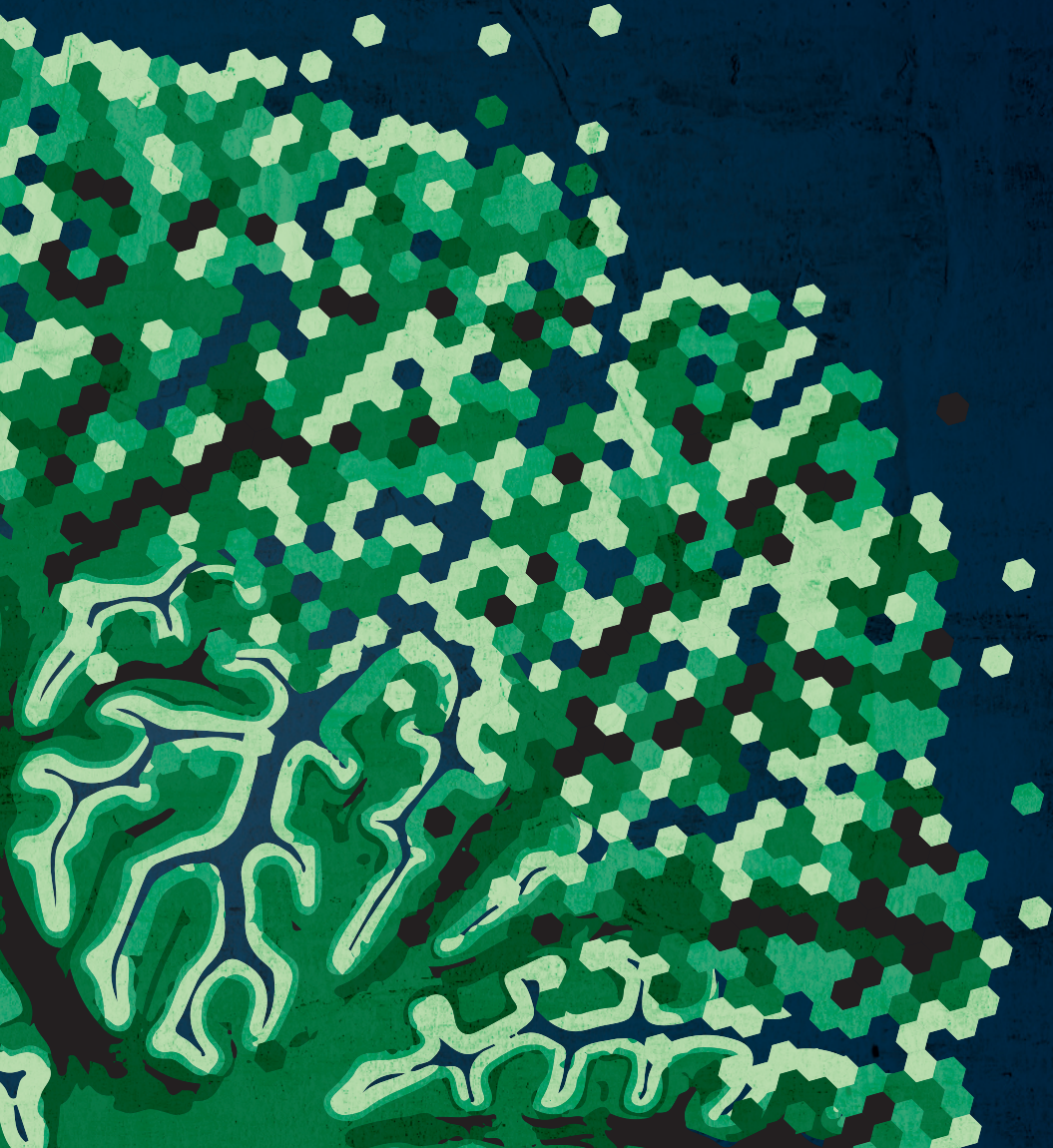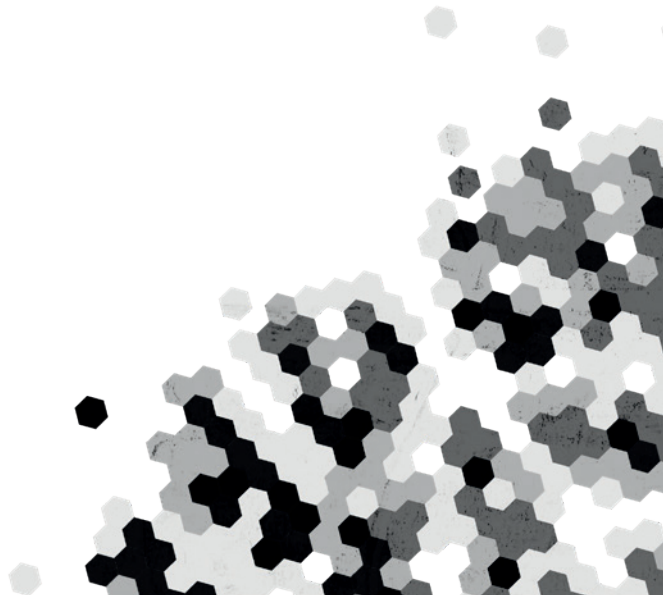THOMAS JAN HULST

CEREBELLAR MOTOR LEARNING DEFICITS

Structural mapping, neuromodulation
and training-related interventions

THOMAS JAN HULST

CEREBELLAR MOTOR LEARNING DEFICITS

Structural mapping, neuromodulation
and training-related interventions

COLOPHON

Cerebellar Motor Learning Deficits

Structural mapping, neuromodulation and training-related interventions

Motorisch leren deficiënties van het cerebellum
Structurele beeldvorming, neuromodulatie en training-gerelateerde interventies

P R O E F S C H R I F T

ter verkrijging van de graad van doctor aan de
Erasmus Universiteit Rotterdam
op gezag van de
rector magnificus

Prof. dr. R.C.M.E. Engels

en volgens besluit van het College voor Promoties.
De openbare verdediging zal plaatsvinden op

woensdag 5 februari 2020 om 15:30

Thomas Jan Hulst
geboren te Rotterdam

Erasmus University Rotterdam

Promotiecommissie

Promotor: Prof. dr. M.A. Frens

Overige leden: Dr. C.E. Catsman-Berrevoets
                       Prof. dr. F.E. Hoebeek
                       Prof. dr. J.B.J. Smeets

Copromotoren: Prof. dr. O. Donchin
                       Dr. J.N van der Geest
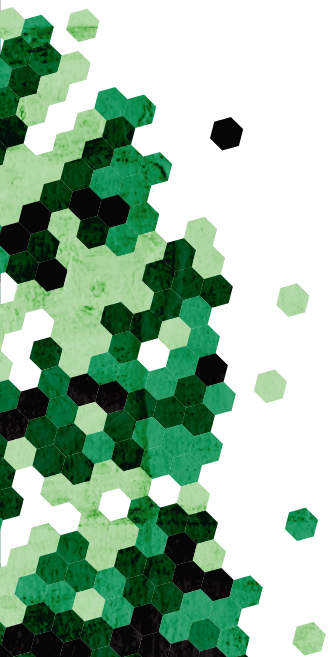
TABLE OF
CONTENTS

1

Introduction

INTRODUCTION

For healthy individuals, movement is trivial. Thoughtlessly and effortlessly, we coordinate muscle contractions to get from uncomfortable situations (a thesis defense), to places with more agreeable conditions (the dinner afterwards). Movement allows us to interact with our direct environment, manipulate objects and communicate with each other. Moreover, we can adjust our movements to fit a remarkable range of situations and circumstances, responding to changes in the environment and task demands. In contrast, individuals with cerebellar dysfunction often suffer from a host of symptoms which makes movement anything but trivial. The clinical manifestation of cerebellar dysfunction, commonly referred to as cerebellar ataxia, typically includes balance and gait disturbances, speech impairments and incoordination of eye and upper-limb movements (Mariotti et al., 2005). Cerebellar ataxia arises due to damage of the cerebellum and related structures which is caused by neuropathology of many different etiologies (Marsden and Harris, 2011). This thesis will focus on the degenerative cerebellar ataxias (DCAs), characterized by the progressive degeneration of the cerebellum and its afferent and efferent pathways. DCA has a huge impact on the quality of life of an individual (López-Bastida et al., 2008; Schmitz-Hübsch et al., 2010) and effective treatment can pose a major challenge (Sarva and Shanker, 2014).

Individuals with DCA often require lifelong supportive therapy to alleviate motor symptoms and maintain activities of daily living (ADL) as no curative treatment currently exists (Ilg et al., 2014). Depending on the unique needs of a patient, supportive therapy can include physical therapy, speech therapy and occupational therapy, for which varying degrees of therapeutic success have been established (Fonteyn et al., 2014). While there is a consensus that supportive therapy is generally beneficial for patients with DCA, little is known about the mechanisms underlying the improvements and how patients can benefit most (Ilg et al., 2014). Effective therapy for individuals with DCA can be especially challenging since they suffer from various motor learning deficits (Maschke et al., 2004a; Sanes et al., 1990; Tseng et al., 2007) which impairs their ability to (re)learn motor sequences required for ADL (Hatakenaka et al., 2012). Investigating the neuroanatomical structure of the diseased cerebellum by means of neuroimaging, as well as investigating the relationship between cerebellar integrity and motor learning deficits, should help us better understand the structural components underlying DCA. Furthermore, by testing whether motor learning deficits can be ameliorated with neuromodulatory or training-related interventions, under experimental conditions, we hope to support the development of interventions relevant for application in a clinical setting.

Thus, this thesis aims to investigate the following:

- The effects of cerebellar disease on cerebellar integrity
- The relationship between cerebellar integrity and motor learning deficits
- The efficacy of non-invasive brain stimulation and training-related interventions to alleviate motor learning deficits of individuals with DCA

The introduction will first cover the anatomy and function of the cerebellum before exploring cerebellar circuitry. Particular attention is given to the role of the cerebellum in motor learning. Finally, the introduction will focus on the etiology of cerebellar disease, therapeutic options, and promising interventions to increase the efficacy of cerebellar therapy.

Cerebellar anatomy

The cerebellum (small brain) is an important functional unit of motor behaviors (e.g. locomotion, speech, grasping etc.) (Holmes, 1917) and cognitive behaviors (e.g. emotion, language, attention etc.) (Strick et al., 2009). Situated below the occipital lobe of the cerebrum (large brain) and bordered ventrally by the brainstem in humans (**Figure 1**), it develops from the rhombencephalon (hindbrain) and is generally well-preserved across species (Bell et al., 2008). The cerebellum is known to hold the majority of neurons in humans with estimates ranging from around 70% to 80% of the total amount of neurons in the human brain (Andersen et al., 1992; Herculano-Houzel, 2010). It consists of a tightly folded layer of cortex around a structure of white matter in which the deep cerebellar nuclei (DCN) are embedded.
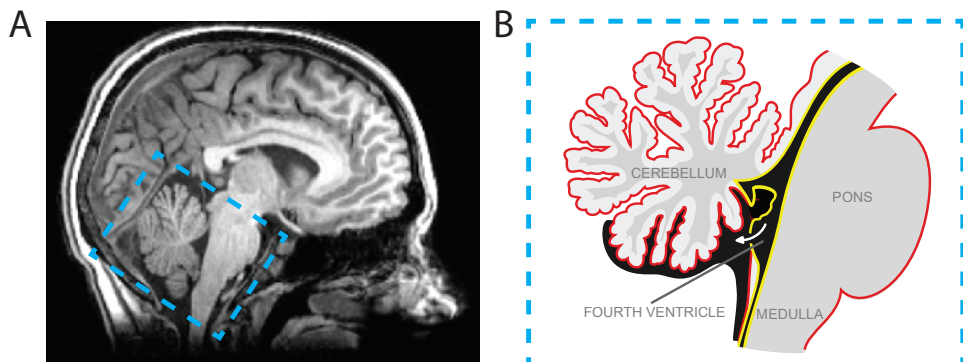

Figure 1. A: Sagittal slice of the human brain (MRI). The location of the cerebellum is indicated by the light blue rectangle. B: The cerebellum and related neural structures, adapted from Gray, 1878.

Macroscopically, the two hemispheres of the cerebellar cortex can be divided into an anterior lobe and a posterior lobe (**Figure 2A**). The anterior lobe is situated above the primary fissure of the cerebellum and consists of several distinct anatomical subregions: lobules I to V after Larsell's nomenclature (Larsell and Jansen, 1972). The posterior lobe, situated below the primary fissure, consists of anatomical lobules VI to IX. The flocculonodular lobe (lobule X) is isolated from the cerebellar hemispheres by the posterolateral fissure and located inferiorly from the posterior lobe. The cerebellum can also be divided mediolaterally, based on the input the cerebellar cortex receives: the vermis, the intermediate zone and the lateral zone (Ghez and Thach, 2000; **Figure 2B**). The vermis and intermediate zone (together: spinocerebellum) occupy the medial parts of the cerebellar cortex and receive the majority of their input from the spinal cord. The spinocerebellum projects, via the deep cerebellar nuclei, onto systems mainly involved in eye movements, locomotion and posture. The lateral zone (or: cerebrocerebellum) comprises the largest volume of the cerebellar cortex and receives the majority of its input from the cerebral cortex. It projects, via the DCN, to motor, premotor and prefrontal cortices in multiple cerebrocerebellar loops (or: cerebello-thalamo-cerebro-cortical circuits, D'Angelo and Casali, 2013). The flocculonodular lobe (also: vestibulocerebellum) receives its inputs from vestibular systems and projects directly onto the vestibular nuclei. While anatomically relevant, the lobular and zonal division does not directly correspond with cerebellar function but provides a common terminology to describe localization in the cerebellum.
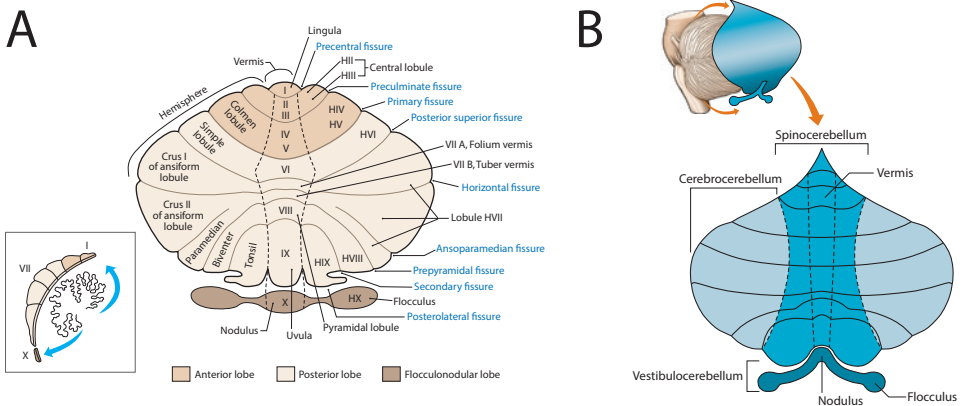

Figure 2. Gross anatomy of the cerebellar cortex. A: Anatomical landmarks of the cerebellar cortex. B: Mediolateral division of the cerebellum. Figure adapted from Klein et al., 2016.

Cerebellar function

Early scientific efforts focused on studying the gross anatomy and major subdivisions of the cerebellum but around the turn of the 19th century experimental research commenced into cerebellar function (Glickstein et al., 2009). After ablation of the cerebellum in various vertebrate animals, Pierre Flourens observed distinct changes in their motor function (Flourens, 1824). Flourens recognized that movements were not completely lost after cerebellar ablation, but irregular and uncoordinated, and suggested a role for the cerebellum in movement coordination. This observation was corroborated by clinical studies of individuals with cerebellar injury, which exhibited various motor deficits, also establishing a role for the cerebellum in motor function in humans (Holmes, 1917). Contemporary clinical and experimental studies also identified the cerebellum as key for cognitive behavior, describing deficits in the executive and emotional domain after damage to the posterior cerebellum (Schmahmann, 1991). Over time, as the methods and techniques to study the cerebellum have gotten more advanced, our understanding and description of cerebellar function has become increasingly detailed.

Breakthroughs in neuroimaging have allowed for a comprehensive mapping of motor and non-motor behavior to anatomical regions of the cerebellum (**Figure 3**). By employing lesion-symptom mapping and functional imaging, a functional topography of the human cerebellum has been developed (Grodd et al., 2001; Timmann et al., 2009). These techniques, in combination with converging evidence from animal studies (Snider and Stowell, 1944), have uncovered two somatotopic maps in the cerebellum. These maps are topographic representations of motor function, i.e. particular regions of the cerebellar cortex are functionally associated with particular motor behavior in a topographically organized manner. The first somatotopic representation of the body is located (mostly) in the anterior lobe and a second somatotopy is located in the posterior lobe [for review, see: Manni and Petrosini, 2004]. More specifically, arm movements are associated with lobule V and the anterior part of lobule VI and have a secondary representation in lobule VIII of the posterior lobe (Diedrichsen and Zotow, 2015; Grodd et al., 2001). Movements of the feet are associated with lobules II-IV (anterior lobe) and lobules VIII and IX (posterior lobe) (Nitschke et al., 1996), while orofacial movements have a representation in lobule VI and VIII (Diedrichsen and Zotow, 2015; Grodd et al., 2001). Furthermore, movements of the trunk, locomotion and eye movements in humans are most commonly associated with the medial zone of the cerebellum (Timmann et al., 2009).

In addition to the mapping of motor functions, recent work has also mapped cognitive functions onto the human cerebellum (Stoodley and Schmahmann, 2009). Cognitive functions like language, spatial processing, reasoning and decision making have all been

associated with regions of the posterior cerebellum, specifically lobule VI and VII (including Crus I, Crus II and lobule VIIb), while emotional processing was primarily associated with the posterior vermis (Stoodley and Schmahmann, 2009). The specific localization of motor function and cognitive function in the cerebellum has led to the characterization of a "sensorimotor cerebellum" and a "cognitive cerebellum". Roughly, the sensorimotor cerebellum is concerned with movement and located primarily in the anterior lobe, with a secondary representation in the posterior lobe (lobule VIII). The cognitive cerebellum is associated with "higher-level" tasks and is localized in the posterior cerebellum, specifically lobules VI and VII (Stoodley and Schmahmann, 2010).
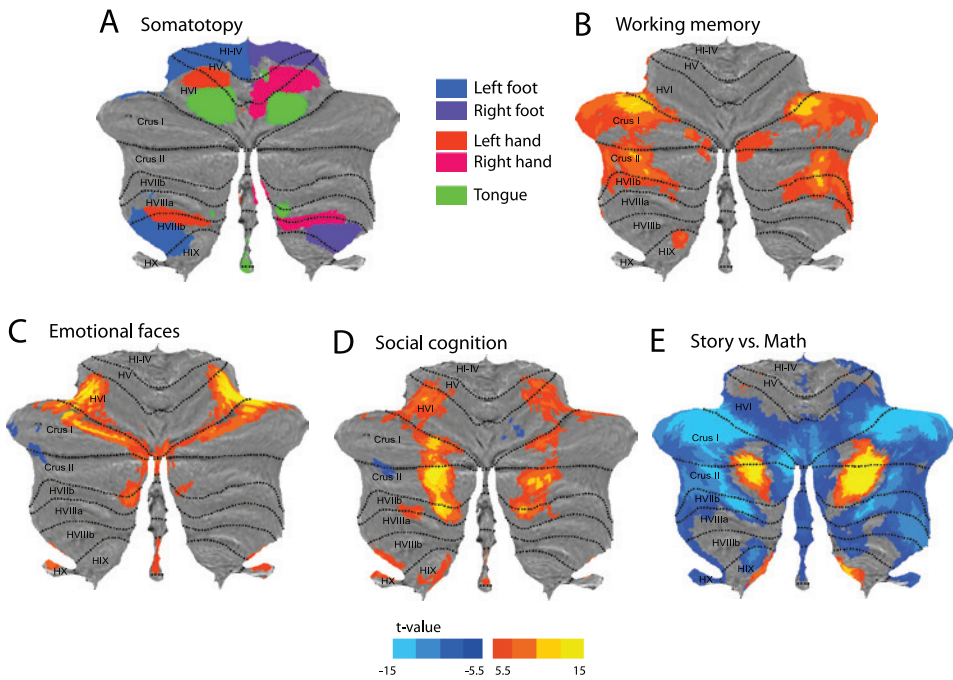
Figure 3. Functional activity flatmaps collected using fMRI, averaged over 100 participants in the Human Connectome Project (Van Essen et al., 2013). A: Functional activity flatmap for hand, foot and tongue movements. Each voxel was assigned the body part associated with the highest activation value. Clearly visible is the primary somatotopic representation of the body in lobules IV-VI and a secondary representation in lobules VIII-IX. B-E: Contrasts of functional activation for various tasks associated with the "cognitive cerebellum". Positive values indicate higher activation during task than contrast, negative values indicate lower activation. All colored voxels survived corrections for multiple comparisons. Functional activity of cognitive tasks is more strongly associated with lobules in the posterior lobe of the cerebellum. NB: functional associations do not adhere to the anatomical divisions of the cerebellum and sometimes overlap between various tasks. Figure adapted from Diedrichsen and Zotow, 2015.

While neuroimaging has been instrumental in our understanding of cerebellar function in humans, it is important to recognize the limits of the technique. Though we can say with reasonable certainty that specific behaviors are associated with specific regions of the cerebellum, less is known about the computations taking place. Therefore, in conjunction with neuroimaging studies, extensive experimental work has been carried out over the past decades to unravel the precise circuitry of the cerebellum.

Cerebellar circuitry

The structure of the cerebellum is highly regular with well-organized input and output connectivity (Lisberger and Thach, 2013). Central in the cerebellar circuit are inhibitory Purkinje cells (PCs) which constitute the sole output of the cerebellar cortex. Purkinje cells, situated between the molecular layer and granular layer of the cerebellar cortex (**Figure 4A**), are a key component of the cerebellar module, considered to be the basic operational unit of the cerebellum (Apps et al., 2018). The cerebellar module consists of longitudinal zones of PCs that receive excitatory climbing fiber (CF) input from specific regions of the inferior olive (IO) in the medulla. In turn, the PCs project onto a specific region of the DCN that has reciprocal connections with the same region of the IO that gave rise to the CFs connected with the PCs (Ruigrok, 2011). The typical olivo-cortico-nuclear connectivity is repeated across the cerebellum with little variance, though recent work has found biochemical differences between distinct cerebellar modules which could also explain physiological differences between modules (Zhou et al., 2014).

Purkinje cells, in addition to having excitatory connections with climbing fibers, also receive excitatory input from parallel fibers (PFs). Parallel fibers arise from granule cells in the granular layer receiving input from mossy fibers that have indirect connections with the cerebral cortex, spinal cord and extracerebellar nuclei. On average, a single Purkinje cell is connected with hundreds of thousands of parallel fibers. The continuous excitatory inputs of parallel fibers on Purkinje cells elicit a stable pattern of discharges, so-called "simple spikes". Contrastingly, each Purkinje cell only receives input from a single climbing fiber and climbing fibers make direct synaptic contact with PCs. The contact between a CF and PC is so extensive that a single action potential in a CF leads to a prolonged and large depolarizing event in the PC, a so-called "complex spike". Together, simple spikes and complex spikes shape the inhibitory output of the cerebellar cortex on the deep cerebellar nuclei (Apps and Garwicz, 2005; **Figure 4B**).
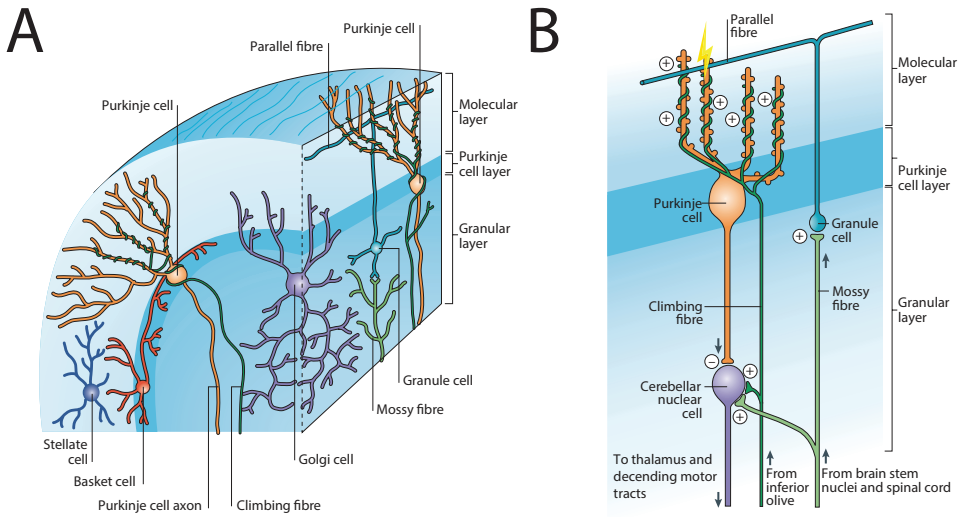
Figure 4. Cerebellar circuitry. A: Basic structure of the cerebellar cortex. The cerebellar cortex consists of a granular layer, Purkinje cell layer and molecular layer. The two main afferents of the cerebellum are mossy fibers, which terminate on granule cells, and climbing fibers, which terminate on Purkinje cells. Also pictured are inhibitory interneurons of the cerebellar cortex: stellate cells, basket cells and Golgi cells. Stellate and basket cells are located in the molecular layer and provide inhibitory input to the dendritic tree and cell body of Purkinje cells respectively. Golgi cells are located in the granular layer and form an inhibitory circuit between parallel fibers and granule cells. B: The prototypical (and simplified) circuit of the cerebellum. Plus (+) symbols indicate excitatory connections, minus (-) symbols indicate inhibitory connections. Not pictured are the connections of inhibitory interneurons, sites of plasticity, and reciprocal connections between the DCN and IO. Figure adapted from Apps and Garwicz, 2005.

Computations of the cerebellar circuit

The well-organized architecture of the cerebellum makes it attractive to study as the uniformity of the circuitry suggests it processes signals in similar ways across the cerebellum. Inspired by the prototypical structure of the cerebellum, David Marr and James Albus developed an influential theory about the computations taking place in the cerebellum (Albus, 1971; Marr, 1969). They hypothesized that the cerebellum can learn to generate appropriate output signals in response to arbitrary (sensory) input patterns via plasticity at the parallel fiber-Purkinje cell synapse. This was later corroborated by experimental work of Masao Ito who identified long-term depression (LTD) at the PF-PC synapse after conjunctive stimulation of PFs and CFs (Ito et al., 1982). Marr and Albus postulated that the cerebellar circuit is the operationalization of an algorithm for adapting movements in response to changes in the internal and external environment, in other words: the cerebellar circuit enables motor learning. In short, they hypothesized that mossy fibers relay motor commands and sensory information via parallel fibers to Purkinje cells, while climbing

fibers relay motor errors. The climbing fiber input acts as a teaching signal that supervises motor learning. Concurrent climbing fiber and parallel fiber input induce LTD at the PF-PC synapse, which in turn decreases the firing rate of Purkinje, disinhibiting the deep cerebellar nuclei after the same parallel fiber input. Disinhibition of the deep cerebellar nuclei can then modulate motor behavior via multiple cerebrocerebellar loops.

The Marr-Albus-Ito model of motor learning has inspired much research in the cerebellar field due to its elegance and well-described properties. The hypotheses of the theory were extensively tested in various motor learning experiments in animals and generally held up under scientific scrutiny [for review, see: Ito, 2001]. However, contemporary cerebellar research challenges the hegemony of the Marr-Albus-Ito model (Galliano and De Zeeuw, 2014). Firstly, when LTD at the PF-PC synapse is blocked, animals are still able to learn new motor behavior which is in direct contradiction with the Marr-Albus-Ito model of motor learning (Schonewille et al., 2011). Secondly, in addition to PF-PC synapse LTD, many other locations and forms of plasticity in the cerebellum have been identified to play a major role in motor learning [for review, see: Gao et al., 2012]. Additionally, spatiotemporal firing patterns (e.g. the synchrony of simple spikes over populations of PCs), shaped by the activity of interneurons in the molecular layer, seem particularly important for adequate motor learning beyond just the modulation of the firing rate of Purkinje cells (De Zeeuw et al., 2011). Furthermore, no consensus has emerged on the exact information signaled by complex spikes and simple spikes (Ebner et al., 2011). Instead, it is hypothesized that the complex spikes could be representative of the sensitivity to error and not the error itself, while simple spikes convey sensory prediction errors (Marko et al., 2012; Popa et al., 2016). Finally, as explored in the previous section, though predominantly associated with motor function, the cerebellum also has clear associations with other types of behavior (Strick et al., 2009).

Nonetheless, trying to understand the cerebellum using (testable) theories from computational neuroscience has been a fruitful endeavor. Building on the work by Marr and Albus, the cerebellar field has made extensive further efforts to unravel the role and computations of the cerebellum. Particularly influential in that regard have been several concepts and vocabulary derived from the domain of engineering and robotics (Doya et al., 2001; Todorov and Jordan, 2002). Motivated to make the movements of robots less clumsy, roboticists studied the fluency of movement in humans and formalized a computational framework of motor control. They recognized that to make accurate and fluent goal-directed movements, the motor system must overcome at least two difficult problems: 1) sensory feedback is noisy and delayed 2) the internal environment (i.e. the body) and external environment (i.e. the world around us) are susceptible to change. Adaptive forward models were suggested as a solution to overcome these problems and

were linked neuroanatomically to the cerebellum (Shadmehr and Krakauer, 2008). Forward models transform motor commands into their sensory consequences, enabling the motor system to act on short latency predictions of sensory consequences, rather than rely on delayed sensory feedback. Furthermore, combining predicted sensory consequences with actual sensory consequences reduces the variance of the state estimates of the body and world around us, facilitating the planning and execution of goal-directed movements as well. However, forward models are only useful if the predictions are accurate. Thus, to maintain optimal motor performance, a forward model should be able to adapt its sensory predictions in response changes in the internal or external environment. Converging lines of research indicate that forward models are updated by sensory prediction error, i.e. the difference between the predicted sensory consequences of a motor command and actual sensory consequences (Shadmehr et al., 2010), and drive a particular type of motor learning behavior: motor adaptation.

Motor adaptation

Motor adaptation is the process of adjusting already learned motor behavior and is considered to be qualitatively different from *de novo* motor learning, i.e. learning to snowboard for the first time is distinct from being an experienced snowboarder who responds to changes in slope conditions or new snowboard shoes. The novice snowboarder is learning a new movement while the experienced snowboarder is adjusting the execution of an already known movement. Importantly, as alluded to in the previous section, this process is hypothesized to rely on sensory-prediction errors, which result from the difference between the predicted outcome of a motor command (the output of a forward model) and the actual outcome of a movement (via sensory feedback). It is important to note that motor adaptation is only one of many mechanisms responsible for the full behavioral spectrum of motor learning in humans (Haith and Krakauer, 2013). For instance, in addition to motor adaptation, mechanisms like reinforcement learning (Izawa and Shadmehr, 2011), use-dependent learning (Diedrichsen et al., 2010) and strategic learning (Taylor and Ivry, 2011) contribute to motor learning behavior, however the rest of this section will focus on motor adaptation, as learning from sensory prediction errors is associated with the cerebellum in particular (Tseng et al., 2007).

While snowboarding is incredibly fun to do, it makes for a poor task to study motor adaptation experimentally. Ski slopes are only open a couple of months per year and are located geographically far away from most laboratories, not to speak of all kinds of data recording challenges. As such, other experimental tasks were developed to study motor adaptation behavior. Reaching movement experiments in particular have long been a staple to investigate motor adaptation in humans (Shadmehr and Wise, 2005). In reaching

experiments, subjects are instructed to move the manipulandum of a robotic device from a starting location to a target location with a quick and accurate hand motion. Direct vision of the hand is purposefully obstructed, but hand position is conveyed to subjects via a cursor on a monitor or horizontal screen (**Figure 5**).
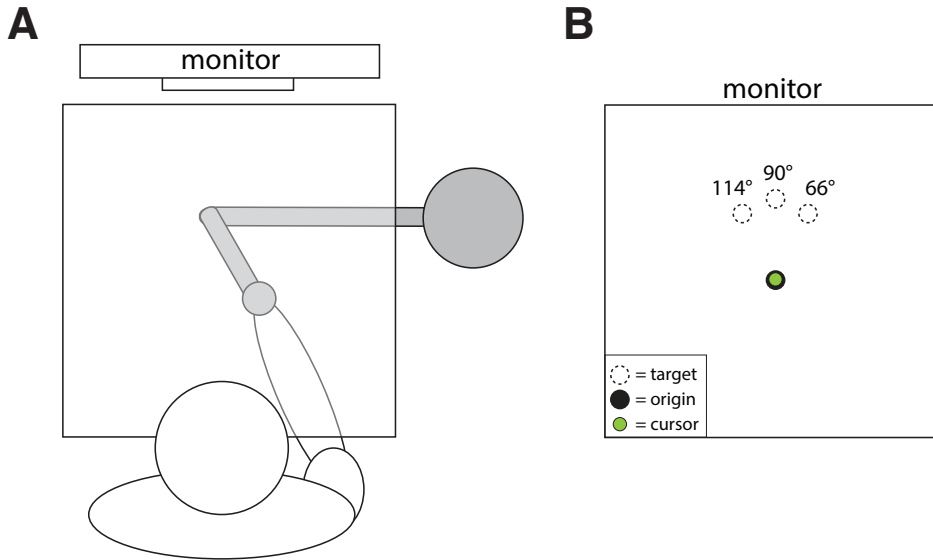
Figure 5. A) Common setup used in reaching movement experiments. The subject is seated behind a robotic device and holds a manipulandum in their right hand. For illustrative purposes the tabletop is pictured as transparent. In reality, the tabletop obstructs the view of the hand and device arm, so hand position can only be inferred from cursor position. B) The cursor position and targets are projected on a monitor or the tabletop in front of subjects. The subject is instructed to move the cursor (green circle) from the starting location (black circle) to one of several pseudorandomly selected target locations (white circles with dotted line). Three different target locations are pictured in this example.

A canonical reaching experiment consists of three phases: a baseline phase, an adaptation phase and a washout phase. During the baseline phase, subjects are familiarized with the device and learn to move the cursor between the starting location and the target location. Subjects usually make almost perfectly straight movements during the baseline phase with little to no movement error (the difference between the cursor position and the target location at the end of the movement), then, during the adaptation phase, visuomotor or forcefield perturbations are introduced while reaching towards the target. Visuomotor perturbations alter the relationship between hand position and cursor position, rotating cursor movement clockwise or counterclockwise when moving the hand towards the target.

In trials with a forcefield perturbation, the robotic device produces a small force, pushing the hand in a clockwise or counterclockwise direction while moving. Thus, visuomotor and forcefield perturbations alter the visual and/or proprioceptive consequences of motor commands, resulting in sensory-prediction errors. Subjects are then tasked with reducing movement errors induced by the perturbation during the adaptation phase. During the washout phase, reaches are made with veridical feedback (as in the baseline phase). A typical result of a visuomotor reaching experiment is displayed in **Figure 6** (Tseng et al., 2007).
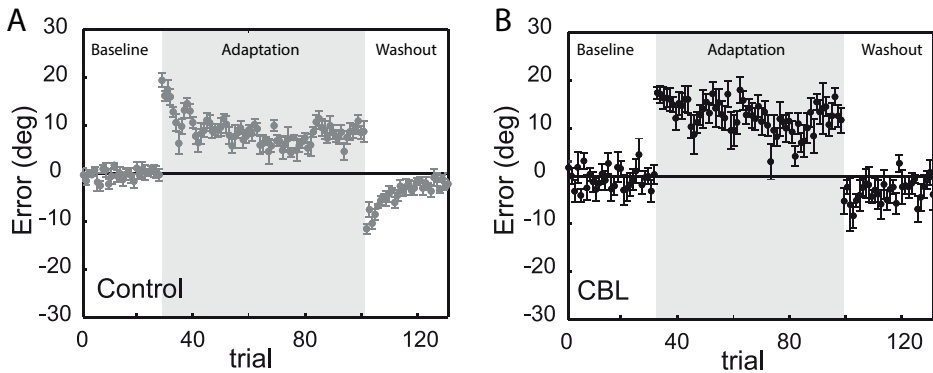
Figure 6. Typical result of a visuomotor reaching experiment in control subjects (A, n =7) and subjects with cerebellar disease (B, n=7), adapted from (Tseng et al., 2007). Movement error in degrees on the y-axis, trial number on the x-axis.

The experiment by Tseng and colleagues was conducted in healthy control subjects (**Figure 6A**) and subjects with cerebellar disease (**Figure 6B**). In control subjects, movement errors during the baseline phase are close to zero degrees (**Figure 6A**). At the start of the adaptation phase a visuomotor perturbation of 20 degrees was introduced. Movement errors in the adaptation phase are initially large (around 20 degrees) but tend towards lower values as the adaptation phase progresses, indicating adaptation to the perturbation. During the washout phase, feedback was veridical and visuomotor perturbations were turned off, so subjects needed to readapt to making reaching movements without visuomotor perturbations. As such, subjects tended to make errors in the opposing direction, indicating retention of adaptation of the preceding phase.

Motor behavior of subjects with cerebellar disease in this experimental task clearly contrasts with that of healthy control subjects. Cerebellar subjects demonstrate more variability in the baseline phase, almost no reduction of movement errors in the adaptation phase, and

less retention of the learned adaptation in the washout phase (**Figure 6B**). Both the total amount and speed of adaptation, as well as the amount of retention, is visibly reduced in subjects with cerebellar disease. This motor learning deficit is typical for cerebellar disease and is hypothesized to be the result of impaired computation and adaptation of forward models (Tseng et al., 2007). It is possibly exactly this motor learning deficit which makes it so challenging to provide effective therapy to patients with cerebellar disease.

Cerebellar disease

The most striking consequence of cerebellar disease is the neurological sign of cerebellar ataxia (Mariotti et al., 2005). Cerebellar ataxia is a neurological dysfunction of motor coordination originating in the cerebellum, with symptoms of balance and gait disturbances, speech impairments and incoordination of eye and upper-limb movements. The etiology of cerebellar ataxia is incredibly diverse and includes neuropathology of many different origins. Generally, a distinction is made between hereditary and nonhereditary ataxias. Nonhereditary ataxias are further subdivided into congenital ataxias, acquired ataxias and non-hereditary degenerative ataxias. (Klockgether, 2007). **Table 1** features an extensive but incomplete overview of many of the cerebellar ataxias.

The clinical history of an individual is often key to determine the etiology of cerebellar ataxia symptoms and proper follow-up (Timmann and Diener, 2007). For instance, acquired ataxias typically present with acute (minutes to hours) or sub-acute (days to weeks) symptoms and should be treated according to the primary disorder (e.g. surgical intervention after stroke, elimination of toxins, symptomatic treatment of infections, tumor resection etc.). To determine the underlying primary disorder, neuroimaging (CT/MRI) and laboratory analyses are most commonly employed (Nachbauer et al., 2015). Patients can recover from acquired ataxias with proper management, but individuals regularly develop chronic cerebellar symptoms (Konczak et al., 2005; Schoch et al., 2006). Congenital ataxias usually present during early childhood with a chronic (months to years) onset of non-progressive symptoms that are either hereditary or non-hereditary in nature (Steinlin, 1998a). The symptoms of congenital ataxias can be severe and curative treatment is generally unavailable (Pavone et al., 2017). Neuroimaging (MRI) is used to distinguish between acquired ataxias and congenital ataxias in childhood but can't predict the severity and progression of the disease (Steinlin, 1998b). Finally, hereditary and sporadic ataxias are marked by slowly progressive and chronic (months to years) onset of symptoms. Progressive and chronic ataxia with a family history of ataxic disease is highly suggestive of a hereditary ataxia (Jayadev and Bird, 2013). Usually, diagnostic follow-up includes neuroimaging (MRI) and molecular genetic testing. Genetic testing can classify the ataxia according to the pattern of inheritance, i.e. autosomal dominant, autosomal recessive

Table 1. Table adapted from Klockgether, 2007.

Hereditary Ataxias

Autosomal Dominant Ataxias (ADCAs)[*]

- Spinocerebellar ataxias (SCA)
- Dentatorubral-pallidoluysian atrophy (DRPLA)
- Episodic ataxias (EA)

Autosomal Recessive Ataxias (ARCAs)

- Friedreich's ataxia (FRDA)
- Ataxia-telangiectasia (AT)
- Ataxia with oculomotor apraxia
- Autosomal recessive spastic ataxia of Charlevoix-Saguenay (ARSACS)
- Abetalipoproteinemia
- Ataxia with isolated vitamin E deficiency (AVED)
- Refsum's disease
- Cerebrotendinous xanthomatosis (CTX)
- Marinesco-Sjogren syndrome (MSS)
- Autosomal recessive ataxia with known gene locus
- Early onset cerebellar ataxia (EOCA)

X-Linked Ataxias (XLAs)

- Fragile X tremor ataxia syndrome (FXTAS)

Nonhereditary Ataxias

Acquired Ataxias

- Alcoholic cerebellar degeneration
- Ataxia due to other toxic reasons (antiepileptics, lithium, solvents)
- Paraneoplastic cerebellar degeneration
- Immune-mediated ataxias (gluten ataxia, GAD antibody associated ataxia)
- Infectious ataxias (acute cerebellitis)
- Acquired vitamin E deficiency
- Hypothyroidism
- Ataxia due to physical causes (heat stroke, hyperthermia)

Congenital Ataxias[#]

- Cerebellar agenesis
- Cerebellar hypoplasia
- Joubert's syndrome
- Dandy-Walker malformation

Sporadic Degenerative Ataxias

- Multiple system atrophy, cerebellar type (MSA-C)
- Sporadic adult-onset ataxia of unknown etiology (SAOA)

* The ADCAs are clinically classified as type 1, 2 or 3 when genetic testing has not been carried out or was inconclusive and is based on the specific symptomatology and a familial history suggestive of dominant disease. # The etiology of congenital ataxia is poorly understood. Occasional appearance of congenital ataxia suggests it might be autosomal recessively inherited, but sporadic cases of congenital ataxia outnumber familial cases by far.

or X-linked inheritance. When genetic testing and family history are inconclusive, and multiple system atrophy (MSA) can be excluded, the ataxia is classified as sporadic adult-onset ataxia of unknown etiology (SAOA). The characteristics of, and therapies for, the most common hereditary ataxias and SAOA (together: the degenerative cerebellar ataxias) are briefly discussed in the next sections.

Degenerative cerebellar ataxias

Of the degenerative cerebellar ataxias, the group of hereditary cerebellar ataxias (HCAs) are most well-described in literature. HCAs are relatively rare, with an estimated prevalence of about 1 case per 10.000 individuals worldwide (Ruano et al., 2014). Cerebellar ataxia with a dominant inheritance pattern (autosomal dominant cerebellar ataxia or ADCA) has an estimated prevalence of about 2.7 (range 1.5 – 4.0) cases per 100.000 individuals (Ruano et al., 2014) and is largely comprised of spinocerebellar ataxias (SCAs). At least 40 different types of SCA have been identified and are named chronologically in order of discovery from SCA1 to SCA40 (Bird, 2016). Regionally, prevalence of ADCAs can be higher than the global average due to founder effects, e.g. there are large (isolated) populations of SCA2 patients in Cuba (Velázquez-Pérez et al., 2011) and SCA10 patients in Mexico (Alonso et al., 2007). The most prevalent SCA genotype worldwide is SCA3, with SCA3 and SCA6 being most common in Germany and the Netherlands (Schöls et al., 1997; van de Warrenburg et al., 2002). Most SCAs are polyglutamine (polyQ) disorders caused by CAG repeat expansions which lead to neural degeneration of the cerebellum and cerebellar pathways, either by aggregation of disease proteins, loss-of-function mutations, or (toxic) gain-of-function mutations (Paulson, 2009). The rate of disease progression differs between SCA types but on average individuals progress towards disability between 10 to 20 years after disease onset (Bird, 2016). Mortality data for SCA is limited but some SCA types are life-limiting while others are compatible with a normal life span (Diallo et al., 2018). Within SCA types, differences in CAG repeat length explain the highly variable clinical phenotype and longer repeat lengths correlate negatively with the age of onset (Tezenas du Montcel et al., 2014). Three essential patterns of neurodegeneration can be observed in SCA radiologically: "pure" cerebellar atrophy (e.g. SCA6 and SCA14), olivopontocerebellar atrophy (e.g. SCA1-3) and a pattern of global cerebral atrophy (e.g. SCA12, SCA17, SCA19) (Manto, 2005).

Ataxias with a recessive inheritance pattern (autosomal recessive cerebellar ataxias or ARCAs) have an estimated prevalence of about 3.3 (range 1.8 – 4.9) cases per 100.000 individuals (Ruano et al., 2014). Friedreich's ataxia (FRDA) is the most prevalent ARCA, accounting for about half of the ARCA cases (Pandolfo, 2009). Friedreich's ataxia is caused by loss of function mutations in the frataxin gene due to abnormally long intronic GAA

triplet repeats (Campuzano et al., 1996). Longer GAA repeat lengths predict an earlier age of onset, quicker disease progression and stronger extracerebellar involvement like cardiomyopathy (Dürr et al., 1996). The symptoms of ataxia, marked by sensory neuropathy, can be severe and the disease is life-limiting (Tsou et al., 2011). Neuroimaging generally reveals mild cerebellar cortical atrophy, but extensive degeneration of the dentate nuclei and spinal cord (Pandolfo, 2009).

The final group of degenerative ataxias, the sporadic adult onset ataxias of unknown etiology (SAOA), are the non-hereditary progressive ataxias with symptom-onset in adulthood. SAOA should not be considered a distinct disease entity (there are no structural or biochemical markers), but as a heterogeneous group of disorders with a common clinical syndrome and unknown etiology (Klockgether, 2012). SAOA is per definition a diagnosis of exclusion, as known causes of ataxia are ruled out. It is difficult to make concrete statements about the prevalence and neuropathology of SAOA since the underlying disease can vary between individuals and new discoveries constantly move the division between known and unknown etiologies. Still, clinical experience dictates that SAOA is more common than hereditary ataxia and isolated cerebellar atrophy is the most frequent radiological sign, though brainstem involvement is also observed (Abele et al., 2007).

Cerebellar therapy

Effective treatment of cerebellar disease in general, and degenerative cerebellar ataxias in particular, poses a major challenge. Apart from acquired ataxias and a small number of congenital ataxias, treatment options are limited (Mitoma and Manto, 2016). The degenerative cerebellar ataxias (hereditary and of unknown etiology) are especially difficult to treat, as curative treatments that target the pathogenic mechanisms of DCAs are still far away (Sarva and Shanker, 2014). Early and hopeful progress has been made in the development of antisense oligonucleotides (ASOs) which can target mRNA-transcripts of specific ataxia genes but ASOs have not reached the phase of clinical trials yet (Pulst, 2016; Toonen et al., 2017). Pharmacological treatment of specific symptoms is possible in a small subset of hereditary ataxias (Strupp et al., 2011) but for the vast majority of symptoms and DCAs no pharmacological treatment exists. Until curative treatment has become a viable option, management of DCA is limited to providing life-long supportive therapy (i.e. physical therapy, occupational therapy and speech therapy), with the goal of reducing ataxia symptoms, slowing down disease progression, and retaining activities of daily living (Ilg et al., 2014).

Physical therapy has proven to be most effective in attaining these goals (Fonteyn et al., 2014). A study by Ilg and colleagues established improvements in motor performance

and ataxia symptoms after an intensive four week physical therapy program (Ilg et al., 2009). Another study combined physical therapy with occupational therapy to improve the functional status of DCA patients. DCA patients, on average, exhibit long-term improvements under this combined therapy program, with larger functional gains for patients with mild symptoms than with severe ataxia (Miyai et al., 2012). In a study of SCA3 patients in Brazil, occupational therapy alone had no effects on motor performance, but did improve symptoms of depression (Silva et al., 2010). Evidence for beneficial effects of speech therapy is limited to case reports but can be considered for patients with severe dysarthria (Perlmutter and Gregory, 2003; Sapir et al., 2003). Taken together, these studies establish the benefits of supportive therapy but also raise several intriguing questions. Firstly, why is supportive therapy more effective in some patients than others? Secondly, what are the underlying mechanisms driving the effects of supportive therapy? Finally, can we improve the efficacy of supportive therapy?

Recent work has provided tentative answers to the first two questions. Firstly, since supportive therapy is more beneficial for cerebellar patients with less severe ataxia (Miyai et al., 2012), it suggests that the ability of patients to improve motor function depends on the residual capacity of the diseased cerebellum. Mitoma and Manto propose a 'restorable phase' in the progression of cerebellar disease, during which the cerebellum can (still) compensate for motor deficits (Mitoma and Manto, 2016). After this phase, the residual capacity of the cerebellum is too low to improve motor function. A second observation elucidates a possible mechanism driving the effects of supportive therapy. Hatakenaka and colleagues observed a correlation between the beneficial effects of supportive therapy and the motor learning capabilities of an individual. That is, cerebellar patients with higher motor learning capabilities exhibit higher gains from a neurorehabilitation program (Hatakenaka et al., 2012). Consequently, individuals with pronounced motor learning deficits, like DCA patients (Maschke et al., 2004a; Sanes et al., 1990; Tseng et al., 2007), are unable to benefit fully from neurorehabilitation. Conceivably, ameliorating motor learning deficits of DCA patients could also improve the efficacy of supportive therapy.

Improving cerebellar therapy

Several interventions have been proposed to ameliorate the motor learning deficit of DCA patients. Two types of intervention in particular have garnered considerable interest over recent years (Ilg et al., 2014). The first type of intervention aims to reduce motor learning deficits by applying non-invasive brain stimulation to the cerebellum or other areas of the brain. Specifically, transcranial direct current stimulation (tDCS) has been suggested as a promising type of non-invasive brain stimulation due to its low cost and ease of application. The technique involves running a small (in the order of 1-2 milliamperes) direct current

(DC) between two electrodes placed on the scalp. It is hypothesized that tDCS modulates the neuronal excitability of the brain areas the electrodes are placed over (Galea et al., 2009; Nitsche et al., 2000).

Over the past couple of years, multiple studies have reported beneficial effects of tDCS on motor adaptation. For instance, healthy subjects adapted more quickly to motor perturbations when tDCS was applied over the cerebellum (Avila et al., 2015; Block and Celnik, 2013; Galea et al., 2010a; Herzfeld et al., 2014a) and short-term retention of adaptation was improved when tDCS was applied over the primary motor cortex (Galea et al., 2010a; Hunter et al., 2009; Panouillères and Jenkinson, 2015). These early tDCS results in healthy subjects were regarded as promising for the development of therapeutic applications of tDCS, as possibly it could reduce the motor learning deficit of cerebellar patients. Pilot results indeed indicated behavioral improvements in cerebellar patients as a result of tDCS warranting follow-up studies (Grimaldi et al., 2014a; Pozzi et al., 2013), however early positive tDCS effects have proven difficult to replicate (Jalali et al., 2017) and whether tDCS has reliable neurophysiologic effects, even in healthy subjects, is still up for debate (Horvath et al., 2014a). Therefore, additional studies are required to establish whether tDCS can reliably elicit motor adaptation improvements, whether tDCS can reduce motor learning deficits in cerebellar patients, and whether the technique can be used to improve therapeutic efficacy.

The second type of intervention focusses on using training-related interventions to reduce motor learning deficits in cerebellar patients. As mentioned before, in addition to motor adaptation, mechanisms like reinforcement learning (Izawa and Shadmehr, 2011), use-dependent learning (Diedrichsen et al., 2010) and strategic learning (Taylor and Ivry, 2011) contribute to motor learning behavior. The central idea of training-related interventions is that training differently could allow motor learning mechanism not affected by pathology to compensate for cerebellar motor learning deficits. Recent evidence provides merit to this idea. For example, when cerebellar patients are provided with an explicit strategy to counter visuomotor perturbations they demonstrate near error-less performance (Taylor et al., 2010). Furthermore, altering the type of feedback from movement-errors to reinforcement signals (success or failure) improves learning from a visuomotor perturbation in cerebellar patients (Therrien et al., 2016). There is also limited evidence that gradually introducing a perturbation can alleviate motor learning deficits of cerebellar patients, hypothesized to be the result of a so-called slow learning mechanism (Criscimagna-Hemminger et al., 2010), however the beneficial effects of training-related interventions might be limited.

Firstly, while cerebellar patients can employ an explicit strategy to counter a visuomotor perturbation (Taylor et al., 2010), they cannot discover an aiming strategy on their own

(Butcher et al., 2017). Similarly, the result by Therrien and colleagues suggested that, while cerebellar patients can learn from reinforcement signals, cerebellar patients can only learn from reinforcement signals if motor noise is tightly controlled (Therrien et al., 2016). Furthermore, improving motor learning in cerebellar patients by the gradual introduction of a perturbation could not be replicated in subsequent work (Gibo et al., 2013; Schlerf et al., 2013). Thus, while training-related interventions look promising, additional research is required to establish a role for them in cerebellar therapy.

Outline of this thesis

Firstly, in **Chapter 2**, the effects of healthy ageing and cerebellar disease on cerebellar cortical integrity are investigated. The chapter compares the pattern of cerebellar degeneration between healthy ageing and cerebellar disease. **Chapter 3** explores the effects of cerebellar disease on integrity of the deep cerebellar nuclei using quantitative susceptibility mapping (QSM). In **Chapter 4**, motor learning in typically developed children and children with autism is examined, emphasizing the interaction between cerebellar integrity and motor learning. In **Chapters 5, 6 and 7**, the effects of non-invasive brain stimulation on motor learning in healthy control subjects and cerebellar patients are examined. **Chapter 5 and 6** investigate whether the motor learning deficit of cerebellar patients can be alleviated using online or offline tDCS. **Chapter 7** is an attempt to reproduce previous positive tDCS findings in healthy subjects. **Chapter 8** studies the explicit and implicit components of motor learning, establishing a method to uncover the use of strategies during motor learning. Finally, **Chapter 9** explores the effect of training-related interventions on motor learning deficits of cerebellar patients.

2

Ageing shows a pattern of cerebellar degeneration analogous, but not equal, to that in patients suffering from cerebellar degenerative disease

Thomas Hulst[ab], Jos N. van der Geest[ac], M. Thürling[d], S. Goericke[e], Maarten A. Frens[ab], Dagmar Timmann[d], Opher Donchin[af]

a Department of Neuroscience, Erasmus MC, 3000 CA Rotterdam, The Netherlands
b Erasmus University College, Rotterdam, The Netherlands
c Department of Radiology, Erasmus MC, 3000 CA Rotterdam, The Netherlands
d Department of Neurology, University of Duisburg-Essen, 45122 Essen, Germany
e Institute of Diagnostic and Interventional Radiology and Neuroradiology, University Clinic Essen, 45122 Essen, Germany
f Department of Biomedical Engineering and Zlotowski Center for Neuroscience, Ben-Gurion University of the Negev, Beer Sheva 81405, Israel

ABSTRACT

Ageing generally leads to impairments in cognitive function and the ability to execute and learn new movements. While the causes of these impairments are often multi-factorial, integrity of the cerebellum in an elderly population is an important predictive factor of both motor function and cognitive function. A similar association between cerebellar integrity and function is true for cerebellar patients. We set out to investigate the analogies between the pattern of cerebellar degeneration of a healthy ageing population and cerebellar patients. We quantified cerebellar regional volumes by applying voxel-based morphometry (VBM) to a publicly available dataset of MR images obtained in 313 healthy subjects aged between 18 and 96 years and a dataset of MR images of 21 cerebellar patients. We observed considerable overlap in regions with the strongest loss of cerebellar volume in the two datasets. In both datasets, the anterior lobe of the cerebellum (lobules I-V) and parts of the superior cerebellum (primarily lobule VI) showed strongest degeneration of cerebellar volume. However, the most significant voxels in cerebellar patients were shifted posteriorly (lobule VII) compared to the voxels that degenerate most with age in the healthy population. The results showed a pattern of significant degeneration of the posterior motor region (lobule VIIIb) in both groups, and significant degeneration of lobule IX and X in the healthy population, but not in cerebellar patients. Furthermore, we saw strong volumetric degeneration of functionally defined cerebellar regions associated with cerebral somatomotor function in both groups. Predominance of degeneration in the anterior lobe and lobule VI suggests impairment of motor function in both groups, while we suggest that the posterior shift of degeneration in cerebellar patients would be associated with relatively stronger impairment of higher motor function and cognitive function. Thus, these results may explain the specific symptomology associated with cerebellar degeneration in ageing and in cerebellar patients.

Keywords: Ageing, voxel-based morphometry, cerebellum, cerebellar degeneration, motor control, cognition

INTRODUCTION

Although the rate and degree of transition into old age varies from individual to individual, ageing can generally be defined as a progressive deterioration of physiological function. Often, ageing leads to impairments in executing movements and learning new movements (Seidler et al., 2010), as well as impairments in cognitive functions (Li et al., 2001; Park and Reuter-Lorenz, 2009). While the causes of functional impairments associated with ageing are multi-factorial, integrity of the cerebellum is an important predictive factor of both motor function and cognitive function in an elderly population (Bernard and Seidler, 2013; MacLullich et al., 2004; Raz et al., 2000; Woodruff-Pak et al., 2001).

Imaging studies have shown that cerebellar grey and white matter volumes are reduced in elderly persons (Hoogendam et al., 2012; Jernigan et al., 2001). Especially the anterior lobe of the cerebellum (lobules I-V) shows a reduced neuronal cell count (Andersen et al., 2003) and reduced volume (Bernard and Seidler, 2013) with increasing age. It is also reported that the posterior lobe of the cerebellum (lobules VI-X) is affected by ageing (Dimitrova et al., 2008; Paul et al., 2009), though this relationship is not as strong as for the anterior lobe. A recent and thorough review links the reductions of cerebellar volume to motor and cognitive impairments in an older population (Bernard and Seidler, 2014).

Patients with cerebellar ataxia also show a strong association between function and cerebellar integrity. It has long been known that damage to the cerebellum, be it a lesion or degenerative disease, lead to impairments in motor function (Flourens, 1824; Holmes, 1908). Recent studies of the diseased cerebellum were able to identify two body representations within the cerebellum; one in the anterior cerebellum and a second in the posterior cerebellum (Manni and Petrosini, 2004). Cerebellar patients suffering from cerebellar degenerative disease (Rabe et al., 2009) and patients with cerebellar infarctions (Donchin et al., 2012) show motor impairments. These impairments are strongly associated with volumetric loss of the anterior motor area (lobules IV – VI) but have a less consistent association between motor impairments and volumetric loss of the posterior motor area (lobule VIIIb). These findings support the notion that motor function and the integrity of particular regions of the cerebellum are intimately linked. Correspondingly, diseases of posterior cerebellar regions like lobule VI and VII, including Crus I/II and VIIb, are linked to a decline in cognitive function (Stoodley and Schmahmann, 2009; Timmann and Daum, 2007) and clinical syndromes like the cerebellar cognitive affective syndrome (CCAS) (Schmahmann and Sherman, 1998).

The similarity of behavioural motor deficits between healthy elderly persons and cerebellar patients suggests cerebellar degeneration of anterior motor area and posterior motor area

as a common factor. Likewise, integrity of the posterior cerebellum is linked to cognitive function in both healthy elderly persons as well as cerebellar patients, but this association is stronger in cerebellar patients. Clinical syndromes like CCAS seem unique for cerebellar patients and are linked to degeneration of the posterior cerebellum as well. These findings could be consistent with the idea that the posterior cerebellum is more severely affected in cerebellar patients than in healthy aging.

The studies reviewed above show converging evidence of an association between cerebellar integrity and function in both healthy elderly persons and in cerebellar patients, but a comparison of the pattern of degeneration between the two populations has not been made so far. In essence, such a comparison would tell us to what extent healthy ageing can be regarded as a proxy or model system of cerebellar degenerative diseases. Studying how similar these two populations are with respect to cerebellar volume integrity, and in which ways they differ, can tell us more about the aetiology of both processes and the symptomatology, or behavioural deficits, of cerebellar degeneration. When making a direct comparison of the regions most affected by ageing with the regions most affected by disease, we expect to see large areas of overlap of degeneration. The most overlap of degeneration is expected in the anterior lobe of the cerebellum, which is implicated to lose integrity both with increasing age and cerebellar disease. Less overlap of degeneration is expected in the posterior lobe of the cerebellum, since age effects on posterior cerebellar volume are less pronounced than the effect of cerebellar disease on posterior cerebellar volume.

We set out to investigate the amount and localization of age-related cerebellar degeneration in a healthy ageing population by applying voxel-based morphometry (VBM) to an open-access dataset of brain images. We applied a similar analysis to a dataset of cerebellar degeneration patients and healthy age-matched controls. Subsequently, we were able to compare the patterns of degeneration of healthy ageing people and cerebellar patients.

METHODS

Datasets

The Open Access Series of Imaging Studies (OASIS) project (Marcus et al., 2007) provides brain imaging data that is freely available to the scientific community (http://www.oasis-brains.org). The OASIS cross-sectional MRI dataset consists of a collection of 416 subjects aged 18 to 96 including healthy individuals and individuals with early-stage Alzheimer's Disease. We excluded subjects who suffered from dementia (Clinical Dementia Rating (CDR) > 0.0) and/or had a low Mini-Mental State Examination score (MMSE < 25).

After visual inspection of the segmentation maps generated during the VBM-analysis, we excluded 3 more subjects whose MRI scans did not successfully segment into grey matter (GM), white matter (WM) and cerebrospinal fluid (CSF). In total, we included 313 subjects from the dataset provided by the OASIS project. **Table 1** gives an overview of the age and gender of subjects.

Table 1. Overview subjects OASIS dataset. Distribution of the age and gender of 313 included subjects (195 females and 118 males).

Group (#)	Age range (years)	Female (n)	Male (n)	All (n)
1	18 – 33	79	66	145
2	34 – 49	23	15	38
3	50 – 65	33	15	48
4	66 – 81	39	15	54
5	82 – 97	21	7	28

Furthermore, we acquired a dataset of MRI scans from the Institute of Diagnostic and Interventional Radiology and Neuroradiology, University Clinic Essen containing data from 23 patients suffering from pure cerebellar degeneration and 59 healthy controls. From this dataset we selected 21 patients whose ages we could match within 3 years with 21 of the healthy control subjects. **Table 2** gives a detailed overview of their individual characteristics.

Image acquisition

MR images in the OASIS data set consist of high-resolution three-dimensional T1-weighted MPRAGE (Magnetization Prepared Rapid Acquisition Gradient Echo) scans acquired by, a 1.5T Siemens MR scanner [TR, 9.7 ms; TE, 4.0 ms; TI, 20 ms; flip angle, 10 deg.; matrix 256 x 256; voxel size, 1.0 x 1.0 x 1.25 mm^3] (Marcus et al., 2007). The OASIS dataset contains at least 3 T1-weighted MRI scans obtained within a single imaging session for each subject. We used the average image [matrix 256 x 256; voxel size, 1.0 x 1.0 x 1.0 mm^3] of a scanning session that was motion-corrected and co-registered to the average of the entire dataset by Marcus et al. for our analysis. MR images in cerebellar patients and their age-matched controls consisted of high-resolution three-dimensional T1-weighted MPRAGE scans using a 3T MRI scanner (Siemens Magnetom Skyra) with a 20-channel head/neck coil [TR, 2300 ms; TE = 2.26 ms, TI = 900 ms; flip angle 10 deg; matrix, 256 x 240; voxel size 1.0 × 1.0 × 1.0 mm^3]. None of the cerebellar subjects had radiological pathologies outside the cerebellum. These images have been used previously (Thieme et al., 2013).

Table 2. Overview of patient and control subject characteristics in the University Clinic Essen dataset. All patients are age-matched with a control subject shown on the right-hand side of the table. Although the diagnosis between patients is heterogeneous, all patients suffer from pure cerebellar degeneration, with similar patterns of degeneration of the cerebellar cortex (Timmann et al., 2009).

Patients						Controls	
ID	Age (years)	Gender	Diagnosis	Disease duration (years)	ICARS (total score of max 100)	Age (years)	Gender
C01	35	F	SAOA	7	51.00	34	F
C02	44	M	SAOA	6	13.00	43	M
C03	45	M	SAOA	15	27.50	45	M
C04	46	F	ADCA III	28	26.50	46	M
C05	48	M	ADCA III	8	12.50	47	M
C06	49	M	ADCA III	10	44.00	47	M
C07	49	M	ADCA III	9	27.50	47	M
C08	49	M	SAOA	13	41.00	49	F
C09	51	M	Cerebellitis	9	50.00	51	F
C10	52	F	SCA 14	13	23.00	52	M
C11	54	M	SAOA	19	51.00	54	F
C12	54	M	SCA 6	7	38.00	55	M
C13	56	F	SCA 6	7	26.50	56	M
C14	58	F	ADCA III	18	24.00	59	M
C15	62	M	SAOA	8	22.50	61	M
C16	63	M	SAOA	13	25.50	62	F
C17	64	F	SCA 6	11	43.50	62	F
C18	72	M	SCA 6	16	63.00	70	M
C19	73	M	SCA 6	12	40.50	70	F
C20	74	F	SCA 6	7	39.50	73	M
C21	76	F	SCA 6	15	47.00	74	M

SCA6 = spinocerebellar ataxia type 6; SCA14 = spinocerebellar ataxia type 14; SAOA = sporadic adult onset ataxia; ADCA III = autosomal dominant ataxia type III (a pure cerebellar disorder with autosomal dominant inheritance and inconclusive genetic testing); ICARS = International Cooperative Ataxia Rating Scale (Trouillas et al., 1997).

Voxel-based morphometry

Voxel-based morphometry analysis was applied to the cerebellar cortex of each subject separately (Ashburner and Friston, 2000). The approach of generating a grey matter volume map of the cerebellum using VBM was based on the approach used by Taig and colleagues (Taig et al., 2012). The entire analysis was automated with an in-house program

written for Matlab 8.1 (The Mathworks, Natick, USA) using the SUIT toolbox (version 2.7), developed by Jörn Diedrichsen (http://www.icn.ucl.ac.uk/motorcontrol/imaging/suit. htm) (Diedrichsen et al., 2009), implemented in SPM12 (http://www.fil.ion.ucl.ac.uk/spm/ software/spm12).

In short, the following procedure was followed for each individual. The program first assigned each voxel of the entire T1-weighted scan a probability of being grey matter, white matter, or CSF according to the voxel intensity by means of the updated segmentation algorithm implemented in SPM12 (Ashburner and Friston, 2005). Subsequently, we isolated the cerebellum from surrounding tissue (Diedrichsen, 2006). We applied a nonlinear normalization algorithm to project the individual cerebellum onto a probabilistic atlas (Diedrichsen et al., 2009). The deformation map generated in this step was used to map the individual cerebellar grey matter image onto the template SUIT cerebellum.

The output of this procedure can be regarded as a voxel-by-voxel assessment of the amount of grey matter associated with all voxels in the template (Ashburner and Friston, 2000). In other words, the grey matter that an individual subject has associated with a particular voxel in the SUIT template is the volume mapped onto that voxel (under the deformation map described above) multiplied by the concentration of grey matter in that volume as determined by the segmentation algorithm (Donchin et al., 2012). Finally, we corrected for head size by dividing grey matter volumes by total intracranial volume (TICV). We smoothed the resulting grey matter map using a 6 x 6 x 6 mm^3 median filter.

Cerebellar volume

The effect of age on cerebellar volume in the OASIS dataset was first examined by linear regression with age as the independent variable and total cerebellar volume as the dependent variable. We also performed linear regressions with age as the independent variable and the tissue types acquired during segmentation (grey matter, white matter and CSF) as the dependent variable. Furthermore, we tested for non-linear age effects on total cerebellar volume and the distinct tissue types. Lastly, we tested for non-linear age effects on specific regions of the cerebellum: the anterior cerebellum (lobules I-V), the posterior cerebellum (lobules VI-X) and each cerebellar lobule as defined by the SUIT atlas.

Statistics

We will first describe the methodology applied to the OASIS dataset and later provide an overview of the similarities and differences between the methodology applied to the University Clinic Essen dataset. The main difference in methodology lies in our choice of statistical test, because in the OASIS dataset we are assessing the correlation of cerebellar

volume and age across subjects, while in the University Clinic Essen dataset we are assessing a difference in cerebellar volume between patients suffering from cerebellar degeneration and healthy age-matched controls. An overview of the methodology for the OASIS dataset and for the University Clinic Essen dataset can be found in **Figure 1 and 2** respectively.
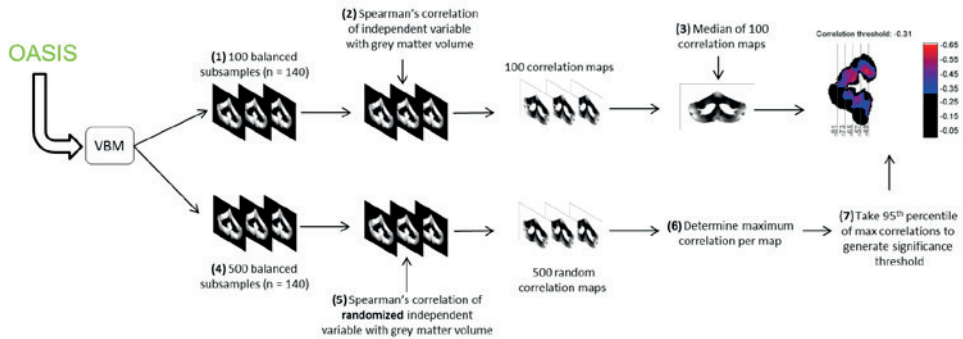

Figure 1. Workflow statistical analysis of the OASIS dataset. Steps 1 – 3 of analysis are described in the Correlation analysis section. Steps 4 – 7 are described in the Permutation analysis section.

Correlation analysis

To assess the localization of degeneration associated with ageing in the OASIS dataset, we calculated the Spearman's correlation between grey matter volume and age group for each subject on a voxel-by-voxel basis. We obtained correlations using randomly selected sub-samples of 28 subjects from each of the five age groups (see **Table 1**), while allowing for duplicates in each age group (k-multi combinations). We chose this number of subjects per age group as this was the number of subjects in the smallest of the five age groups. We repeated this random sampling procedure a 100 times (**Figure 1**, step 1). In this balanced subsample of 140 subjects in total, we calculated the correlations of grey matter volume and categorical age data for each voxel in the cerebellum (**Figure 1**, step 2). From these 100 correlation maps we took the median correlation for each individual voxel to generate a balanced correlation map of the entire OASIS database (**Figure 1**, step 3). We applied a minimum filter to the balanced correlation map, substituting each voxel with the minimum correlation value in a 3 x 3 x 3 voxels neighborhood.

We performed similar correlation analyses with grey matter volume for other subject characteristics provided by the OASIS project, namely education level and socio-economic status (SES). The dataset provided information about the education level of 134 subjects and information about the socio-economic status (SES) in the 132 subjects. Both measures

were categorized into a high and low category. High and low education level contained 67 and 67 subjects respectively. High and low SES contained 79 and 53 subjects respectively. By repeated sampling (100 repetitions) of a balanced subsample as described above, a balanced correlation map for both education level and SES was calculated.

To assess whether there was a difference between females and males in ageing-related patterns of cerebellar degeneration, we calculated the correlation with age as described above for both male subjects and female subjects separately. Again, we made sure to keep both subsamples balanced by applying the same resampling method (100 repetitions) as described above. We selected 22 subjects per age-group for both females and males, as this was the number of subjects in the smallest of age-groups. For this comparison age was categorized into 3 age-categories instead of 5 age-categories, to retain enough subjects per age-category: 18-33 years (79 female, 66 male), 34-65 years (56 female, 30 male) and 66-97 years (60 female, 22 male). We applied a Fisher r-to-z transformation on both the female and male correlation maps and tested for the significance of the difference between the two correlation maps.

Permutation analysis

We determined the significance of correlations calculated in the OASIS database by performing a permutation analysis which allowed us to correct for the multiple testing problem. We first took 500 balanced subsamples (**Figure 1**, step 4) and calculated balanced correlation maps as described above, but for each of these maps we randomly permuted the association between subject age and grey matter volume, essentially generating an estimation of the null distribution of our test statistic (**Figure 1**, step 5). We then took the maximum voxel correlation per permutation map (**Figure 1**, step 6). The significance threshold was then calculated as the 95th percentile of absolute maximum voxel correlations of all random correlation maps (**Figure 1**, step 7). In this way, our significance threshold corrected appropriately for the reduction in significance caused by testing many voxels, and the reduction in the number of effective tests caused by spatial correlations across voxels.

University Clinic Essen dataset

The methodology for assessing cerebellar degeneration in the University Clinic Essen dataset is similar to that of the methodology for the OASIS dataset, but here we test for a difference between patients and age-matched controls with a t-score as our test statistic.

We first performed a paired sample t-test on the grey matter volume of individual voxels in the cerebellum between patient cerebella and age-matched controls (**Figure 2**, step 1). To test for significance, we generated 500 permutations maps of the original dataset where, for

each permutation, the match between MRI data and subject category (patient or control) was randomized (**Figure 2**, step 2). Finally, we determined the maximum t-score per permutation map (**Figure 2**, step 3) and a significance threshold was calculated by taking the 95th percentile of all maximum voxel t-scores (**Figure 2**, step 4).
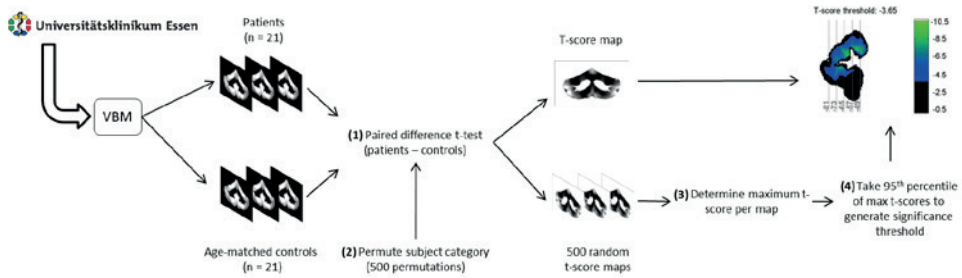
Figure 2. Workflow statistical analysis of the University Clinic Essen dataset. Steps 1 – 4 are described in the University Clinic Essen dataset section.

RESULTS

Cerebellar volume

There is a marked decline of total cerebellar volume (TCV) in the OASIS dataset with age; the linear coefficient of the regression line (b1) is: -586 mm^3 per year, R2 = 0.37, F = 184, p < 0.00001. When TCV was corrected for TICV, the linear model was able to predict the relationship between age and cerebellar volume with more accuracy (b1 = -350 mm^3 per year, R2 = 0.52, F = 337, p < 0.00001). **Table 3** gives a detailed overview of the effect of ageing on cerebellar volume and cerebellar tissue type corrected for TICV, as well as a gender specific analysis. It is clear from the table that the reduction in volume is primarily a result of the loss of grey matter, and that the effect is not markedly different between males and females. A voxel-by-voxel assessment of the difference between males and females as described in the last paragraph of the correlation analysis section was also made, but did not reveal a significant difference.

We also tested for non-linear age effects on total cerebellar volume, but a linear model provided the best fit. Similarly, we tested for non-linear age effects on distinct tissue types

and cerebellar regions, but here as well a linear model provided the best fit. Reporting a linear model thus has our preference, since it is able to explain age-related degeneration just as well, or better, as a model with more polynomials.

Table 3. Regression reliability measures of a simple linear regression with age as independent variable and volume (mm³) as dependent variable in the OASIS dataset. All volumes are corrected for total intracranial volume.

	Coeff (b1) mm³/year	R²	F	p
TCV (all subjects)	-350	0.52	337	<0.00001
Males	-403	0.55	139	<0.00001
Females	-339	0.54	224	<0.00001
GM (all subjects)	-301	0.60	463	<0.00001
Males	-331	0.57	156	<0.00001
Females	-297	0.64	342	<0.00001
WM (all subjects)	-69	0.21	81	<0.00001
Males	-83	0.28	45	<0.00001
Females	-69	0.21	53	<0.00001
CSF (all subjects)	+20	0.18	69	<0.00001
Males*	+11	0.06	8	<0.01
Females	+27	0.32	91	<0.00001

* = significant difference of age effects between males and females (ANCOVA, F = 10.59, p = 0.0013). TCV = Total cerebellar volume; GM = Grey matter; WM = White matter; CSF = Cerebrospinal fluid.

Degeneration maps

The definition of lobule anatomy and nomenclature used in the forthcoming results and discussion are as described in the SUIT atlas by Diedrichsen et al., 2009. Our analysis generated a map of age-dependent degeneration in SUIT atlas space, where the value of each voxel is the correlation between grey matter volume and age for that particular voxel. Slices from this map are shown in **Figure 3**, with a threshold set at significance level (a negative correlation of -0.31). The range of correlations for individual voxels ranged between -0.65 to +0.2. Almost the entire cerebellum undergoes significant volume reduction with age, but the strongest reduction can be found in the anterior lobe (lobules I-V) spreading towards parts of the superior cerebellum (in particular lobule VI). A large part of the posterior cerebellum, specifically Crus I/II and lobule VIIb, does not show significant volume reduction with age. Furthermore, the degeneration map shows significant volume reduction in the posterior motor area of the cerebellum (lobule VIIIb) and lobule IX. From all voxels in the cerebellum approximately 52.9% tested as having a significant correlation.
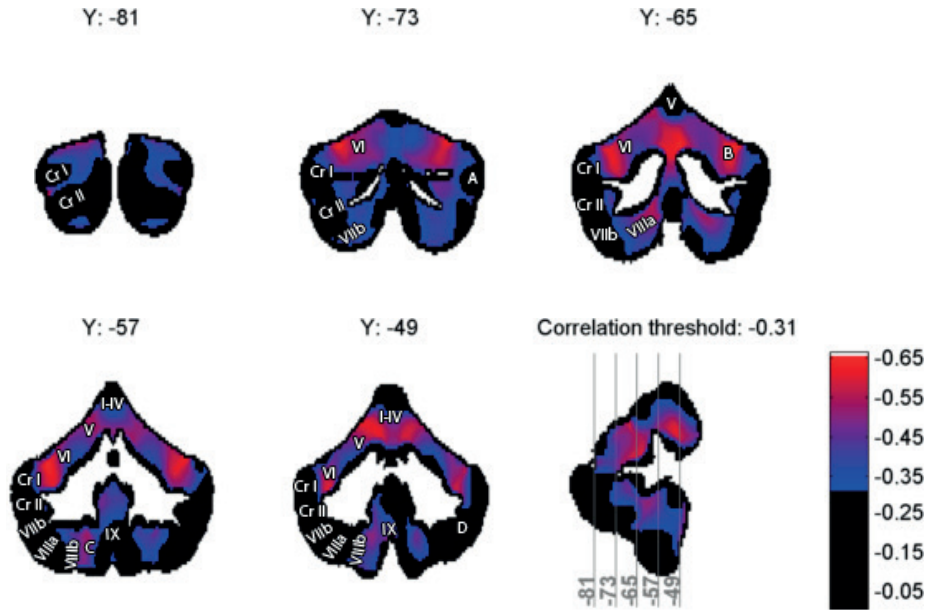
Figure 3. Pictured are slices of the cerebellum showing the correlation between grey matter volume and age in the OASIS database. A threshold was set at the calculated significance threshold, meaning that each voxel with a correlation less strong than -0.31 is color-coded as black. Weak significant correlations are color-coded as blue, while strong significant correlations are color-coded as red. Letters A, B, C and D correspond with approximate positions of voxel clusters in figures 6A-D. Definition of lobule anatomy and nomenclature as described in Diedrichsen et al., 2009. Cr I = Crus I, Cr II = Crus II.

Figure 4 shows a similar map for the University Clinic Essen dataset. This map shows t-scores of the difference between cerebellar patients and age-matched controls (threshold set at the significance threshold of t = -3.65). The range of t-scores for individual voxels ranged between -10.5 to +3.5. In this dataset too, we see that degeneration is most pronounced in the anterior part of the cerebellum (lobules I-V). Degeneration is widespread, but unlike the healthy ageing population, we see more pronounced degeneration in Crus I/II and lobule VIIb, while the posterior motor area (lobule VIIIb) and lobule IX seem less affected. From all voxels in the cerebellum approximately 59.1% tested as having a significant t-score.
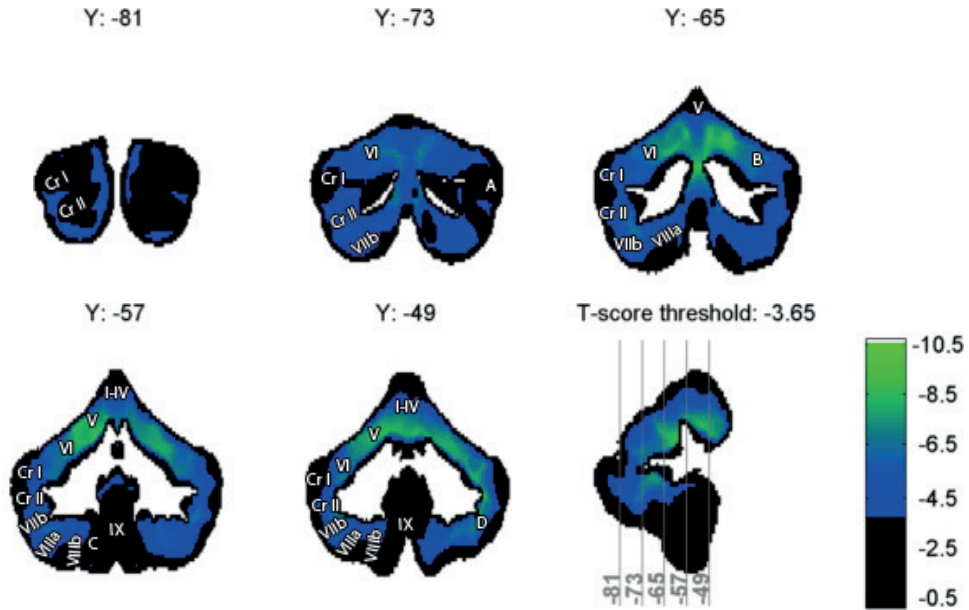
Figure 4. Pictured are slices of the cerebellum showing t-scores of the grey matter volume difference between patients and age-matched controls in the University Clinic Essen dataset. A threshold was set at the calculated significance threshold, meaning that each voxel with a t-score that is less strong than -3.65 is color-coded as black. Low significant t-scores are color-coded as blue, while high significant t-scores are color-coded as green. Letters A, B, C and D correspond with approximate positions of voxel clusters in figures 6A-D. Definition of lobule anatomy and nomenclature as described in Diedrichsen et al., 2009. Cr I = Crus I, Cr II = Crus II.

In order to compare the areas undergoing age-related degeneration and the areas affected in patients, we generated a map of the overlap of degeneration. To make this comparison fair, we took the 25% most degenerated voxels in both datasets. The results are more significant in cerebellar degeneration than in ageing, so any specific significance cut-off would have included many more voxels from the cerebellar degeneration maps. Using the 75th percentile meant that the number of voxels taken from each map was the same. **Figure 5** shows slices from the overlap map. The combination map corroborates the impression that similar areas undergo degeneration in ageing as in cerebellar patients. In both the healthy ageing population and the cerebellar patients, the anterior lobe of the cerebellum (lobules I-V) and parts of the superior cerebellum (primarily lobule VI) show the strongest degeneration of cerebellar volume. However, the most significant voxels in cerebellar patients are shifted posterior (Crus I/II and lobule VIIb) compared to the voxels that degenerate most with age in the healthy population. This map also shows strong degeneration of the posterior motor region (lobule VIIIb) and lobule IX in the healthy population, but not in cerebellar patients.
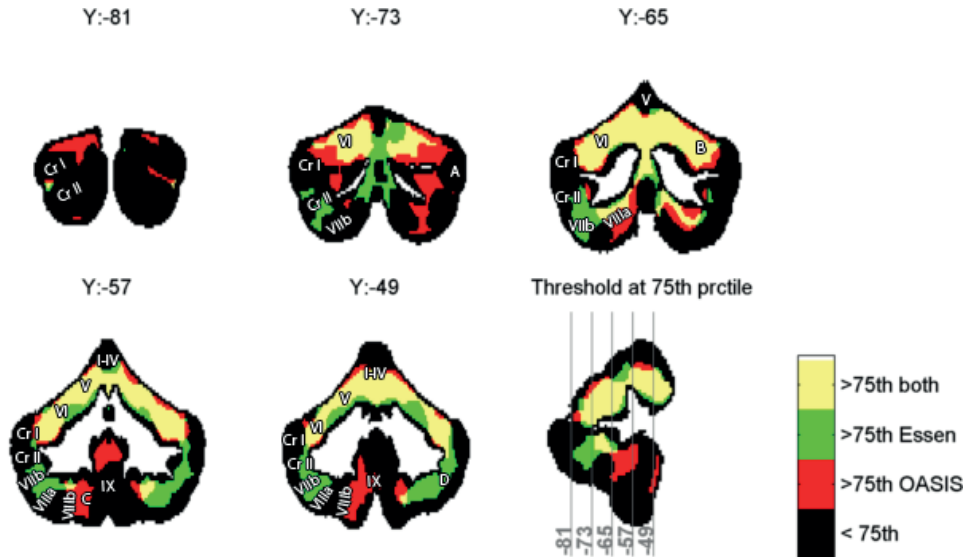
Figure 5. A combination of the correlation map of the OASIS dataset and the t-score map of the University Clinic Essen dataset. Individual voxels in both the OASIS dataset and the University Clinic Essen dataset with a correlation or t-score above the 75th percentile respectively are color-coded as yellow. Individual voxels with a correlation above the 75th percentile in the OASIS dataset, but no overlap with University Clinic Essen dataset, are color-coded as red. Individual voxels with a t-score above the 75th percentile in the University Clinic Essen dataset, but no overlap with the OASIS dataset, are color-coded as green. Individual voxels with both a correlation in the OASIS dataset and a t-score in the University Clinic Essen dataset below the 75th percentile respectively are color-coded as black. Letters A, B, C and D correspond with approximate positions of voxel clusters in figures 6A-D. Definition of lobule anatomy and nomenclature as described in Diedrichsen et al., 2009. Cr I = Crus I, Cr II = Crus II.

Permutation analysis of socio-economic status and level of education yielded no significant results. Correlations for both socio-economic status and level of education ranged between -0.2 and +0.2, below the generated significance threshold.

Voxel clusters

To elaborate upon the effect of ageing on cerebellar volume at the voxel-level, we present several boxplots showing the median volume of typical clusters of 27 voxels (3 x 3 x 3 mm^3 sized cube) plotted against their age-group (**Figure 6A-D**). The locations of selected voxel clusters are highlighted by the letters A, B, C and D on the correlation and t-score maps of **Figures 3-5**. **Figure 6** serves to illustrate the 'raw' data underlying **Figures 3-5**. In principle, we could generate this figure for each location (voxel cluster) in the cerebellum, but that would be impractical given the large amount of voxels in the cerebellum. The voxel

clusters depicted in **Figure 6** were chosen based on the varying levels of significance as described below. **Figure 6A** shows the median volume per age-group of a voxel cluster that is not significant in both datasets. **Figure 6B** shows a voxel cluster that is significant in both datasets. **Figure 6C** shows a voxel cluster that is significant in the OASIS dataset, but not the University Clinic Essen dataset, while **Figure 6D** shows the reverse. The boxplots reveal that voxel-clusters with strong age-related volume reduction in the OASIS dataset have similar age-related reduction in the control subjects of the University Clinic Essen dataset. Although cerebellar patients tend to have less grey matter volume in the selected voxel-clusters, the grey matter volume does not seem to decrease with age. An analysis for ageing effects on total grey matter volume of the cerebellum in patients did not reveal a significant effect ($R^2 = 0.06$, $F = 1.22$, $p = 0.28$).

Lobules

To explore the effect of ageing on cerebellar volume at the level of cerebellar lobules, we took the median of all lobule volumes for each subject in the OASIS dataset and each control subject and patient in the University Clinic Essen dataset respectively. All volumes were corrected for TICV. Similarly, we took the median of all voxel correlations per lobule in the OASIS dataset and the median of all voxel t-scores per lobule in the University Clinic Essen dataset. **Table 4** shows the median volume and interquartile range (IQR) of all cerebellar lobules, as well as the median correlation and IQR between voxel volume and age per lobule for subjects of the OASIS dataset. Similarly, it shows the median volume and IQR of cerebellar lobules for all controls and patients of the University Clinic Essen dataset, as well as the volume difference per voxel between controls and patients in median t-score and IQR.
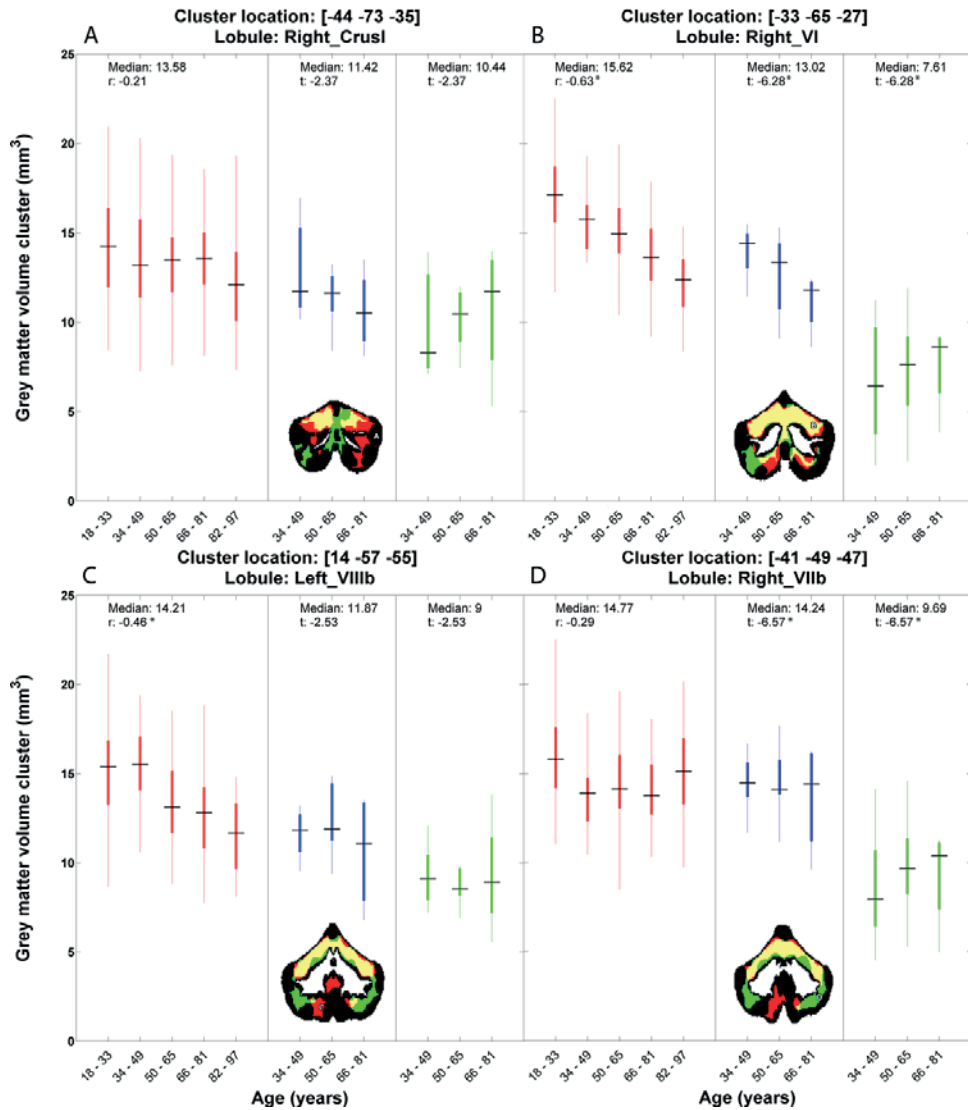
Figure 6. Median grey matter volume of 3x3x3 cluster of voxels per age-group in OASIS dataset (red), Essen controls (blue) and Essen patients (green). Cluster locations are in XYZ coordinates of the MNI atlas. The location of a voxel cluster is depicted with a letter on the slice of the overlap map below the box plots. All subjects in both datasets were included in this analysis. * = significant voxel cluster with significance threshold set at level of permutation analysis.

Table 4. Median volumes of cerebellar lobules in the OASIS dataset and University Clinic Essen dataset. Definition of lobule anatomy and nomenclature as described in Diedrichsen et al., 2009. All volumes are corrected for total intracranial volume. Number between parentheses is the interquartile range (Q3 – Q1). Also shown are the correlations of the OASIS dataset and t-scores of the University Clinic Essen dataset. IQR of correlations and t-scores are printed between parentheses.

	OASIS dataset		Essen Controls	Essen Patients	Difference
Lobule	Volume (mm³)	Correlation (r)	Volume (mm³)	Volume (mm³)	T-score
Left I_IV	1465 (362)	-0.46 (0.21)*	1066 (130)	571 (184)	-5.67 (3.38)*
Right I_IV	1491 (358)	-0.39 (0.21)*	1168 (189)	651 (250)	-5.45 (2.96)*
Left V	2159 (482)	-0.44 (0.21)*	1713 (230)	869 (362)	-6.55 (2.81)*
Right V	2031 (476)	-0.41 (0.20)*	1682 (227)	924 (348)	-6.13 (2.67)*
Left VI	5123 (973)	-0.47 (0.12)*	4072 (680)	2224 (1045)	-6.03 (1.80)*
Vermis VI	1057 (228)	-0.44 (0.22)*	802 (139)	424 (235)	-5.74 (1.90)*
Right VI	4610 (855)	-0.45 (0.13)*	3871 (574)	2301 (913)	-6.18 (2.16)*
Left Crus I	6758 (1428)	-0.29 (0.26)	5293 (1109)	3705 (1608)	-3.64 (1.48)
Vermis Crus I	9 (3)	-0.37 (0.07)*	5 (2)	2 (3)	-4.38 (1.97)*
Right Crus I	6729 (1469)	-0.32 (0.21)*	5498 (839)	3861 (1877)	-3.42 (2.13)
Left Crus II	4425 (870)	-0.21 (0.17)	3784 (597)	2632 (1074)	-3.97 (1.53)*
Vermis Crus II	266 (66)	-0.23 (0.15)	211 (59)	120(67)	-4.51 (1.68)*
Right Crus II	4446 (877)	-0.23 (0.13)	3684 (497)	2695 (1408)	-3.38 (1.07)
Left VIIb	2321 (491)	-0.27 (0.22)	1955 (301)	1315 (581)	-4.88 (1.39)*
Vermis VIIb	104 (26)	-0.43 (0.08)*	90 (20)	47 (23)	-6.61 (0.90)*
Right VIIb	2379 (476)	-0.29 (0.20)	1989 (287)	1300 (710)	-4.27 (0.99)*
Left VIIIa	2432 (545)	-0.29 (0.24)	2099 (386)	1507 (561)	-4.21 (1.89)*
Vermis VIIIa	604 (122)	-0.29 (0.24)	488 (118)	320 (161)	-4.78 (3.28)*
Right VIIIa	2269 (419)	-0.28 (0.20)	1972 (299)	1281 (574)	-4.78 (1.67)*
Left VIIIb	1951 (405)	-0.34 (0.27)*	1789 (408)	1147 (457)	-3.37 (1.63)
Vermis VIIIb	343 (73)	-0.33 (0.22)*	272 (51)	205 (63)	-3.26 (1.97)
Right VIIIb	1984 (394)	-0.29 (0.20)	1765 (251)	1255 (311)	-4.17 (1.83)*
Left IX	1521 (362)	-0.33 (0.16)*	1189 (359)	790 (469)	-1.72 (1.41)
Vermis IX	406 (77)	-0.33 (0.22)*	363 (65)	283 (89)	-2.32 (1.52)
Right IX	1572 (345)	-0.23 (0.18)	1376 (402)	934 (509)	-2.38 (1.64)
Left X	126 (29)	-0.35 (0.15)*	108 (27)	61 (47)	-2.45 (2.96)
Vermis X	84 (15)	0.03 (0.09)	49 (13)	37 (30)	-2.57 (0.73)
Right X	114 (29)	-0.43 (0.15)*	80 (16)	49 (26)	-2.77 (3.23)

* = significant lobule correlation with significance threshold set at level of permutation analysis for the OASIS dataset and significant lobule t-score with significance threshold set at level of permutation analysis for the University Clinic Essen dataset.

The results in **Table 4** confirm what we previously saw in **Figures 3-5**: the anterior lobe (lobules I-V) and lobule VI are affected in healthy ageing as well as in patients suffering from cerebellar degenerative diseases. More posteriorly in the cerebellum, we see that patients are more severely affected than healthy ageing individuals. The analysis particularly shows degeneration of Crus II and lobule VIIb in cerebellar patients, but not healthy ageing individuals. The analysis shows less consistent degeneration of the posterior motor area (lobule VIIIb) in both healthy individuals and patients. Finally, the analysis shows strong degeneration of lobule XI and X in healthy individuals, but not in patients. **Supplementary Material 1** (online) contains a similar correlation map and t-score map as depicted in **Figure 3-4**, but for lobule volumes instead of voxel volumes. **Supplementary Material 2** (online) contains boxplots of median lobule volume plotted against age-group for both the OASIS data set and the University Clinic Essen dataset. **Supplementary Material 3** (online) contains histograms of the voxel correlations per lobule of the OASIS dataset, as well as histograms of the voxel t-score per lobule of the University Clinic Essen dataset. The volumes depicted in the Supplementary Materials are all corrected for TICV.

Functionally defined regions

Finally, we applied the same approach as we did for cerebellar lobules to the defined regions (networks) of a 7-network functional connectivity atlas of the cerebellum developed by Buckner et al., 2011. Cerebellar voxels in this atlas are classified as functionally connected to a cortical network when there is a high temporal correlation in BOLD signal between the cerebellar voxel and a specific cortical network. We applied the Buckner network parcellation to the cerebellum of each subject in both datasets and measured the volume of the functionally defined regions. We then correlated the grey matter volume of each functionally defined region with that subjects age in the OASIS dataset (see **Figure 7**) or calculated a t-score for the difference between healthy controls and patients in the University Clinic Essen dataset (**Figure 8**). This analysis does not measure the effects of cerebellar degeneration on functional connectivity directly, as we would require resting-state fMRI data for such an analysis, but measures the effect on volume of age- and disease-related cerebellar degeneration in the regions defined by the Buckner atlas. **Supplementary Material 4** (online) contains a table alike **Table 4**, but for volumes, correlations and t-scores of the functional connectivity atlas.
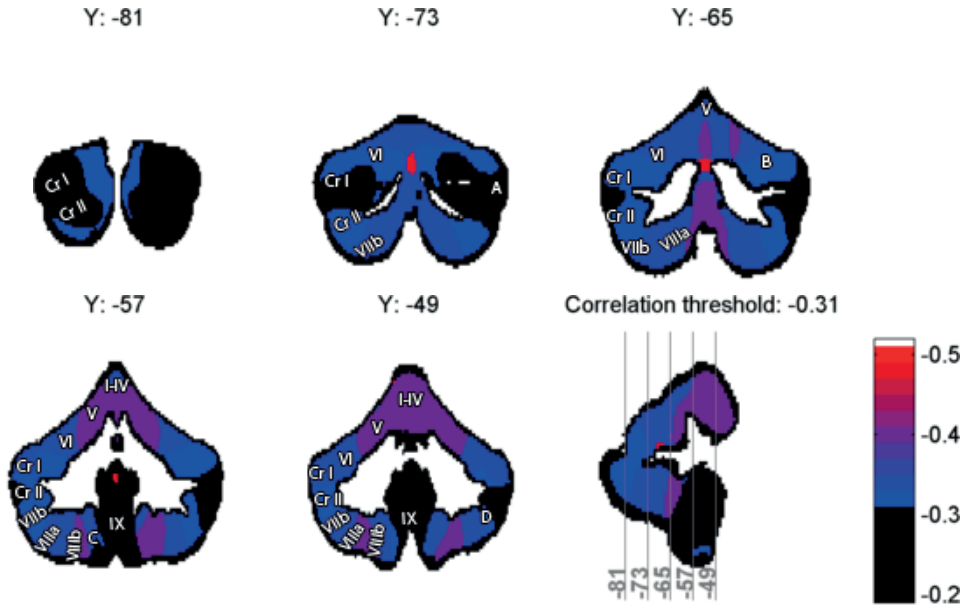
Figure 7. Correlation map of functionally defined regions in the OASIS dataset. Pictured are slices of the cerebellum showing the correlation between grey matter volume and age of functional connectivity networks in the OASIS database. A threshold was set at the calculated significance threshold, meaning that each voxel with a correlation less strong than -0.31 is color-coded as black. Weak significant correlations are color-coded as blue, while strong significant correlations are color-coded as red. Letters A, B, C and D correspond with approximate positions of voxel clusters in figures 6A-D. Definition of lobule anatomy and nomenclature as described in Diedrichsen et al., 2009. Cr I = Crus I, Cr II = Crus II.

To illustrate the effect of degeneration of functionally defined cerebellar regions on the cerebral cortex, we projected the correlation values and t-scores of each functionally defined region in the cerebellum onto a map of the functionally defined regions in the cerebral cortex. Thus, the voxels that belonged to a certain functional connectivity network in the cerebral cortex each got the correlation value or t-score of the corresponding network in the cerebellum, see **Figure 9** and **Figure 10**. Again, this analysis does not show the effects of cerebellar degeneration on functional connectivity in the cerebral cortex directly, but serves to illustrate which networks of the cerebral cortex are likely affected by degeneration of cerebellar regions defined by the Buckner atlas.
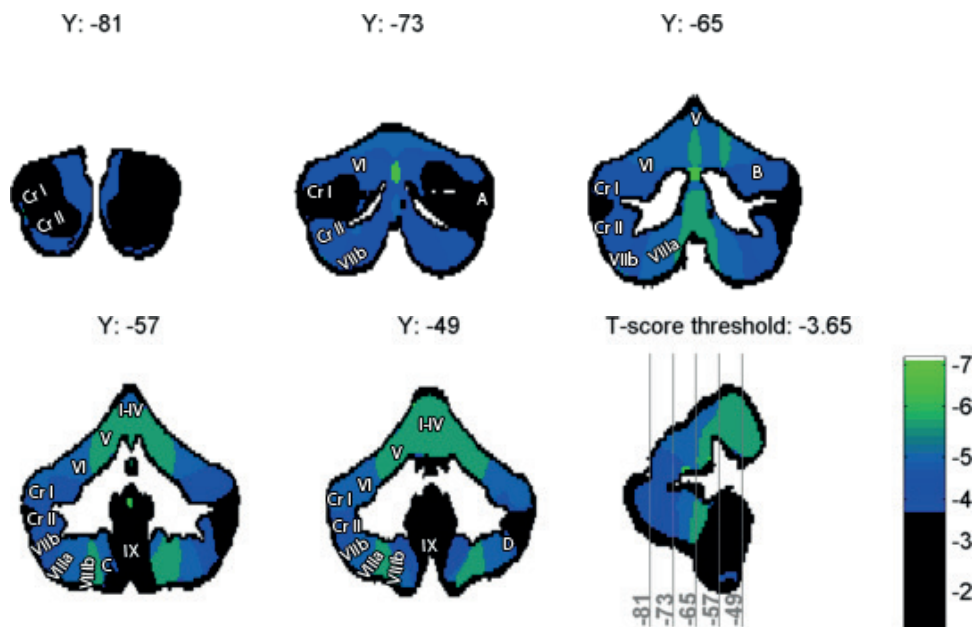
Figure 8. T-score map of functionally defined regions in the University Clinic Essen dataset. Pictured are slices of the cerebellum showing t-scores of the grey matter volume difference between patients and age-matched controls of functional connectivity networks in the University Clinic Essen dataset. A threshold was set at the calculated significance threshold, meaning that each voxel with a t-score that is less strong than -3.65 is color-coded as black. Low significant t-scores are color-coded as blue, while high significant t-scores are color-coded as green. Letters A, B, C and D correspond with approximate positions of voxel clusters in figures 6A-D. Definition of lobule anatomy and nomenclature as described in Diedrichsen et al., 2009. Cr I = Crus I, Cr II = Crus II.

It becomes apparent from this analysis that similar functionally defined cerebellar regions degenerate in ageing and cerebellar patients. The functionally defined region that is most degenerated in both datasets is the visual network, but one should take into account that the visual network has a very small representation in the cerebellum. The functionally defined region of the somatomotor network degenerates strongly in both ageing subjects and cerebellar patients, while the dorsal attention, ventral attention and frontoparietal networks degenerate less strongly. The volumes of the limbic network (network 5) and the default network (network 7) both do not degenerate in ageing subjects and cerebellar patients.
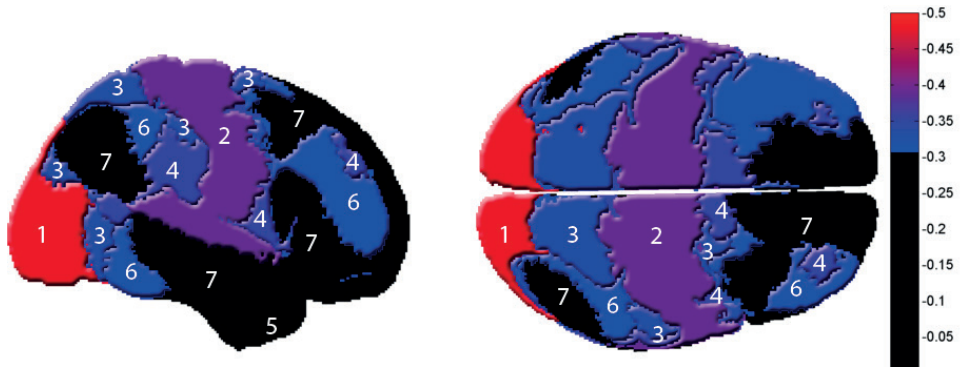
Figure 9. Correlation map of functionally defined regions in the OASIS dataset. Pictured is the lateral surface of the left hemisphere of the cerebral cortex (left) and the lateral surface of both hemispheres of the cerebral cortex from a craniocaudal view (right). A threshold was set at the calculated significance threshold, meaning that each voxel with a correlation less strong than -0.31 is color-coded as black. Weak significant correlations are color-coded as blue, while strong significant correlations are color-coded as red. Numbers correspond with functional connectivity networks as described in Thomas Yeo et al., 2011. 1 = visual network, 2 = somatomotor network, 3 = dorsal attention network, 4 = ventral attention network, 5 = limbic network, 6 = frontoparietal network, 7 = default network.
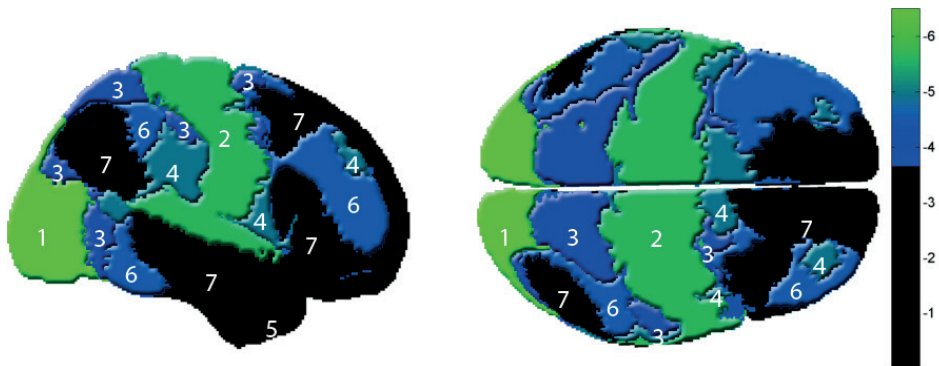
Figure 10. T-score map of functionally defined regions in the University Clinic Essen dataset. Pictured is the lateral surface of the left hemisphere of the cerebral cortex (left) and the lateral surface of both hemispheres of the cerebral cortex from a craniocaudal view (right). A threshold was set at the calculated significance threshold, meaning that each voxel with a t-score that is less strong than -3.65 is color-coded as black. Low significant t-scores are color-coded as blue, while high significant t-scores are color-coded as green. Numbers correspond with functional connectivity networks as described in Thomas Yeo et al., 2011. 1 = visual network, 2 = somatomotor network, 3 = dorsal attention network, 4 = ventral attention network, 5 = limbic network, 6 = frontoparietal network, 7 = default network.

DISCUSSION

This study investigated the relationship between cerebellar volume and ageing. More specifically, it quantified the amount and localization of age-related cerebellar degeneration in a healthy population and compared these findings with a group of cerebellar patients. The results show a striking pattern of cerebellar degeneration in the healthy OASIS dataset. The areas of the cerebellum that are most affected by ageing lie in the anterior lobe of the cerebellum (lobules I-V), with degeneration spreading towards the superior cerebellum (lobule VI). This suggests that the anterior motor area (lobule IV – VI), which has previously been linked to motor adaptation and performance in cerebellar patients (Donchin et al., 2012), is affected. Earlier work on motor adaptation and the cerebellum in healthy ageing indeed suggests a connection between integrity of the anterior motor area and motor performance (Bernard and Seidler, 2013). We also saw degeneration of the posterior motor area (lobule VIIIb) in healthy subjects, although the degeneration of this area was less consistent than degeneration of the anterior motor area.

The strong correlation between ageing and degeneration of specifically the anterior cerebellum raises the question of its selective vulnerability. It has been suggested before that the anterior cerebellum is particularly vulnerable to the effects of ageing (Andersen et al., 2003; Torvik et al., 1986), although the exact mechanism is unknown. Possible explanations for cerebellar degeneration in ageing include an increased exposure to toxins (i.e. alcohol) due to localized higher CSF flow (Cavanagh et al., 1997), changes in the cerebrovascular system (Raz et al., 1998), and functional factors (Chung, 1985). Recently Zhou and colleagues found higher firing frequencies of zebrin-negative Purkinje cells in awake mice, mainly located in the anterior cerebellum, which could have an effect on cerebellar integrity (Zhou et al., 2014). Likely, the cause of selective vulnerability of the anterior cerebellum is multi-factorial.

Cerebellar patients showed widespread degeneration of the anterior cerebellum and lobule VI, similar to healthy ageing individuals. However, when comparing degeneration of the posterior cerebellum (lobule VI – X) between healthy individuals and cerebellar patients, the most significant voxels were shifted posteriorly in cerebellar patients. Taig et al. have suggested recently that there is an anterior-posterior gradient of increasing abstraction in these areas of the cerebellum, suggesting a possible cognitive impairment in cerebellar patients. Indeed, there is evidence that lesions of the posterior lobe of the cerebellum lead to cognitive and higher motor function impairments in patients (Schmahmann and Sherman, 1998), but cognitive impairments in cerebellar degeneration might be subtle and hardly distinct from normal function (Timmann and Daum, 2010). What is interesting to note is

the apparent lack of an ageing effect in cerebellar patients, both in the anterior and posterior cerebellum. This could be in part a floor effect; when the cerebellar cortex is severely degenerated by disease, ageing might not have an effect on cerebellar volume anymore.

There are several limitations of our method that need to be considered. First, segmentation into tissue types can be problematic in cerebellar foliations which are close to the voxel size, thus some voxels might be incorrectly regarded as grey or white matter. We think this does not compromise our current results, because we show regions of degeneration well above the size of single voxels and our filtering methods should correct for incorrect classification of tissue type sufficiently. Secondly, we utilized the standard SUIT atlas template for normalization, which was developed based on scans of neurological healthy individuals aged 22 – 45 years, while the eldest individuals in our datasets are well above the age range included in the SUIT atlas template. Ideally, a specialized atlas template that includes elderly individuals should be developed and used for normalization of our dataset. Relatedly, the entire procedure as described in the voxel-based morphometry section of our methods was applied automatically without hand-correction, barring the exclusion of 3 subjects that failed segmentation into different tissue types. This has the advantage that the procedure is repeatable and can easily be applied to large populations, however a recent paper by (Price et al., 2014) showed limited reliability and validity of the SUIT-atlas when hand correction of isolation-masks was not applied. Future work on large aging populations could benefit from using a specialized aging atlas template and alternative automated normalization approaches.

Overall, our findings corroborate the idea that healthy ageing individuals show a pattern of cerebellar degeneration that is partly analogous to patients suffering from cerebellar degenerative disease. While both healthy ageing individuals and patients show degeneration of the anterior cerebellum (lobule I –V) and lobule VI, the degeneration in patients spreads towards lobules in the posterior cerebellum (Crus I/II and lobule VIIb). Degeneration of the posterior motor area (lobule VIIIb) is less consistent in healthy individuals and cerebellar patients, while lobule XI and X show strong degeneration in healthy individuals but not in cerebellar patients. Predominance of degeneration in the anterior lobe spreading towards lobule VI suggests impairment of motor function in both groups, while we predict that the posterior shift of degeneration in cerebellar patients would be associated with relatively stronger impairment of higher motor function and cognitive function. Thus, our results may explain the specific symptomology associated with cerebellar degeneration in ageing and in cerebellar patients.

Acknowledgements

Author contributions

Thomas Hulst conceived and designed the research; analyzed data; interpreted results; prepared figures; drafted manuscript; edited and revised manuscript; approved the final version of the manuscript.

3

Age-related changes of cerebellar cortex and nuclei: MRI findings in healthy controls and its application to spinocerebellar ataxia (SCA6) patients

Dominik Jäschke[1], Katharina M. Steiner[1], Dae-In Chang[1,2], Jens Claaßen[1], Ellen Uslar[1], Andreas Thieme[1], Marcus Gerwig[1], Viktor Pfaffenrot[3], Thomas Hulst[1,4], Stefan Maderwald[3], Sophia L. Göricke[5], Martina Minnerop[6,7], Mark E. Ladd[3,8,9], Jürgen R. Reichenbach[10], Dagmar Timmann[1,3,#], Andreas Deistung[1,3,10,#]

[1] Department of Neurology, Essen University Hospital, University of Duisburg-Essen, 45147 Essen, Germany
[2] Department of Psychiatry and Psychotherapy, LVR-Hospital Essen, Faculty of Medicine, University of Duisburg-Essen, 45147 Essen, Germany
[3] Erwin L. Hahn Institute for Magnetic Resonance Imaging, University of Duisburg-Essen, 45141 Essen, Germany
[4] Erasmus University College, 3011 HP Rotterdam, The Netherlands
[5] Institute of Diagnostic and Interventional Neuroradiology, Essen University Hospital, University of Duisburg-Essen, 45141 Essen, Germany
[6] Institute of Neuroscience and Medicine (INM-1), Research Centre Juelich, 52425 Jülich, Germany
[7] Center for Movement Disorders and Neuromodulation, Department of Neurology and Institute of Clinical Neuroscience and Medical Psychology, Medical Faculty, Heinrich-Heine University, Düsseldorf, Germany
[8] Medical Physics in Radiology, German Cancer Research Center (DKFZ), 69120 Heidelberg, Germany
[9] Faculty of Physics and Astronomy and Faculty of Medicine, Heidelberg University, 69120 Heidelberg, Germany
[10] Medical Physics Group, Institute of Diagnostic and Interventional Radiology, Jena University Hospital, 07743 Jena, Germany
# Authors contributed equally

ABSTRACT

Understanding cerebellar changes due to healthy aging is of utmost importance. It provides a reference point against which pathological changes in late-onset disease, for example spinocerebellar ataxia type 6 (SCA6), can be contrasted. In the present study, we investigated the influence of aging on the cerebellar nuclei and cerebellar cortex in 111 healthy controls (age range: 16 – 78 years) using 3 Tesla magnetic resonance imaging (MRI). Findings were contrasted with 25 SCA6 patients (age range: 38 – 78 years). A subset of 16 SCA6 patients and 40 controls received an additional MRI scan at 7 Tesla and were re-scanned after one year. MRI included T1-weighted, T2-weighted FLAIR, and multi-echo T2*-weighted imaging. The T2*-weighted images were converted to effective transverse relaxation rate (R2*) and quantitative susceptibility maps. Since the cerebellar nuclei are characterized by elevated iron content with respect to their surroundings, two independent raters manually outlined them on the susceptibility maps. T1-weighted images acquired at 3T were utilized to automatically identify the cerebellar gray matter (GM) volume. Linear correlations revealed significant atrophy of the cerebellum due to tissue loss of cerebellar cortical GM in healthy controls with increasing age. Decline of the cerebellar GM was substantially stronger in SCA6 patients. We were able to robustly delineate the dentate, but less frequently the smaller cerebellar nuclei (globose, emboliform, and fastigial nuclei) on susceptibility maps even at a magnetic field strength of 3T. Interestingly, the globose and emboliform nuclei were even better discernible on 3T than on 7T images. The volume of the dentate nuclei and the smaller cerebellar nuclei did not exhibit a significant relationship with age, at least in the age range between 18 and 70 years, whereas mean susceptibilities and R2* of both the dentate and globose nuclei increased with age. The cerebellar nuclei volumes, except for the emboliform nuclei, were smaller in SCA6 patients compared to age- and sex-matched controls. The significant dentate volume loss in SCA6 patients could be confirmed with 7T MRI, while the smaller cerebellar nuclei followed the trend observed at 3T, but did not reach statistical significance due to the lower number of subjects. Additionally, lower magnetic susceptibilities and R2* were found in the dentate of the patients, whereby the effect sizes for differentiating between the controls and patients were similar. Neither patients nor controls showed significant changes in volume, susceptibility and R2* of the dentate after one year. Importantly, dentate volumes were more sensitive to differentiate between SCA6 (Hedges' g = 2.83) and controls than the cerebellar cortex volume (g = 1.97). Since iron content in the cerebellar nuclei has been shown to be highest in neuroglia, our findings suggest that atrophy of dentate nuclei in SCA6 patients reflects at least partly a decrease of iron-containing glia cells.

Keywords: MRI, ataxia, spinocerebellar ataxia type 6, cerebellum, quantitative susceptibility mapping, dentate nucleus

INTRODUCTION

The aging healthy brain undergoes various structural changes leading to impairments in executing movements and learning new movements (Seidler et al., 2010), as well as cognitive decline (Li et al., 2001; Park and Reuter-Lorenz, 2009). It is well known that the cerebellum and the cerebellar white matter (WM) tissue degenerate during aging of healthy adults (Hoogendam et al., 2012; Koppelmans et al., 2015; Raz et al., 2001; Sullivan and Pfefferbaum, 2006). Imaging studies have also shown that volumes of cerebellar gray and white matter are reduced in elderly people (Hoogendam et al., 2012; Hulst et al., 2015; Jernigan et al., 2001). Especially, the anterior lobe of the cerebellum (lobules I–V) exhibits reduced neuronal cell count (Andersen et al., 2003) and reduced volume (Bernard and Seidler, 2013) with increasing age. The posterior lobe of the cerebellum (lobules VI–X) is also affected by ageing (Dimitrova et al., 2008; Paul et al., 2009), though this relationship is not as strong as in the anterior lobe. Age-related degeneration of the cerebellum likely has an effect on behaviors associated with cerebellar function, i.e. motor behaviors (Trewartha et al., 2014) and cognitive behaviors (Bernard and Seidler, 2014; MacLullich et al., 2004).

Apart from all these studies of aging induced effects in the cerebellar cortex and white matter, little is known about the involvement of the deep cerebellar nuclei in aging. More than 60 years ago, Höpker (1951) reported volume decreases of the dentate nuclei with increasing age. He obtained volumes of the dentate ranging between 320 mm^3 and 420 mm^3 for adults, whereas individuals older than 70 years exhibited volumes between 200 mm^3 and 300 mm^3, representing a decrease by approximately 30% in the elderly. Histopathological studies reported increased iron concentration in the dentate nucleus compared to the surrounding WM tissue (Benkovic and Connor, 1993; Drayer et al., 1986; Koeppen et al., 2012) as well as evaluated iron content for elderly (Hallgren and Sourander, 1958; Ramos et al., 2014). Utilizing the elevated iron levels in the dentate as a source of contrast in magnetic resonance imaging (MRI), *in vivo* studies could confirm increasing iron concentrations in the dentate nucleus over the lifespan (Aoki et al., 1989; Bilgic et al., 2012; Ghassaban et al., 2019; Li et al., 2014; Maschke et al., 2004b). In addition to the dentate, elevated amounts of iron were also identified in histological stains for the globose, emboliform and fastigial nuclei relative to their surrounding tissue (Benkovic and Connor, 1993). The smaller deep cerebellar nuclei (DCN), however, have not yet been assessed systematically and non-invasively across the lifespan.

Understanding brain changes due to healthy aging is of utmost importance as it provides a reference point against which pathological changes can be contrasted. Spinocerebellar ataxias, for instance, represent a group of rare hereditary neurodegenerative disorders that go along with damages in the cerebellum and its pathways (Klockgether, 2011). Age-related

changes are of special interest in late-onset disease, such as, for example, spinocerebellar ataxia type 6 (SCA6). In contrast to many forms of hereditary ataxias, pathology in SCA6 is mostly confined to the cerebellum (Schöls et al., 2004). Clinically, SCA6 manifests commonly with a late onset around the sixth decade. Slowly progressing gait ataxia, oculomotor disorders and dysarthria are central symptoms (Schöls et al., 1998). Histological studies concerning structural changes in SCA6 are inconsistent. While some older studies found mainly a degeneration of the cortex with little or no changes in the DCNs (Koeppen, 2005; Sasaki et al., 1998), later observations suggested possible alterations in the DCN (Gierga et al., 2009; Wang et al., 2010).

Susceptibility weighted MR imaging (SWI) (Haacke et al., 2004; Reichenbach and Haacke, 2001) with high spatial-resolution at ultra-high magnetic fields ($B_0 \geq 7T$) offers a detailed non-invasive view of the DCN in healthy controls (Diedrichsen et al., 2011; Maderwald et al., 2012) and SCA6 patients (Stefanescu et al., 2015). Stefanescu et al. (2015) reported severe atrophy of the dentate nuclei in SCA6 patients that was even more striking than in SCA3 and Friedreich ataxia patients. With quantitative susceptibility mapping (QSM), the logical successor of SWI that directly maps the distribution of the magnetic susceptibility across the human brain, exquisite contrast and detail of the DCN has been demonstrated (Deistung et al., 2016; Li et al., 2015) at the clinically available MRI field strength of 3T. While accurate identification of iron containing structures may be impaired on SWI due to blooming and non-local phase contributions, QSM is expected to overcome those drawbacks, providing a local view of the anatomy (Deistung et al., 2013) and a more direct link to the underlying iron concentration (Hametner et al., 2018; Langkammer et al., 2012; Zheng et al., 2013).

In the present study, we investigated the influence of healthy aging on DCN and the cerebellar cortex in healthy controls based on MRI, and related the outcome to patients suffering from SCA6. A comparison of physiological changes during the normal aging process with changes under the influence of SCA6 as a neurodegenerative disease might help to better understand the pathophysiology of hereditary ataxias and to facilitate interpretation of MRI data in a clinical context. We assessed the need of ultra-high field (7T) MRI for accurate depiction of cerebellar nuclei compared to imaging at 3T and compared R2* and susceptibility mapping with respect to their potential to display iron induced changes. In addition, cross-sectional and longitudinal structural changes of the DCN and cerebellar cortex were assessed in both SCA6 and healthy subjects and related to ataxia scores in order to find MRI correlates with the participants' physiological condition. In this context, the smaller cerebellar nuclei (globose, emboliform and fastigial nuclei) were incorporated for the first time in such an MRI-based analysis.

METHODS

Subjects

Twenty-five SCA6 patients as well as 126 healthy controls underwent 3T-MRI and clinical assessments at least once. Fifteen healthy subjects were excluded due to incidental pathological findings, incomplete MRI data due to interruption of the measurement or unacceptable artifacts due to movement. Among the participants included, 16 SCA6 patients and 40 controls additionally received a 7T-MRI scan. Nineteen SCA6 patients (3T: 19, 3T and 7T: 13) and 33 controls (3T: 33, 3T and 7T: 22) received a one-year follow-up examination. The study was approved by the internal Ethics Committees of the Essen University Hospital and the Jena University Hospital. Written informed consent was obtained from all participating subjects.

The healthy controls served to study age-related changes of the cerebellum. In addition, a subset was selected that was age- and sex-matched to the SCA group. The demographic and clinical details are summarized in **Table 1**.

All patients had genetically proven disease. The CAG repeat length and disease duration were recorded. Clinical ataxia scores were assessed based on the Scale for the Assessment and Rating of Ataxia (SARA) (Schmitz-Hübsch et al., 2006), the International Cooperative Ataxia Rating Scale (ICARS) (Trouillas et al., 1997), and the SpinoCerebellar Ataxia Functional Index (SCAFI) (Schmitz-Hübsch et al., 2008b). Both SARA (range: 0 – 40) and ICARS (range: 0 – 100) are sum scores and increase the more severe the degree of ataxia. The SCAFI represents the sum of the z-scores of an 8 meter walk test, a 9-hole peg-test, and a speech test, whereas the individual z-scores were calculated with respect to the corresponding mean values of our healthy control group (n = 111). Consequently, the SCAFI deviates from zero the more the subject's values deviate from the average of the healthy control population. A negative SCAFI indicates a decreased performance of the tasks in relation to the healthy control group. The lower the SCAFI, the worse the performance.

MRI Data Acquisition

MRI data of all patients and the majority of controls (n=106) were collected with a human whole-body combined MRI-PET system (Siemens Healthineers, Erlangen, Germany), operating at a magnetic field strength of 3T, by using a 16-channel head array coil (Siemens Healthineers). Further, 20 controls underwent 3T-MRI on a PRISMA Fit (Siemens Healthineers) equipped with a 64-channel head array coil (Siemens Healthineers). The same acquisition protocols were used for the two 3T-MRI systems. Multi-echo, three-dimensional (3D) gradient-echo (GRE) imaging was carried out in transverse-to-coronal

Table 1. Overview of the study population. Statistics for disease duration and disease onset of the SCA6 group were only calculated for 23 and 14 patients at 3T and 7T, respectively, because one patient was not aware of the exact start of the disease and another patient did not show any symptoms at the time of data collection. For the 1 year follow-up, the latter exhibited first symptoms and was included in the statistics. One patient was excluded from the descriptive statistics of the clinical ataxia scores because of a confounding comorbidity. The cell entries with brackets are mean (minimum - maximum) across the cohort.

	age study		group study: SCA6 vs. controls			
	baseline		baseline		follow-up	
MRI field strength	3T	7T	3T	7T	3T	7T
Control subjects						
• N	111	40	25	16	19	13
• age (years)	45.3 (16 – 78)	50.2 (24 – 76)	60.1 (36-78)	57.2 (36-76)	57.8 (37-77)	55.5 (37-74)
• sex (m/f)	56/55	25/15	15/10	11/5	13/6	9/4
• visit interval (days)					353.9 (321-385)	359.8 (321-386)
SCA6 patients						
• n			25	16	19	13
• age (years)			61.6 (38-78)	59.4 (38-76)	59.7 (39-77)	57.3 (39-75)
• sex (m/f)			15/10	11/5	13/6	9/4
• visit interval (days)					374.2 (343-504)	369.4 (357-392)
• disease duration (years)			11.3 (1-25)	10.5 (1-24)	12.3 (0-25)	10.3 (0-24)
• SARA (0-40)			13.3 (0.5-26)	13.2 (0.5-26)	14.0 (0.5-28)	13.3 (0.5-26)
• ICARS (0-100)			37.0 (3-24)	35.4 (3-62.5)	38.9 (4-69)	36.6 (4-69)
• INAS (0-16)			1.8 (0-4)	1.8 (0-4)	1.9 (0-5)	2.1 (0-4)
• SCAFI (z-score)			-2.7 (-5.2 – -0.4)	-2.6 (-5.2- -0.4)	-2.7 (-5.2-0)	-2.5 (-4-0)
• CAG repeats (short)			12.4 (10-13)	12.3 (10-13)	12.3 (10-13)	12.2 (10-13)
• CAG repeats (long)			22.4 (21-27)	22.4 (21-27)	22.5 (21-27)	22.4 (21-27)

SARA – Scale for the Assessment and Rating of Ataxia (SARA) (Schmitz-Hübsch et al., 2006). ICARS – International Cooperative Ataxia Rating Scale (ICARS) (Trouillas et al., 1997). INAS – Inventory of non-ataxia symptoms (INAS) (Schmitz-Hübsch et al., 2008a). SCAFI – SpinoCerebellar Ataxia Functional Index (SCAFI) (Schmitz-Hübsch et al., 2008b).

orientation for subsequent quantitative susceptibility and R_2^* mapping. To this end, four echoes with monopolar read-out were recorded (TE_{1-4} = 6.47 ms/17.23 ms/27.99 ms/38.75 ms, TR=62 ms, flip angle (FA)=17°, BW_{1-4} = 120 Hz/px, phase encoding direction: right/left, acquisition matrix = 384 × 324 × 160) with an interpolated voxel size of 0.5 mm × 0.5 mm × 0.5 mm in an acquisition time (TA) of 13:09 min:sec. Data were collected with partial parallel undersampling (GRAPPA) with an undersampling factor (R) of 2 and 48 reference lines along the phase encoding direction and 75% partial Fourier along the slice encoding direction. Both phase resolution and slice resolution were adjusted to 74% to further reduce acquisition time, resulting in an acquired voxel size of 0.5 mm × 0.67 mm × 0.67 mm. Saturation pulses were positioned inferior and superior to the field-of-view (FoV) to avoid non-local artifacts due to pulsatile blood flow in vessels close to the cerebellum. In addition, whole-head T1-weighted (T1w) MRI data sets were collected with a magnetization prepared rapid gradient echo (MP-RAGE) sequence for determining the total intracranial volume (TIV) and automatically identifying the cerebellar lobules. The T1w data were acquired in sagittal orientation with an isotropic voxel size of 1 mm, TE=3.26 ms, TR=2530 ms, inversion time (TI)=1100 ms, FA=7°, acquisition matrix = 256 × 256 × 176, BW = 200 Hz/Px, GRAPPA with R = 2 and 48 reference lines, resulting in an acquisition time of 6:24 min:sec. Finally, fluid-attenuated inversion recovery (FLAIR) images covering the whole brain were acquired using a 2D sequence with TI = 2500 ms, TE = 94 ms, TR = 9000 ms, FA = 150°, acquisition matrix = 256 × 208, 55 contiguous slices and an acquired voxel size of 0.9 mm × 0.9 mm × 3 mm that was interpolated to 0.45 mm × 0.45 mm × 3 mm. MPRAGE and FLAIR images were inspected by a neuroradiologist. Controls were excluded from the study in case cerebral abnormalities were identified.

To validate the features and appearances detected on 3T-MR images, we carried out additional MRI exams of 19 patients and 40 controls on a 7T whole-body MRI system (Siemens Magnetom 7T, Siemens Healthineers) using a 32-channel head array coil (NOVA Medical Inc., Wilmington, MA, USA). The lower coil was covered with two dielectric pads (dimensions: 170 mm × 110 mm × 10 mm, provided by the Leiden Medical Center [Leiden, The Netherlands]) made of calcium titanate ($CaTiO_3$, permittivity: 110, loss tangent: 0.05) to increase both field strength and homogeneity of the transmit radiofrequency field, B_1^+, in the area of the cerebellum. Gradient-echo images for QSM and R2* mapping were acquired with 4 echoes (TE_{1-4} = 4.49 ms/11.23 ms/17.97 ms/24.71 ms, BW_{1-4} = 280Hz/px, monopolar echo readout, TR = 30 ms, FA = 10°) and an isotropic voxel size of 0.38 mm (matrix: 552 × 552 × 192, GRAPPA with R = 3 and 48 reference lines in phase encoding direction, 75% partial Fourier in slice encoding direction, phase-encoding direction = anterior/posterior) within an acquisition time of 16:32 min:sec. To enable retrospective correction of slight head movements, the sequence was equipped with 3D fat navigators (voxel size = 4 mm × 4 mm × 4 mmm, GRAPPA [R=4 × 4]) (Gallichan et al., 2016). The fat navigators (n = 215)

were measured after the 4th gradient-echo for each phase encoding step (phase encoding loop outside the slice encoding loop). The gradient-echo k-space data were reconstructed offline by adjusting the Matlab scripts of the retroMoCoBox (https://github.com/dgallichan/retroMoCoBox) to mitigate motion related artifacts.

QSM and R2*

Single-channel GRE magnitude and phase images were combined using the sum-of-squares method (Roemer et al., 1990) and the MCPC-3D-S approach (Eckstein et al., 2018), respectively. A spatially adaptive non-local means denoising algorithm (Manjón et al., 2010) was applied to the real and imaginary parts of the combined complex-valued images to mitigate noise. The denoising strength (υ) was constant across the echoes of the 3T data (u_{1-4} = 100%), but was increased with longer echo times at 7T (υ_{1-4} = 25%/50%/75%/85%). Quantitative susceptibility maps were computed based on these denoised phase images. To this end, the phase images for each echo were unwrapped using a 3D best-path algorithm (Abdul-Rahman et al., 2007), divided by $2\pi \cdot TE_i$ to obtain the Larmor frequency variation in Hz, and then combined across the different TEs in an optimized way that takes into account the local echo-time dependent contrast-to-noise ratio of the Larmor frequency images (Wu et al., 2012a). Background frequency contributions were eliminated using sophisticated harmonic artifact removal for phase data (SHARP) (Schweser et al., 2011) with 10 different spherical kernels (Wu et al., 2012b) with varying radii, ranging from 1 to 10 voxels and employing a high-pass filter (Özbay et al., 2017) of 0.01 for regularization. Susceptibility mapping was performed based on the SHARP-processed frequency images using homogeneity-enabled incremental dipole inversion (HEIDI) (Schweser et al., 2012). We referenced all susceptibility maps to the average susceptibility of the brain tissue within the field of view and stated susceptibility values in parts-per-billion (ppb).

Maps of the effective transverse relaxation rate constant, R_2^*, were calculated from the magnitude signal decay employing the power method utilizing a logarithmic calculus (McGibney and Smith, 1993; Miller and Joseph, 1993).

Segmentation and Volume Estimation

Susceptibility maps were used to demarcate the cerebellar nuclei. The cerebellar nuclei were manually traced by two independent raters, who were blinded to the diagnosis and age, following the same delineation strategy. Data obtained from the SCA6 patients and matched controls were demarcated two times by the raters. If clearly discernible, the DCN were manually traced in both hemispheres on the axial, sagittal and coronal susceptibility maps using MRICroN (http://people.cas.sc.edu/rorden/mricron/). Drawings were done directly on the susceptibility maps taking into account information of magnitude and SHARP-

processed frequency images as well. Two different volumes of interest (VOIs) were created for the dentate nucleus. The first VOI was manually traced and followed the corrugated wall of the dentate nucleus (DN_o) as well as possible. The second dentate VOI (DN_h) represents the convex hull obtained from the first manually traced VOI and, thus, also included the white matter surrounded by the dentate. The absolute volumes were determined for each cerebellar nucleus. To account for different head sizes, the DCN volumes were divided by the total intracranial volume (TIV). The TIV was estimated based on the T1w images acquired at 3T using the standard pre-processing pipeline of the Computational Anatomy Toolbox 12 (CAT12, http://www.neuro.uni-jena.de/cat/).

Subject-specific segmentations were generated by Freesurfer's (https://surfer.nmr.mgh.harvard.edu/) automatic processing pipeline for T1w data (Destrieux et al., 2010; Fischl et al., 2002). The resulting segmentation of the cerebellum was further refined using an automated cerebellar lobule segmentation method that relies on the incorporation of multi-atlas labeling and tissue classification outcomes in a graph cut framework (Yang et al., 2016). The absolute volumes of the individual cerebellar lobules and cerebellar white matter were calculated. The cerebellum volume was determined as the sum of all segmented cerebellar lobules, vermis, and the cerebellar white matter segment. We also computed volumes for the cerebellar GM and cerebellar cortical GM. The former was defined as the sum of the volumes of all lobules, vermis and cerebellar nuclei, whereas the latter represents only the sum of all lobules. In addition, the absolute volumes were normalized to the TIV.

Iron Mass

To enable a more detailed investigation on the variation of iron within the cerebellar nuclei, we determined their iron mass ($m_{Fe,c}$) according to

$$m_{Fe,c} = c_{Fe,c} \cdot V_c \cdot \rho, \tag{1}$$

where $m_{Fe,c}$ is the iron concentration and V_c is the volume of each cerebellar nucleus $c.p$ denotes the density of brain tissue assumed to be 1.058 kg/dm³ (Barber et al., 1970). With the linear relation between magnetic susceptibility and iron concentration, we estimated the iron mass by using the following formula (Schweser et al., 2018):

$$m_{Fe,c} = \left(\chi_c \cdot 1.47 \, \frac{\text{mg}}{\text{kg wet weight} \cdot \text{ppb}} + 48.85 \, \frac{\text{mg}}{\text{kg wet weight}} \right) \cdot V_c \cdot 1.058 e^{-6} \, \frac{\text{kg wet weight}}{\text{mm}^3}. \tag{2}$$

Statistical Analysis

To assess the reliability of the manually delineated cerebellar nuclei VOIs, their volumes and the average susceptibilities were investigated using Cronbach's alpha (Cronbach, 1951) between the two raters (inter-rater) and between repeated demarcation (intra-rater), respectively.

We investigated the presence of linear correlations of the relative volumes of the cerebellum, cerebellar lobules, white matter and nuclei, as well as magnetic susceptibility, R2*, and iron mass with respect to age using Pearson correlation. Correlations between MRI measures, ataxia scores (SCAFI, SARA, ICARS), disease onset and genetics (repeat length) were calculated using Spearman correlation. If the correlation yielded statistical significance, linear least-squares regression was performed.

Group comparisons between SCA6 patients and controls were carried out using Mann-Whitney U test. Repeated measures analysis of variance (rmANOVA) was performed to compare findings at 3T and 7T, and to compare findings at baseline and one-year follow-up.

All statistical analyses were performed with SPSS (version 25; IBM, Armonk, NY, United States) and Matlab (Mathworks Inc., Natick, MA, United States). Type 1 error correction for multiple comparisons was conducted using the Bonferroni-Holm approach (Holm, 1979), where appropriate. Corrected p-values smaller than 0.05 were considered statistically significant, while uncorrected p-values of less than 0.05 were considered a trend.

RESULTS

Identification of Cerebellar Nuclei

We were able to identify the dentate nuclei in all healthy controls and nearly all SCA6 patients on 3T and 7T images. Only one MRI exam in an SCA6 patient carried out at 7T did not provide a clear demarcation of the dentate nuclei. The other three cerebellar nuclei (globose, emboliform, fastigial nuclei) exhibited a lower contrast with respect to surrounding white matter in comparison to the dentate nuclei (**Figure 1**).

Consequently, we were not able to demarcate these small nuclei in all healthy controls and even less frequently in the SCA6 patients (see summary in **Table 2**). The emboliform nuclei were the most difficult to demarcate. Interestingly, the globose and emboliform nuclei were less visible on 7T than on 3T images. Only the fastigial nuclei were more often depicted at 7T (except: rater 2.1 in the MC-7T cohort).
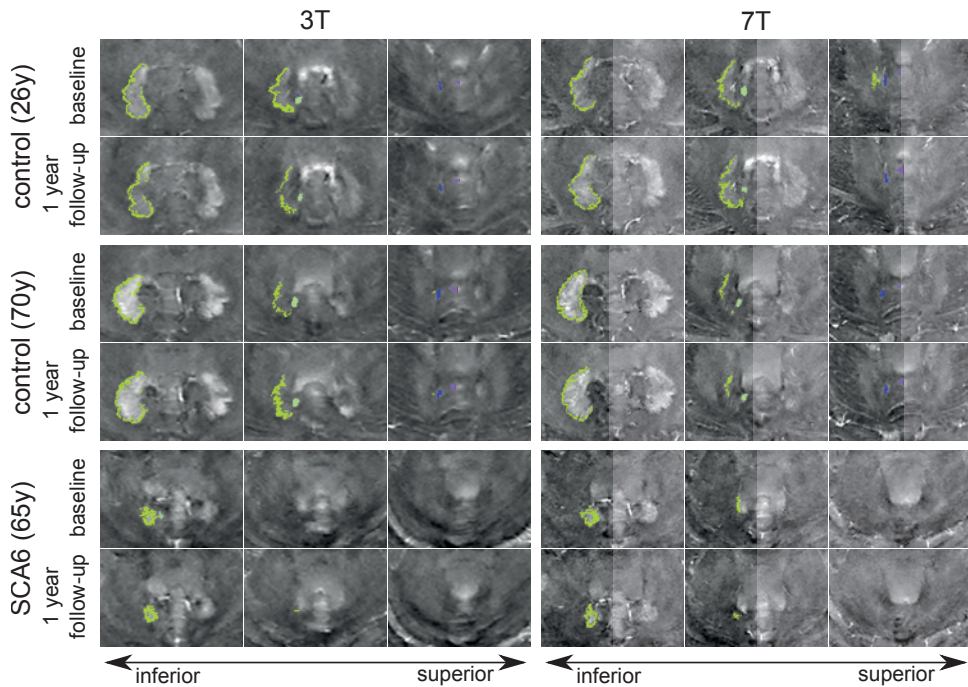
Figure 1. Quantitative susceptibility maps of the cerebellum of a young healthy control (male, 26y, TIV = 1766 cm³), an elderly control (male, 70y, TIV = 1814 cm³), and an SCA6 patient (male, 65y, TIV = 1724 cm³) are presented from the top to the bottom row, respectively. The cerebellar nuclei of the left hemisphere are clearly seen on the maps. The manual delineations of the cerebellar nuclei are depicted for the right hemisphere (green [large area]: dentate nucleus, light green [small area]: globose nucleus, blue: emboliform nucleus, purple: fastigial nucleus). The dentate nucleus of the SCA6 patient is substantially smaller compared to the age matched controls. The emboliform, globose, and fastigial nuclei were not discernible on the maps of the SCA6 patient.

Cronbach´s alpha values ($α_c$) for the volume and magnetic susceptibility of the individual DCN are presented in **Table 3**. Independent of field strength, values for Cronbach´s alpha exceeding 0.84 for the volume measurements suggest very high consistency for the demarcation of the dentate both within the delineations of the raters (intra-rater consistency) and between the raters (inter-rater consistency). Lower values for Cronbach's alpha were found for the volumes of the smaller cerebellar nuclei with highest values for the globose nuclei ($α_c > 0.68$). Cronbach's alpha values were higher for the intra-rater comparison of rater 1 and overall higher than the inter-rater comparison. Higher $α_c$, in particular in the patient cohort, were observed for the volumes extracted from the demarcations at 7T compared to 3T. Cronbach's alpha values were higher for the susceptibility measures compared to the volumes and exceeded 0.745 for all cerebellar nuclei demarcations.

Table 2. Cerebellar nuclei identified on quantitative susceptibility maps. The absolute number (and percentage) of identified cerebellar nuclei by the two raters are presented for different cohorts and different field strengths (B_0). Direct comparison of the identified nuclei on susceptibility maps between 3T and 7T acquisitions is warranted by considering the SCA-7T and MC-7T cohort at 3T. The number in brackets denotes the percentage amount of detected nuclei.

B0	rater	cohort	nc	dentate	globose	emboliform	fastigial
3T	R1.1	HC	111	111 (100)	106 (95)	104 (94)	100 (90)
		SCA6	25	25 (100)	10 (40)	3 (12)	9 (36)
		MC	25	25 (100)	25(100)	25 (100)	21 (84)
		SCA6-7T	16	16 (100)	8 (50)	2 (12.5)	6 (37.5)
		MC-7T	16	16 (100)	16 (100)	16 (100)	14 (87.5)
	R2.1	HC	111	106 (94)	97 (87)	89 (80)	103 (93)
		SCA6	25	25 (100)	8 (32)	6 (24)	12 (48)
		MC	25	25 (100)	24 (96)	24 (96)	23 (92)
		SCA6-7T	16	16 (100)	7 (43.75)	7 (43.75)	10 (62.5)
		MC-7T	16	16 (100)	16 (100)	16 (100)	15 (93.75)
7T	R1.1	HC	40	40 (100)	38 (95)	37 (93)	37 (93)
		SCA6	16	16 (100)	2 (12.5)	1 (6.25)	12 (75)
		MC	16	16 (100)	14 (87.5)	13 (81.25)	14 (87.5)
	R2.1	HC	40	40 (100)	26 (65)	25 (63)	26 (65)
		SCA6	16	15 (93.75)	5 (31.25)	3 (18.75)	12 (75)
		MC	16	16 (100)	14 (87.5)	12 (75)	14 (87.5)

B_0 – field strength. R1.1 – rater 1, delineation 1. R2.1 – rater 2, delineation 1. HC – healthy controls. SCA6 – SCA6 patients, MC – age- and sex-matched controls to the SCA6 patients. SCA6-7T – SCA6 patients who also underwent 7T-MRI. MC-7T – age- and sex-matched controls to the SCA6 patients who also underwent 7T-MRI.

Table 3. Cronbach's alpha values (α_c) of the volumes and the average magnetic susceptibilities determined for VOIs identified on 3T and 7T data sets by two independent raters. The numbers in brackets denote the number of values incorporated into the analysis. Hemisphere denotes the localization of specific nuclei (that is within the right or left cerebellar hemisphere). Hemisphere "both" indicates that the sum of the left and right VOIs was considered in the analysis.

	hemisphere	3T intra-rater R1.1/R1.2	R2.1/R2.2	7T inter-rater R1.1/R2.1	R1.1/R2.1
volume					
healthy controls					
DN$_o$	left	0.908 (27)	0.896 (27)	0.878 (106)	0.842 (40)
	right	0.902 (27)	0.857 (27)	0.879 (106)	0.845 (40)
emboliform	left	0.657 (26)	0.694 (26)	0.416 (86)	0.681 (33)
	right	0.603 (26)	0.566 (26)	0.552 (86)	0.774 (33)
globose	left	0.806 (26)	0.591 (26)	0.727 (95)	0.755 (34)
	right	0.684 (26)	0.696 (26)	0.698 (95)	0.681 (34)
fastigii	both	0.960 (22)	0.597 (25)	0.552 (93)	0.811 (33)
SCA6+MC					
DN$_o$	left	0.988 (48)	0.978 (50)	0.979 (50)	0.986 (31)
	right	0.989 (48)	0.977 (50)	0.981 (50)	0.987 (31)
emboliform	left	0.756 (27)	0.675 (29)	0.387 (27)	0.862 (13)
	right	0.640 (27)	0.574 (29)	0.409 (27)	0.915 (13)
globose	left	0.857 (34)	0.740 (30)	0.698 (31)	0.814 (15)
	right	0.824 (34)	0.811 (30)	0.396 (31)	0.756 (15)
fastigii	both	0.963 (28)	0.531 (33)	0.533 (26)	0.882 (17)

Table 3. Continued.

hemisphere	3T intra-rater		7T inter-rater	
	R1.1/R1.2	R2.1/R2.2	R1.1/R2.1	R1.1/R2.1
susceptibility				
healthy controls				
DN_o left	0.915 (27)	0.929 (27)	0.804 (106)	0.870 (40)
right	0.848 (27)	0.855 (27)	0.783 (106)	0.796 (40)
DN_h left	0.945 (27)	0.978 (27)	0.988 (106)	0.957 (40)
right	0.990 (27)	0.985 (27)	0.985 (106)	0.925 (40)
emboliform left	0.960 (26)	0.846 (26)	0.900 (86)	0.945 (33)
right	0.961 (26)	0.896 (26)	0.881 (86)	0.933 (33)
globose left	0.963 (26)	0.896 (26)	0.940 (95)	0.958 (34)
right	0.981 (26)	0.971 (26)	0.965 (94)	0.956 (34)
fastigii both	0.830 (22)	0.824 (25)	0.928 (93)	0.747 (33)
SCA6+MC				
DN_o left	0.935 (48)	0.901 (50)	0.911 (50)	0.874 (31)
right	0.917 (48)	0.816 (50)	0.878 (50)	0.825 (31)
DN_h left	0.972 (48)	0.948 (50)	0.985 (50)	0.845 (31)
right	0.978 (48)	0.969 (50)	0.976 (50)	0.841 (31)
emboliform left	0.948 (27)	0.881 (29)	0.848 (27)	0.978 (13)
right	0.963 (27)	0.878 (29)	0.886 (27)	0.905 (13)
globose left	0.936 (34)	0.906 (30)	0.799 (31)	0.895 (15)
right	0.977 (34)	0.923 (30)	0.918 (31)	0.907 (15)
fastigii both	0.935 (28)	0.860 (33)	0.801 (26)	0.926 (17)

R1.1 – rater 1, delineation 1. R1.2 – rater 1, delineation 2. R2.1 – rater 1, delineation 2. R2.2 – rater 1, delineation 2. Healthy controls – Cronbach's alpha values computed across all healthy controls. SCA6 + MC – Cronbach's alpha values computed for the group comprising SCA6 patients and the correspondingly matched controls. DN_o – outlined dentate nucleus. DN_h – hull of the dentate nucleus.

Age Dependency

Results of univariate linear correlation analysis of cerebellar tissues, individual cerebellar nuclei and lobule volumes with respect to age are summarized in **Table 4** for healthy controls and SCA6 patients.

Linear correlations show a significant decline of the cerebellum due to significant tissue loss of the cerebellar GM in healthy controls with increasing age (see also **Figure 2**). The volume loss of the cerebellar GM in healthy controls is mainly driven by significant tissue declines in Crus I and lobule VIIb and to a lesser extent by tissue decline in lobules I-V, VI, VIII and vermal lobule VII (**Table 4**).

Figure 2. Linear correlations of volume, susceptibility, R_2^* and iron mass with respect to age in healthy controls and the SCA6 patients. The volumes normalized to the TIV of the whole cerebellum, the cerebellar cortical gray matter, as well as the outlined dentate nuclei (DN_o) are presented as functions of age in A, B, and C, respectively. The lower row illustrates the relationship between (D) magnetic susceptibility, (E) R2* and (E) the iron mass of the dentate hull (DN_h). The dots and crosses indicate the parameters measured in healthy controls and SCA6 patients, respectively. The solid line indicates the regression line. The 95% confidence interval and the 95% percent prediction interval are illustrated as shaded area and dashed line, respectively. The black color indicates elements related to the healthy controls, whereas the red elements are associated with the SCA6 patients. Pearson's correlation coefficient, r, is provided if the uncorrected p-value indicates statistical significance. [#] – uncorrected p-value < 0.05. [*] – corrected p-value < 0.05 (details on Bonferroni-Holm correction are provided in the additional information of *Table 4*). While not statistically significant, the regression line, confidence interval and prediction interval are also plotted for the normalized volume of the dentate in healthy controls to visually highlight the absence of correlation and to show the differences between the controls and patients.

In SCA6 patients, we observed a trend (uncorrected p-value < 0.05) of cerebellar GM decline with increasing age, which appeared to be more pronounced than for controls. In patients, GM decline is mostly driven by tissue breakdown in Crus I but also, though only statistically significant for uncorrected p-values while exhibiting a distinct correlation, in lobules I-V, lobule VIIb, and lobule VIII. The results of the automatic segmentation for the cerebellar lobules of a young and an elderly control are shown in **Figure 3,** indicating accurate segmentation across age.

Table 4. Results of univariate linear correlations between selected parameters (volume, susceptibility, iron mass, R2*) and age separated for the healthy controls and the SCA6 patients. Statistically significant correlation coefficients and the corresponding slopes and offsets are printed bold. * – corrected p-value < 0.05 (Bonferroni-Holm correction; for correction of p-values obtained from different tests of volumes vs. age, the 22 different cerebellar regional volumes [DCN, whole cerebellum, cerebellar GM and WM, lobules, vermis] as well as the dentate surface were considered; for correcting p-values observed from multiple tests of iron estimates vs. age, the 5 different DCN regions with 3 different metrics [QSM, R_2^*, iron mass] were considered).

	healthy controls			SCA6 patients		
	r	slope	offset	r	slope	offset
volume normalized to TIV						
cerebellum	-0.29*	**-1.18e-4**	**8.88e-2**	-0.40#	-4.25e-4	8.87e-2
cerebellar WM	0.08			-0.41#	-3.33e-5	8.42e-3
cerebellar GM[1]	-0.31*	**-1.20e-4**	**8.18e-2**	-0.40#	-4.00e-4	8.11e-2
cerebellar cortical GM[2]	-0.32*	**-1.18e-4**	**7.71e-2**	-0.40#	-3.86e-4	7.72e-2
DN_o	0.05			-0.31#	-1.45e-06	1.71e-4
DN_h	0.09			-0.33#	-4.35e-6	3.99e-4
globose	-0.17#	-3.49e-8	9.53e-6	-0.74*	**-2.02e-7**	**1.56e-5**
emboliform	-0.07					
fastigial	-0.1			-0.15		
lobule I-V	-0.15#	-4.79e-6	5.29e-3	-0.34#	-2.57e-5	5.09e-3
lobule VI vermis	-0.05			-0.12		
lobule VI	-0.16#	-8.05e-6	6.31e-3	-0.27		
lobule VII vermis	-0.20#	-1.89e-6	7.88e-4	-0.25		
Crus I	-0.32*	**-2.19e-5**	**0.10e-2**	-0.44*	**-6.06e-5**	**1.03e-2**
Crus II	-0.09			-0.21		
lobule VIIb	-0.24*	**-7.96e-6**	**3.92e-3**	-0.29#	-1.70e-5	3.73e-3
lobule VIII vermis	-0.14			0.04		
lobule VIII	-0.17#	-1.01e-5	6.23e-3	-0.38#	-3.73e-5	6.23e-3
lobule IX vermis	0.03			-0.161		

Table 4. Continued.

	healthy controls			SCA6 patients		
	r	slope	offset	r	slope	offset
lobule IX	-0.11			-0.22		
lobule X vermis	0.22			0.10		
lobule X	0.08			0.01		
susceptibility						
DN_o	0.25[#]	0.23	45.33	-0.21		
DN_h	**0.47***	0.73	51.86	-0.21		
globose	**0.32***	0.34	40.2	-0.03		
emboliform	0.21[#]	0.22	48.7			
fastigial	**-0.3***	0.32	43.85	-0.21		
iron mass						
DN_o	0.13			-0.32		
DN_h	**0.32***	**1.82**	**193.63**	-0.33		
globose	-0.09			-0.79[#]	-0.10	7.83
emboliform	-0.03					
fastigial	-0.06			-0.18		
R2*						
DN_o	**0.43***	**0.072**	**21.70**	-0.18		
DN_h	**0.52***	**0.126**	**21.93**	-0.10		
globose	**0.41***	**0.11**	**18.87**	-0.42		
emboliform	**0.3***	**0.076**	**21.74**			
fastigial	0.19			0.12		

 # – uncorrected p-value < 0.05. Since the emboliform nuclei were only seen in three SCA6 patients, results of univariate regression are not provided, [1] – volume of the whole GM including vermis and cerebellar nuclei. [2] – volume of the cerebellar cortical GM excluding the vermis. DN_o – outlined dentate nuclei. DN_h – hull of the dentate nuclei.
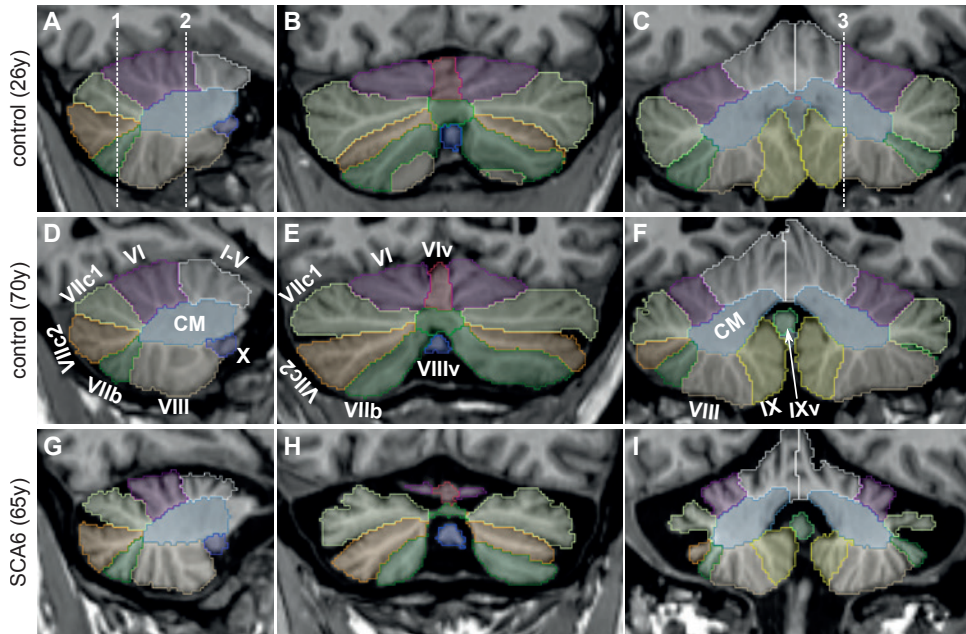
Figure 3. T1-weighted images of the cerebellum with superimpositions of the cerebellar lobules in a young healthy control (male, 26y, TIV = 1766 cm³), an elderly control (male, 70y, TIV = 1814 cm³) and an SCA6 patient (male, 65y, TIV = 1724 cm³) are presented from top to bottom row, respectively. The left column shows the sagittal view of the cutting plane indicated by dashed line 3 in (C). The middle and right columns display coronal slices at the locations indicated by dashed line 1 and 2 in (A), respectively. The cerebellum of the SCA6 patient (G-I) exhibits considerable atrophy compared to the elderly control (D-F). The color scheme of the cerebellar segmentation is indicated in the middle row: I-V – lobules I to V, VI – lobule VI, VIv – vermis lobule VI, VIIc1 – Crus I, VIIc2 – Crus II, VIIb – lobule VIIb, VIII – lobule VIII, VIIIv – vermis lobule VIII, IX – lobule IX, IXv – vermis lobule IX, X – lobule X and CM – corpus medullare.

The volumes of the outlined and filled dentate did not exhibit a significant relationship with age in healthy controls. The same held true for the volumes of the globose, emboliform and fastigial nuclei. In patients, a relationship between the globose nuclei volume and age was observed and a trend to smaller dentate nuclei volumes with increasing age.

Magnetic susceptibility, $R2^\star$ and iron mass of the dentate hull (DN_h) are presented as functions of age in **Figure 2D-F**. In healthy controls, both mean susceptibilities and $R2^\star$ of the dentate and globose significantly increased with age with correlation coefficients being slightly higher for $R2^\star$ (**Table 4**). While the susceptibility of the fastigial nuclei correlated significantly with age, their $R2^\star$ values were not linked to age. In contrast to magnetic susceptibility and $R2^\star$, only the iron mass of the dentate hull was correlated with age in the healthy controls. The iron mass of the globose nuclei exhibited a trend to decrease in SCA6 patients with increasing age (**Table 4**).

Table 5. Volumes and surfaces of the cerebellar nuclei determined based on susceptibility maps recorded at 3T and 7T are presented for all healthy controls, healthy controls age- and sex-matched to the SCA6 patients and SCA6 patients. Values are presented as mean ± standard deviation. HC (all) – all control subjects, HC (SCA6) – control subjects matched to SCA6 patients, SCA6 – SCA6 patients. * indicates statistical significance between SCA6 patients and matched healthy controls (Bonferroni-Holm correction accounting for the statistical tests of 22 different cerebellar regional volumes [DCN, whole cerebellum, cerebellar GM and WM, lobules, vermis], and the dentate surface).

cohort		3T			7T			histology1
		HC (all)	HC (SCA6)	SCA6	HC	HC (SCA6)	SCA6	HC
n		111	25	25	40	16	16	10
volume [cm³]								
cerebellum		133.4±14.70	133.0 ±15.7*	98.9 ± 22.0*				
cerebellar GM[1]		122.0±13.6	121.2 ± 14.5*	89.3 ± 20.8*				
cerebellar cortex[2]		114.7±13.0	113.7 ± 13.9*	84.5 ± 19.8*				
volume [mm³]								
outlined dentate	left	319.0±49	332.6±52	135.5±90	267.4±48	256.0±41	120.0±64	394.5±95
	right	312.2±47	322.9±49	130.2±89	272.8±48	257.1±46	115.1±61	390.2±99
	sum	631.2±94	655.5±98*	265.7±178*	540.2±91	513.1±84*	235.1±124*	784.7±193
globose	left	12.8±6	11.5±6	6.4±4	13.3±5	14.2±7	8.2±3†	9.5±4
	right	12.7±6	11.9±4	5.8±4	13.4±5	13.5±6	9.6±3†	9.5±5
	sum	25.5±11	23.4±9*	12.2±7*	26.7±10	27.7±12	17.8±0.3†	19.0±9
emboli-form	left	13.3±7	11.0±5	4.8±4†	9.9±5	9.7±4	3.5†	50.2±12
	right	14.4±7	12.0±4	7.3±4†	10.6±6	9.8±5	3.8†	49.5±12
	sum	27.7±12	23.0±9	12.0±8†	20.5±9.4	19.5±8	7.3†	99.7±24
fastigial	sum	23.6±15	26.7±22	13.9±21	21.7±11	21.6±13	10.8±4	91.4±20

Table 5. Continued.

volume / TIV		3T	7T	histology[1]	3T	7T	histology[1]
volume / TIV [$\ast 10^{-4}$]							
cerebellum		836.9±70.5	813.7±68.2*	625.2±115.0*			
cerebellar GM[1]		764.1±67.1	741.3±63.3*	564.2±109.2*			
cerebellar cortex[2]		717.8±63.7	695.6±61.0*	533.6±104.0*			
volume / TIV [$\ast 10^{-6}$]							
outlined dentate	left	200.4±32.4	204.3±32.7	83.4±51.1	167.0±34.2	154.8±27.5	72.2±34.6
	right	196.1±30.6	198.2±29.5	80.0±50.6	170.5±34.9	155.6±31.3	69.5±33.0
	sum	396.5±61.7	402.5±60.5*	163.4±101.1*	337.4±67.0	310.4±57.1*	141.7±67.1*
globose	left	8.0±3.5	7.1±3.6	3.7±1.9	8.3±3.3	8.6±3.9	4.5±1.5†
	right	8.0±3.6	7.3±2.5	3.4±2.4	8.3±3.0	8.1±3.2	5.2±1.3†
	sum	16.0±6.4	14.4±5.3*	7.1±4.1*	16.5±6.7	16.7±6.7	9.7±0.3†
emboli-form	left	8.3±4.4	6.8±2.8	2.8±2.2†	6.2±3.3	5.9±2.6	2†
	right	9.0±4.3	7.4±3.4	4.3±2.2†	6.6±3.5	6.0±3.0	2.1†
	sum	17.3±7.9	14.2±5.8	7.1±3.9†	12.9±6.1	11.9±5.0	4.1†
fastigial	sum	14.8±9.3	16.6±13.8*	8.4±11.5*	13.7±7.4	13.2±7.7	6.3±2.7
surface [mm^2]							
outlined dentate	left	1000.6±139	1035.4±143	430.4±285	1064.4±183	1041.9±151	493.0±261
	right	976.4±134	1000.7±133	413.8±283	1074.0±177	1030.1±162	474.0±250
	mean	988.5±134	1018.0±135*	422.1±283*	1069.2±173	1036.0±152*	483.5±255*

† indicates that only three or less nuclei could be demarcated across the whole group and, thus, no statistical comparison between patients and matched controls was performed.
[1] – volume of the whole GM including vermis and cerebellar nuclei. [2] – volume of the cerebellar GM excluding the vermis.

3T Baseline Measurements

Volumes of the cerebellar nuclei are summarized for both controls and SCA6 patients in **Table 5** and **Figure 4**. The whole cerebellum, the cerebellar GM, the cerebellar cortex and the cerebellar WM exhibited significantly reduced volumes in SCA6 patients compared to age- and sex-matched healthy controls. A closer look into the substructure of the cerebellar cortex revealed a significant volume loss of all individual cerebellar and vermal lobules in SCA6 patients, with the exception of lobules IX and X as well as vermal lobule X (**Figure 4E** and **F**). Volumes of the outlined and hull dentate nuclei as well as the outlined dentate surface were significantly smaller in SCA6 patients with effect sizes (Hedges's g) above 2.8. The globose and fastigial nuclei but not the emboliform nuclei exhibited significantly smaller volumes in patients than in controls.

Magnetic susceptibilities, R2* and iron masses of the cerebellar nuclei are presented for controls and SCA6 patients in **Figure 5**. The outlined dentate exhibited significantly lower values of the magnetic susceptibility (Hedges' g=0.92), R2* (g=0.88) and iron mass (g=2.2) in SCA6 patients. For the dentate hull, we observed a trend to lower R2* values in the patients (g=0.65), whereas the numerically lower susceptibilities measured in patients did not reach statistical significance even without alpha error correction (g=0.47). Magnetic susceptibilities and R2* values in the smaller cerebellar nuclei (globose, emboliform, fastigial nuclei) did not significantly differ between patients and controls, whereas iron masses of the globose and fastigial nuclei were substantially decreased in the patient cohort driven by the lower volume of the nuclei.
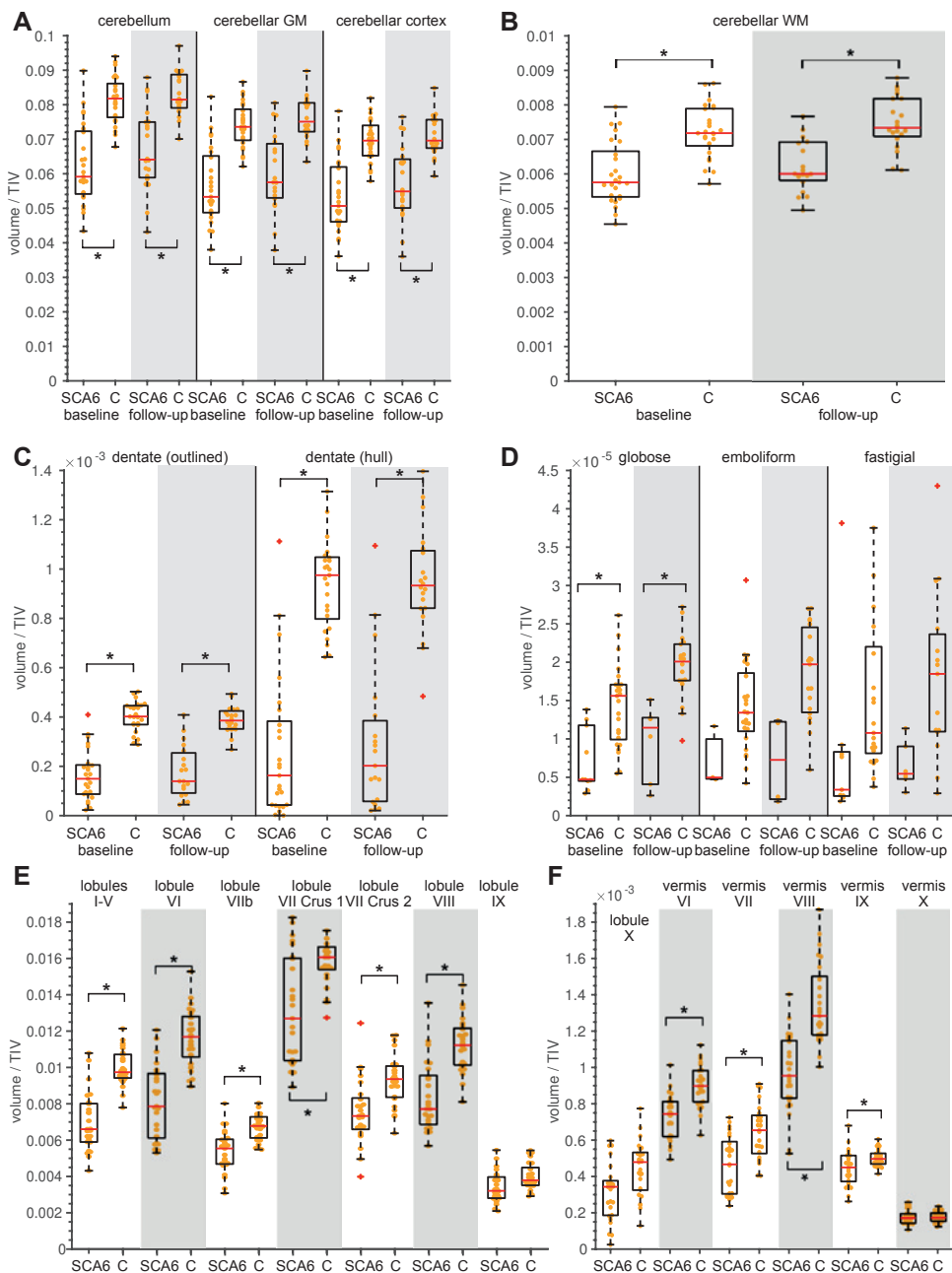
Figure 4. Boxplots of relative volumes (with respect to the total intracranial volume (TIV)) for the baseline and 1 year follow-up examinations at 3T of SCA6 patients and their age- and sex-matched healthy controls. The relative volumes of the cerebellum, cerebellar cortex (without vermis) and cerebellar GM (including vermis and cerebellar nuclei) are plotted in A. Relative volumes of cerebellar white matter are displayed in B. The middle row shows the relative volumes measured for (C) the dentate as well as the (D) smaller cerebellar nuclei. The plots in E and F show the relative volumes of the individual cerebellar lobules measured at baseline. In each box, the solid red line indicates the median, and the bottom and top edges of the box indicate the 25th and 75th percentiles, respectively. The solid orange dots indicate individual measurements. In in A to D, the findings for the 1 year follow-up are highlighted in light gray. Statistical significant differences between SCA6 patients and controls are indicated by the asterisk (Mann-Whitney U test, p < 0.05; Bonferroni-Holm correction accounting for the statistical tests of 22 different cerebellar regional volumes [DCN, whole cerebellum, cerebellar GM and WM, lobules, vermis], and the dentate surface). SCA6 – SCA6 patients. C – healthy control matched to SCA6 patients.
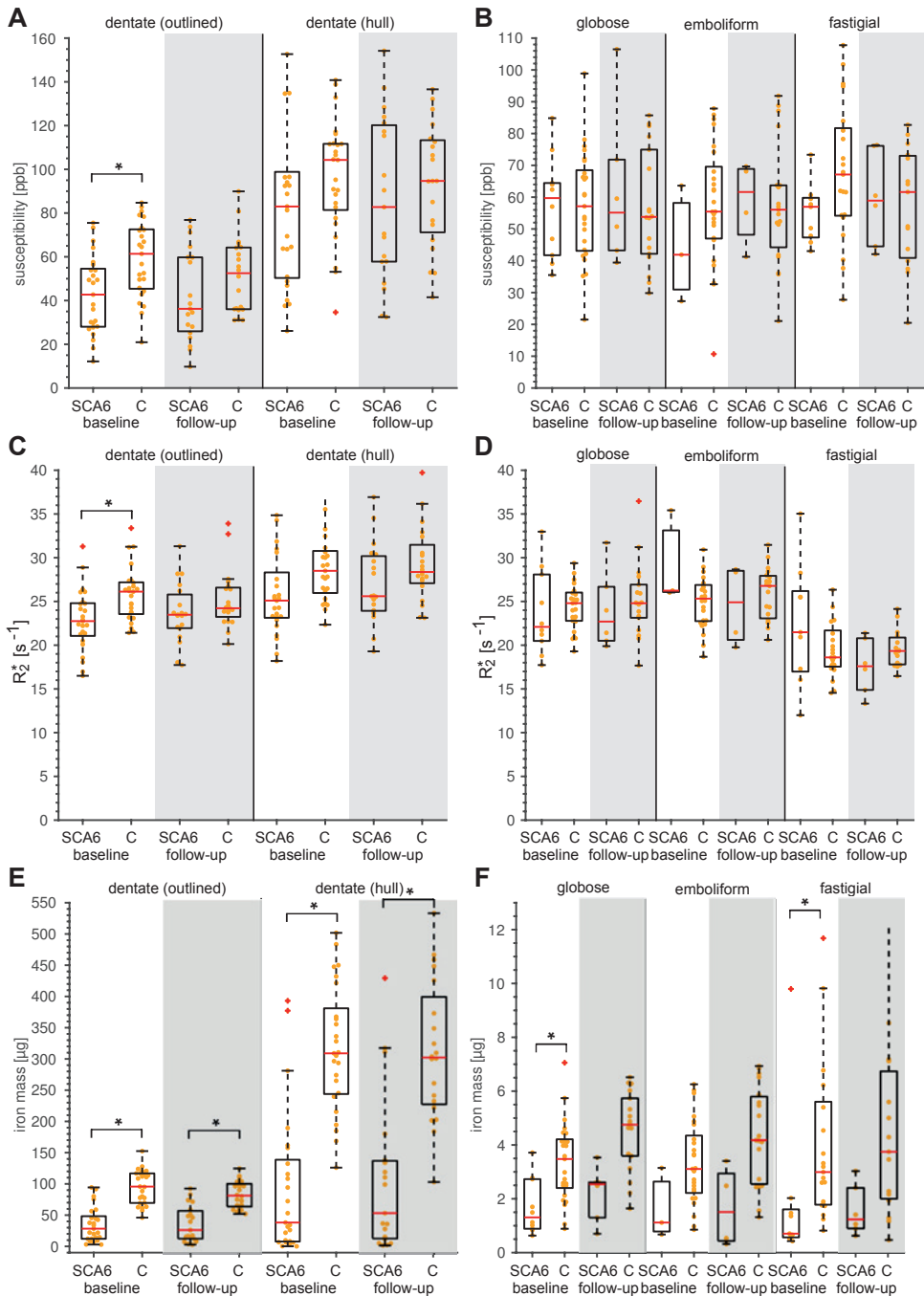
Figure 5. Boxplots of mean magnetic susceptibility (A, B), R2* (C, D), and iron mass (E, F) of the individual cerebellar nuclei for the baseline and 1 year follow-up examinations at 3T of SCA6 patients and their age- and sex-matched healthy controls. The plots in the left column (A, C, E) display the measures for the outlined dentate and the hull of the dentate, whereas the right column summarizes the measures for the globose, emboliform and fastigial nuclei. In each box, the solid red line indicates the median, and the bottom and top edges of the box indicate the 25th and 75th percentiles, respectively. The solid orange dots indicate individual measurements. The findings for 1 year follow-up are highlighted light gray. Statistical significant differences between SCA6 patients and controls are indicated by the asterisk (Mann-Whitney U test, p < 0.05; Bonferroni-Holm correction accounting for the statistical tests of 5 different DCN regions with 3 different metrics [QSM, R_2^*, iron mass]). SCA6 – SCA6 patients. C – healthy control matched to SCA6 patients.

3T Measurements vs. 7T Measurements

We found smaller volumes for the outlined dentate nuclei on 7T susceptibility maps compared to the ones traced on 3T maps (**Table 5**). rmANOVA revealed a significant main effect of field strength (F $(1,30)$ = 102.4, p <0.001, η_p^2 = 0.77). As the accuracy of the DCN volumes strongly depend on voxel size (see Discussion: Volumes of Cerebellar Nuclei and Lobules), we also investigated the dentate surface as potential marker. In contrast to the volume, the surface of the dentate nuclei did not show a statistically significant main effect with changing field strength (F $(1,30)$ = 1.0, p = 0.32), indicating higher robustness against variations in voxel size.

While it is expected that magnetic susceptibility is independent of the main magnetic field strength ($B_0 \leq 7T$) (Yao et al., 2009), we observed slightly smaller susceptibilities for the dentate hull at 7T compared to 3T (rmANOVA, DN_h: F$(1,30)$ = 42.2, p <0.001, η_p^2 = 0.59). With mean susceptibilities of the dentate across both controls (n=16) and patients (n=16) of (91.5 ± 32.2) ppb at 3T and (77.0 ± 25.0) ppb at 7T, most of the 7T values are still in the uncertainty range of the 3T measures. One reason for the small variations might be a slightly different delineation of the dentate between the two different field strengths. In line with the previous evaluations (volume and susceptibility of the dentate), iron mass was also affected by magnetic field strength (rmANOVA, DN_h: F$(1,30)$ = 28.6, p <0.001, η_p^2 = 0.49). Since it is known that R2* increases linearly with magnetic field strengths (Peters et al., 2007; Yao et al., 2009), we did not investigate field strength effects for R2*.

The rmANOVAs revealed significant main effects of the group (i.e. SCA6 vs. controls) for the volume (DN_o, η_p^2 = 0.68), surface (η_p^2 = 0.65), susceptibility (η_p^2 = 0.9) and iron mass (η_p^2 = 0.8) of the dentate, supporting the statistical significances reported previously.

Longitudinal Changes

To assess longitudinal changes for both the SCA6 patients and the age- and sex-matched controls we set up rmANOVAs for each field-strength separately, with the group identifier as between-subject factor and the measurement time point as inner-subject factor. While both the volume and the surface of the outlined dentate showed statistical significance between the two groups (volume 3T: F$(1,36)$ = 56.1, p < 0.001, η_p^2 =0.61; volume 7T: F$(1,24)$ = 40.9, p < 0.001, η_p^2 = 0.63; surface 3T: F$(1,36)$ = 55.4; p < 0,001; η_p^2 = 0.61; surface 7T: F$(1,24)$ =37.0; p < 0.001, η_p^2 = 0.62), no significant changes were found between the baseline and the 1-year follow-up measurement for both groups. Among magnetic susceptibility, R2*, and iron mass, only the iron mass showed a statistically significant group difference (iron mass 3T: F$(1,36)$=27.8, p<0.001, η_p^2 =0.44; iron mass 7T: F$(1,24)$=22.5, p<0.001, η_p^2

=0.48). None of these tests showed a significant effect along the 1-year period between the baseline and follow-up scan. Interactions between year effect and group also did not reach statistical significance (all p values > 0.05).

Correlation with Clinical Scores

In SCA6, volumes of the whole cerebellum, cerebellar cortical GM, cerebellar WM as well as the dentate and globose nuclei showed a significant negative correlation with SARA and ICARS (**Table 6**), indicating that a more pronounced atrophy goes along with a more severe degree of ataxia. This finding is further supported by the fact that these structures also correlate positively with the SCAFI (**Table 6**). Susceptibility, R2* and iron mass of the dentate tend to correlate positively with SARA and ICARS as well as negatively with SCAFI (**Table 6**). In addition, the iron mass of the globose nuclei revealed trends to correlate with these clinical scores, however, the correlations are mainly driven by the volume change.

No significant linear relationships between the volumes of the whole cerebellum and selected cerebellar structures (lobules, nuclei, GM, WM) as well as susceptibility, R2* and iron mass of the cerebellar nuclei were observed with respect to the CAG repeat length or the disease duration. The lack of correlation with CAG repeat length is not surprising due to its small variation in SCA6 patients. The CAG repeat length in the pathological allele correlated significantly with the age of the initial clinical disease manifestation (Spearman $r = 0.546$, $p = 0.006$), while no correlation was found for the number of repeats in the non-affected allele.

Combining all study participants (controls and SCA6 patients: $n = 111 + 25$), significant linear relationships with correlation coefficients of about -0.58 were observed when correlating the normalized volume of the cerebellum, the cerebellar cortical GM and the outlined dentate nuclei with SARA (**Figure 6D-F**). The absolute values of the correlation coefficients increased substantially to about 0.73, when correlating these volumes with SCAFI (**Figure 6A-C**).

Table 6. Spearman's correlation coefficients between selected structural parameters (volume, surface, susceptibility, R_2^*, iron mass) and clinical disease scores calculated across the SCA6 cohort. Statistically significant correlation coefficients are printed bold.

	SARA	ICARS	SCAFI
volume / TIV			
cerebellum	**-0.70***	-0.61[#]	**0.71***
cerebellar GM[1]	**-0.70***	-0.63*	**0.73***
cerebellar cortex[2]	**-0.68***	-0.61[#]	**0.71***
cerebellar WM	**-0.63***	-0.54[#]	0.57[#]
DN$_o$	**-0.54***	**-0.55***	**0.64***
DN$_h$	**-0.51***	**-0.56***	**0.60***
globose	**-0.7***	**0.72***	**0.72***
surface area			
dentate	-0.54[#]	-0.56[#]	**0.64***
susceptibility			
DN$_h$	-0.5[#]	-0.59[#]	0.53[#]
globose	0.01	-0.05	0.18
iron mass			
DN$_h$	-0.52[#]	-0.58[#]	0.61[#]
globose	-0.83[#]	-0.81[#]	0.87[#*]
R2*			
DN$_h$	-0.44[#]	-0.54[#]	0.49[#]
globose	-0.43	-0.34	0.31

* – corrected p-value < 0.05 (Bonferroni-Holm correction; correction for multiple tests of the volumes/surface vs. clinical scores was carried out considering the 22 different cerebellar regional volumes [DCN, whole cerebellum, cerebellar GM and WM, lobules, vermis], the dentate surface as well as the 3 different scores [SCAFI, SARA, ICARS]; to correct for multiple testing of iron estimates vs. clinical scores the 5 different DCN regions with the 3 different metrics [QSM, R_2^*, iron mass] and the 3 different scores [SCAFI, SARA, ICARS] were considered). # – uncorrected p-value < 0.05. No correlations are presented for the emboliform and fastigial nuclei because of their low number detected in SCA6 patients.
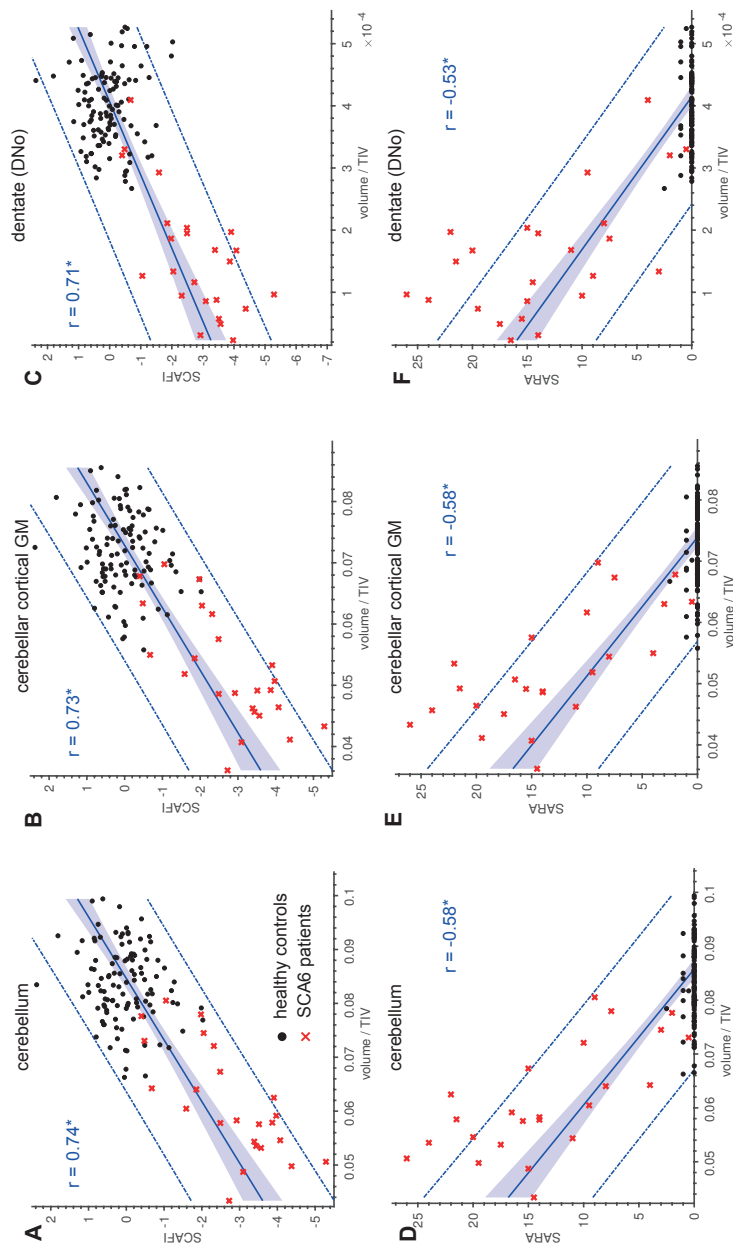
Figure 6. Linear correlations of SCAFI (upper row) and SARA scores (lower row) with respect to volumes of selected structures for both healthy controls and the SCA6 patients. Correlations are presented as functions of normalized volumes of the whole cerebellum, the cerebellar cortical gray matter (without vermis) as well as the outlined dentate nuclei (DN_o). The black dots and red crosses indicate the parameters measured in the healthy controls (n=111) and the SCA6 patients, respectively. The solid blue line indicates the regression line computed across both the healthy controls (n=111) and the SCA6 patients. The 95% confidence interval and the 95% percent prediction interval are illustrated as shaded area and dashed line, respectively. The upper row presents Pearson's correlation coefficient, while the lower row shows Spearman's correlation coefficient. * − corrected p-value < 0.05; Bonferroni-Holm correction (multiple tests of 22 different cerebellar regional volumes [DCN, whole cerebellum, cerebellar GM and WM, lobules, vermis] for 3 different clinical scores [SCAFI, SARA, ICARS] were considered).

DISCUSSION

We investigated the cerebellum and its substructures non-invasively in healthy aging controls and were able to associate these findings with SCA6 patients. While the volume of the cerebellar nuclei does not significantly vary with age, the magnetic susceptibility and iron content of the DCN significantly increase during the lifespan. The decrease in volume of the entire cerebellum and selected cerebellar lobules with increasing age was confirmed. In SCA6 patients, increased atrophy of the cerebellar cortex as well as a tendency of dentate tissue loss was observed with increasing age. We were able to reliably visualize and identify the dentate but less frequently and accurately the smaller cerebellar nuclei on susceptibility maps even at a magnetic field strength of 3T. The globose and emboliform nuclei were even better delineable on 3T than on 7T images. In addition, we observed similar sensitivity to disease-related iron changes in the dentate for susceptibility and R2*. The volumes of the cerebellar nuclei (except for the emboliform nuclei) were smaller in SCA6 patients compared to age- and sex-matched controls. In addition, lower magnetic susceptibilities and R2* were found in the dentate considering the group of all SCA6 patients. After one year, neither patients nor controls showed significant changes of the dentate volume or susceptibility and R2*. Cerebellar GM and dentate volumes significantly correlated with clinical ataxia scores, while susceptibilities and R2* of the dentate only showed a tendency to correlate with these scores.

Identification of Cerebellar Nuclei

We were able to reliably identify the dentate nuclei on quantitative susceptibility maps acquired at 3T and 7T. The smaller nuclei (i.e., fastigial, globose and emboliform nuclei) of the controls could be traced in at least 75% of the data sets. Importantly, dentate nuclei could reliably be identified using the conventional field strength of 3T. In fact, these nuclei were detected even more frequently at 3T than at 7T (**Table 2**). Although improved spatial resolution was used at 7T, the slightly longer acquisition time of about 3 minutes resulted in greater proneness to head motion. We tried to cope with these head movements with retrospective motion correction, which, however, failed in cases of severe head movements of several millimeters during the measurement. In addition, despite using dielectric pads, in some cases the more heterogeneous B1+ field yielded inferior excitation of the cerebellum at 7T. While the higher sensitivity to susceptibility variations with increasing field strength is beneficial for structural imaging (Deistung et al., 2008), it is also the cause of increased sensitivity to physiological fluctuations. Deep breathing, for instance, results in magnetic field fluctuations during the measurement and, thus, degrades the image quality.

Most of the extracted parameters from the manual demarcations were highly consistent between and within the raters (**Table 3**). In particular, the dentate nuclei could reliably be demarcated by the two raters (Cronbach´s alpha values for the volume > 0.84). Volumes of the smaller cerebellar nuclei exhibited lower Cronbach alpha values within and between the raters when comparing with the dentate values. The smaller Cronbach´s alpha values are not surprising as the volumes of these individual nuclei only range between 10 and 50 mm³ (Tellmann et al., 2015) and the accuracy for demarcation is limited by the imaging resolution. Consequently, partial volume effects were more prominent for the 3T acquisitions, resulting in lower inter-rater values at 3T than at 7T.

Volumes of Cerebellar Nuclei and Lobules

While some MRI studies determined the dentate volume based on the extent of the main body of the dentate nucleus (i.e., nuclei's gray matter rim including the enclosed white matter) (Dimitrova et al., 2006; He et al., 2017), we assessed the nuclei volume based on its corrugated thin walls, in line with histological observations (Tellmann et al., 2015; Voogd and Ruigrok, 2012). Our dentate volumes in healthy subjects are well within the range reported in the histological literature. While Höpker (1951) determined an average dentate volume of 315.7 mm³ (27 subjects; age: 6 to 99 years), Tellmann et al. (2015), using up-to-date histological techniques, reported 784.7 ± 193 mm³ (10 subjects; age: 30 to 85 years). For comparison, Diedrichsen et al. (2011) and Stefanescu et al. (2015) reported average dentate volumes of 729 mm³ (23 subjects, age: 21 – 61 years) and 400.2 mm³ (23 subjects, age: 22 – 75 years, individual volume (200.1 ± 89.3) mm³) by analyzing 0.5 mm isotropic 7T-MRI images. Assuming the dentate volume from Tellmann et al. (2015) as ground truth, the volume was most accurately mapped by Diedrichsen et al. (2011) using SWI phase images at 7T, followed by our own 3T and 7T QSM measurements and by Stefanescu et al. (2015) relying on SWI images at 7T. The highest accuracy of the dentate volume measured on phase images instead on susceptibility maps compared to the histologically observed volume by Tellmann et al. (2015) seems to be unexpected at first. QSM should provide a more accurate depiction of the dentate and our resolution of 0.38 mm at 7T was even 24% higher than the one used by Diedrichsen et al. (2011). As QSM is expected to be more accurate in anatomically delineating iron stores compared to phase or SWI images (Deistung et al., 2013, 2016, 2017; Ghassaban et al., 2019), a possible explanation for our lower volumes could be attributed to an inhomogeneous iron distribution within the dentate nucleus. From histology it is known that the ventromedial portion of the dentate nucleus exhibits less amounts of iron compared to the dorsolateral part (Gans, 1924; Höpker, 1951; Jansen and Brodal, 1958). As a consequence, some parts of the nuclei area might be only barely seen or even invisible on QSM, whereas due to the non-locality of the phase (Schäfer et al., 2009) the remaining structures gathered with phase images are overestimated.

Dentate volumes at 7T (DN_o, healthy controls, (540.2 ± 92) mm³) were smaller than at 3T (DN_o, healthy controls, (631.2 ± 94) mm³). This is most likely explained by different spatial imaging resolutions. Of note, voxel volume at 7T was 56% smaller than at 3T. Thus, the contribution of partial volume effects was markedly reduced at 7T. In fact, the surfaces of the dentate nuclei were approximately 8% larger at 7T than at 3T (**Table 5**) indicating that the folding pattern of the dentate could be more accurately traced at 7T. In addition, we did not observe statistical significances of the dentate surfaces when comparing exactly the same cohort at 3T and 7T. Thus, the surface is more robust against different image resolutions than the volume measure.

Although our volumes for the globose nuclei are in excellent agreement with the histological measures reported by Tellmann et al. (2015), we obtained substantially smaller volumes for the emboliform and fastigial nuclei (**Table 5**). As suggested by histologic sections in rodents (Benkovic and Connor, 1993), the evaluated iron is most likely not distributed equally across the (smaller) nuclei and, thus, some nuclear areas are not seen on the susceptibility maps. So far, only one previous MRI study reported data on the smaller nuclei. Diedrichsen et al. (2011) reported substantially smaller volumes (fastigial nuclei 17.4 mm³; and interposed nuclei, that is the sum of emboliform and globose nuclei, 72 mm³) compared to our estimates at 3T and 7T. Thus, QSM allowed more detailed delineation of the smaller nuclei, but except for the globose, volumes were still underestimated compared to histology.

Age Dependency

We could verify a loss of cerebellar volume with increasing age in healthy subjects, which was mainly due to a decline of cortical gray matter (Bernard and Seidler, 2013). The volume reduction with increasing age was mostly driven by the decline of cortical GM in Crus I (as part of lobule VIIa) and lobule VIIb as well as to a lesser extent by lobules I-V, lobule VI, lobule VIII and vermal lobule VII. This finding is in agreement with Bernard and Seidler (2013), who observed gray matter volume loss mainly in the anterior lobes and Crus I when comparing young (age: 22.04 ± 3.47 years) with elderly subjects (age: 65.03 ± 6.42 years) using the SUIT-approach (Diedrichsen, 2006; Diedrichsen et al., 2009). By analyzing T1w images from the OASIS database, which contains 313 subjects ranging from 18 to 97 years, with voxel-based morphometry (VBM), Hulst et al., (2015) reported significant volume declines with age in lobules I-VII, Vermis Crus I, Vermis VIIb, lobules VIIIb, IX and X. Age-related decline of cerebellar volume has been described to be particularly prominent after the age of 70 years (Torvik et al., 1986). One explanation why we did not see significant age relationships for lobules IX and X is that our sample included only few subjects above 70 years (nine subjects with an age range from 70 to 78 years). Different to previous reports (Dimitrova et al., 2008; Hoogendam et al., 2012; Jernigan et al., 2001), we could not find

a significant reduction of cerebellar white matter for healthy controls with increasing age. The reason might be different definitions of cerebellar white matter. In the present study, only the corpus medullare (i.e., the central white matter without the cerebellar nuclei) was defined as cerebellar white matter, whereas the other studies also added white matter areas that branch more deeply into the folia and the area of the cerebellar nuclei.

In addition, we found a tendency of linear relationships of the cerebellar cortex (uncorrected $p < 0.05$) and the whole cerebellar volumes (uncorrected $p < 0.05$) with age in the SCA6 patients. Interestingly, the slopes observed for the SCA6 cohort were substantially steeper than the ones calculated for the healthy controls indicating faster age-related tissue decline in SCA6 patients. This finding is further supported by Schmitz-Hübsch et al. (2008) who reported that only age at onset and disease duration determine disease-related symptoms as detected with the SARA score.

Regarding the cerebellar nuclei we observed that their size remained relatively stable across the lifespan of healthy subjects. This observation coincides with findings for the extent of the main body of the dentate nucleus ("dentate hull") by He et al. (2017). Compared to He et al. (2017), we assessed the dentate volume more accurately and across a larger cohort with a broader range of age. Furthermore, we could not replicate the results of the histological post mortem study by Höpker (1951) who stated a loss of dentate volume at higher age. This discrepancy could be due to a relatively low number of subjects that were examined by Höpker (1951) and the histological techniques which do not reflect today's state-of-the-art. Maybe most importantly, histological shrinkage was mainly seen in an age group above 70 years, which made up only a small part of our investigated study population.

In line with previous literature (Acosta-Cabronero et al., 2016; Ghassaban et al., 2019; Li et al., 2014; Persson et al., 2015), we found a strong relationship of susceptibility and $R2^*$ with age for the main body of the dentate. The origin of the susceptibility- and $R2^*$-age relationship is the changing iron content within the dentate during lifespan. This is supported by findings of Hallgren and Sourander (1958), who histochemically observed that iron values within the dentate increase rapidly during the first two decades, and Ramos et al. (2014), who measured slightly lower amounts of iron for a subject group between 53 and 59 years ([244 ± 135] µg/g dry weight) than for subject groups larger than 60 years (about 290 µg/g dry weight). The statistically significant relationship of iron mass with age observed by us is mainly driven by the change of the underlying susceptibility in the dentate body, rather than the gray matter rim of the dentate nucleus. As discussed in more detail below, these changes likely reflect changes in glia but not in neurons. Of note, our iron mass in the dentate (DN_o) measured at 3T for all healthy controls of (88.2 ± 23.8) µg is in excellent agreement with the amount of (69.1 ± 34.1) µg that we observed by converting

the histochemically determined dentate iron concentration of (103.5 ± 48.6) mg iron/kg wet weight (Hallgren and Sourander, 1958) using our dentate volume of (631.2 ± 94) mm³ and Eq. 1.

SCA6 vs. Healthy Controls

We were able to demonstrate significant cerebellar tissue decline in SCA6 patients compared to matched controls, manifesting itself not only in the cerebellar cortex, vermis and cerebellar white matter but also in the DCN. Our cerebellar volumes observed in SCA6 patients and controls are in excellent agreement with previous MRI reports (Eichler et al., 2011; Schulz et al., 2010) and reflect a severe cerebellar tissue decline by about 25% in SCA6 patients. Our volume reductions observed in the cerebellar lobules and vermis in SCA6 patients are in line with previous reports relying on manual (Jung et al., 2012) and automatic volume segmentations (Yang et al., 2016) as well as VBM (Lukas et al., 2006; Schulz et al., 2010). In contrast to previous VBM studies, we also observed a significant decrease of white matter volume in SCA6 patients compared to controls. Reduced white matter volumes in SCA6 have also been reported in another volume-of-interest based analysis of structural T1w images (Yang et al., 2016) and is also supported by tissue decline of the superior and middle cerebellar peduncles as measured with diffusion tensor tractography (Falcon et al., 2015). Our findings show that white matter degeneration (most likely secondary to the Purkinje cell loss) is also present at the level of the corpus medullare (definition see above).

The significantly reduced dentate volumes in the SCA6 group compared to matched controls confirm data of a recent 7T MRI study (Stefanescu et al., 2015). They are also in line with previous histological findings, which suggest an involvement of the cerebellar nuclei in SCA6 (Gierga et al., 2009; Wang et al., 2010). Furthermore, we could demonstrate a loss of volume in SCA6 for the smaller cerebellar nuclei (**Figure 4D**), although their delineation was less reliable than the one for the dentate nucleus for reasons given above.

SCA6 is a form of more pure cerebellar degeneration, which primarily results in degeneration of the Purkinje cells. In transgenic mouse models, Triarhou et al. (1987) and Sultan et al. (2002) showed that a loss of Purkinje cell input led to a loss of volume in the cerebellar nuclei that could not be explained by the loss of dentate neurons. In fact, investigations by Heckroth, 1994 revealed that the reduction of nuclei volume is mainly driven by the loss of myelinated axons and synapses with a proportion of more than 50 %. About one third of dentate volume loss was due to glial processes, vessels and intercellular space, whereas only a minor proportion could be accounted to the depletion of neurons.

We measured significantly reduced R2* and magnetic susceptibilities in the gray matter rim of the dentate wall as well as significantly lower R2* and a trend to lower susceptibilities in the body ("hull") of the dentate in the group of all SCA6 patients compared to healthy controls at baseline (**Table 5, Figure 5**). The one year follow-up examination still revealed reduced magnetic susceptibilities and R2* of the dentate, however, statistical significance could not be reached, most likely due to the lower sample size resulting from a drop out of six SCA6 patients and controls, respectively. There was also a trend toward lower iron masses in the smaller cerebellar nuclei in the patients. These findings suggest a depletion of iron in the DCN of the patients. Of note, studies in rats have shown that iron in the cerebellum and its nuclei is primarily stored in oligodendrocytes and microglia (Benkovic and Connor, 1993). Thus, our findings suggest that the decreased nuclei size does not reflect a decrease in the number of neurons. Rather it likely reflects a decrease of oligodendrocytes and/or microglia – which is exactly what one would expect based on the findings in transgenic mouse models (Heckroth, 1994; Sultan et al., 2002; Triarhou et al., 1987). As yet, glia cell involvement has not yet been studied in SCA6. To prove the involvement of glial cells in SCA6 further histological studies are required.

It is commonly assumed that the Purkinje cell loss is the primary deficit in SCA6 (Falcon et al., 2015; Gomez et al., 1997). In that case, the assumed reduction of the oligodendroglia would be secondary. However, it cannot be excluded that oligodendroglia are primarily involved. This assumption is supported by neuropathological changes in transgenic MBP-TK mice. Here, selective ablation of oligodendrocytes during the first weeks of postnatal life resulted in disruption of the cortical cytoarchitecture and neuronal network (Collin et al., 2007; Mathis et al., 2003), resembling histological findings in human SCA6 brains (Gierga et al., 2009; Yang et al., 2000).

Of note, the susceptibility and R2* decreases measured in patients may not only be influenced by changes in iron but also by myelin degradation. However, this would increase susceptibility but decrease R2* (Deistung et al., 2013).

MRI Measures and Clinical Parameters

In line with Stefanescu et al. (2015), we were able to replicate the significant negative correlations comparing the whole cerebellum and the dentate volumes with clinical ataxia scores (SARA; ICARS) already at 3T (**Table 6**). In addition to the volumes, the iron sensitive measures (susceptibility, R2* and iron mass) of the dentate nuclei tended to inversely correlate with the clinical disease scores (SARA; ICARS) and positively with the SCAFI. Thus, lower dentate iron content is linked to a more severe degree of ataxia.

The volumes of the dentate nuclei were more sensitive to differentiate between SCA6 and controls (Hedges' g = 2.83) compared to the volumes of the cerebellar cortex (g = 1.97). **Figure 2C** demonstrates that the majority of SCA6 patients exhibit dentate nuclei volumes outside of the 95% prediction interval of the healthy controls. In five patients, however, the nuclei volumes were within the prediction interval of the controls. Two of these five patients were presymptomatic, whereas the remaining three patients were symptomatic and showed signs of ataxia (SARA scores; patient 3 = 4, patient 4 = 2, patient 5 = 9.5). Thus, although a reduced dentate volume allows identifying symptomatic patients with a high sensitivity, it does not appear to be an early marker of the disease. The latter, however, has to be confirmed in a larger group of presymptomatic patients. Of note, we did not observe a significant reduction of the dentate nuclei after a one year follow-up. Thus, volume of the dentate nuclei is of diagnostic value, but apparently not a sensitive biomarker of SCA6.

Limitations

There are two main limitations. Firstly, QSM has turned out to be a valid method to assess the volume of the dentate nuclei even at the conventional field strength of 3T. However, QSM was unable to display the corrugated wall of the dentate nuclei with an accuracy that comes close to histology. This is because QSM likely does not show the extent of the dentate neurons, but rather the distribution of the iron-containing glia cells (as discussed above). As a consequence, QSM shows more than the thin wall of the dentate nucleus, and the white matter inside the nucleus is also visible (see e.g. **Figure 1**). If one goes back to the early iron stainings by Gans (1924), a similar distribution of iron positive cells can already be seen.

Secondly, we like to note that although Stefanescu et al. (2015) showed significantly smaller nuclei in SCA6 compared to controls (very similar to our study), the absolute volumes for the dentate nuclei were significantly smaller compared to the present study, presumably because of different strategies in manual delineation of the nuclei. Therefore, automated strategies for delineation of the cerebellar nuclei are needed to achieve improved reproducibility and, thus, comparability among different studies.

CONCLUSIONS

QSM enabled us to assess the dentate nuclei and the smaller cerebellar nuclei already at a magnetic field strength of 3 Tesla, which is widely used in clinical settings. Volume measures of the dentate nuclei were in good accordance with histological data. In contrast to the well-known age-dependent decline of cerebellar GM, the volume of the dentate nuclei did not depend on age, at least in the age range of 18 and 70 years, whereas its iron load increased during lifespan. Previous findings of markedly reduced volumes of the cerebellar lobules
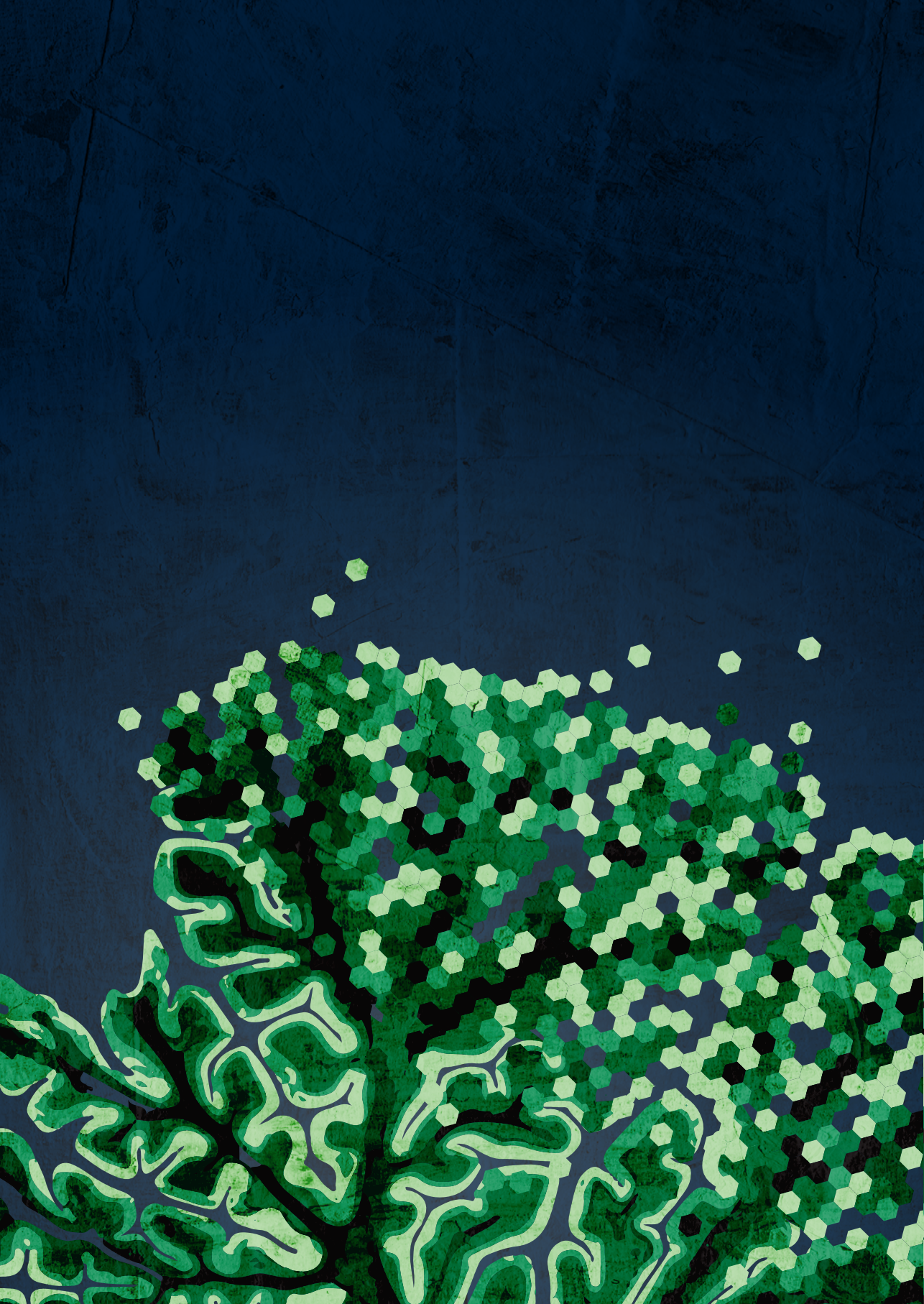
and dentate nuclei in SCA6 at 7 Tesla were confirmed at 3 Tesla. Finally, the present data suggest that the loss of dentate volume in SCA6 is due to the loss of iron-containing glial cells.

Acknowledgments

Author contributions

Thomas Hulst performed experiments; edited and revised manuscript; approved the final version of the manuscript.

4

Behavioral and neural basis of anomalous motor learning in children with autism

Mollie K. Marko[1], Deana Crocetti[2], Thomas Hulst[3], Opher Donchin[4], Reza Shadmehr[1], and Stewart H. Mostofsky[2,5]

[1] Laboratory for Computational Motor Control, Department of Biomedical Engineering, Johns Hopkins School of Medicine
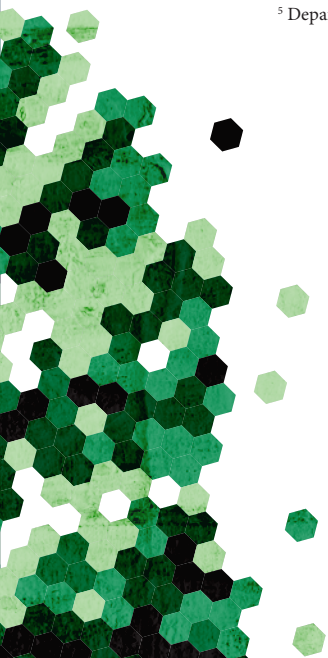[2] Center for Neurodevelopmental and Imaging Research, Kennedy Krieger Institute
[3] Department of Neuroscience, Erasmus MC
[4] The Motor Learning Laboratory, Department of Biomedical Engineering, Ben Gurion University of the Negev, and
[5] Departments of Neurology and Psychiatry and Behavioral Sciences, Johns Hopkins University School of Medicine

ABSTRACT

Autism spectrum disorder (ASD) is a developmental disorder characterized by deficits in social and communication skills and repetitive and stereotyped interests and behaviors. Though not part of the diagnostic criteria, individuals with autism experience a host of motor impairments, potentially due to abnormalities in how they learn motor control throughout development. Here, we used behavioral techniques to quantify motor learning in ASD, and structural brain imaging to investigate the neural basis of that learning in the cerebellum. Twenty children with ASD and twenty typically developing (TD) controls, ages 8-12, made reaching movements while holding the handle of a robotic manipulandum. On random trials the reach was perturbed, resulting in errors sensed through vision and proprioception. The brain learned from this error and altered the motor commands on the subsequent reach. We measured learning from error as a function of the sensory modality of that error, and found that children with ASD outperformed TD children when learning from errors that were sensed through proprioception, but underperformed TD children when learning from errors that were sensed through vision. Previous work had shown that this learning depends on the integrity of a region in the anterior cerebellum. Here we found that the anterior cerebellum, extending into lobule VI, and parts of lobule VIII were smaller than normal in children with ASD, with a volume that was predicted by the pattern of learning from visual and proprioceptive errors. We suggest that the abnormal patterns of motor learning in children with ASD, showing an increased sensitivity to proprioceptive error and a decreased sensitivity to visual error, may be associated with abnormalities in the cerebellum.

Keywords: error sensitivity, proprioception, motor learning, reaching, cerebellum, autism

INTRODUCTION

Autism spectrum disorder (ASD) is a developmental disorder characterized by impairments in social and communication skills, coincident with repetitive, stereotyped behaviors. Though the underlying physiological cause is unknown, the cerebellum has been highlighted as a key region of interest due to the relative frequency of cerebellar abnormalities found in individuals with ASD. For example, in post-mortem studies, reduced Purkinje cell numbers are the most common neuropathological finding (Bailey, 1998; Kemper and Bauman, 1998; Ritvo E, 1986; Whitney et al., 2008). Furthermore, imaging studies have found that individuals with ASD exhibit reduced volumes in the cerebellar vermis (Courchesne et al., 2001; Hashimoto et al., 1995; Murakami et al., 1989; Scott et al., 2009), with some tendency for an overall increase in cerebellar volume (Courchesne et al., 2001; Murakami et al., 1989; Sparks et al., 2002; Stanfield et al., 2008).

Though damage to the cerebellum can lead to a host of cognitive deficits (Schmahmann and Sherman, 1998), a prominent symptom of cerebellar damage is motor learning impairment (Criscimagna-Hemminger et al., 2010; Donchin et al., 2012; Smith and Shadmehr, 2005; Xu-Wilson et al., 2009). Cerebellar dependent motor learning is believed to occur through the construction of internal models of action in which the brain predicts the sensory consequences of a movement (Izawa et al., 2012a). If the actual sensory feedback is different from predicted, the resulting prediction error drives motor learning by updating an internal model (Donchin et al., 2003). Individuals with ASD present a broad range of motor impairments, including impairments in simple timed movements (Jansiewicz et al., 2006), handwriting (Fuentes et al., 2009), skilled gestures (Dowell et al., 2009; Mostofsky, 2006) and imitation (Dziuk et al., 2007). Potentially, this broad spectrum of motor impairments, present even in infancy (Provost et al., 2006), is related to the inability of individuals with ASD to appropriately learn internal models, a lifelong developmental process.

Understanding how internal models are learned in ASD is useful, as motor learning may parallel learning of communication, language, and social skills (Gallese et al., 2004; Gidley Larson et al., 2008; Iacoboni, 2009). In a recent series of studies we examined motor learning in ASD, focusing on a reaching task in which the children learned to compensate for a perturbation. We found that children with ASD constructed an internal model that was different than healthy controls, potentially relying more than normal on proprioception, as evidenced by their generalization patterns (Haswell et al., 2009; Izawa et al., 2012b). In contrast, children (Johnson et al., 2013) and adults (Mosconi et al., 2013) with ASD showed slower learning in a saccade adaptation paradigm, in which errors were purely visual in

nature. These findings raise the possibility that during motor learning children with ASD have a greater than normal reliance on errors that are sensed by proprioception and less than normal reliance on errors sensed by vision.

Here, we examined both the behavioral and the neural basis of motor learning abnormalities in autism. We quantified how children with ASD learned from visual and proprioceptive errors in their reaching movements. Using anatomical MRI, we related our behavioral measures to the volume of the cerebellar regions known to be important for learning control of reaching. We hypothesized that children with ASD would show greater than normal learning from proprioceptive errors, but less than normal learning from visual errors, and that this would be related to the volume of the sensorimotor regions of the cerebellum.

METHODS

Participants

We recruited n=40 children, ages 8-12. Among these 40 children, there were an equal number of typically developing children (TD, n = 20, age 10.3 ± 0.3, mean ± SEM, one left handed, 16 male), and children who were diagnosed with ASD (n = 20, age 10.95 ± 0.2, one left handed, 18 male). The protocol was approved by the Johns Hopkins Institutional Review Board and a legal guardian for all children provided written, informed consent.

Autism diagnosis was established using both the Autism Diagnostic Observation Schedule (ADOS-G: first 9 participants, 14.6 ± 1.8, mean ± SEM, or ADOS-2: final 11 participants, 11.4 ± 1.3, mean ± SEM) and the Autism Diagnostic Interview-Revised (ADI-R). Diagnoses were confirmed by a child neurologist with over two decades of experience with autism spectrum diagnosis (S.H.M.). Children were excluded if they had a known etiology for autism, documented prenatal/perinatal insult, or showed evidence of psychiatric disorders based on the Diagnostic Interview for Children and Adolescents – IV (DICA-IV), with the exception of anxiety disorders, obsessive compulsive disorder, oppositional defiant disorder, or attention deficit hyperactivity disorder (ADHD). We found no effect of comorbid diagnoses on our results. Children from the TD group were excluded if they scored < 80 on the Wechsler Intelligence Scale for Children - IV (WISC-IV) Full Scale IQ (FSIQ), while children from the ASD group could be included if the FSIQ was below 80 as long as either the Verbal Comprehension Index (VCI) or Perceptual Reasoning Index (PRI) was 80 or higher, and the other was 65 or higher. Subjects were matched for gender (Fischer's exact test, p = 0.66), age [$t_{(38)}$ = 1.70, p = 0.09], PRI [$t_{(38)}$ = 1.74, p = 0.09], and Edinburgh Handedness score, [$t_{(38)}$ = -0.64, p = 0.52] (see **Table 1**). Groups were further

found to match for VCI [$t_{(38)}$ = 1.72, p = 0.09] but not FSIQ [$t_{(38)}$ = 2.67, p = 0.01], however prior research indicates that perceptual, task based assessments of intelligence are more appropriate for children with ASD, rather than full scale measures of IQ (Mottron, 2004). Thus, standard practice in our lab is match groups on PRI alone. MRI scans were examined by a radiologist for abnormalities and all children were found healthy.

Table 1. Participant information (mean ± SD). Groups showed no significant difference in gender, age, PRI, or handedness.

	ASD	TD
n	20	20
Males	18	16
Age	10.95±1.0	10.30±1.4
Perceptual Reasoning Index	109.6 ± 13.1	117.7 ± 16.1
Verbal Comprehension Index	111.7 ± 15.3	120.1 ± 15.6
Full scale IQ	105.6 ± 13.7	118.1 ± 15.9
Edinburgh Handedness Score	0.737 ± 0.5	0.828 ± 0.4
ADOS-G/ADOS-2	14.6 ± 3.5/11.4 ± 4.2	N/A

Task

The children participated in a game in which they were instructed to hold a robotic arm in their hand and "shoot through a target", following a protocol similar to (Marko et al., 2012). Briefly, children sat in a dark room while holding the handle of a robotic manipulandum (**Figure 1A**). A screen over their hand projected information about the game. Each trial began with the child bringing the cursor, indicating hand position, into a 6x6 mm start box. A second, 6x6 mm target box then appeared 8 cm in front of the start box. Children were instructed to shoot through the target, crossing through it between 150 and 250 ms after movement onset. After their reached exceeded 8 cm in extent, a "pillow" force field slowed the movement and guided the hand back to the target. Movements that were too fast or slow were indicated by coloring the target box red or blue, respectively. Successful trials were indicated by a target explosion and a point added to the child's score. With every point, a cartoon coin temporarily appeared above the score and children were encouraged to collect as many coins as possible. At the end of the experiment the children were further rewarded by giving them the option of choosing a small toy from a collection in a bag.
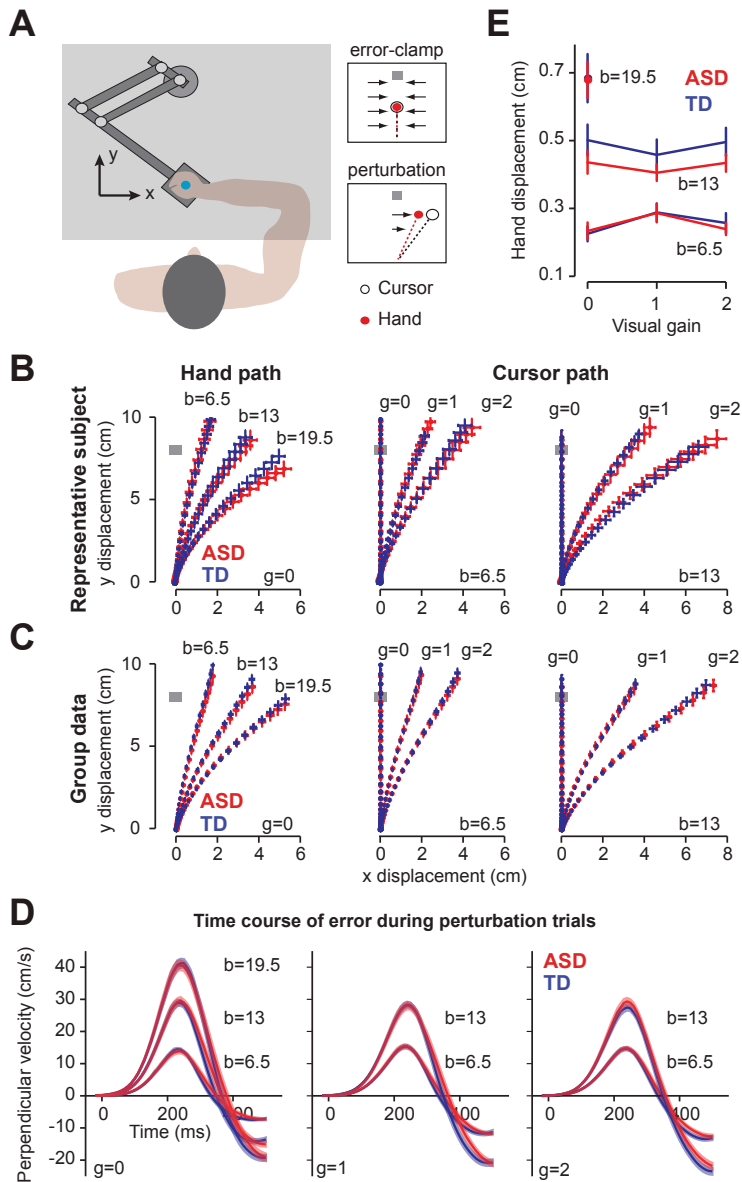
Figure 1. Experimental task. A) Children made reaching movements to a target while holding the handle of a robotic manipulandum. On random trials, the robot perturbed the reach, causing an error. Learning from this error was measured through error-clamp trials, in which the error was clamped to zero and the forces that the children produced against the clamp walls were measured. B, C) Hand path and cursor paths for a representative TD and ASD subject (B) and for the group (C). For both groups, hand error increased with increasing field strength and cursor error increased with increasing visual gain. Data was sampled at 100 Hz, and error bars represent SEM. D) Time course of error during the reach in the perturbation trials, as quantified via velocity perpendicular to the direction of the target. Perpendicular velocity reflects both the perturbation to the hand and the online-feedback response. Perpendicular velocity increased with increasing perturbation strength, reflecting the effect of field size, but was not different between groups. E) Proprioceptive error, experienced by the hand, measured at 50% of the max velocity for each movement for all perturbation conditions. Increasing field strength increased the proprioceptive error, but increasing visual gain did not. The errors experienced by the children were not different between groups.

The experiment consisted of two sessions, each approximately 40 minutes long. Each session began with a warm up block of 40 trials, followed by five perturbation blocks of 55 trials each. After the first session, the child left the room and returned later in the same day for a second session. Analysis was collapsed across sessions.

Perturbations

Our perturbations had two components: a proprioceptive component generated by a force field that displaced the hand, and a visual component generated by a displacement to the cursor. The perturbation to the hand was a curl force field that pushed the hand perpendicular to the direction of motion (the x- and y-coordinates are specified in **Figure 1A**):

$$f = \begin{bmatrix} 0 & b \\ -b & 0 \end{bmatrix} \begin{bmatrix} \dot{x} \\ \dot{y} \end{bmatrix} \qquad\qquad \text{(Eq. 1)}$$

In Eq. (1), $\dot{x}$ and $\dot{y}$ are components of the hand velocity vector, and f is the force that the robot applied to the hand. There were three field strengths, resulting in small, medium, or large proprioceptive errors: $b = \pm 6.5$, $b = \pm 13$, or $b = \pm 19.5$ N.s/m.

The visual perturbation was applied through displacement of the cursor. As the hand moved, the position of the cursor c was perturbed with respect to position of the hand as:

$$c = \begin{bmatrix} g & 0 \\ 0 & 1 \end{bmatrix} \begin{bmatrix} x \\ y \end{bmatrix} \qquad\qquad \text{(Eq. 2)}$$

In Eq. (2), x and y are components of hand position. Thus, similar to a force field, the visual perturbation acted to perturb the position of the cursor perpendicular to the direction of the target. This perturbation was a scaling via variable g, which took on one of three values: $g = 0$, $g = 1$ or $g = 2$. When $g = 0$, the cursor did not deviate from a straight line to the target. When $g = 1$, the cursor faithfully followed the position of the hand. When $g = 2$, the cursor magnified the x-displacement of the hand. These visual gains were applied to the small ($b = \pm 6.5$) and medium ($b = \pm 13$) field strengths, and the $g = 0$ condition was applied to the large field strength ($b = \pm 19.5$), creating seven possible perturbation types. For each perturbation block, each of the seven types of perturbations were applied twice, in random order, once to perturb the arm to the right, and once to perturb the arm to the left.

Our aim was to measure how much the brain learned from each type of error. To do so, we used triplets of trials (Huang and Shadmehr, 2007): error-clamp C_1, perturbation P, error-clamp C_2 (**Figure 1A**). During an error-clamp trial, the robot guided the handed along a stiff "channel" from the start position through the target (spring coefficient = 2.5 kN/m, damping coefficient = 25 N.s/m). A force transducer in the handle of the manipulandum measured the forces produced by the hand of the child against the channel wall, which captured the motor output of the subject during that trial. We looked at the change in motor output from trial C_1 to C_2 as a proxy for the learning from error that was experienced in trial P.

Estimating learning from error

When the hand experiences a perturbation during a movement, on the next trial the brain will produce motor commands that predict and partially compensate for the perturbation (Thoroughman and Shadmehr, 2000). Our goal was to quantify how much the brain compensated for the experienced perturbation, as this represented how much the brain learned from error. To examine this learning on a trial-to-trial basis, we subtracted the force produced in trial C_1 from the force produced in trial C_2, thus treating the force in trial C_1 as a baseline. This isolated the force production that occurred as a consequence of learning in response to the error that was experienced on trial P. However, throughout our experiment, errors varied in size, driving varying amounts of learning. Therefore, we chose to further examine sensitivity to error by normalizing learning by the experienced error (Marko et al., 2012). We did this for measures of proprioceptive learning and visual learning, producing a modality- and error-specific quantification of the sensitivity to error for each child.

To quantify learning from error, we use the state-space framework for error-dependent adaptation (Donchin et al., 2003):

$$f^{(n+1)} = \alpha f^{(n)} + \lambda\left(e_v^{(n)}, e_p^{(n)}\right)$$

(Eq. 3)

In Eq. (3), $f^{(n)}$ is motor output on trial n, e_v is error as sensed by vision, e_p is error as sensed by proprioception, λ is a function that describes learning from error, and α is a decay term. If trial n-1 is an error-clamp, then $f^{(n)} = \alpha f^{(n-1)}$ (by definition, there are no errors in an error-clamp trial). It follows that in an [error-clamp, perturbation, error-clamp] triplet, learning from error is:

$$\lambda\left(e_v^{(n)}, e_p^{(n)}\right) = f^{(n+1)} - a^2 f^{n-1} \tag{Eq. 4}$$

Results of our previous work (Marko et al., 2012) suggest that learning from error can be well approximated by a linearly separable function of visual and proprioceptive errors. In this framework, learning from error can be thought of as the sum of learning from visual error, labeled as λ_v, and learning from proprioceptive error, labeled as λ_p:

$$\lambda\left(e_v^{(n)}, e_p^{(n)}\right) \equiv \lambda_v + \lambda_p$$
$$\approx \beta_v(e_v)e_v + \beta_p(e_p)e_p \tag{Eq. 5}$$

Using Eqs. (4) and (5), we calculated sensitivity to visual and proprioceptive errors, $\beta_v(e_v)$ and $\beta_p(e_p)$. The coefficient α in Eq. (4) was found using instances of two consecutive error-clamp trials. This occurred 52 times across the duration of the experiment. We regressed the force profile in the second of the consecutive error-clamp trials onto the first, telling us how much of the motor output was retained in two consecutive movements. We found that $\alpha = 0.91 \pm 0.05$ (mean $\pm$ SEM). There was no significant difference in the value of α between groups [$t_{(38)} = 0.60$, p = 0.55].

In Eqs. (4) and (5), force and error are represented as scalar quantities for each trial. To find force in a given error-clamp trial, we measured force that the children produced at 50% of peak speed of the movement. Similarly, we measured error in perturbation trials as displacement of the hand or cursor with respect to the target at 50% of peak speed (Taig et al., 2012). This midpoint of speed did not differ between groups [$t_{(38)} = -0.12$, p = 0.91], and occurred on average at 149 ms after movement onset (ASD: 149.2 $\pm$ 3.8 ms, TD 148.5 $\pm$ 3.9 ms, mean $\pm$ SEM).

To find $\lambda(e_v^{(n)}, e_p^{(n)})$, we used Eq. (4). Triplets were removed from analysis if 50% of max speed occurred prior to 100 ms from movement onset, if the hand did not successfully complete the 8 cm reach, if the hand moved further than 2x the width of the target box (0.6 cm) from the midline during an error-clamp trial, or if the hand experienced a substantial error in the wrong direction (> $\pm$ 0.5 cm) in response to a perturbation. Additionally, within each condition, outliers were identified and removed using the p < 0.001 criterion of the median absolute deviation method. In total, this removed 6.6% $\pm$ 0.76% (mean $\pm$ SEM) of triplets per subject, with no difference in percentage of removed triplets between groups [$t_{(38)}$ =

-1.1, p = 0.29]. Learning from error and error size were corrected for sign and collapsed to one direction. For ease of presentation, learning and error or sensitivity and error will be plotted in the first quadrant. All analysis was completed using Matlab (Mathworks), Excel (Microsoft), SPSS (IBM) or SPM (http://www.fil.ion.ucl.ac.uk/spm/).

Estimating Sensitivity to Error

To estimate learning from proprioceptive error, labeled as λ_p, we focused on trials in which visual error was zero (i.e., = 0 condition). For this condition, from Eq. (5) we have:

$$\lambda\left(0, e_p^{(n)}\right) = \beta_v(0)0 + \beta_p(e_p)e_p$$
$$= \lambda_p$$

(Eq. 6)

We further examined learning from proprioception by finding the sensitivity to proprioceptive error at each field size, using the following equation:

$$\beta_p(e_p) = \frac{\lambda(0,e_p)}{e_p}$$

(Eq. 7)

In Eq. (7), learning from error is normalized to the specific error that was experienced by each subject. The term β_p estimates how much the subject learned from proprioceptive error of size e_p.

To estimate sensitivity to visual error alone, we measured how the trial-to-trial change in motor commands was affected when proprioceptive perturbations were kept constant (at $b = 6.5$ or $b = 13$) and the visual perturbations were changed (from $g = 0$ condition to $g = 1$ or 2). Mathematically, this is equivalent to setting $\lambda_p = \lambda(0,e_p)$ in Eq. (5), which we measured in the $g = 0$ condition, resulting in the following estimate of sensitivity to visual error:

$$\beta_v(e_v) = \frac{\lambda(e_v,e_p) - \lambda(0,e_p)}{e_v}$$

(Eq. 8)

This produced a measure of sensitivity to visual error alone, and eliminated the effects of concurrent proprioceptive error.

Brain imaging

Given the well-established role of the cerebellum in motor adaptation, we focused our imaging analyses on this structure. Specifically, we examined brain-behavior associations with regions of the cerebellum known to be important for sensorimotor control and reach adaptation. In order to focus our analysis on these relevant cerebellar regions, we employed the mappings described by (Buckner et al., 2011). In that work, the cerebellum was parcellated based on shared signal properties with regions of the cerebral cortex. This produced two functional atlases of the cerebellum. One atlas labeled each cerebellar voxel as being connected with one of 7 identified regions within the cerebral cortex. The other atlas labeled each cerebellar voxel as being connected with one of 17 identified regions within the cerebral cortex (each cortical map covered the entire cortex). For the 7 network atlas, Buckner and colleagues found a region of the cerebellum that exhibited resting state functional connectivity to the motor and somatosensory cortices, which we will refer to as the coarse-scale sensorimotor region of the cerebellum. In Buckner et al., the connectivity between the cerebral cortex and this region of the cerebellum was validated using a movement task of the tongue, hand and foot. For the 17 network atlas, the cortical sensorimotor area was split, separating the tongue from the hand and foot representations. In the cerebellum, the sensorimotor region was more finely resolved into two corresponding networks. We focused on the cerebellar region that contained the hand representation, which we will term the fine-scale sensorimotor region of the cerebellum. Both the 7 and the 17 network cerebellar atlases were recently published as a standardized atlas with the Spatially Unbiased Infra-Tentorial (SUIT) toolbox (Diedrichsen, 2006), allowing us to isolate and examine these sensorimotor regions of the cerebellum in our participants. As we will show, we found that the anterior cerebellum, extending into lobule VI, and parts of lobule VIII, corresponded to these sensorimotor regions of the cerebellum.

For each child, we acquired a T1-weighted 3D MP-RAGE brain image using a 3T Philips Gyroscan NT (Royal Philips Electronics, Amsterdam, The Netherlands). The MP-RAGE scans were acquired using the following parameters: 155 coronal slices, 1 mm slice thickness, 8° flip angle, TE=3.0 ms, TR=7 ms, matrix=256x256. Two children were excluded from the analysis due to poor image quality: one due to severe motion artifact, and one for poor gray/white matter segmentation. The cerebellum was isolated and the resulting image was then registered to the SUIT template. This produced a deformation matrix, which morphed the native image to the standardized template of the cerebellum, and a cropped version of

the original T1 image. We used SPM to segment the cropped image into gray matter, white matter and cerebrospinal fluid. Using a threshold of 0.5, we then generated binary maps of the cropped image for each of the three tissue types.

To find the volume of the sensorimotor regions of the cerebellum, we used the deformation matrix of each child, produced by SUIT, to invert the atlas of the 7 and 17 network cerebellar parcellations into each child's native space. This was multiplied by the binary tissue maps, allowing us to calculate regional volumes based on the network parcellation, for each tissue type. For both the coarse- and fine-scale sensorimotor networks, we summed the gray and white matter volume to produce a measure of total tissue volume for each child. The resulting sum was termed the coarse (or fine) scale sensorimotor cerebellar volume.

RESULTS

Learning from error

The children held the handle of a robotic manipulandum and reached toward a target. A visual or proprioceptive perturbation perturbed their movements, as illustrated for an example ASD and TD subject in **Figure 1B**, and for groups in **Figure 1C**. As a proxy for the error induced by the perturbations, we used displacement of the hand or cursor perpendicular to the direction of the target at 50% of max speed (**Figure 1E**). An ANOVA with a within-subject measure of hand displacement for various visual gains, and between-subject factor of group showed a significant effect of field strength [$F_{(1,38)}$ = 1575.1, p < 0.001], but found no effect of visual gain [$F_{(2,37)}$ = 0.623, p = 0.54], and no effect of group [$F_{(1,38)}$ = 0.66, p = 0.42]. The time course of the error during movements is shown via the perpendicular velocity trace in **Figure 1D**. The time course of error experienced during the reaching movements appeared identical in the two groups, suggesting that the errors that the two groups experienced were comparable.

Despite experiencing similar errors, the groups differed in how they learned from error.

Figure 2A, left, shows learning from proprioceptive error as estimated in each of the three field sizes. ANOVA with a within subject repeated measure of field strength and a between-subject factor of group resulted in a significant main effect of group [$F_{(1,38)}$ = 5.7, p = 0.022], but no significant effects of field size [$F_{(2,37)}$ = 1.36, p = 0.27] or group by field interaction [$F_{(2,37)}$ = 0.009, p = 0.99]. Therefore, children with autism learned more from a given proprioceptive error than typically developing children.

To further examine learning from proprioception, we calculated the sensitivity to proprioceptive error at each field size using Eq. (7). The results are displayed in **Figure 2A** (right panel). ANOVA with a within subject repeated measure of field strength and between-subject factor of group revealed that across both groups, there was a significant effect of field [$F_{(2,37)}$ = 4.72, p = 0.015] such that sensitivity to proprioceptive error was highest for smallest errors, a pattern that we had also seen in healthy adults (Marko et al., 2012). Unique to this study, we also found a significant effect of group [$F_{(1,38)}$ = 4.7, p = 0.035], suggesting that sensitivity to proprioceptive error was significantly larger than normal in the ASD group, and that the ASD group learned more from proprioceptive errors than the TD group. There was no significant group by field interaction [$F_{(2,37)}$ = 0.29, p = 0.75].

We next examined the patterns of learning from visual errors. We began by first measuring learning in trials in which there were both visual and proprioceptive errors (Eq. 5). This learning, labeled as $\lambda(e_v, e_p)$, is plotted as a function of visual error for the small field (b = 6.5, right) and the medium field (b = 13, left) in **Figure 2B**. ANOVA with a within subject effect of field and gain and a between-subject factor group revealed a significant effect of field [$F_{(1,38)}$ = 5.1, p = 0.029], a significant effect of gain [$F_{(2,37)}$ = 20.9, p < 0.001], and a significant gain by group interaction [$F_{(2,37)}$ = 3.53, p = 0.039]. All other effects were not significant (p > 0.05). As there was both a proprioceptive and visual component of adaptation in these measurements, we would not anticipate any specific group effect. The interaction suggests that the rate of increasing adaptation in response to increasing visual error was different between groups. In fact, we found that the slope of learning with respect to visual gain was significantly greater in TD children [$t_{(38)}$ = -2.51, p = 0.016], implying decreased visual sensitivity in the ASD group.

It is also interesting to note that there were no group differences in adaptation for either of the g = 1 conditions (the middle data point in **Figure 2B**, left and right). This condition represents "typical" adaptation conditions, for which prior work has indicated that the ASD group was comparable to controls (Gidley Larson et al., 2008; Haswell et al., 2009): ANOVA with a with-in subject repeated measure of field strength and between subject factor of group found no significant effect of group [$F_{(1,38)}$ = 0.28, p = 0.61], a significant effect of field [$F_{(1,38)}$ = 4.45, p = 0.042] and no significant group by field interaction [$F_{(1,38)}$ = 0.006, p = 0.94].

We then used Eq. (8) to examine sensitivity to visual error alone. The results of this analysis are shown in **Figure 2C**. Similar to proprioceptive errors, ANOVA with a within subject repeated measure of perturbation size and between-subject factor of group revealed a significant effect of perturbation size [$F_{(3,36)}$ = 5.4, p = 0.004] such that sensitivity to visual

error was largest for smallest visual errors, something that we also had seen in healthy adults (Marko et al., 2012). Unique to this study, we also found a significant effect of group [$F_{(1,38)}$ = 6.4, p = 0.016], suggesting that sensitivity to visual error was significantly smaller than normal in the ASD group and that the ASD group learned less from visual errors than the TD group. There was no significant interaction [$F_{(3,36)}$ = 0.21, p = 0.89].
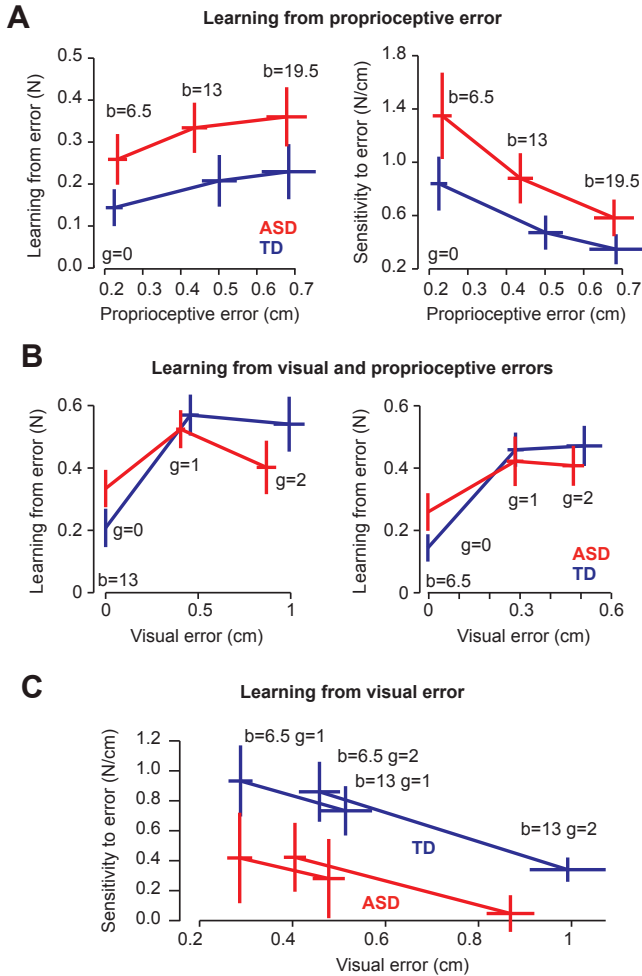

Figure 2. Learning in response to visual and proprioceptive errors. All error-bars are between-subject SEM. A) Adaptive response (left) and sensitivity (right) to proprioceptive errors. We found children with ASD showed increased adaptation and sensitivity to proprioceptive error of different sizes. B) Adaptive response to the b = 13 force field (left) and to the b = 6.5 force field (right). There was no group difference in adaptation in response to proprioceptive and visual errors given together, most clearly demonstrated by the g = 1 condition. C) Sensitivity to visual error alone. We found children with ASD exhibited less sensitivity to visual error than TD children.

As the symptoms of ASD vary along a spectrum, we wondered how sensitivity to error was distributed across subjects. In **Figure 3A** we have plotted the average visual and proprioceptive error-sensitivities of each child. We found that children who exhibited greater proprioceptive error-sensitivity tended to have smaller visual error-sensitivity. This trend was true within in the ASD population alone [r = -0.57, p = 0.0089], as well as across the two populations [r = -0.54, p < 0.001]. There was no significant correlation in the TD population alone [r = -0.35, p = 0.13].

We have summarized the behavioral data in **Figure 3B**. We found that sensitivity to proprioceptive error was significantly larger in the ASD group [$t_{(38)}$ = -2.1, p = 0.035], and sensitivity to visual error was significant larger in the TD group [$t_{(38)}$ = 2.5, p = 0.016]. To ensure these results were not the product of our sensitivity analysis or due to the process of normalizing by error, we looked at the average proprioceptive adaptation, λ_p, and average visual adaptation, λ_v, as well. We again found that children with ASD show greater adaptation in response to proprioceptive error [$t_{(38)}$ = 2.4, p = 0.022] and less adaptation in response to visual error [$t_{(38)}$ = -2.6, p = 0.013]. Corresponding to our sensitivity results, there was a negative correlation between the amount of adaptation in response to visual and proprioceptive errors [r = -0.32, p = 0.044]. Therefore, our findings appear robust to our methods of calculating sensitivity to error.

Relationship to cerebellar anatomy

Reach adaptation is known to depend on the integrity of the cerebellum (Criscimagna-Hemminger et al., 2010; Donchin et al., 2012; Smith and Shadmehr, 2005), in particular those regions known to be involved in sensorimotor control. Thus, we hypothesized that the behavioral differences between groups may be associated with anatomical differences in the cerebellum.

To test our hypothesis, we acquired anatomical MRIs and identified the coarse- and fine-scale sensorimotor cerebellum in each child. The coarse-scale sensorimotor cerebellum is the region that, in adults, exhibits the largest resting state connectivity to the sensorimotor network of the cerebral cortex (Buckner et al., 2011). The cortical network includes the entire motor and somatosensory cortices (Thomas Yeo et al., 2011), and in the cerebellum includes the anterior cerebellum, extending into lobule VI, and parts of lobule VIII. The coarse-scale sensorimotor cerebellum is identified for a typical ASD and a typical TD child in **Figure 4A** in red. The volume of coarse-scale sensorimotor cerebellum appeared smaller in the ASD child. Indeed, we found a significant difference in volume between groups [$t_{(36)}$ = -2.39, p = 0.022], with the ASD group showing a smaller volume than TD children (**Figure 4B**).
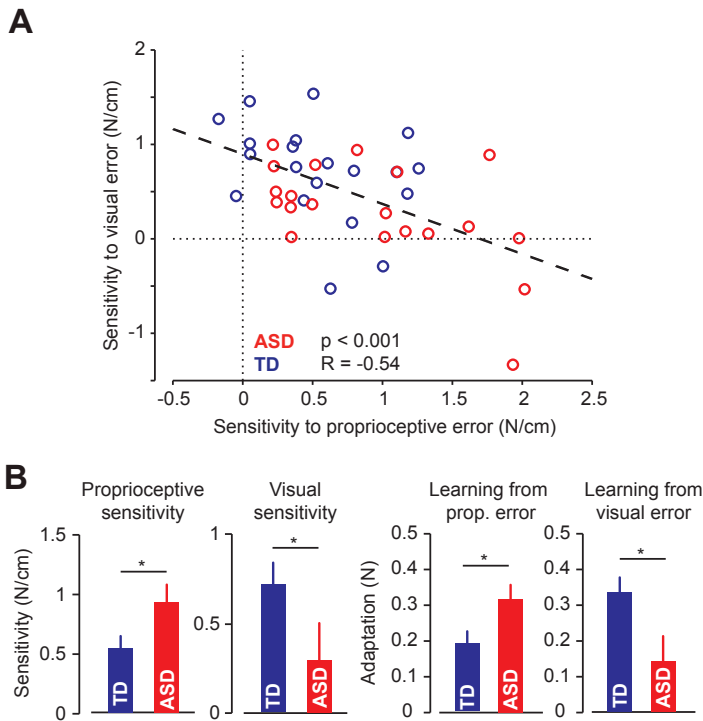
Figure 3. Relationship between sensitivity to visual and proprioceptive errors. A) Average proprioceptive sensitivity (x-axis) and visual sensitivity (y-axis) for each subject. We found a significant trade-off between sensitivities, such that as sensitivity to error in one modality increased, sensitivity in the other modality decreased. B) Overall response to error. We found children with ASD to have a greater sensitivity to proprioceptive errors and greater adaptation in response to a proprioceptive error, and TD children to have greater sensitivity to visual errors and greater adaptation in response to visual errors.

We then refined our atlas by focusing only on regions of the sensorimotor cerebellum that included the hand and foot representation, but excluded the tongue representation (Thomas Yeo et al., 2011). For this fine-scale sensorimotor representation of the cerebellum, we again found that the ASD group had a significantly smaller volume [$t_{(36)}$ = -2.59, p = 0.013], as shown in **Figure 4B**. This finding is independent of our behavioral data, and suggests that the region of the cerebellum involved in control of movements is smaller than normal in children with ASD

To check the specificity of this result, we considered two other volumes – the total cerebellar volume (TCV), and the total brain volume (TBV). TCV was found as the sum of the volumes of the entire cerebellum calculated using the 7 network atlas. TBV was measured by FreeSurfer, which includes the grey matter and white matter for the whole cerebrum and

cerebellum, and excludes the dura, CSF, and ventricles. We found no significant difference between groups, for both total cerebellar volume [$t_{(36)}$ = -1.67, p = 0.10] and total brain volume [$t_{(36)}$ = -0.54, p = 0.59].
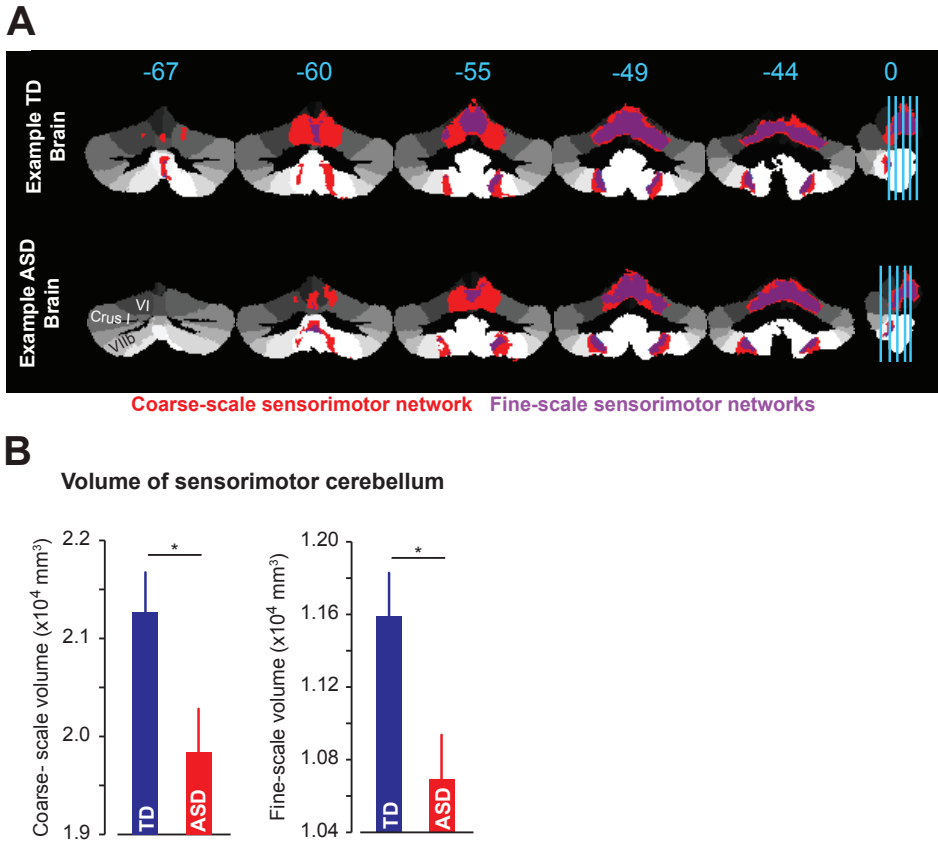

Figure 4. Volume of the sensorimotor cerebellar regions. A) Example TD subject (top) and example ASD subject (bottom), highlighting the coarse-scale sensorimotor region in red and the fine-scale sensorimotor region in purple. The ASD subject had a smaller than normal volume for both regions. B) Group data for the volume of both the coarse- and fine-scale sensorimotor regions, demonstrating a smaller sensorimotor cerebellar volume for children with ASD. Error bars are between-subject SEM.

Does the volume differences in the cerebellum relate to differences in the learning task? To understand the relationship between sensitivity to error and volume of the sensorimotor cerebellum, we used a generalized linear model (GLM). In the GLM, the volume of the coarse-scale sensorimotor cerebellum for each child was the dependent variable, and the

sensitivity to visual and proprioceptive errors of each child were the independent variables. As a result, the GLM included factors of group, sensitivity to proprioceptive error, sensitivity to visual error, and group by sensitivity interactions. We found that the GLM was significant (p = 0.008, **Table 2**), suggesting that these factors were important correlates of sensorimotor cerebellum volumes. The GLM identified a main effect of group, a main effect of visual sensitivity, and a group by proprioceptive sensitivity interaction. The main effect of visual sensitivity indicates that, across both groups of children, as the volume of the sensorimotor cerebellum increased, visual sensitivity increased. The interaction suggests that there was a significantly more positive relationship between proprioceptive sensitivity and volume for the ASD group.

Table 2. GLM Results for the coarse-scale sensorimotor volume. GLM analysis revealed a significant main effect of visual sensitivity and a significant group by proprioceptive sensitivity interaction on the volume of the coarse-scale sensorimotor region.

Omnibus Test	Likelihood Ratio Chi-Square	df	Sig.
	15.65	5	0.008
Tests of Model Effects			
Source	Type III		
	Wald Chi-Square	df	Sig.
(Intercept)	901.142	1	<0.001
Group	10.482	1	0.001
Proprioceptive Sensitivity	1.593	1	0.207
Visual Sensitivity	4.799	1	0.028
Group * Proprioceptive Sensitivity	6.705	1	0.01
Group * Visual Sensitivity	1.988	1	0.159

All of these results were confirmed when we repeated our analysis on the volume of the fine-scale sensorimotor cerebellum (**Table 3**). Further, we found that the model fit improved for the fine-scale sensorimotor cerebellum (Akaike's Information Criterion: 638.7) as compared to the coarse-scale sensorimotor cerebellum (Akaike's Information Criterion: 680.9).

Table 3. GLM Results for the fine-scale sensorimotor volume. GLM analysis found a significant main effect of visual sensitivity and a significant group by proprioceptive sensitivity interaction on the volume of the fine-scale sensorimotor region, matching the findings for the GLM analysis of the coarse-scale sensorimotor volume.

Omnibus Test	Likelihood Ratio Chi-Square	df	Sig.
	16.953	5	0.005
Tests of Model Effects			
Source	Type III		
	Wald Chi-Square	df	Sig.
(Intercept)	804.05	1	<0.001
Group	12.126	1	<.001
Proprioceptive Sensitivity	1.269	1	0.26
Visual Sensitivity	4.605	1	0.032
Group * Proprioceptive Sensitivity	7.585	1	0.006
Group * Visual Sensitivity	2.323	1	0.127

DISCUSSION

Prior to being able to complete complex motor actions, one must be able to learn to produce appropriate motor commands. From infancy, these motor abilities adapt and develop as our body changes in size and strength, and as we interact with tools that have distinct dynamics. Motor impairments are present in ASD from infancy (Provost et al., 2006), and are potentially rooted in an abnormal ability to learn motor control. In the present study, we considered an elementary motor learning task in which reaching movements were perturbed (Shadmehr and Mussa-Ivaldi, 1994), resulting in errors that were sensed by proprioceptive and visual feedback. We found that children with ASD responded normally to these perturbations during the movement, demonstrating an intact sensorimotor reflex loop. The children also learned from this error, altering their motor commands on the next trial. Remarkably, children with ASD outperformed health controls when learning from proprioceptive errors, but underperformed when learning from visual errors. Because the task that we studied depended critically on the integrity of the cerebellum, we quantified the volume of sensorimotor regions of this structure via anatomical MRIs. We found that whereas the volume of the cerebellum as a whole, and the volume of the brain as a whole, was normal in ASD, the volume of sensorimotor cerebellum was smaller than normal in the children with autism, and that this volume related to the patterns of learning from error. Therefore, the deficits in the sensorimotor regions of the cerebellum may underlie the motor learning abnormalities exhibited in autism.

Sensitivity to error

Perhaps one of the most interesting aspects of studying a disorder such as autism is that in certain tasks, individuals with the disorder can outperform healthy controls. For instance, Nakano and colleagues (Nakano et al., 2009, 2012) studied adults with autism in their ability to integrate sensory information for the identification of an object. When asked to identify the object from visual cues, individuals with ASD made more errors than controls. However, when asked to identify an object based on haptic tracing, the ASD group made fewer errors than controls. In light of our results, these findings seem consistent with the idea that people with ASD may be better than normal in utilizing proprioceptive information, but worse than normal in utilizing visual information.

In another example of better than normal performance in autism, and the inspiration for our current study, we found that children with ASD showed greater than normal generalization of force field adaptation in intrinsic, or proprioceptive, coordinates (Haswell et al., 2009; Izawa et al., 2012b). In other words, after learning to fully compensate for a force field, children with ASD expressed that learning better than controls in a new workspace that was proprioceptively similar to the original workspace. We had interpreted this to reflect an increased ability to learn from proprioceptive error during motor adaptation (Haswell et al., 2009; Izawa et al., 2012b), but had been unable to directly measure learning from proprioception. In the current paper, we relied on single trial learning with a mix of visual and proprioceptive errors, and were able to measure learning from proprioceptive and visual errors to directly test our hypothesis.

Here, we found that children with ASD showed increased learning in response to proprioceptive feedback. Importantly, we also found that children with ASD showed deficient learning in response to visual feedback. This pattern is perhaps consistent with the often reported finding that individuals with ASD are less able to imitate (Dowell et al., 2009; Stieglitz Ham et al., 2007; Vanvuchelen et al., 2007; Williams et al., 2004) or recognize biological (Cattaneo et al., 2007; Cook et al., 2009). Specifically, individuals with ASD show difficulties in imitation of movement kinematics, rather than emulation of a movement goal (Gowen, 2012; Hobson and Hobson, 2008; Wild et al., 2011). If the ability to learn from visual feedback regarding one's own movements is impaired, it could potentially hinder the ability to learn a complex series of movement kinematics performed by others.

We note, however, that our measure of learning from visual error is not an absolute quantity, as learning from error can change with task parameters (Burge et al., 2008; Marko et al., 2012; Wei and Kording, 2008). For instance, in a force field adaptation task in which visual feedback was removed, adaptation occurred normally compared to adaptation with cursor feedback available, reflecting an increase in proprioceptive sensitivity (Scheidt, 2005).

Additionally, task structure can alter sensitivity to error (Herzfeld et al., 2014b), such that subjects up-regulate learning in the presence of consistent errors (Gonzalez Castro et al., 2014). Perhaps this can explain our previous findings: when children with ASD were asked to make reaching movements in the presence of a visual rotation, a perturbation in which the cursor feedback is rotated relative to the reach direction causing a visual error but no proprioceptive error, children with ASD were able to adapt at normal speeds (Gidley Larson et al., 2008). Given the flexible nature of sensitivity to error, it is possible that consistent, repeated visual errors up-regulate sensitivity in the ASD group. In our task, the history of the perturbations and the resulting errors were similar between the two groups, suggesting that the differences that we observed in learning from error were due to inherent between group differences in error sensitivity

Autism and the cerebellum

Despite the range of potential upstream physiological causes of autism, there are still key diagnostic features that define the disorder – deficits in social and communication skills, and repetitive and stereotyped interests and behaviors. How might the cerebellum contribute to these features? It is important to note that the cerebellum is not simply a motor structure, and is reciprocally connected to association regions within the frontal cortex (Middleton and Strick, 2001) and the basal ganglia (Middleton, 2000). Children with congenital or early cerebellar insults show a range of autistic symptoms (Tavano et al., 2007), while adults with acquired cerebellar disease experience a host of non-motor symptoms, termed the Cerebellar Cognitive Affective Syndrome, impacting executive function, visual spatial abilities, language, and affect (Schmahmann and Sherman, 1998). Therefore, damage to the cerebellum can have effects far outside of the motor domain.

Importantly, the cerebellum has been the location of a number of physiological abnormalities for individuals with autism. Lower Purkinje cell numbers are the most consistent post mortem finding (Bailey, 1998; Kemper and Bauman, 1998; Ritvo E, 1986; Whitney et al., 2008). Imaging studies with targeted measurements of the vermis have found it to be smaller in size in autism (Courchesne et al., 2001; Hashimoto et al., 1995; Murakami et al., 1989; Scott et al., 2009). However, the results are not always clear, and reports of overall cerebellar volume are mixed, tending to find an overall larger volume compared to controls (Courchesne et al., 2001; Murakami et al., 1989; Sparks et al., 2002; Stanfield et al., 2008). Likewise, functional imaging studies have found children with ASD to have both reduced (Mostofsky et al., 2009) and increased (Allen and Courchesne, 2003) cerebellar activation during a simple movement task. Here, rather than examining cerebellar volume based on

anatomical distinctions, we were able to examine a functional region of the cerebellum, and found a clear relationship between cerebellar volume and learning from proprioceptive and visual errors.

The sensorimotor cerebellar network and motor learning

Dating back to the 1940's, recordings during proprioceptive and tactile stimulation found two sets of sensory maps in the cerebellum: an inverted homunculus stretching primarily over the anterior lobe, and two smaller representations in the hemispheres of lobule VIII (Adrian, 1943; Snider and Stowell, 1944). This sensory information reaches the cerebellum through both spinocerebellar projections and neocortical afferents projected through the pontine nuclei (Manni and Petrosini, 2004). It came as no surprise, therefore, that Buckner and colleagues (Buckner et al., 2011) chose to validate the findings of their resting state connectivity maps with a motor task, and found corresponding functional activation for simple hand, foot, and tongue movements (see Figure 5 in Buckner et al., 2011). But do these sensorimotor maps relate to motor adaptation? In a study of cerebellar patients using voxel based morphometry, or a voxel-by-voxel quantification relating the density of grey matter to performance in a reaching task, Donchin et al. (2012) found that anterior regions from lobules IV-VI were related to the ability to adapt in a force field or visual motor rotation paradigm. Importantly, the region of the cerebellum most relevant to learning in our task appears to correspond to the sensorimotor cerebellum described by Buckner et al., 2011.

Apart from our behavioral results, we found that the volume of the sensorimotor region of the cerebellum was smaller than normal in children with ASD. When relating this volume to learning from error, we found a main effect of visual sensitivity and a group by proprioceptive sensitivity interaction. The main effect of visual sensitivity on volume echoes that which was described in Donchin et al. (2012): that visual motor adaptation depended on integrity of this region, and greater volume will allow for improved performance. For our task, higher visual sensitivity can be considered comparable to improved visual performance, which correlates with higher volume. Potentially, cerebellar Purkinje cell loss in ASD (Bailey, 1998; Kemper and Bauman, 1998; Ritvo E, 1986; Whitney et al., 2008) may cause this reduced volume, and may subsequently reduce one's ability to learn from visual error.

The group by proprioceptive interaction is more difficult to interpret. We found that there is a more positive relationship between volume and proprioceptive sensitivity in the ASD group than in the TD group. A popular theory explaining the underlying basis of ASD claims that there is a bias towards short range connections in the brain, and against long range connections (Mostofsky and Ewen, 2011). With no direct connections between the

visual cortex and the cerebellum, visual information likely travels through the parietal cortex before it is relayed to the cerebellum through the pons (Glickstein, 2000). Proprioceptive information, however, is relayed both through the pons from the cortex, and through the spinocerebellar tract (Manni and Petrosini, 2004). Therefore proprioceptive feedback may have an advantage, relative to visual feedback, in that it can be received by the cerebellum both from the shorter path through the somatosensory cortex as well as directly through the spinocerebellar tract. This may alter the path of development, subsequently impacting volume.
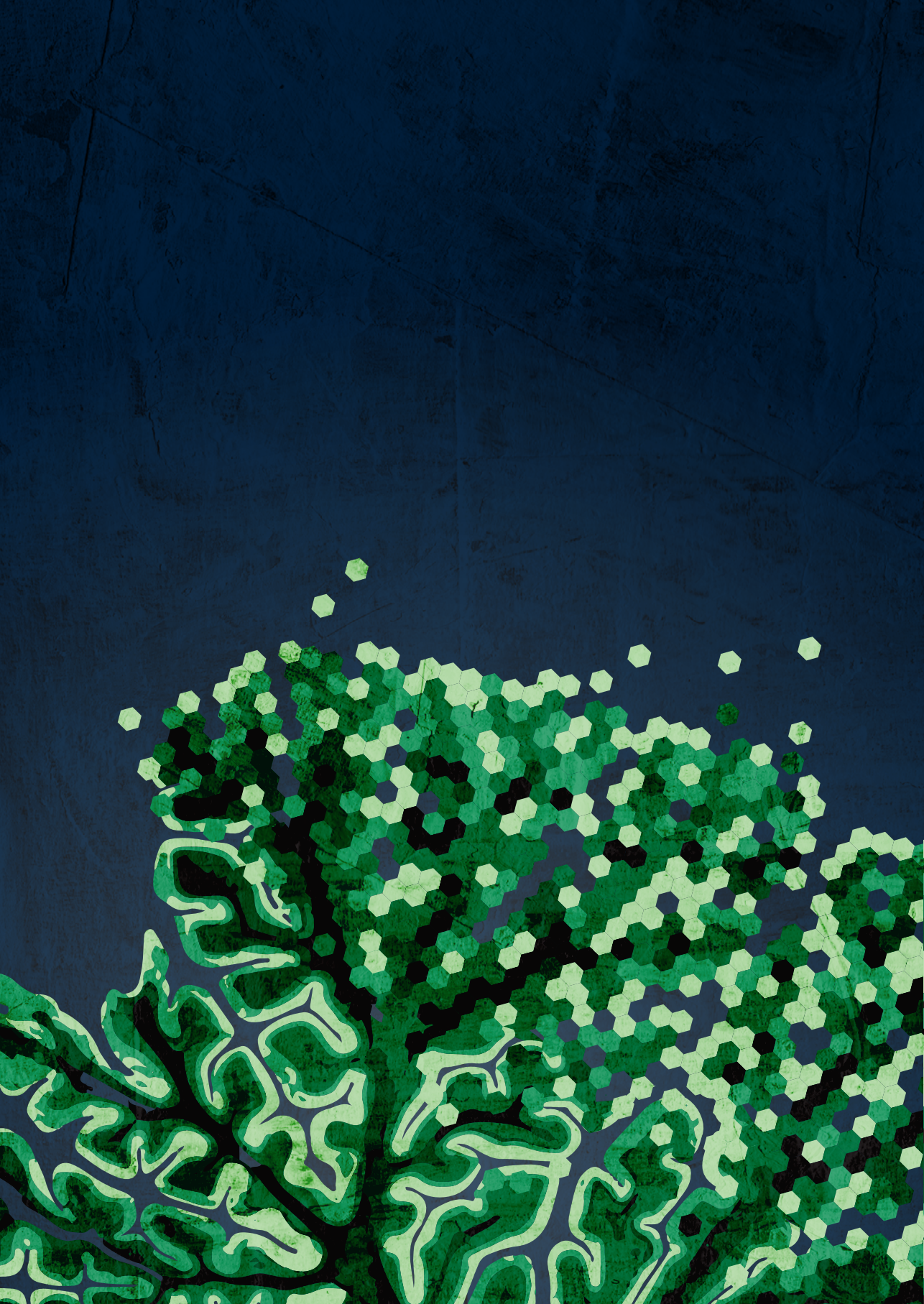
A limitation of our work is that our analysis of the cerebellum relied on an atlas that was developed from anatomical data of healthy adults (Buckner et al., 2011). Our analysis is focused not only on children, but children with a developmental disorder. Though the cerebellum does have a protracted development, reaching peak volume around age 15 (Tiemeier et al., 2010), the children in our study were restricted in age and likely at a similar developmental stage. It would be exciting to track the evolution of a functional cerebellar atlas through development, even more so within an autism population. Regardless, based on anatomy alone, the region that we can best predict to be related to motor learning in the cerebellum is smaller than normal in children with ASD. This anatomical finding highlights a potential contributor to the multitude of motor impairments that impact children with ASD.

Acknowledgements

Author contributions

Thomas Hulst analyzed data; interpreted results; approved the final version of the manuscript.

Cerebellar patients do not benefit from cerebellar or M1 transcranial direct current stimulation during force field reaching adaptation

Thomas Hulst [1,2], Liane John [1], Michael Küper [1], Jos N. van der Geest [3], Sophia L. Göricke [4], Opher Donchin [5], Dagmar Timmann [1]

[1] Department of Neurology, Essen University Hospital, University of Duisburg-Essen, 45122 Essen, Germany
[2] Erasmus University College, Rotterdam, The Netherlands
[3] Department of Neuroscience, Erasmus MC, 3000 CA Rotterdam, The Netherlands
[4] Department of Diagnostic and Interventional Radiology and Neuroradiology, Essen University Hospital, University of Duisburg-Essen, 45122 Essen, Germany
[5] Department of Biomedical Engineering, Zlotowski Center for Neuroscience, Ben-Gurion University of the Negev, Beer-Sheva 8410501, Israel
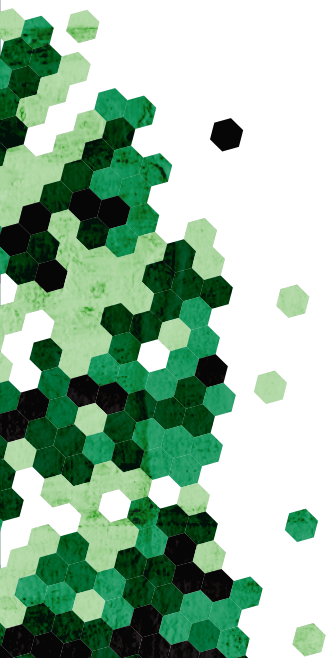
ABSTRACT

Several studies have identified transcranial direct current stimulation (tDCS) as a potential tool in the rehabilitation of cerebellar disease. Here, we tested whether tDCS could alleviate motor impairments of subjects with cerebellar degeneration. Three groups took part in this study: twenty individuals with cerebellar degeneration, twenty age-matched controls and thirty young controls. A standard reaching task with force field-perturbations was used to compare motor adaptation between groups and to measure the effect of stimulation of the cerebellum or primary motor cortex (M1). Cerebellar subjects and age-matched controls were tested during each stimulation type (cerebellum, M1 and sham) with a break of one week between each of the three sessions. Young controls were tested during one session under one of three stimulation types (anodal cerebellum, cathodal cerebellum or sham). As expected, individuals with cerebellar degeneration had a reduced ability to adapt to motor perturbations. Importantly, cerebellar patients did not benefit from anodal stimulation of the cerebellum or M1. Furthermore, no stimulation effects could be detected in ageing and young controls. The present null results cannot exclude more subtle tDCS effects in larger subject populations and between-subject designs. Moreover, it is still possible that tDCS affects motor adaptation in cerebellar subjects and control subjects under a different task or with alternative stimulation parameters. However, for tDCS to become a valuable tool in the neurorehabilitation of cerebellar disease, stimulation effects should be present in group sizes commonly used in this rare patient population and be more consistent and predictable across subjects and tasks.

Keywords: tDCS, cerebellar degeneration, motor adaptation, rehabilitation.

INTRODUCTION

The cerebellum is widely regarded as an essential structure for motor control and motor adaptation. Damage to the cerebellum leads to a number of specific motor impairments commonly referred to as ataxia (Flourens, 1824; Holmes, 1908). One specific symptom of ataxia, easily reproduced in the laboratory, is difficulty adapting to perturbations of the motor system (Sanes et al., 1990). Specifically with regard to reaching movements, patients with cerebellar degeneration demonstrate impaired motor adaptation during reaching tasks with force field (Maschke et al., 2004a) and visuomotor perturbations (Tseng et al., 2007). While the motor performance deficits of patients with cerebellar degeneration are well-described, the therapeutic options for the treatment of cerebellar disease are limited (Ilg et al., 2014; Marsden and Harris, 2011).

In recent years, transcranial direct current stimulation (tDCS) has accrued considerable interest of the neuroscientific community for its scientific applications and therapeutic potential (Fregni and Pascual-Leone, 2007; Nitsche et al., 2008; Stagg and Nitsche, 2011). The technique has been identified as a possible tool in the rehabilitation after stroke (Hummel and Cohen, 2006) and it has also been suggested recently that it may provide benefits to patients with cerebellar disease (Grimaldi et al., 2014b). Several studies have explored the physiological basis of tDCS effects and provide us with likely mechanisms how tDCS can aid in neurorehabilitation. The studies demonstrated that polarity-specific excitability changes and LTP-like (long-term potentiation) plasticity are induced by stimulation of the primary motor cortex (M1) (Nitsche et al., 2000; Stagg and Nitsche, 2011). Furthermore, it was demonstrated that cerebellar tDCS can influence the excitability of the cerebellum, which in turn has a polarity-specific effect on cerebellar-M1 connectivity (Galea et al., 2009). These underlying mechanisms likely form the basis of tDCS effects that are observed in motor adaptation experiments. For instance, in healthy subjects, adaptation to motor perturbations are quicker when anodal tCDS is applied over the cerebellum (Avila et al., 2015; Block and Celnik, 2013; Herzfeld et al., 2014a; Jayaram et al., 2012). Moreover, short-term retention (Galea et al., 2010a; Hunter et al., 2009; Panouillères and Jenkinson, 2015) and long-term retention (Reis et al., 2009) is improved when anodal tDCS is applied over M1. Motor adaptation experiments utilizing non-invasive brain stimulation in cerebellar patients are much rarer, but two recent pilot experiments have revealed behavioral improvements in cerebellar patients during tDCS stimulation (Grimaldi et al., 2014a; Pozzi et al., 2013). This has further established the potential role for tDCS in the treatment of degenerative cerebellar ataxia. However, it remains unclear if all aforementioned effects of tDCS apply to cerebellar ataxia patients, since cerebellar degeneration may hamper tDCS excitability effects (Ugawa et al., 1994).

On the other hand, a recent study identified several areas of the cerebellum which degenerate similarly in both cerebellar ataxia patients and healthy ageing subjects (Hulst et al., 2015). Although older adults are generally slower to adapt to perturbations of the motor system (Seidler et al., 2010), motor adaptation in healthy elderly subjects is enhanced when anodal tDCS is applied to the cerebellum (Hardwick and Celnik, 2014). Therefore, motor adaptation may be enhanced in patients after cerebellar tDCS as well. Likewise, M1 stimulation improves motor learning and retention in ageing subjects (Goodwill et al., 2013; Panouillères and Jenkinson, 2015; Zimerman et al., 2013), which in turn indicates potential beneficial effects of M1 stimulation for cerebellar patients.

The aim of the present study was to compare motor adaptation in cerebellar patients with age-matched controls, and to test whether the positive effects of tDCS as described in healthy ageing could also be established in cerebellar patients. Furthermore, a second between-subject experiment was carried out in a group of young controls to control for possible carryover effects. A standard reaching task with force field-perturbations was used to measure motor adaptation. Neuroimaging was used to identify the degree and pattern of cerebellar degeneration in patients. We expected to find impaired motor adaptation in cerebellar patients, characterized by slower and incomplete adaptation to the force field-perturbations. If tDCS could significantly alleviate the difficulties patients have in adapting to perturbations, this would further suggest a potential role for tDCS as a supportive treatment in cerebellar disease.

METHODS

Experiment 1

Twenty individuals with cerebellar degeneration (8 females; mean age ± SD of 53.7 ± 10.8 years; range 30–74 years) and twenty age-matched controls without any known neurological diseases (9 females; mean age ± SD 54.6 ± 11.2 years; range 28–74 years) participated in this study. All subjects were right-handed as assessed by the Edinburgh Handedness Inventory (Oldfield, 1971). An overview of the subjects' characteristics can be found in **Table 1**. The severity of cerebellar symptoms in cerebellar participants were assessed by one of two experienced neurologists (DT & MK) based on the International Cooperative Ataxia Rating Scale (ICARS; Trouillas et al., 1997) and the Scale for the Assessment and Rating of Ataxia (SARA; Schmitz-Hübsch et al., 2006). Eight cerebellar participants had a genetically defined spinocerebellar ataxia (SCA). Four participants presented with autosomal dominant cerebellar ataxia (ADCA) type III. Seven cerebellar participants had sporadic adult onset ataxia of unknown etiology (SAOA). One cerebellar participant

presented with cerebellar degeneration caused by cerebellitis. These disorders are known to primarily affect the cerebellum (Gomez et al., 1997; Timmann et al., 2009). All subjects gave informed oral and written consent. The experiment was approved by the ethics committee of the medical faculty of the University of Duisburg-Essen and conducted in accordance with the Declaration of Helsinki.

Table 1. Overview Cerebellar subjects and Control subjects. Cerebellar subjects were age-matched with the control subject on the right side of the table.

Cerebellar subjects								Controls			
ID	Age	Sex	Diagnosis	Disease duration	ICARS (total/100)	ICARS UL (total/20)	LI	ID	Age	Sex	LI
P01	30	M	SAOA	9 years	38.5	7.5	0.16	C01	28	M	0.79
P02	34	M	SAOA	22 years	17	3	0.46	C02	33	M	0.69
P03	46	M	SAOA	7 years	8	0	0.50	C03	47	M	0.55
P04	47	M	ADCA III	17 years	32.5	4.5	0.18	C04	47	M	0.77
P05	48	M	SCA 14	25 years	20	3	0.22	C05	50	M	0.81
P06	48	F	ADCA III	28 years	19	1	0.33	C06	47	F	0.75
P07	50	F	SCA 14	17 years	17	1	0.30	C07	52	F	0.61
P08*	51	M	SAOA	20 years	61	9	-0.08	C08*	55	F	0.50
P09	51	M	ADCA III	11 years	47	5	0.30	C09	51	M	0.59
P10	52	M	ADCA III	6 years	19.5	3	0.43	C10	54	M	0.67
P11	53	M	Cerebellitis	10 years	46	5	0.25	C11	63	M	0.72
P12	54	F	SCA 14	25 years	27	3.5	0.40	C12	55	F	0.68
P13	54	F	SAOA	18 years	31	4.5	0.30	C13	55	F	0.57
P14	58	F	SCA 6	8 years	43.5	10	0.34	C14	57	F	0.67
P15	61	M	SCA 6	4 years	9	0	0.20	C15	63	M	0.74
P16	63	M	SAOA	9 years	20.5	5	0.56	C16	64	M	0.70
P17	66	F	SCA 6	12 years	43.5	5	0.19	C17	64	F	0.71
P18	66	F	SCA 6	15 years	47	5	0.28	C18	65	F	0.78
P19	67	F	SCA 6	3 years	33	5	0.22	C19	68	F	0.64
P20	74	M	SAOA	16 years	12	2	0.22	C20	74	M	0.58

*SCA6 = spinocerebellar ataxia type 6; SCA14 = spinocerebellar ataxia type 14; SAOA = sporadic adult onset ataxia; ADCA III = autosomal dominant ataxia type III; ICARS = International Cooperative Ataxia Rating Scale (Trouillas et al., 1997). ICARS UL = score of right upper limb in finger-to-nose test, finger-to-finger test, pronation/supination and Archimedes spiral drawing. Disease duration is years since presentation of the first symptoms. LI = average final learning index over 3 experimental sessions. * = Cerebellar subject and age-matched control which were removed due to a high number of disregarded movements in the cerebellar subject.*

Task

All subjects participated in a standard force field task (Shadmehr and Mussa-Ivaldi, 1994) on a setup largely similar to the one used by Rabe and colleagues (Rabe et al., 2009). Subjects held the handle of a two-joint robotic manipulandum in their right hand while seated in a comfortable chair. The handle of the robotic manipulandum was able to move freely in the horizontal plane underneath a horizontal projection screen located above the subjects' hand (**Figure 1A**). Hand position was recorded using encoders on each of the manipulandum's motors with a resolution of 106 counts per revolution and a sample rate of 200 Hz using the analog inputs of a motor controller card (DMC-1826; Galil Motion Control). The distance to the manipulandum and the chair height were adjusted individually to ensure a comfortable position and good vision of the projection screen. Vision of the subjects' arm was blocked by a cloth stretched from the projection screen to the subjects' neck. The position of the handle was represented by a green circular cursor with diameter of 6 mm and directly corresponded with the position of the right hand of the subject. The origin was indicated by a black circle with a diameter of 14 mm in the middle of the projection screen. Participants were instructed to move the cursor into the origin at the start of each trial. After a delay of 2500 ms, a black circular target with a diameter of 14 mm appeared in one of six target locations positioned 10 cm from the origin. The target locations were located at an angle of 30°, 90°, 150°, 210°, 270° and 330° from the origin and were presented in a pseudorandom order so that each target position appeared once every six trials. Subjects were instructed to move the cursor from the origin to the target by making a rapid hand-movement as soon as the target appeared (**Figure 1B**). Subjects received instructions to move through the target and not stop at the target location, as the handle was gently brought to a stop by a simulated cushion implemented by the manipulandum motors. The cursor was extinguished after it passed out of a 10 cm radius from the position of the origin. The disappearance of the cursor indicated the end of a movement, at which point a cushioning force was applied by the robot to safely slow the hand to a stop. After the movement ended, the robot motors pushed the handle of the manipulandum back to the starting position. The cursor reappeared when the handle came within 2 cm of the origin location. During the cushion phase and push back phase, subjects received feedback on movement speed and whether they hit the circular target. When subjects hit the target and the movement was neither too fast nor too slow, the target became green and a sound was played to indicate success. When subjects hit the target, but the movement was too fast, the target turned yellow. The target turned blue when the cursor hit the target, but the movement was too slow. If participants failed to hit the target, the target was turned off and provided no further feedback. An adaptive mechanism based on movement duration was used to determine whether a movement was too fast, too slow or had the correct speed. Initially, a movement was considered to have the correct speed when it was completed within a time window

centered at 500 milliseconds with an upper- and lower-bound of 250 milliseconds. In other words, movement durations between 250 ms and 750 ms were considered as having the correct speed, movement durations below 250 ms were considered too fast and movement durations above 750 ms were considered as too slow. From the first movement onwards, the upper- and lower-bound of the time window was reduced by 10% each time a movement was the correct speed and increased by 10% when a movement was either too fast or too slow. The adaptive time window and feedback from the experimenter encouraged subjects to move at similar speeds, while it also made sure participants received similar amounts of positive feedback thereby preventing motivational differences that might be driven by differences in performance.
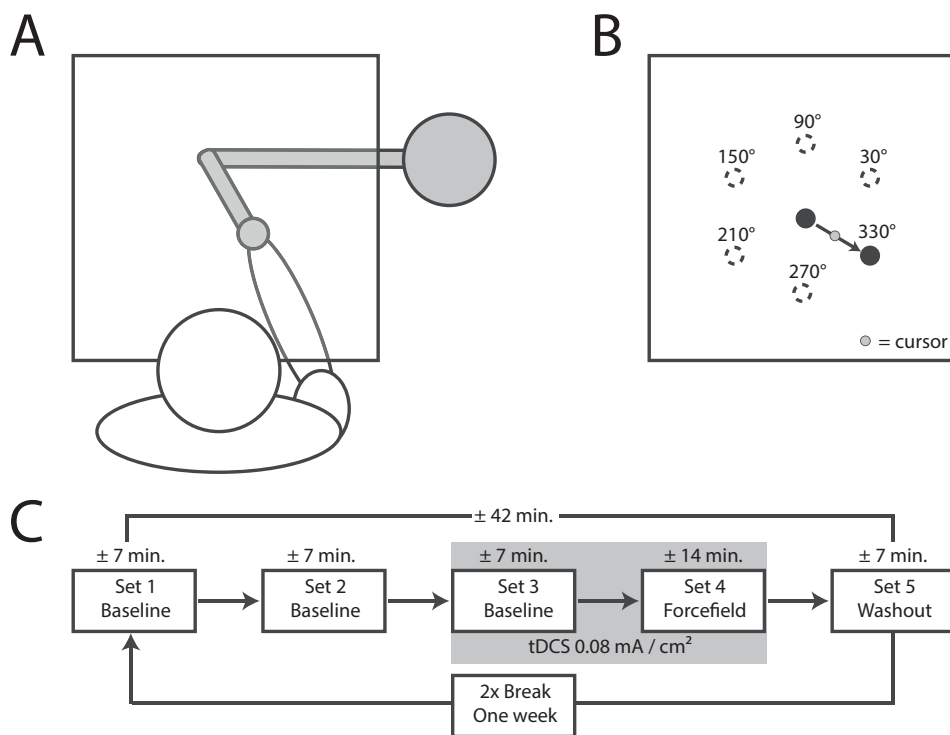
Figure 1. Experimental setup. A: An overview of the setup used in the behavioral task. Drawings are not to scale. The horizontal projection screen is illustrated as transparent for the purpose of this figure. Subjects were unable to see the position of their own hand and robot manipulandum in the experiment, because the horizontal screen was covered with a blank paper. A piece of cloth stretched from the screen to the subjects' neck blocked vision of the subjects' arm. B: Targets were located 10 centimeters from the origin at 30°, 90°, 150°, 210°, 270° and 330° around the origin location. Subjects were instructed to move the cursor from the origin to the target as soon as the target appeared. C: Subjects performed 5 sets of movements in quick succession after which a break of exactly one week followed. Upon resuming the experiment one week later, subjects started with the first baseline set.

Each participant performed 5 sets of movements. The first three sets consisted of 84 trials without perturbations to allow participants to familiarize with the task (baseline phase). The fourth set consisted of 168 trials, of which 144 trials were force field (FF) trials and 24 trials were catch trials. In FF trials a velocity dependent force of $13N \cdot m^{-1} \cdot s^{-1}$ was applied by the robot motors perpendicular to the movement direction, pushing the participants' hand in the clockwise direction. In catch trials no external forces were applied, which in adapted participants produced movements in the opposite of the direction of the perturbation. Catch trials to each of the six target locations were pseudo-randomly interspersed over the entire set. The final set consisted of 84 trials without the application of external forces and without feedback on hand position by the cursor, as well as no visual or auditory feedback on movement time and success (washout phase) (**Figure 1C**).

tDCS-stimulation parameters

Participants were invited for three experimental sessions separated by exactly one week. During each session participants performed the same motor adaptation task, but under different stimulation regimes. In two of the three sessions, each participant received anodal tDCS stimulation: once over M1 and once over the cerebellum. In the third session, the recipient received sham tDCS stimulation over either M1 or cerebellum. The order of the three sessions was counterbalanced between participants. Stimulation parameters were largely similar to (Galea et al., 2010b). In short, anodal tDCS was delivered through two rubber electrodes (surface area: 25 cm^2) covered with conductive paste (Ten20 Conductive; Weaver) via a NeuroConn device (DC-Stimulator PLUS; NeuroConn). For cerebellar stimulation the anodal electrode was placed on the position of the right cerebellar cortex, with the center of the anodal electrode being 3 cm lateral to the inion, and the cathodal electrode was placed on the right buccinator muscle. The anodal electrode for M1 stimulation was placed by finding the area of the left cortex which elicited a response of the first dorsal interosseous muscle after single TMS (transcranial magnetic stimulation) pulses. TMS was delivered by a MagPro magnetic stimulator (MagPro; Dantec). The cathodal electrode was placed on the skin overlying the contralateral supraorbital region. During each experimental session, electrodes were placed over all the stimulation locations, so participants were blinded for stimulation location.

In both cerebellar and M1 anodal stimulation, the target stimulation intensity was set at 2 mA, resulting in a current density of 0.08 mA/cm^2. At the start of the third baseline set, current was ramped up from 0 mA to 2 mA in a period of 30 seconds after which anodal tDCS was applied for the entirety of the third and fourth sets (last baseline set and force field set). Due to variances in movement times between subjects, this resulted in slightly different stimulation times for each subject. On average, subjects were stimulated

for approximately 22 minutes (mean duration 1,289 ± SD 150 seconds). At the end of tDCS stimulation, current was ramped down from 2 mA to 0 mA in 30 seconds. In sham stimulation current was ramped-up in 30 seconds, remained at 2 mA for a duration of 60 seconds, after which current was ramped down again for the remainder of the experiment. This method of applying anodal and sham stimulation has shown to achieve a good level of blinding for participants (Gandiga et al., 2006). One experimenter (LJ) ran all the behavioral experiments and used a prepared set of stimulation codes in order to remain blind for stimulation polarity (sham or anodal). An experimenter (BB) who was not involved in the collection of behavioral data, deblinded the stimulation codes after data collection had ended.

Analysis of behavioral data

Behavioral data was analyzed using MATLAB with the Statistics Toolbox (MATLAB 8.5; Mathworks). Baseline aiming errors in the second baseline set (before tDCS onset) were averaged per target direction and subtracted from aiming errors in the force field and washout phase to correct for movement biases. Short movements with less than 2 centimeters of travel distance, movements in which hand velocity did not exceed 0.12 m/s and movements with aiming errors more than 4 absolute deviations from the median were discarded. Effectively, this removed trials in which a subject did not move or made a movement with no effective movement towards the target direction (i.e. oscillating movements around the starting location). In the case of one cerebellar participant (P08 in **Table 1**) this led to more than 50% of all trials being filtered, so we decided to exclude this participant and its age-matched control from group analyses. On average approx. 2.7% of all movements were filtered, with the amount of filtered trials not being significantly different between cerebellar subjects and healthy controls [paired t-test, $t_{(18)} = 0.06$, p = 0.94; range 0.8% - 9.1%].

Movement onset was defined to be the first time in a trial at which hand speed exceeded 0.04 m/s. For each trial, a straight movement would be along a line from the position at movement onset to the target. For each time point in each movement, the perpendicular distance of the cursor from the line determining a straight movement was called the error. The moment of maximum error (ME) was determined by finding the maximum perpendicular displacement after movement onset. The aiming error (AE), our primary measure of the error in each movement, was then the angle between a straight line movement and a line from the starting position to the position of ME. A learning index (LI) was also calculated based on the amount of AE in force field trials versus catch trials. This measure of learning has been described previously (Criscimagna-Hemminger et al., 2003; Maschke et al., 2004a) and corrects for subjects stiffening the arm in force field trials to compensate for movement

errors. When stiffening the arm, performance in force field trials will improve, but catch trials will not show a significant AE error in the opposite direction (Smith and Shadmehr, 2005). The LI was calculated as follows:

$$LI = \frac{AE_{Catch\ Trials}}{|AE_{Catch\ Trials}| + |AE_{Force\ Field\ Trials}|}$$ (Eq. 1)

In this definition, learning indexes can range between -1 and 1, with values between -1 and 0 indicating no learning and a LI of 1 indicating maximum learning. The LI was calculated per bin of seven consecutive trials (six force field trials and one catch trial). To assess final performance values, the LI was calculated over a bin of 36 trials (30 force field trials and 6 catch trials in each target direction). Mixed design ANOVAs in SPSS (SPSS Statistics 23.0; IBM) were used to test for differences in average movement times and speeds, with the between factor group (cerebellar subjects or healthy controls) and within factors stimulation type (cerebellum, M1 or sham) and set number. Greenhouse-Geisser adjustments were performed where appropriate. Differences in aiming errors during adaptation and washout were tested with a linear mixed model assuming compound symmetry for the fixed effects of group, simulation type and bin number. Differences in final learning indices were tested with the fixed effects of group and stimulation type. The unknown parameters in all mixed models were estimated via restricted maximum likelihood estimation and we report adjusted type III errors for the fixed effects. The degrees of freedom were estimated via Satterthwaite approximation. The linear mixed models described are essentially similar to a repeated measures ANOVA, but also allowed us to control for a continuous covariate (movement time). Furthermore, order effects were analyzed by testing with measurement day as a factor, instead of stimulation type, for both aiming errors and final learning indices. The p-values of pairwise comparisons were adjusted for multiple comparisons using the Bonferroni correction. Null results were tested for equivalence using the TOST-procedure (Schuirmann, 1987; Seaman and Serlin, 1998).

MR imaging

MR images in cerebellar subjects and their age-matched controls consisted of high-resolution three-dimensional T1-weighted MPRAGE scans using a 3T MRI scanner (Siemens Magnetom Skyra) with a 20-channel head/neck coil [TR, 2500 ms; TE = 4.37 ms, TI = 1100 ms; flip angle 7 deg; matrix, 256 x 100; voxel size $1.0 \times 1.0 \times 1.0$ mm³]. All MR scans were evaluated by an experienced neuroradiologist (SLG). None of the participants had radiological pathologies outside the cerebellum.

VBM

A voxel-based morphometry analysis was applied to the cerebellum of each subject as described previously (Hulst et al., 2015; Taig et al., 2012). The procedure will be briefly explained. The analysis was automated with an in-house program written for MATLAB 8.5 using the SUIT toolbox (version 3.1) (Diedrichsen et al., 2009), implemented in SPM12 (http://www.fil.ion.ucl.ac.uk/spm/software/spm12). First, each subjects' brain was segmented into grey matter, white matter and cerebrospinal fluid. Next, the grey matter of each subjects' cerebellum was normalized onto the template SUIT cerebellum. Each normalized cerebellum was then smoothed using a 6 x 6 x 6 mm^3 median filter. To test for differences in grey matter volume between cerebellar subjects and age-matched controls, a paired sample t-test was performed on the grey matter volume of individual voxels. The resulting map of t-scores was smoothed using a minimum filter, substituting each voxel with the minimum t-score in a 3 x 3 x 3 mm^3 neighborhood. To correct for multiple testing, 500 permutations maps of the original dataset were generated where, for each permutation, the match between MRI data and subject category (cerebellar subject or control) was randomized. The maximum t-score of each min-filtered permutation map was determined and a significance threshold was calculated by taking the 95th percentile of all maximum t-scores. Voxels with t-scores above the significance threshold in the original grey matter map were defined as significant. The result of this analysis was an assessment of the grey matter volume difference between cerebellar subjects and healthy controls on a voxel-by-voxel basis. To assess the correlation of the final learning index with cerebellar volume, Spearman's correlations between grey matter volume and final LI were calculated for both subject groups separately. Similarly to our analysis of t-scores, 500 permutations of the original dataset were generated and the significance threshold was calculated by taking the 95th percentile of all maximum correlations. The result of this analysis was an assessment of the correlation between grey matter volume and learning within the group of cerebellar subjects and within the group of healthy controls.

Experiment 2

The first experiment was carried out using a crossover design, testing the same subjects over multiple sessions under different stimulation conditions. A within-subject design has increased power over a between-subject design, which is an advantage when it is difficult to recruit enough subjects for a sufficiently powered between-subject experiment (like in the case of cerebellar patients). However, crossover designs can introduce carryover effects between measurement sessions. Although literature has described limited carryover effects during force field-adaptation when proper washout is applied (Caithness, 2004), to eliminate the possibility of carryover effects influencing consecutive measurement sessions,

an additional between-subject experiment was carried out. The experimental procedures of this second experiment were largely similar to the first experiment with several important differences described below.

Thirty young healthy controls were recruited (17 females; mean age ± SD of 23.9 ± 2.7 years; range 18–29 years) and gave informed oral and written consent. All subjects were measured during one session of the task described in Experiment 1. Ten subjects received sham stimulation of the cerebellum, ten subjects received anodal stimulation of the cerebellum and ten subjects received cathodal stimulation of the cerebellum. No subjects received stimulation of M1. Other stimulation parameters were equal to Experiment 1. On average, subjects were stimulated for approximately 22 minutes (mean duration 1,343 ± SD 114 seconds). The processing and analysis of behavioral data matched the methods described in Experiment 1. Approximately 2.7% of all movements were filtered, with the amount of filtered trials not being significantly different between groups [$F_{(2, 29)}$ = 1.98, p = 0.16; range 0.2% - 9.9%]. No MRI data was collected from these subjects.

RESULTS

Experiment 1: Movement times and speeds

An analysis of average movement times indicated no differences between cerebellar subjects and controls or a main effect of set and stimulation, but did uncover an interaction of set and group (**Table 2**). Analysis of the average movement speeds revealed a significant main effect of group and an interaction between set and group (**Table 2**). Whereas control subjects on average tended to speed up during the experiment, cerebellar subjects slowed down (**Figure 2**). Importantly, movement times and speeds in the set with velocity dependent force field trials (set 4) were not significantly different [movement time, pairwise comparisons, p = 0.22; speed, pairwise comparisons, p = 0.10], thus control subjects and cerebellar subjects were exposed to similar perturbation magnitudes.

Table 2. ANOVAs of average movement times and speeds.

ANOVA	Factors		F statistics	p
Average movement time				
	Between	**Group**	$F_{(1, 36)} = 2.48$	**0.12**
	Within	**Set**	$F_{(1.76, 63.4)} = 2.81$	**0.07**
		Set*Group	$F_{(1.76, 63.4)} = 6.183$	**0.005***
		Stimulation	$F_{(2, 72)} = 0.08$	**0.92**
		Stimulation*Group	$F_{(2, 72)} = 0.70$	**0.5**
		Set*Stimulation	$F_{(3.81, 137)} = 1.12$	0.35
		Set*Stimulation*Group	$F_{(3.81, 137)} = 0.61$	0.65
Average movement speed				
	Between	**Group**	$F_{(1, 36)} = 4.50$	**0.04***
	Within	**Set**	$F_{(2.18, 78.5)} = 2.42$	**0.09**
		Set*Group	$F_{(2.18, 78.5)} = 8.5$	**<0.001***
		Stimulation	$F_{(2, 72)} = 0.03$	**0.97**
		Stimulation*Group	$F_{(2, 72)} = 1.06$	**0.35**
		Set*Stimulation	$F_{(3.19, 115)} = 1.35$	0.26
		Set*Stimulation*Group	$F_{(3.19, 115)} = 0.84$	0.48

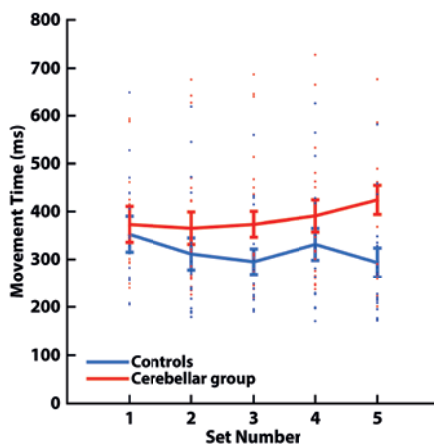*Boldface highlights important (in-text) comparisons. * = significant at the α = 0.05 level.*

Figure 2. Average movement times of age-matched controls in blue (n = 19) and cerebellar subjects (n = 19) in red. Movement times in this figure are averaged over all stimulation types. Movement times were calculated from movement onset to the moment the cursor extinguished after moving out of a 10 cm radius from the starting position. Set number 4 refers to the set with force field-perturbation trials. Error bars indicate standard error of the mean. There was no significant difference in movement times of the fourth set between age-matched controls and cerebellar subjects [pairwise comparisons, p = 0.22].

Data per subject

An overview of the raw data of one healthy control subject and one cerebellar subject from an adaptation set can be found in **Figure 3**. Movement trajectories initially deviate strongly from a straight trajectory in both the control and cerebellar subject. The control subject is able to adapt to the force field perturbation and produces straighter movement trajectories later in the set (**Figure 3A**). As a consequence, the average aiming error of the control subject during the force field set decreases, while the aiming error in the negative direction in catch trials increases. This in turn leads to a higher learning index for the control subject, indicating adaptation to the force field perturbation. In contrast, the cerebellar subject maintains curved movement trajectories throughout the adaptation set (**Figure 3B**). The average aiming error does not significantly decrease during the set, and catch trials do not show an increase in aiming errors in the negative direction. Evidently, the learning index in the cerebellar subject does not consistently increase during the adaptation set. These observations generalized to other control and cerebellar subjects in the experiment and are consistent with observations of force field adaptation in controls and patients in previous studies (Donchin et al., 2012; Smith and Shadmehr, 2005).

Movement trajectories and perpendicular velocities

Next, average movement trajectories and perpendicular velocities were compared between stimulation types in control subjects and cerebellar subjects. **Figure 4** depicts the movement trajectories and perpendicular velocities during the last baseline trials and various stages of the force field set (early, middle and late adaptation). During the last trials of the baseline set (bins 11-12), the movement trajectories were relatively straight in both control and cerebellar subjects, and there was no apparent difference between the stimulation types (**Figure 4A and 4C**). During early adaptation (bins 1-2 of the force field set), movement trajectories of control and cerebellar subjects deviated strongly from a straight trajectory to the target. Control subjects adapted more quickly and adequately to the force field perturbation than cerebellar subjects, illustrated by straighter movement trajectories in the middle of the set (bins 12-13) and late in the set (bins 23-24). Importantly, in both groups, the development of the average movement trajectories was indistinguishable between stimulation types. This observation will be quantified when aiming errors are analyzed below (see *Average aiming errors*).
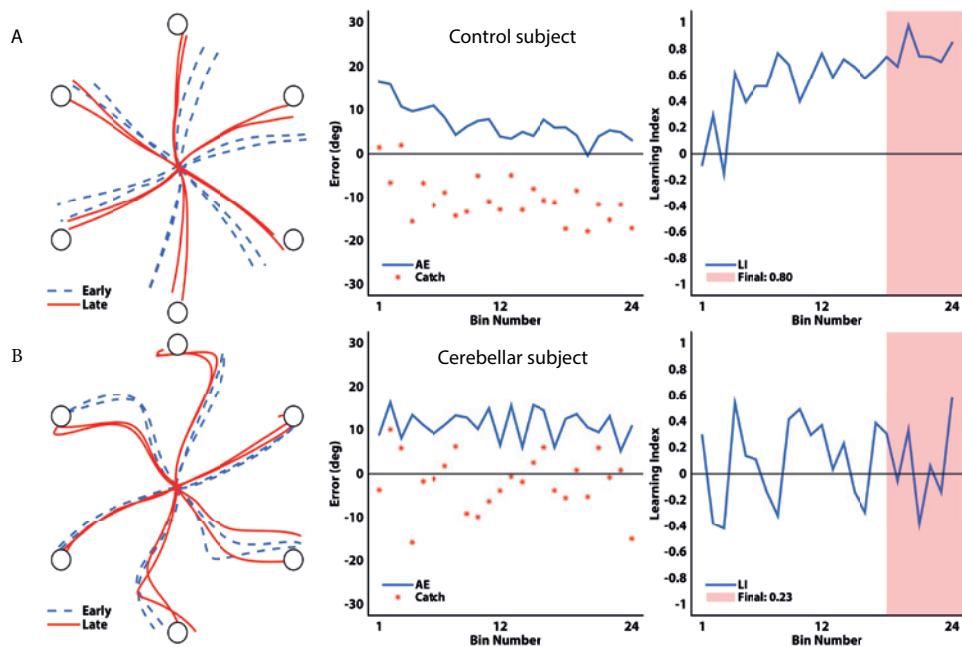
Figure 3. Movement trajectories, aiming errors and learning indices from two typical subjects during the adaptation set of a single experimental session. A: Healthy control subject (C05, **Table 1**). B: Cerebellar subject (P19, **Table 1**). The left panel displays movement trajectories early and late in adaptation. Blue lines represent movement trajectories of the first twelve movements in the set and red solid lines represent movement trajectories of the last twelve movements in the set. The target locations are depicted by white circles. The middle panel shows aiming errors (degrees) of perturbed trials and catch trials corresponding to the same set of the movement trajectories. The blue solid line represents the average aiming error during force field trials. Aiming errors were averaged over bins of six trials. Red stars represent the aiming error of catch trials. When a subject adapts to the force field, the average aiming error will decrease and catch trials will show increasing errors in the opposite direction of the force. The right panel displays the learning index during the force field set. The learning index was calculated over bins of six perturbed trials and one catch trial. The blue line represents the average learning index during adaptation. The red area of the plot represents the bins over which the final learning index was calculated (last six bins).

The perpendicular velocity traces painted a similar picture. Control subjects demonstrated smaller perpendicular velocities than cerebellar subjects, earlier in the set (**Figure 4B and 4D**). Furthermore, only control subjects developed a slight overcompensation for the perturbation early in the movement, illustrated by the negative perpendicular velocity around 50-60 ms in the second half of the set. This is regarded as a characteristic of force field learning in healthy individuals (Izawa et al., 2008), and is reduced in individuals with cerebellar damage (Criscimagna-Hemminger et al., 2010). Previously, tDCS effects have been described on the development of overcompensation in force field learning (Herzfeld et al., 2014a). However, tDCS effects on perpendicular velocity during overcompensation were not apparent in this experiment. This observation was quantified by performing a statistical analysis on perpendicular velocity at the moment of maximum overcompensation, defined as 55 ms after movement onset (between factor: group, within factor: stimulation type, bin number). As with the movement trajectories, the perpendicular velocity traces were indistinguishable between stimulation types in control subjects and cerebellar subjects [$F_{(2, 71.1)}$ = 1.03 p = 0.36, 95% CIs of difference [-0.19 cm/s, 0.06 cm/s] and [-0.19 cm/s, 0.06 cm/s] for sham vs M1 stimulation and sham vs cerebellum stimulation respectively], while cerebellar subjects did not show overcompensation compared to controls [$F_{(1, 35.1)}$ = 13.4, p = 0.001].

Average aiming errors

Figure 5 provides an overview of the development of average aiming errors during all sets in control subjects and cerebellar subjects. Aiming errors in control and cerebellar subjects reach near zero values during baseline and do not differ between stimulation conditions [$F_{(2, 71.1)}$ = 0.67, p = 0.51, 95% CIs of difference [-0.43°, 1.12°] and [-0.50°, 1.06°] for sham vs M1 stimulation and sham vs cerebellum stimulation respectively]. Equivalency between stimulation types during baseline was established with the smallest effect size of interest (SESOI) set at -1 and +1 degrees [p = 0.02 and p = 0.01 for sham vs M1 stimulation and sham vs cerebellum stimulation respectively].
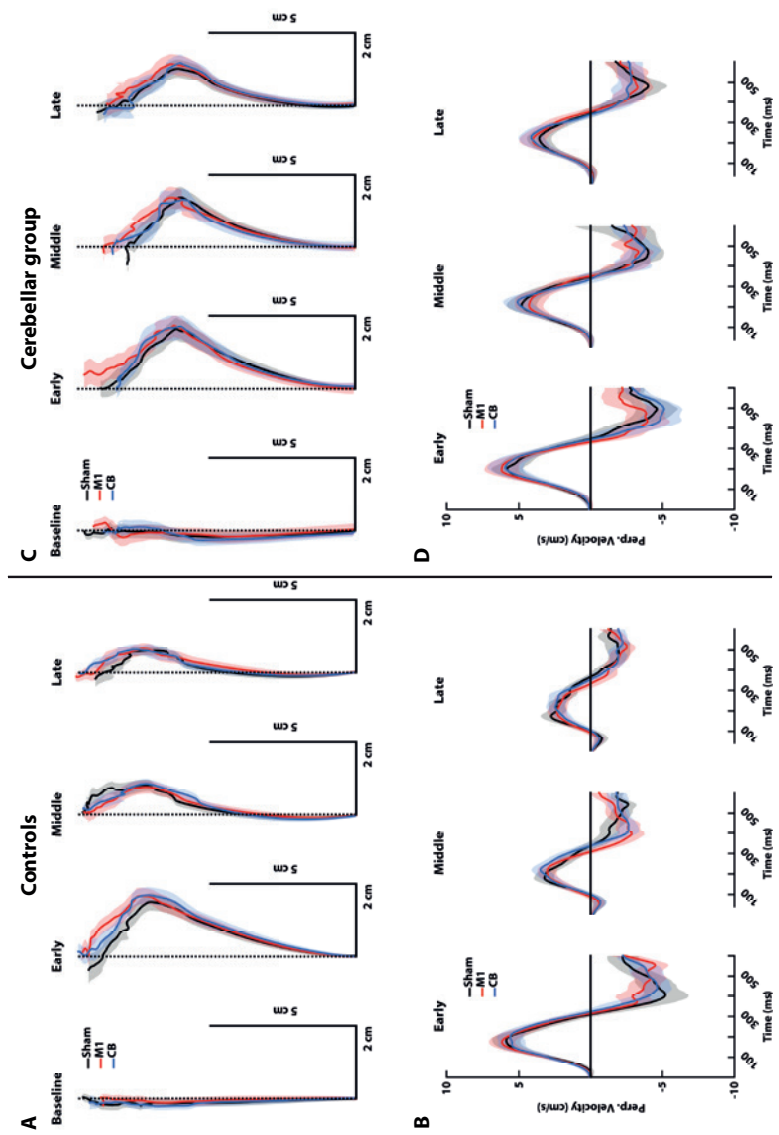
Figure 4. Average movement trajectories and perpendicular velocity traces of age-matched controls (n = 19) and cerebellar subjects (n = 19). Movements were rotated so each movement was towards the same target direction and then averaged over two bins (twelve trials). Movement trajectories and velocity traces show mean ± SEM. A: Movement trajectories of control subjects. Movements start at the bottom of the panel and end at the top. Baseline refers to the last twelve baseline trials (bins 11-12). Early refers to bins 1-2 of the force field set, middle refers to bins 12-13 and late refers to bins 23-24. CB = cerebellar stimulation. B: Velocity perpendicular to target direction in control subjects. C: Movement trajectories of cerebellar subjects D: Velocity perpendicular to target direction in cerebellar subjects. There was no significant difference in perpendicular velocity at 55 ms between stimulation types [$F_{(2,711)}$ = 1.03, p = 0.36].
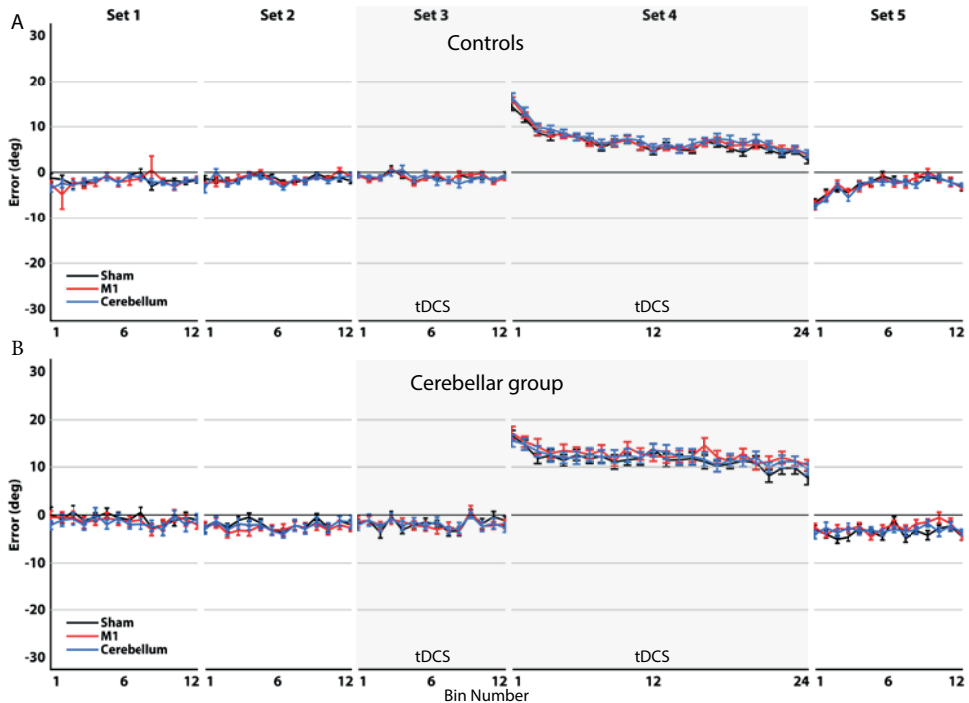
Figure 5. Mean aiming errors. A: Mean aiming errors of healthy ageing controls (n = 19). B: Mean aiming errors of cerebellar subjects (n = 19). Mean aiming errors (degrees) are shown during baseline (set 1-3), force field adaptation (set 4) and washout (set 5) for sham (black), M1 (red) and cerebellum (blue) stimulation. Aiming errors were averaged over bins of 6 movements. Set 4 and Set 5 were corrected for baseline movement biases. The shaded area represents the sets in which tDCS was applied. Error bars indicate standard error of the mean. There was no significant difference in mean aiming errors of the adaptation set between stimulation types [$F_{(2, 71.2)} = 2.31$, $p = 0.11$].

Initially, aiming errors are high in the positive direction during the force field set, but decrease as subjects adapt to the perturbation. Control subjects make movements with negative aiming errors (towards the direction of the force field) in the beginning of the washout set, exhibiting an after-effect of the perturbation. To assess the effects of tDCS during adaptation and washout, we analyzed the means of aiming errors of healthy controls and cerebellar subjects in the fourth and fifth set. This analysis did not reveal a main effect of stimulation type in both the adaptation set and the washout set and there was no significant interaction of stimulation and group in the adaptation set and washout set (**Table 3**). When comparing mean aiming errors of controls and cerebellar subjects, we found a significant difference during adaptation, but not of after-effects in the washout set (**Table 3**). The analysis further revealed a main effect of bin number in the adaptation set and interaction effects of bin number and group, indicating that subjects significantly decrease aiming

errors as the set progresses, but healthy controls more than cerebellar subjects (**Table 3**). In the washout set we saw similar main effects of bin number and interaction effects of bin number and group, indicating different washout effects between healthy controls and cerebellar subjects (**Table 3**).

Table 3. Linear mixed model aiming errors with movement time as continuous covariate.

Linear mixed model	Fixed effects		F statistics	p
Aiming errors adaptation				
	Between	**Group**	$F_{(1, 36.2)} = 23.6$	**<0.001***
	Within	**Bin**	$F_{(23, 828)} = 39.9$	**<0.001***
		Bin*Group	$F_{(23, 828)} = 6.16$	**<0.001***
		Stimulation	$F_{(2, 71.2)} = 2.31$	**0.11**
		Stimulation*Group	$F_{(2, 71.6)} = 0.86$	**0.43**
		Bin*Stimulation	$F_{(46, 1656)} = 0.84$	0.77
		Bin*Stimulation*Group	$F_{(46, 1656)} = 0.74$	0.90
Aiming errors washout				
	Between	**Group**	$F_{(1, 38)} = 0.30$	**0.59**
	Within	**Bin**	$F_{(13, 470)} = 10.9$	**<0.001***
		Bin*Group	$F_{(13, 468)} = 6.94$	**<0.001***
		Stimulation	$F_{(2, 71.9)} = 1.01$	**0.37**
		Stimulation*Group	$F_{(2, 71.7)} = 1.07$	**0.35**
		Bin*Stimulation	$F_{(26, 934)} = 1.36$	0.11
		Bin*Stimulation*Group	$F_{(26, 933)} = 0.95$	0.54

Boldface highlights important (in-text) comparisons. * = significant at the α = 0.05 level.

To investigate the null result of stimulation on average aiming errors during the adaptation set, group means were tested for equivalency and 95% confidence intervals of differences were calculated. Although equivalency between group means could not be established (SESOI = [-1°, +1°], p = 0.35 for sham vs M1 stimulation and p = 0.29 for sham vs cerebellum stimulation), the confidence intervals show the differences between sham and M1 stimulation (95% CI of difference [-1.91°, 0.22°]) and sham and cerebellum stimulation (95% CI of difference [-1.83°, 0.30°]) are small. Furthermore, the mean aiming error of sham stimulation (8.98° ± SE 0.58°) was on average slightly lower than M1 stimulation (9.83° ± SE 0.58°) and cerebellar stimulation (9.74° ± SE 0.58°), which is against the prediction of improved learning with anodal tDCS.

Similar analyses were performed to investigate the null result of stimulation in the washout set. Equivalency could not be established between sham and M1 stimulation (SESOI = [-1°, +1°], p = 0.06), but could be established between sham and cerebellar stimulation (p = 0.01). During washout the differences between sham and M1 stimulation (95% CI of difference [-1.30°, 0.39°]) and sham and cerebellar stimulation (95% CI of difference [-0.91°, 0.77°]) were also small. Two additional analyses were performed to compare aiming errors in the second baseline set with aiming errors in the washout set. This revealed that control subjects initially made movements with negative aiming errors in the washout set, which differentiated significantly from aiming errors in the second baseline set [$F_{(1, 35.9)}$ = 11.1, p = 0.002], indicating an after-effect of the force field-perturbation. Cerebellar subjects made movements in the washout set which could not be distinguished from baseline set movements [$F_{(1, 35.3)}$ = 0.80, p = 0.38], indicating no after-effects in cerebellar subjects.

Next, aiming errors were analyzed over measurement day to test for carryover effects. The analysis of aiming errors over measurement day was carried out separately for control subjects and cerebellar subjects, because we noticed a marked decrease in the means of controls with measurement day, but not in cerebellar subjects. For control subjects there was a significant effect of measurement day [$F_{(2, 35.0)}$ = 4.82, p = 0.01]. The mean aiming error of the first day (7.71° ± SE 0.52°) was significantly higher than the third day (6.44° ± SE 0.52°, p = 0.02) and there was a trend of a difference between the first day and second day (6.67 ± SE 0.52°, p = 0.06), both indicating a slight carryover effect. The 95% CIs for the difference in means were [-0.04°, 2.14°] for day 1 vs day 2 and [0.17°, 2.38°] for day 1 vs day 3.

No significant effect of measurement day could be detected in the cerebellar group [$F_{(2, 36.0)}$ = 0.11, p = 0.89]. Although equivalency between measurement days in cerebellar subjects was not established (SESOI = [-1°, +1°], p = 0.19 and p = 0.15 for day 1 vs day 2 and day 1 vs day 3 respectively), no indication of a carryover effect was observed in the means of aiming errors (day 1: 12.2° ± SE 1.01°, day 2: 11.9° ± SE 1.01°, day 3: 12.2° ± SE 1.01°) or 95% CIs of differences in means ([-1.54°, 2.20°] for day 1 vs day 2 and [-1.82°, 1.93°] for day 1 vs day 3). We also separately analyzed aiming errors of subjects during the first session only. This can be regarded as a between-subject comparison of the stimulation effect during the first session (i.e. without possible carry-over effects). Here as well, we could not detect stimulation effects on average aiming errors [$F_{(2, 31.8)}$ = 1.66, p = 0.21]. The power of this between-subject analysis is low due to the limited amount of subjects (n = 6 or 7 for each stimulation type), but the results are in accordance with the findings of the main results of the within-subject experiment. **Figure 6** provides an overview of the development of aiming errors on the first day of measurement. From the figure one could conclude there is a trend of a difference between the stimulation types in the cerebellar patient group, i.e.

the cerebellar stimulation group seems to be learning slower than other stimulation types. However, this is due to one particularly slow learner in the cerebellar stimulation group on the first day.
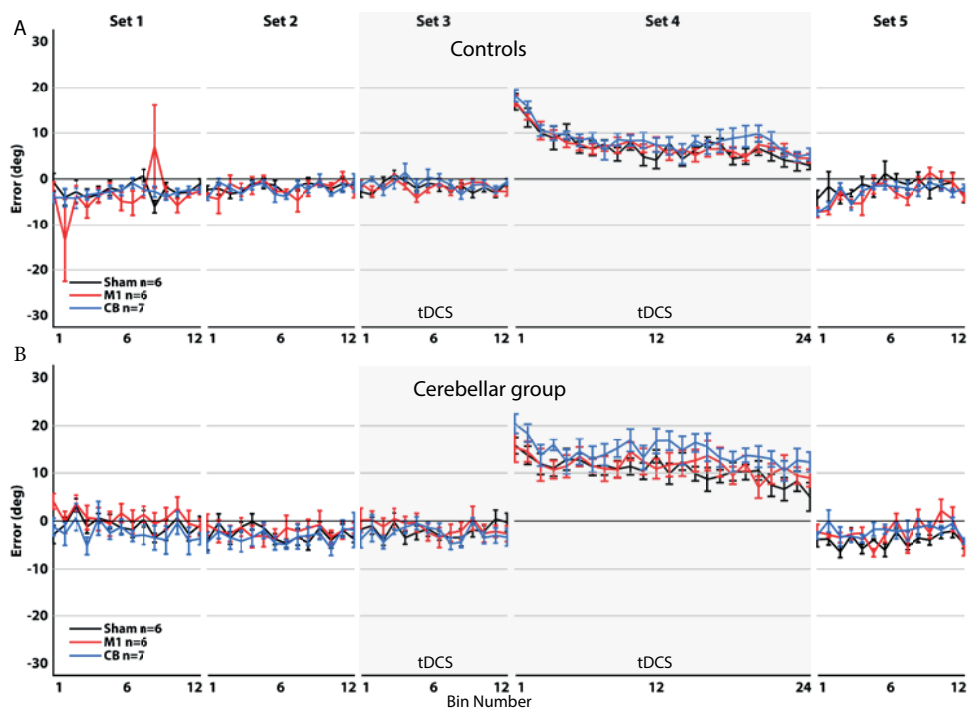

Figure 6. Mean aiming errors first day. A: Mean aiming errors of healthy ageing controls on the first measurement day (n = 6/7). B: Mean aiming errors of cerebellar subjects on the first measurement day (n = 6/7). Mean aiming errors (degrees) are shown during baseline (set 1-3), force field adaptation (set 4) and washout (set 5) for sham (black), M1 (red) and cerebellum (blue) stimulation. Aiming errors were averaged over bins of 6 movements. Set 4 and Set 5 were corrected for baseline movement biases. The shaded area represents the sets in which tDCS was applied. Error bars indicate standard error of the mean. There was no significant difference in mean aiming errors of the adaptation set between stimulation types [$F_{(2, 31.8)}$ = 1.66, p = 0.21].

To test whether non-significant stimulation effects were due to a lack in statistical power, a post hoc power analysis was conducted in G*Power (Faul et al., 2007), as well as a simulation-based power analysis. The simulation-based power analysis was carried out to control for differences in repeated measure ANOVAs and our statistical model, since G*Power can calculate power of RM ANOVAs, but not of linear mixed models. In the stimulation-based approach we approximated power by generating many (n = 1000 per effect size) permutations of the original dataset where the alternative hypothesis was true. That is, for

each of the permutations the true effect of tDCS was not zero, with effect sizes ranging between 0.05 and 1.00. Then, we calculated the fixed effect of tDCS for each permutation and determined the proportion of significant simulations ($p < 0.05$) for each effect size. We wanted to find out what the minimum effect size necessary was to reliably reject the null hypothesis and how sensitive our experiment was in picking up clinically relevant stimulation effects. While calculated power was generally similar between G*Power and simulations, in cases where there was a small difference, we report the results of the analysis with the lowest power.

For two groups of 19 subjects (total n = 38) with α = 0.05 and 1 – β = 0.80, we calculated we could reliably reject the null hypothesis if the true effect size was f = 0.21 or higher (d ≥ 0.42). Taking into account carryover effects, we also calculated the minimum true effect size required if we only conducted the experiment in one subject group (total n = 19) (e.g. only the cerebellar group). With α = 0.05 and 1 – β = 0.80 and n = 19, we could reliably reject the null hypothesis if the true effect size was f = 0.30 or higher (d ≥ 0.6). This would mean that, given the standard deviation of the cerebellar group, we could reliably detect aiming errors of 2.6° degrees and larger. To put this into perspective, the difference in aiming error between control subjects and cerebellar subjects we found is about 5°. Galea et al. report a difference of approximately 5° between sham and cerebellar stimulation during reaching adaptation in a group of young controls (Galea et al., 2010a). A recent study by Jalali et al. report a Cohen's d of 0.7 of pooled experimental data (difference of ± 2.6°) in similar tasks and young control subjects (Jalali et al., 2017). Others have suggested a true effect size of tDCS around d = 0.5, depending on the task (Hashemirad et al., 2016; Minarik et al., 2016). We thus fully expected to pick up on clinically relevant stimulation effects, even in groups of 19 subjects.

Learning index

The final measure of performance for each stimulation type was calculated by taking the learning index of the last 6 bins (30 force field trials and 6 catch trials in each target direction). An overview of the development of the learning index through the adaptation set averaged over stimulation types is shown in **Figure 7**. As expected, healthy controls initially improve their performance strongly, after which they plateau around a mean learning index of 0.68 ± SD 0.10. The increase of the learning index in cerebellar subjects is much less consistent, with a mean learning index of 0.31 ± SD 0.11 at the end of the adaptation set.
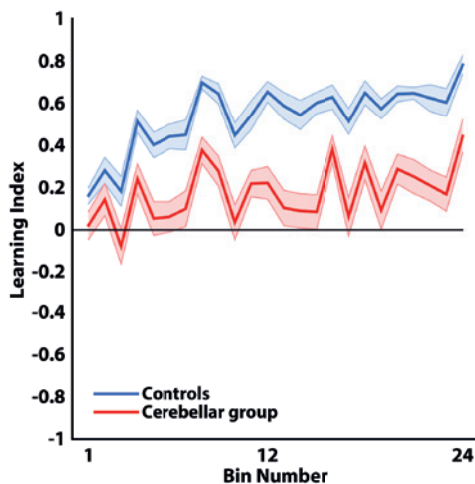
Figure 7. Learning index during the adaptation set averaged across stimulation types for age-matched controls (n = 19) and cerebellar subjects (n = 19). Learning index was calculated for each bin of 7 trials (6 force field trials and one catch trial). A value of 1 indicates full adaptation to the force field perturbation, while values between 0 and -1 indicate no learning. Shaded area depicts standard error of the mean. There was no significant difference in the final learning index between stimulation types [$F_{(2, 72.1)} = 0.41$, $p = 0.67$].

The final learning index was significantly different between cerebellar participants and healthy subjects (**Table 4**). Importantly, the final learning index was not affected by stimulation type and there was no interaction of stimulation type and group (**Table 4**). Equivalency between stimulation types could not be established (SESOI = [-0.05, 0.05], $p = 0.09$ for sham vs M1 stimulation and $p = 0.27$ for sham vs cerebellum stimulation). There was a trend for an effect of session number when comparing final learning over experimental sessions instead of stimulation type, indicating possible interference of previous measurement days (**Table 4**). As was investigated when aiming errors were analyzed, the source of this difference was a carryover effect of measurement day in the healthy control group. When analyzing the final learning index in controls over measurement day, pairwise comparisons revealed significantly higher final learning indices of the third measurement day in comparison with the first day (mean difference = 0.07, $p = 0.02$).

Table 4. Linear mixed model final learning index with movement time as continuous covariate.

Linear mixed model	Fixed effects		F statistic	p
Final learning index				
(over stimulation type)	Between	**Group**	$F_{(1, 35.7)} = 185$	**<0.001***
	Within	**Stimulation**	$F_{(2, 72.1)} = 0.41$	**0.67**
		Stimulation*Group	$F_{(2, 73.0)} = 1.42$	**0.25**
Final learning index				
(over measurement order)	Between	**Group**	$F_{(1, 35.6)} = 187$	**<0.001***
	Within	**Day**	$F_{(2, 73.0)} = 2.78$	**0.07**
		Day*Group	$F_{(2, 72.5)} = 1.87$	0.16

*Boldface highlights important (in-text) comparisons. * = significant at the α = 0.05 level.*

The learning index required the use of catch trials to calculate. Catch trials can cause a non-trivial amount of trial-by-trial unlearning (Thoroughman and Shadmehr, 2000) which in combination with improved (un)learning due to tDCS could lead to complex mixed results. However, not using catch trials during the adaptation set is not optimal, as catch trials give us a measure of the internal state of the motor system and allow us to assess whether subjects are stiffening the arm in response to the force field perturbation. As a way to assure unlearning by catch trials was not affected by stimulation type, the difference between perpendicular displacement right before a catch trial and directly after a catch trial in the healthy control group was assessed as follows:

$$\text{Unlearning} = PD_{\text{catchtrial+1}} - PD_{\text{catchtrial-1}} \qquad \text{(Eq. 2)}$$

The analysis revealed no effect of stimulation on unlearning, but did reveal a significant effect of catch trial number (**Table 5**). The mean value of unlearning per catch trial was about 0.80 cm ± SE 0.06 cm for each of the stimulation types. Unlearning was stronger in the beginning of the adaptation set, than later in the adaptation set, which can be explained by a motor memory which is more resistant to unlearning later in the set (i.e. more 'slow learning', (Smith et al., 2006). In all, the analysis shows unlearning by catch trials during the adaptation set is not affected by stimulation type and complex mixed results are thus unlikely.

Table 5. Linear mixed model unlearning with movement time as continuous covariate.

Linear mixed model	Fixed effects		F statistic	p
Unlearning				
	Within	**Stimulation**	$F_{(2, 35.0)} = 1.00$	**0.38**
		Catch trial	$F_{(23, 412)} = 17.8$	**<0.001***
		Stimulation*Catch trial	$F_{(46, 821)} = 0.83$	0.79

*Boldface highlights important (in-text) comparisons. * = significant at the α = 0.05 level.*

Voxel-based morphometry

Figure 8 shows a cerebellar map of the difference in grey matter volume between healthy controls and cerebellar subjects on a voxel-by-voxel basis, reported in t-scores. The significance threshold as estimated by the permutation analysis was set at t = -3.94 and t = 3.93, meaning voxels with t-scores below -3.94 and t-scores above 3.93 were significant. Voxel t-scores ranged between -10.62 and 1.66, yielding 44.02% of voxels as significant, with significant voxels only being negative t-scores. The highest percentage of significant voxels was found in the anterior lobe (lobule I-V) and superior parts of the posterior cerebellar lobe (lobule VI). This confirms earlier observations where the strongest degeneration in cerebellar patients was also found in the anterior and superior cerebellum (Hulst et al., 2015), although that study also reports strong degeneration of the more inferior parts of the posterior cerebellum (in particular lobule VII). Previous studies have found that integrity of the anterior lobe of the cerebellum, in particular lobule IV and lobule V, is important for adaptation to force-field perturbations (Donchin et al., 2012; Rabe et al., 2009). Thus, the loss of cerebellar volume in the anterior lobe of the cerebellum is the likely cause of the observed motor impairments in cerebellar patients.

Analysis of the correlation between the final learning index and grey matter volume yielded no results in both healthy control subjects (correlation thresholds between r = -0.72 and r = 0.75, voxel correlations between r = -0.47 and r = 0.45, no significant voxels) and cerebellar subjects (correlation thresholds between r = -0.74 and r = 0.75, voxel correlations between r = -0.39 and r = 0.67, no significant voxels). This is likely due to conservative corrections for multiple testing and the low amount of variance in the final learning index of cerebellar subjects.
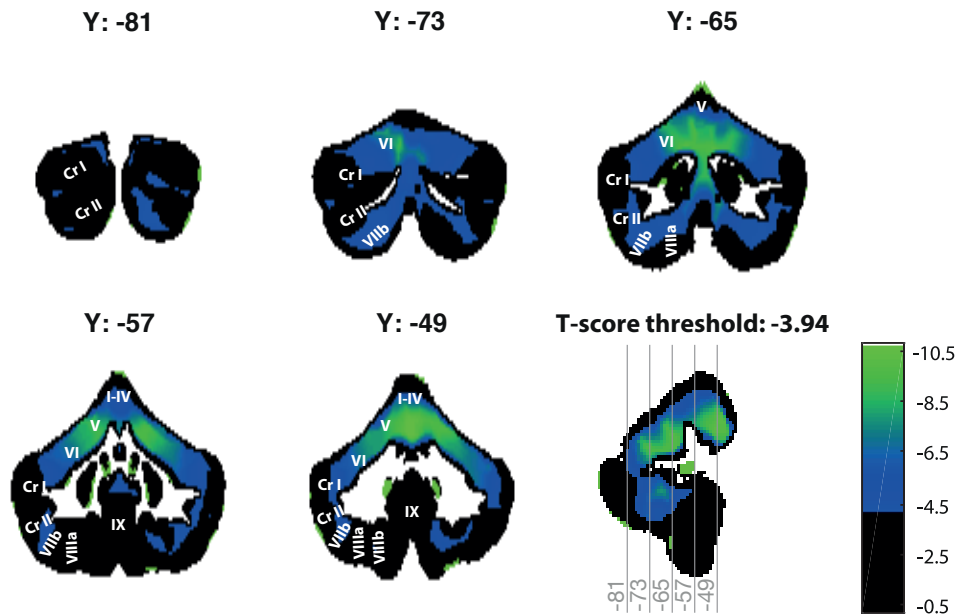
Figure 8. Slices of the cerebellum showing t-scores of the grey matter volume difference between cerebellar subjects and controls (MNI-coordinates). A threshold was set at the calculated significance threshold, meaning that each voxel with a t-score that is less strong than −3.94 is color-coded as black. Low significant t-scores are color-coded as blue, while high significant t-scores are color-coded as green. Definition of lobule anatomy and nomenclature as described in Diedrichsen et al., 2009. Cr I=Crus I, Cr II=Crus II.

Experiment 2

The second experiment was analyzed using the same methodology described in Experiment 1. We will summarize the most important results and the effects of cerebellar stimulation on our main performance measures.

Average movement times and movement speed indicated no differences between stimulation types, but did uncover a main effect of set number (**Table 6**). Like elderly controls, young controls tended to speed up during the course of the experiment. Movement times in the first set were about 100 ms longer (353 ms ± SE 19.9) than in the last set (255 ms ± SE 18.2), and were comparable to movement times of the elderly control group [unpaired t-test, $t_{(84.9)}$ = -1.66 p = 0.10]. A univariate test of mean movement times [$F_{(2, 27)}$ = 0.37, p = 0.69] and movement speeds [$F_{(2, 27)}$ = 0.30, p = 0.74] in the fourth set revealed no differences between the three stimulation types, indicating all groups were exposed to similar perturbation magnitudes.

Table 6. ANOVAs of average movement times and speeds.

ANOVA	Factors		F statistics	p
Average movement time				
	Between	**Stimulation**	$F_{(2, 27)} = 0.69$	**0.51**
	Within	**Set**	$F_{(2.04, 64.1)} = 13.5$	**<0.001***
		Set*Stimulation	$F_{(4.08, 64.1)} = 0.28$	0.71
Average movement speed				
	Between	**Stimulation**	$F_{(2, 27)} = 0.41$	**0.67**
	Within	**Set**	$F_{(2.47, 66.6)} = 10.9$	**<0.001***
		Set*Stimulation	$F_{(4.93, 66.6)} = 0.28$	0.92

*Boldface highlights important (in-text) comparisons. * = significant at the α = 0.05 level.*

Secondly, perpendicular velocities were analyzed at the moment of maximal overcompensation. Like elderly controls, young control subjects developed an overcompensation to the force field perturbation around the 55 ms mark of a movement. Negative perpendicular velocities during the beginning of a movement were observed in all stimulation types as the adaptation set progressed. No difference between stimulation types could be detected at 55 ms [$F_{(2, 26.8)} = 0.27$, p = 0.78]. Here, as well, the magnitude of the overcompensation in young controls was comparable to that of healthy elderly controls [-0.75 cm/s ± SE 0.14 vs -0.65 cm/s ± SE 0.10 in the final bin of the set, unpaired t-test, $t_{(85)}$ = -0.51 p = 0.61].

Next, the development of average aiming errors during the experiment was plotted and investigated (**Figure 9**). Young controls, like healthy elderly controls, learn to adapt to the perturbation quickly and exhibit aiming errors at the end of learning with near-zero values. Also, like in elderly controls, an aftereffect was observed during the washout phase of the experiment (**Figure 9**). No difference was found between the average of aiming errors of the adaptation set between young and elderly controls [unpaired t-test, $t_{(85)}$ = -0.32 p = 0.75].

Importantly, no stimulation effects could be detected in young controls in the baseline set [$F_{(2, 27.4)} = 0.44$, p = 0.65, 95% CIs of difference [-1.95°, 1.31°] for sham vs cathodal and [-1.34°, 1.90°] for sham vs anodal], as well as the adaptation set [$F_{(2, 25.7)} = 0.10$, p = 0.91, 95% CIs of difference [-3.19°, 4.10°] for sham vs cathodal and [-3.05°, 4.24°] for sham vs anodal] and washout set [$F_{(2, 27.1)} = 0.03$, p = 0.97, 95% CIs of difference [-2.87°, 3.11°] for sham vs cathodal and [-2.72°, 3.25°] for sham vs anodal]. Here as well, we were interested in how sensitive our experiment was in detecting stimulation effects. Given α = 0.05 and 1 – β = 0.80, we calculated we could reliably reject the null hypothesis if the true effect size

was f = 0.43 or higher (d ≥ 0.86). This meant we could detect a true effect in aiming errors of 2.72° or more. Although less sensitive than Experiment 1, we would argue that it is still reasonable to expect stimulation effects which are as large or larger than this.

Lastly, we investigated the effect of stimulation of the cerebellum on the final learning index. The final learning index reached values which were on average a little higher than the final learning index of elderly controls [0.74 ± SD 0.12, unpaired t-test, $t_{(85)}$ = 2.22, p = 0.03], indicating young controls achieve slightly higher final learning than elderly controls. Importantly, here as well, no effects of stimulation were detected [$F_{(2, 26)}$ = 0.52, p = 0.60]. Equivalency between group means could not be established for all of the aforementioned measures under the equivalency criteria from Experiment 1.
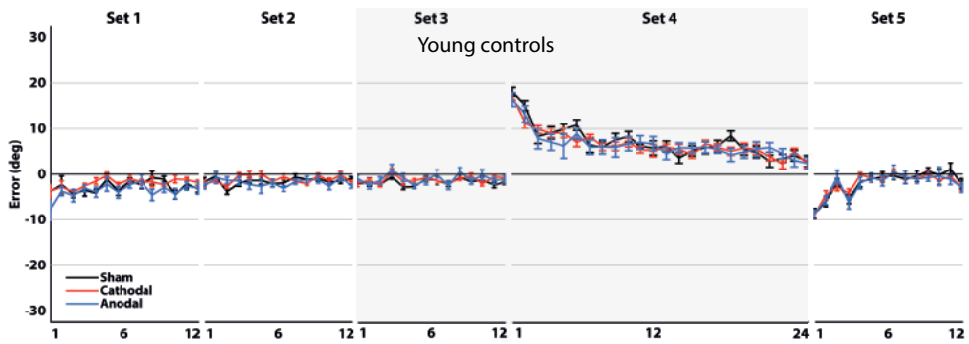

Figure 9. Mean aiming errors of young controls (n = 30, n =10 for each stimulation type). Mean aiming errors (degrees) are shown during baseline (set 1-3), force field adaptation (set 4) and washout (set 5) for sham (black), cathodal (red) and anodal (blue) stimulation of the cerebellum. Aiming errors were averaged over bins of 6 movements. Set 4 and Set 5 were corrected for baseline movement biases. The shaded area represents the sets in which tDCS was applied. Error bars indicate standard error of the mean. There was no significant difference in mean aiming errors of the adaptation set between stimulation types [$F_{(2, 25.7)}$ = 0.10, p = 0.91].

DISCUSSION

As expected, individuals with cerebellar degeneration were slower to adapt to force field-perturbations and displayed no after-effects in the washout phase. These findings are in line with earlier work on motor adaptation in cerebellar patients (Maschke et al., 2004a; Tseng et al., 2007). Against our expectations, cerebellar subjects did not benefit from transcranial direct current stimulation. Cerebellar subjects did not adapt more quickly to force field-perturbations during stimulation of the cerebellum or primary motor cortex

when compared to sham stimulation. Similarly, retention in the washout phase did not improve after stimulation of the cerebellum or M1 when compared to sham stimulation. No effects of transcranial direct current stimulation were observed in the elderly age-matched controls as well as young controls.

In short, we were unable to detect faster learning rates and higher retention after anodal stimulation, which is in contrast with previous reports [for review, see Buch et al., 2016]. We cannot exclude, however, that tDCS elicits behavioral improvements under different task and stimulation parameters, in larger subject populations, or that carryover effects have masked potential benefits of tDCS in elderly controls. Nonetheless, our results suggest that tDCS of the cerebellum or M1, using currently available stimulation techniques, is unlikely to lead to improvements which are clinically relevant for cerebellar patients. When stimulation effects cannot be detected in the controlled environment of a laboratory, any potential benefits of stimulation are likely going to be small, and stimulation techniques should first be further developed before they can be applied in the clinic. Possible reasons for the lack of detectable stimulation effects and several limitations of this study are discussed below.

tDCS effects may be highly task-dependent

Studies investigating tDCS effects in reach adaptation in young healthy subjects have reported different effects of stimulation depending on the task and the performance measures. A recent study demonstrated that anodal stimulation of the cerebellum led to quicker overcompensation of a force field perturbation and cathodal stimulation of the cerebellum led to slower overcompensation, as evidenced by a significant difference in perpendicular velocities between stimulation types (Herzfeld et al., 2014a). We were unable to replicate this finding in both of our experiments. In agreement with our results, the study by Herzfeld et al. did not find anodal stimulation effects on maximum perpendicular displacement, a measure which closely relates to our main performance measure, as well as no effects of anodal stimulation of M1. This contrasts with a study by Galea et al. who report anodal stimulation effects of M1 in a visuomotor task (Galea et al., 2010a). Moreover, the authors found anodal stimulation of the cerebellum sped up adaptation to visuomotor perturbations when measuring angular end point error, a measure which closely relates to our performance measure. Although the experiments by Herzfeld et al. and Galea et al. appear similar to our experiment, there are significant differences in experimental design and task parameters. Differences in task parameters include the types of perturbation, the amount of movements, the number and direction of target locations, the projection of the hand position (horizontal plane or vertical monitor), the inclusion of clamp or catch trials and the type and amount of feedback. Since nuances in task parameters have an effect on

how the nervous system learns and retains a motor adaptation (Joiner and Smith, 2008; Kitago et al., 2013), it is possible that these differences in task parameters explain the different stimulation effects. A recent study by Jalali et al. has further established the task-specificity of stimulation effects in reach adaptation(Jalali et al., 2017), suggesting that the parameters of a task influence how tDCS effects performance, and stimulation effects in one task and performance measure might not generalize to others.

tDCS effects on critical areas may have been insufficient

Other factors which could possibly have influenced tDCS efficacy in both our control subjects and cerebellar subjects were the stimulation parameters. A recent modelling study of the cerebellar electrode placement, demonstrated that the majority of current is distributed over the cerebellar hemisphere under the anode (Rampersad et al., 2014). The highest electrical field strengths are found on the inferior surface of the cerebellum, below the primary fissure. This could indicate that when applying tDCS with an electrode placed 3 centimeters right from the inion, inferior areas of the cerebellum are mainly stimulated and to a lesser extent the anterior cerebellum. Because adaptation to force field-perturbations depends on lobule IV and lobule V of the anterior cerebellum (Donchin et al., 2012; Rabe et al., 2009), this could possibly explain the lack of cerebellar stimulation effects in our study. Due to the anatomical structure of the neck region and cerebellum it is however unlikely that alternative cerebellar montages will alter the distribution of current, as variations in the cerebellar montage produce only small changes in current distribution (Parazzini et al., 2014). The same modelling study also revealed that the placement of electrodes during M1 stimulation in our study might be suboptimal for stimulation of the target area, which could have affected tDCS efficacy during M1 stimulation (Rampersad et al., 2014). However, as Rampersad et al. point out, several simplifications and assumptions are made when modelling tDCS (e.g. in tissue conductivity) and the models still need to be validated in animal studies.

The tDCS montages used in our experiment are the most commonly agreed upon montages for stimulation of the cerebellum and primary motor cortex (Nitsche et al., 2008; Woods et al., 2015) and the physiological basis for using these stimulation locations is well-established [cerebellum: Galea et al. (2009); M1: Stagg and Nitsche (2011)]. Furthermore, several studies have found stimulation effects during motor learning utilizing the exact cerebellar montage and exact M1 montage used in this experiment [for review, see Buch et al., 2016]. It is therefore unlikely that the montage of electrodes was the driving force behind the lack of stimulation effects in this experiment, but alternative electrode montages could be considered depending on the task parameters and stimulation target.

tDCS effects may depend on cerebellar integrity

The specific task- and stimulation-parameters are the most likely candidates for the lack of stimulation effects in this experiment, but even when these methodological difficulties have been worked out (i.e. tDCS effects can robustly and predictably be elicited across healthy subjects and tasks), it could be difficult to elicit behavioral improvements in subjects with cerebellar atrophy. When stimulation is applied over an area of the cerebellum which is atrophied, the amount of cerebellar neurons left could be too low to institute a behavioral change. This can be demonstrated by the absence of cerebellar excitability effects on cerebellar-M1 connectivity in hereditary ataxia for instance (Ugawa et al., 1994). Furthermore, since internal model formation is impaired in cerebellar patients due to degeneration of the cerebellum (Smith and Shadmehr, 2005), it is likely that consolidation of an impaired internal model does not lead to functional improvements. The primary motor cortex plays a crucial role in the retention of a newly formed motor memory (Hadipour-Niktarash et al., 2007) and any potential benefits of anodal stimulation of M1 in cerebellar patients could thus be masked by impaired internal model formation by the cerebellum. Since both cerebellar patients and ageing subjects are affected by cerebellar atrophy of the anterior cerebellum (Hulst et al., 2015), the effect of stimulation on behavior might be limited. Of course, loss of cerebellar volume cannot have impeded tDCS efficacy in our group of young control subjects, and the null results in healthy elderly and cerebellar patients are likely independent from cerebellar atrophy, but this caveat should be considered when further exploring the clinical potential of tDCS.

Limitations

Several limitations have to be taken into account for the interpretation of the results in this study. Since the focus of this experiment was to determine whether tDCS could be effective in reducing motor learning deficits of cerebellar patients, we chose to stimulate anodally in cerebellar patients exclusively. Cathodal stimulation most commonly impairs the ability of healthy subjects to learn and retain a motor adaptation (Herzfeld et al., 2014a; Jayaram et al., 2012) likely due to a decrease of cortical and cerebellar excitability (Galea et al., 2009; Nitsche et al., 2000), but positive cathodal stimulation effects have also been reported (Orban de Xivry et al., 2011; Pope and Miall, 2012). It is therefore still possible that cathodal stimulation would have improved the ability of cerebellar patients to adapt to force field-perturbations, although we consider this unlikely because of the lack of effects of cathodal stimulation in the second experiment.

Furthermore, we did not assess physiological effects of tDCS. Even when we could not establish behavioral effects of tDCS, stimulation of the cerebellum and M1 has likely had an effect on neuronal excitability. If physiological effects of cerebellar or M1 stimulation

could have been established, but not behavioral effects, it would have further cemented the task-dependency of tDCS effects. Moreover, we did not control for BDNF-polymorphisms (brain-derived neurotrophic factors), which are known to effect cortical plasticity between individuals (Antal et al., 2010; Fritsch et al., 2010), and did not quantify the sensitivity to TMS in subjects, which is a promising proxy measure of an individuals' sensitivity to brain stimulation (Labruna et al., 2015). After review of individual behavioral data, however, we could not distinguish between responders and non-responders, something one would have expected if some of the subjects carried a BNDF-polymorphism or in the case of interindividual differences in TMS sensitivity.

Another difference between our application of tDCS and several aforementioned studies is the use of rubber electrodes which are covered in conductive paste instead of covered by saline-soaked sponges. Rubber electrodes covered in conductive paste are expected to apply current over the scalp more consistently than electrodes covered in saline-soaked sponges, for which improper usage can lead to oversaturation and alter the distribution of current between subjects and experimental sessions (Woods et al., 2015). While we cannot rule out the possibility of different stimulation effects due to the use of different electrode configurations, we do not think this has an impact on the interpretation of our findings.

Two additional limitations of our experimental design have to be taken into account. Firstly, our learning index required catch trials during adaptation to calculate which can cause significant trial-to-trial unlearning. Although unlearning due to catch trials was not affected by stimulation type, it would have been desirable to use error-clamp trials instead. Error-clamp trials cause unlearning as well, but less than catch trials (Kitago et al., 2013).

Secondly, Experiment 1 was carried out using a within-subject design, which has the advantage of increased power, but comes with the disadvantage of introducing possible carryover effects between sessions. Indeed, the healthy elderly control group demonstrated a carryover effect between measurement days which might have masked potential stimulation effects. However, the carryover effect was only present in the group of healthy elderly controls and relatively minor. If doing more learning sessions in healthy elderly is more effective than stimulation, it is unlikely that tDCS can affect learning in cerebellar patients to a degree which is therapeutically relevant. Furthermore, a second experiment was carried out to control for stimulation effects possibly being masked by carryover effects. The second experiment also did not detect an effect of tDCS in a between-subject design, which makes it more likely that improper task- and stimulation-parameters were at the root of our null result.
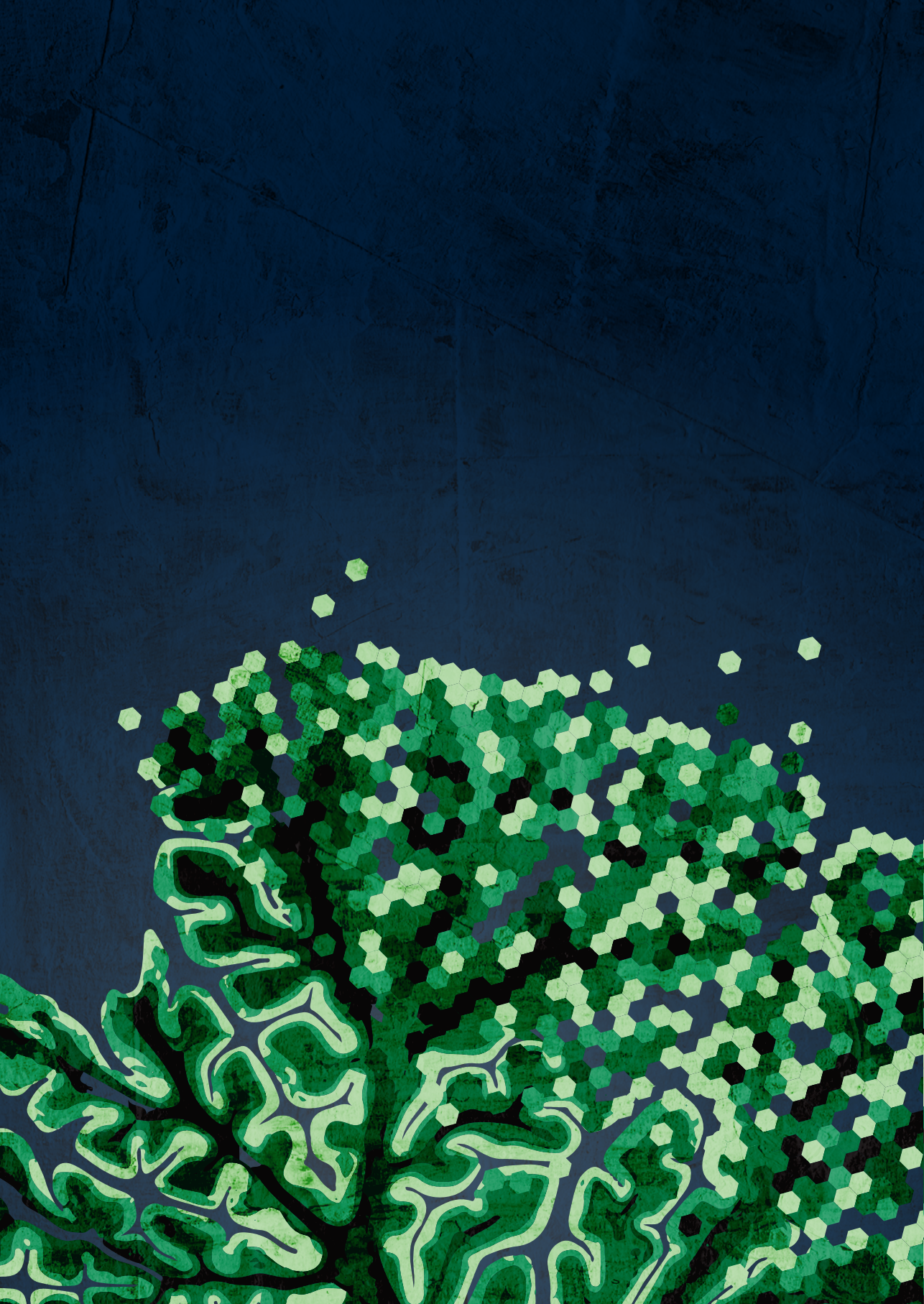
CONCLUSIONS

The present study did not find stimulation effects of tDCS in young control subjects, healthy ageing subjects and individuals with cerebellar degeneration during reach adaptation. Not fully developed task- and stimulation-parameters may explain the lack of stimulation effects. Carryover effects were present in healthy elderly controls and could have masked stimulation effects, but carryover effects were not present in the group of cerebellar patients. Furthermore, the second experiment, which controlled for carryover effects, was also unable to establish a significant relationship between tDCS and behavior. The second experiment was performed in a relatively small group of young control subjects and still needs to be replicated in a larger group of elderly controls. Despite these limitations, the results of our study require a reevaluation of the clinical potential of tDCS in cerebellar patients. Currently, this study does not provide evidence that tDCS changes learning or retention rates in cerebellar patients. For tDCS to become a valuable tool in the neurorehabilitation of cerebellar disease, stimulation effects should be consistent and predictable between subjects and tasks, and lead to behavioral improvements in cerebellar patients which are large enough to be clinically relevant.

Acknowledgements

Author contributions

Thomas Hulst conceived and designed the research; analyzed data; interpreted results; prepared figures; drafted manuscript; edited and revised manuscript; approved the final version of the manuscript.

6

Effects of transcranial direct current stimulation on grip force control in patients with cerebellar degeneration

Liane John[1*], Michael Küper[1*], Thomas Hulst[1,2],
Dagmar Timmann[1], Joachim Hermsdörfer[3]

[1] Department of Neurology, University Hospital Essen, University of Duisburg-Essen, Essen, Germany
[2] Erasmus University College, Rotterdam, The Netherlands
[3] Department of Sport and Health Sciences, Institute of Movement Science, Technical University of Munich, Germany
[*] Authors contributed equally
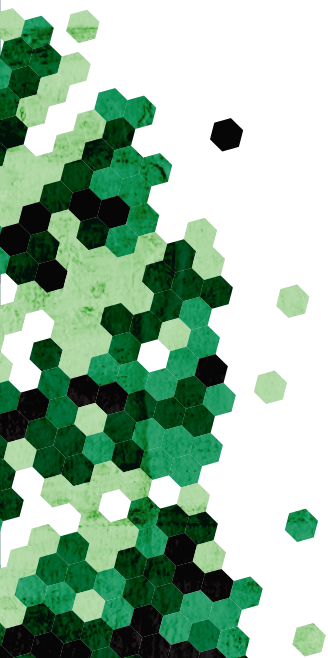
ABSTRACT

Background: The control of grip forces when moving a hand held object is impaired in patients with cerebellar degeneration. We asked the question whether after-effects of anodal transcranial direct current stimulation (tDCS) applied to the lateral cerebellum or M1 improved grip force control in cerebellar patients.

Methods: Grip force control while holding an object during cyclic arm movements was assessed in patients with pure cerebellar degeneration (n= 14, mean age 50.2 years ± SD 8.8 years) and age- and sex-matched control participants (n=14, mean age 50.7 years ± SD 9.8 years). All subjects were tested before and after application of tDCS (2mA, 22 minutes) in a within-subject design. Each subject received anodal tDCS applied to the cerebellum, anodal tDCS applied to M1 or sham-stimulation with a break of one week between the three experimental sessions.

Results: There were no clear after-effects of tDCS on grip force control neither in control participants nor in cerebellar patients. Cerebellar patients showed typical impairments with higher grip forces, a higher variability of movements.

Conclusion: In the present study, deficits in grip force control were neither improved by tDCS applied over the cerebellum nor M1 in cerebellar degeneration.

Keywords: After effects, Motor Cortex, Cerebellum, Direct current

INTRODUCTION

While moving hand-held objects, inertial loads arise from the acceleration of the object mass and grip forces must prevent slippage of the object despite the destabilizing loads (Brandauer et al., 2010). In healthy subjects, grip and load force change in parallel indicating that the grip force is adjusted in a predictive way in order to compensate changing load forces (Flanagan and Wing, 1990; Flanagan et al., 2006). Apart from load perturbations grip force control depends on physical object properties such as weight, shape and surface friction (Flanagan and Johansson, 2002; Johansson and Westling, 1988). During free movement of a hand held object cerebellar patients typically show slower movements, higher peak grip forces and higher movement variability compared to healthy controls (Brandauer et al., 2010; Küper et al., 2011a). Less efficient coupling of grip and load forces was reported in some studies (Nowak and Hermsdörfer, 2004; Rost et al., 2005) but was not detected in others (Brandauer et al., 2010; Küper et al., 2011a). The impaired grip force control found in cerebellar patients likely adds to patients´ disability in everyday life. As yet, controlled studies are lacking of rehabilitative interventions to improve grip force control in cerebellar patients.

Because of its ability to modify cerebellar excitability and to induce plastic modifications without significant side effects, cerebellar transcranial direct current stimulation (tDCS) may be a powerful tool in the rehabilitation of cerebellar patients (Ferrucci et al., 2016). As yet, it is unknown whether tDCS improves deficits of cerebellar patients in grip-force control.

A seminal study conducted by Galea et al. (2010b) demonstrated that anodal cerebellar tDCS led to faster visuomotor-adaptation in young and healthy subjects. Galea et al. applied anodal stimulation over the right cerebellum during the experimental task ("online stimulation") (Flanagan and Wing, 1990). In a recent sham-controlled study, a single session of cerebellar anodal tDCS was followed by significant improvement of ataxia (Benussi et al., 2015) as assessed by the Scale for the Assessment and Rating of Ataxia (SARA; Schmitz-Hübsch et al., 2006) and the International Cooperative Ataxia Rating Scale (ICARS; Trouillas et al., 1997). Importantly, there was also a better performance in the 9-hole peg test as a marker of upper limb coordination and finger dexterity. These results were replicated in a study looking at long-term effects. Anodal tDCS was applied 5 days a week for two weeks. Positive effects were still present after 3 months (Benussi et al., 2017). In both studies anodal stimulation was applied over the cerebellum bilaterally. Outcome measures were assessed after the stimulation ("offline stimulation").

TDCS of the motor cortex may also be helpful in treatment of cerebellar disease because motor cortex excitability is reduced in patients with cerebellar disease (Liepert et al., 2009; Manto and Taib, 2008). Bilateral M1-stimulation was followed by improvement of ataxic gait with better symmetry of step execution and reduction of base-width in three patients with cerebellar disease (Pozzi et al., 2013) (anodal electrode placed over M1 contralateral to the most affected side, offline stimulation). Authors also reported improvements in the SARA score for upper limb function. Therefore, M1 stimulation maybe another promising approach to improve grip-force modulation in cerebellar patients.

Few studies have assessed the effects of tDCS on the learning and retention of the control of grip forces. One study found a better reproduction of an irregular force pattern in participants who received five days of anodal tDCS over the contralateral M1 (offline stimulation). Consolidation of performance was improved over the night in the tDCS group (Reis et al., 2009). Other studies reported heterogeneous findings, such as absent effects of anodal tDCS stimulation over contralateral M1 (online and offline stimulation) in a grip force tracking task (Minarik et al., 2016) or performance decrements in the form of increased variability in an isometric constant grip force task (Parikh and Cole, 2014). Investigating the grasping and lifting of objects with different surface material in elderly subjects, the authors reported a decrease of the grip force in those subject who practiced a different fine motor task during tDCS stimulation of contralateral M1 compared to subjects who practiced with sham stimulation (Parikh and Cole, 2015). The effect of stimulation was particularly evident with a more slippery surface and less with the rougher surface and the timing of the lifting act was not affected. Interestingly, the application of dual hemisphere tDCS (online and offline stimulation) in a group of stroke patients resulted in a decrease of grip forces and a decreased time to establish the grip during a similar grasping and lifting task (Lefebvre et al., 2013a). Heterogeneous effects of tDCS over M1 have been reported in healthy subjects, elderly subjects or stroke patients. As yet, effects of tDCS on disordered grip force control in cerebellar patients are lacking.

In the present study we assessed the effect of tDCS applied to the cerebellum or M1 on grip-force modulation during self-generated, sinusoidal up-down movements with a handheld object in healthy subjects and patients with cerebellar degeneration. We hypothesized that anodal tDCS over the cerebellum or M1 improves grip-force control in cerebellar patients. We expected higher movement frequencies, lower grip forces and more precise coupling after stimulation in the patient group.

MATERIALS AND METHODS

Participants

Fourteen individuals with pure cerebellar degeneration (6 females; mean age ± SD of 51.2 ± 7.6 years) and fourteen age-matched controls without any known neurological diseases (5 females; mean age ± SD 50.8 ± 10.1 years) participated in this study. All subjects were right-handed as assessed by the Edinburgh Handedness Inventory (Oldfield, 1971). A summary of the subjects' characteristics can be found in **Table 1**. The severity of cerebellar symptoms in cerebellar participants were assessed by two experienced neurologists (DT & MK) based on the International Cooperative Ataxia Rating Scale (ICARS; Trouillas et al., 1997) and the Scale for the Assessment and Rating of Ataxia (SARA; Schmitz-Hübsch et al., 2006). Five cerebellar participants had a genetically defined spinocerebellar ataxia (SCA6, SCA14). Five participants presented with autosomal dominant cerebellar ataxia (ADCA) type III. Three cerebellar participants had sporadic adult onset ataxia of unknown etiology (SAOA). One cerebellar participant presented with cerebellar degeneration caused by cerebellitis. These disorders are known to primarily affect the cerebellum (Gomez et al., 1997; Timmann et al., 2009). All subjects gave informed oral and written consent. The experiment was approved by the ethics committee of the medical faculty of the University of Duisburg-Essen and conducted in accordance with the Declaration of Helsinki. This study was conducted as part of another study investigating the direct tDCS effects on reach adaptation (Hulst et al., 2017).

Task

All subjects participated in a task designed to analyze grip force adjustments according to movement induced load changes while holding an object. The task has been introduced by Flanagan and Wing (Flanagan and Wing, 1990). The set-up in the present study has been used by Brandauer et al. in previous studies (Brandauer et al., 2010; Flanagan and Wing, 1990).

Subjects' grasped a custom-made instrumented object with their right hand. The object had a rectangular form with two grasping surfaces (60 x 60mm) and a width of 26 mm. The grasping surfaces were covered with medium grain sandpaper (No. 240).

Table 1. Overview Cerebellar subjects and Control subjects. Cerebellar subjects were age-matched with the control subject on the right side of the table.

Cerebellar subjects							Controls		
ID	Age	Sex	Diagnosis	Disease duration	ICARS (total/100)	ICARS UL (total/20)	ID	Age	Sex
P01	30	M	SAOA	9 years	38.5	7.5	C01	28	M
P02	47	M	ADCA III	12 years	43.5	4.5	C02	33	M
P03	47	M	ADCA III	17 years	32.5	4.5	C03	47	M
P04	48	F	ADCA III	28 years	19	1	C04	47	M
P05	48	M	SCA 14	25 years	20	3	C05	50	F
P06	50	F	SCA 14	17 years	17	1	C06	51	F
P07	52	M	ADCA III	6 years	19.5	3	C07	52	M
P08	53	M	Cerebellitis	10 years	46	5	C08	54	M
P09	54	F	SCA 14	25 years	27	3.5	C09	55	M
P10	54	F	SAOA	18 years	31	4.5	C10	55	M
P11	55	M	SAOA	18 years	48	5	C11	55	F
P12	58	F	SCA 6	8 years	43.5	10	C12	57	F
P13	60	F	ADCA III	13 years	23	11	C13	63	F
P14	61	M	SCA 6	4 years	9	0	C14	65	M

SCA6 = spinocerebellar ataxia type 6; SCA14 = spinocerebellar ataxia type 14; SAOA = sporadic adult onset ataxia; ADCA III = autosomal dominant ataxia type III; ICARS = International Cooperative Ataxia Rating Scale (Trouillas et al., 1997). ICARS UL = score of right upper limb in finger-to-nose test, finger-to-finger test, pronation/supination and Archimedes spiral drawing. Disease duration is years since presentation of the first symptoms.

The object incorporated sensors to record the grip force on each side (0–100 N, accuracy ± 0.1 N), the linear vertical and horizontal accelerations tangential to the grasping surfaces (± 50 m/s^2, accuracy ± 0.2 m/s^2), and the load force (0–60 N, accuracy ± 0.1 N).

The grip force of both sensors for each side was averaged. To increase the amplitude of the movement-induced sinusoidal load changes, a weight of 300 g was fixed to the object which increased the total weight of the object to 500 g. Vertical acceleration (AccZ) was defined as pure kinematic acceleration due to movement. The net load force was calculated as the vectorial sum of weight ($m \times g$), acting vertically, and the acceleration-dependent inertial loads in the vertical and sagittal directions ($m \times$ AccZ, $m \times$ AccY), acting tangential to the grip surfaces

$$LF = m \times \sqrt{(AccZ + g)^2 + AccY^2}$$

Participants were asked to grasp the object and to hold it with the right hand in front of their trunk with grip surfaces vertical and parallel to their front. This orientation was kept constant during the movement. It was required to grasp the center of the object with the thumb on one side and the index and middle fingers on the opposite side. The three-finger grip was used to minimize rotational torques that arise when the object is grasped away from the center of mass.

After a verbal command subjects had to move the object along a vertical line up and down with an amplitude of about 30 cm at a frequency of about 0.8 Hz, which was demonstrated by the examiner sitting opposite to the subject by moving the hand up and down. The accurate movement execution was visually monitored by the examiner.

Following one practice trial, five trials of 22 seconds duration were performed successively.

Data analysis

As the first step of data analysis, the first two seconds of each trial were discarded and the remaining 20 s divided into two 10 s-intervals so that 10 intervals per condition resulted.

The following measures were determined for each intervals:

- Movement frequency and vertical acceleration
- Variation of maximal/minimal acceleration during up/down movements as a measure for arm movement variability
- Peak grip force levels
- Coupling of grip and load forces

To quantify the performance in each interval, a computer algorithm first searched for peaks (local maxima and minima) in the sinusoidal profile of the vertical acceleration. Positive acceleration peaks corresponding to load force peaks occur at the lower turning point of the movement, negative accelerations and minimum loads occur at the upper turning point. The magnitude of vertical acceleration was calculated as the averaged acceleration range between positive and negative acceleration peaks. Variability was calculated as the standard deviation of positive and negative acceleration peaks within each interval (averaged for positive and negative peaks) related to the vertical acceleration magnitude described above. Movement frequency was determined from the power spectra of the acceleration profile.

To quantify the magnitude of the produced grip forces, the grip force peaks were determined in a window around each load force peak. In addition, minima of the ratio between grip-

force and load-force were determined in the windows. Both values were averaged for each 10 second interval. The force ratio represents a measure of the efficiency of the grip-force output related to the load.

The coupling between the modulation of grip-force and load-force was evaluated by calculating the cross-correlation function between both time series. The maximum cross-correlation coefficient was taken as the indicator of the precision of the coupling.

The resulting data values were averaged across the intervals of each participant and each condition.

tDCS

Participants were invited for three experimental sessions separated by one week. In two sessions, subjects received verum tDCS stimulation, in one session sham stimulation. Anodal tDCS was performed over M1 and over the cerebellum. Sham tDCS stimulation was performed either over M1 or cerebellum. The order of the three sessions was counterbalanced between participants.

The grasping task was performed as part of another study (Hulst et al., 2017). In that study tDCS was applied during reach adaptation. The grasping task was performed before the reach adaptation task (and therefore prior tDCS) and after the reach adaptation task. The second testing took place on average 10:52 min (mean, ± 1:34 min SD) after the end of tDCS in patients, and 9:52 min (mean, ± 3:55 min SD) in the control group.

Stimulation parameters were chosen in close accordance with previous studies of Galea et al. (Galea et al., 2009, 2010a). Anodal tDCS was delivered through two rubber electrodes (5 cm x 5 cm; surface area: 25 cm^2) covered with conductive paste (Ten20 Conductive; Weaver) via a NeuroConn device (DC-Stimulator PLUS; NeuroConn). For cerebellar stimulation the anodal electrode was placed over the right cerebellar cortex, with the center of the electrode being 3 cm lateral to the inion, and the cathodal electrode was placed on the right buccinator muscle. The anodal electrode for M1 stimulation was centered over the area of the left primary motor cortex which elicited a response of the first dorsal interosseous muscle after single transcranial magnetic stimulation (TMS) pulses. TMS was delivered by a MagPro magnetic stimulator (MagPro; Dantec). The cathodal electrode was placed on the skin overlying the contralateral supraorbital region. During each experimental session, the electrodes were placed over all four stimulation locations, so participants were blinded for stimulation location.

In both cerebellar and M1 anodal stimulation, the target stimulation intensity was set at 2 mA, resulting in a current density of 0.08 mA/cm^2. Current was ramped up from 0 mA to 2 mA in a period of 30 seconds. At the end of tDCS stimulation, current was ramped down from 2 mA to 0 mA in 30 seconds. In sham stimulation current was ramped-up in 30 seconds, remained at 2 mA for a duration of 60 seconds, after which current was ramped down again.

On average, subjects were stimulated for 25:34 min (mean, ± 6:34 min SD) in the patient group and for 21:37 min (mean, ± 2:32 min SD) in the control group.

One experimenter (LJ) ran all the behavioral experiments and used a prepared set of stimulation codes in order to remain blinded for stimulation polarity (sham or anodal). An experimenter (BB) who was not involved in the collection of behavioral data, deblinded the stimulation codes after data collection had ended.

Statistical analysis

To assess the differences between the single-task conditions, repeated-measures ANOVAs were calculated with the between-subject factor "group" (controls, patients) and the within-subject factors "stimulation" (cerebellum, M1, sham) and "time" (pre stimulation, post stimulation). We expected to find differences between patients and control subjects obvious as effects (main and interactions) involving the factor "group" for the different measures. In addition, we expected that the ANOVA reveals effects of tDCS stimulation obvious as interactions between "stimulation" and "time" and also as a three way interaction to indicate differences in the effects of stimulation between patients and control subjects. T-tests were used for post hoc analyses. An alpha level of 0.05 was chosen to indicate statistical significance.

Intervals were excluded from statistical analyses if movements were performed very slowly (movement frequency < 0.3 Hz, 0.4% of 10 second intervals) or if values of behavioral measures were out of two standard deviations of the mean (14.3% 10 second intervals in controls excluded, 12.9% 10 second intervals in patients excluded). The number of excluded intervals in each subject and condition never exceeded three, resulting in a minimum of seven data values that were averaged for each condition. In one patient, pre-stimulation data for the M1 session were missing preventing the inclusion of the subject in the statistical analysis. Acceleration data were missing due to technical problems in another patient for sham stimulation (pre and post tDCS).

RESULTS

Performance of single patient

Figure 1 shows the profiles of the vertical acceleration of the grasped object (AccZ), the combined gravitational and inertial load that result from the movements (LF) and the produced grip force (GF) in one patient and in one healthy control subject before and after the anodal stimulation of the cerebellum. The patient moved faster after the stimulation as obvious from higher accelerations. The patient's grip force profile is clearly more irregular than the load force profile indicating decreased precision of the coupling between both forces. Nevertheless, most grip force peaks coincide in time roughly with main peaks of the load force profiles indicated some preservation of anticipatory control of the grip force. In the control subject, the grip force profile is regular and the timing of grip force peaks anticipates the loads force peaks. The magnitudes of the grip force peaks are substantially higher in the patient compared to the control subject. In general, the individual patient's behavior reflects the performance of the patients' group. No clear changes of grip force control were obvious before and after the stimulations and for the different stimulation conditions.

Group data

Subjects produced cyclic movements with frequencies slightly lower than instructed (overall data including patients and controls prior and post stimulation: mean 0.73 ± 0.17 Hz). Movement frequencies were somewhat higher for controls compared to patients without statistical significance (patients: 0.69 ± 0.16 Hz, controls: 0.76 ± 0.15 Hz, main effect of "group": P> 0.1). The only significant effect was an increase of frequency after the stimulation compared to pre-stimulation values for all participants including patients and controls (pre tDCS: 0.72 ± 0.16 Hz, post tDCS: 0.74 ± 0.15 Hz, main effect of "time": $F(1,25) = 7.8$, P= 0.010). The ANOVA results for the magnitude of arm acceleration reflected the findings for the frequency with higher accelerations produced post-stimulation (pre-tDCS: $11.3 \pm 4.6 m/s^2$, post-tDCS: $13.0 \pm 4.7 m/s^2$, main effect of "time": $F(1,24)= 42.9$, P<0.001) regardless from the group and whether cerebellar, M1 or sham stimulation was applied (all other main effects and interactions: P> 0.1). Thus, the kinematics of arm movements and consequently also the self-generated loads where comparable in magnitude between patients and control subjects as intended by the procedure.
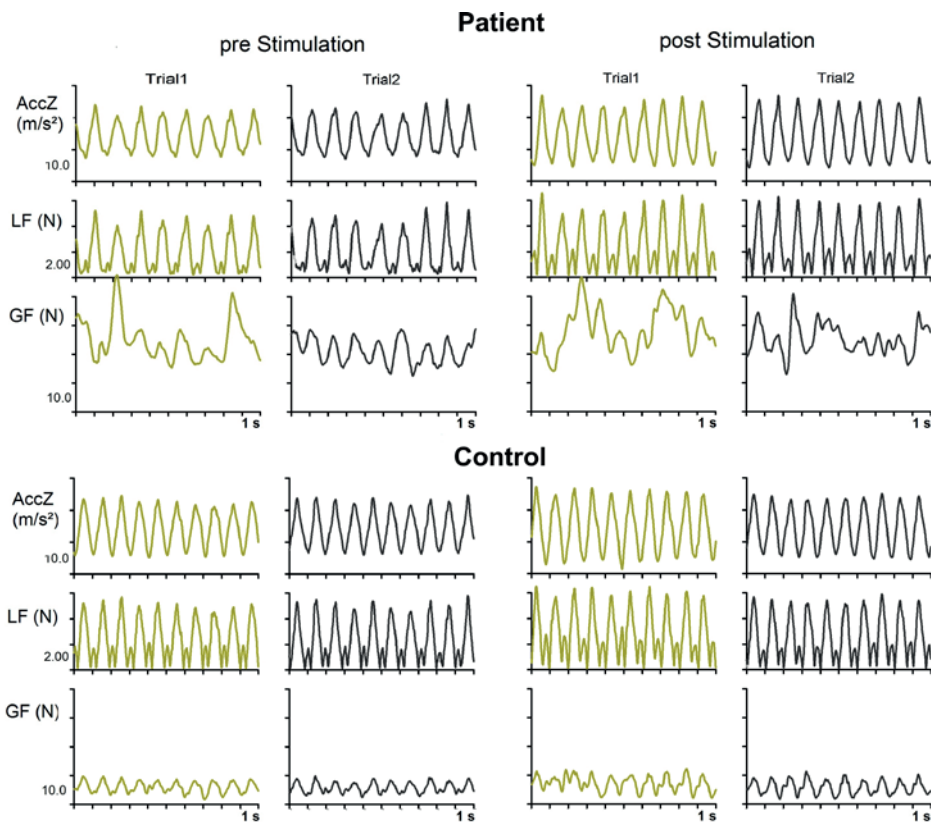
Figure 1. Individual subject data. Vertical acceleration (AccZ), load force (LF) and grip force (GF) during 10 second intervals of continuous cyclic up-and-down movements of the grasped manipulandum. The first interval (2-12 s) of two out of five test trials before and after cerebellar tDCS of one individual patient and one healthy control subject is shown.

Variability of arm movements was higher in patients through all conditions compared to controls (main effect of "group": $F(1,24) = 6.0$, $P = 0.022$, see **Figure 2**). Variability was lower post-stimulation for both groups (main effect of "time": $F(1,24) = 20.8$, $P < 0.001$) and a statistically significant interaction between "time" and "group" ($F(1,24) = 9.9$, $P = 0.004$) indicates that the difference between groups was most prominent before the stimulations. Indeed the post-hoc test found a difference between patients and control subjects for the tests prior to tDCS ($t = 2.6$, $P = 0.016$), but not after tDCS ($P > 0.1$). No significant main effect nor any interaction were found for the factor "stimulation" ($P > 0.1$).
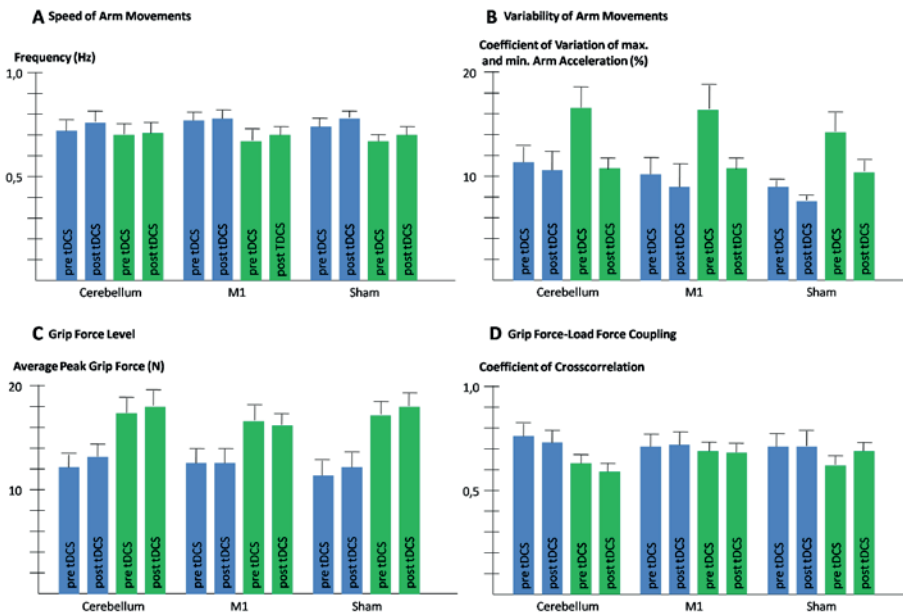
Figure 2. Group effects. Effects of tDCS on Movement speed (A), variability of movements (B), grip force levels (C) and grip force-load force coupling (D). Blue bars = controls, green bars = cerebellar patients.

The average magnitude of peak grip forces exhibited by patients were clearly higher through all conditions compared to controls (main effect of "group": $F(1,24) = 11.0$, $P = 0.003$, see **Figure 2**). The analysis for the ratio of grip force to load force confirmed the findings for the absolute value for grip force (main effect of "group": $F(1,24) = 8.3$, $P = 0.008$). No other factor nor any interaction reached statistical significance ($P > 0.1$).

The maximum coefficient of cross-correlation that measures the precision of the coupling between the grip force and the load force was higher in control subjects than in patients (see **Figure 2**). The main effect of "group" was however not statistically significant ($P > 0.1$). The factor "group" was statistically significant for the interaction with "stimulation" ($F(2,50) = 5.8$, $P = 0.005$). **Figure 2** suggests that particularly in the session with cerebellar stimulation, patients were less precise than control subjects. Pair-wise post-hoc tests detected a trend for this group difference ($t = -2.0$, $P = 0.059$), while no differences were obvious in the other stimulation conditions ($P > 0.1$). Furthermore, an interaction of "stimulation" x "time" was detected ($F(2,50) = 3.3$, $P = 0.044$). **Figure 2** suggests that the coupling improved after the sham stimulation and deteriorated after cerebellar stimulation. However, pairwise post-hoc tests failed to prove difference between pre and post stimulation values in any of the three stimulation conditions (all $P > 0.1$). No interaction was found between "group" and

"time" nor was the 3-way interaction between all factors significant. Thus, no differential effects of stimulation were evident in the patient group. There was no benefit on grip force control neither in cerebellar patients nor in controls following anodal tDCS applied over the cerebellum or M1.

DISCUSSION

Contrary to our hypothesis, there were no consistent tDCS effects on disordered grip-force control in cerebellar patients. Patients with cerebellar degeneration exhibited higher grip-forces and higher variability of movements, which is in good accordance with previous studies (Brandauer et al., 2010; Nowak and Hermsdörfer, 2004). While impaired coupling of grip- and load-forces are also often observed in cerebellar patients (Brandauer et al., 2010; Küper et al., 2011a, 2011b), deficits in this measure were only present at a trend level in the current study. An increase in movement speed and acceleration post-stimulation was observed in patients and controls and irrespective of the stimulation condition and therefore likely attributed to practice effects. A further practice effects was evident for movement variability particularly in cerebellar patients. Possible reasons for the lack of cerebellar tDCS effects are discussed below.

Firstly, in the current study after-effects of tDCS were investigated. After-effects of tDCS have been detected up to 90 min following M1 stimulation based on changes in motor evoked potential amplitudes (Nitsche and Paulus, 2001). Most studies examining therapeutic effects of tDCS in cerebellar patients, including the studies conducted by Benussi et al. (2015, 2017), used off-line stimulation (Dun et al., 2016). The influential studies by Galea et al. (2009, 2010b), however, examined direct effects of tDCS, that is they applied an online stimulation approach. We cannot exclude that direct tDCS may have stronger effects on grip force control in cerebellar patients than tDCS after-effects.

Secondly, electrode positioning may have been suboptimal for the present task. Benussi et al. (2015, 2017), used a location which was centered in the midline, while we used a location centered over the right lateral cerebellum. A modelling study using the same electrode placement as we did, demonstrated current distribution mainly over the lateral posterior cerebellum sparing the vermis and intermediate cerebellum (Rampersad et al., 2014). Yet, deficits in grip force control in degenerative cerebellar patients were associated with atrophy of the intermediate cerebellum (Brandauer et al., 2008). The reach adaptation studies of Galea et al. (2009, 2010b), on the other hand, showed clear effects of cerebellar

tDCS using a similar electrode location as in the current study. An association of impaired prehensile movements has also been demonstrated with more lateral cerebellar areas in focal cerebellar patients (Küper et al., 2011a, 2011b).

Thirdly, cerebellar tDCS effects may differ depending on the type of cerebellar degeneration. The pattern of cerebellar atrophy differs depending on the type of spinocerebellar ataxia, and extra-cerebellar areas are affected to various degrees (Jacobi et al., 2013; Reetz et al., 2013).

Fourthly, one must also consider variability of performance as a critical factor that could obscure intervention effects. While on average we succeeded to standardize the movement generated load profiles, individual trials deviated from the indented movement. Movements with relatively low frequency may have reduced the benefit of a precise coupling between grip force and load in control subjects and may therefore have been responsible for the missing group differences in coupling. Variability of the outcome measures may also have played a role. For example, it is difficult to reconcile the difference for coupling precision between patients and control subjects in the session with cerebellar stimulation compared to the other conditions. Since this interaction was independent of the time of testing, also the pre-stimulation data supported this effect. Therefore, variability of baseline performance in the cerebellar patients may have influenced this finding. Variability was however lower for the grip force and not even a tendency supporting any effect of stimulation was obvious. It therefore seems improbable that variability alone could explain the missing effects of stimulation.

Fifthly, we cannot exclude that the performance of the reach adaption task, which was performed during tDCS stimulation, had interfered with tDCS after-effects on grip force control.

Finally, cerebellar tDCS effects may be highly task dependent. Recently, Jalali et al. (2017) did not replicate effects on cerebellar tDCS on visuomotor adaptation reported previously (Galea et al., 2010a) when a range of task parameter were systematically varied. Besides, other studies report that cerebellar tDCS had no effects on motor learning in healthy controls and patients with cerebellar degeneration (Hulst et al., 2017; Steiner et al., 2016). Due to these inconsistencies it has been questioned whether cerebellar tDCS could become a valuable tool in clinical neurorehabilitation (Hulst et al., 2017; Jalali et al., 2017).

Like cerebellar stimulation, M1-stimulation was not followed by significant effects on grip force control. There was a major difference in the setup used in a prior study reporting reduction of ataxia (Pozzi et al., 2013). The authors used bilateral M1 stimulation. The

anodal electrode was placed on the motor cortex contralateral to the most affected side and the cathode stimulation was placed on motor cortex of the less affected side of the body. In the present study the cathodal electrode was placed over the contralateral supraorbital region. It cannot be excluded that bilateral M1 stimulation leads to changes in grip force control. Reminiscent of the above findings, bilateral stimulation of the M1 lead to improved control of grip force during grasping and lifting of an object in stroke patients (Lefebvre et al., 2013a). In a similar task tested in a sample of elderly subjects, unilateral stimulation of M1 also resulted in an increase efficiency of grip force control. However, results were not consistent. They were significant only for one of two object surface materials and not obvious for a temporal measure (Parikh and Cole, 2015).
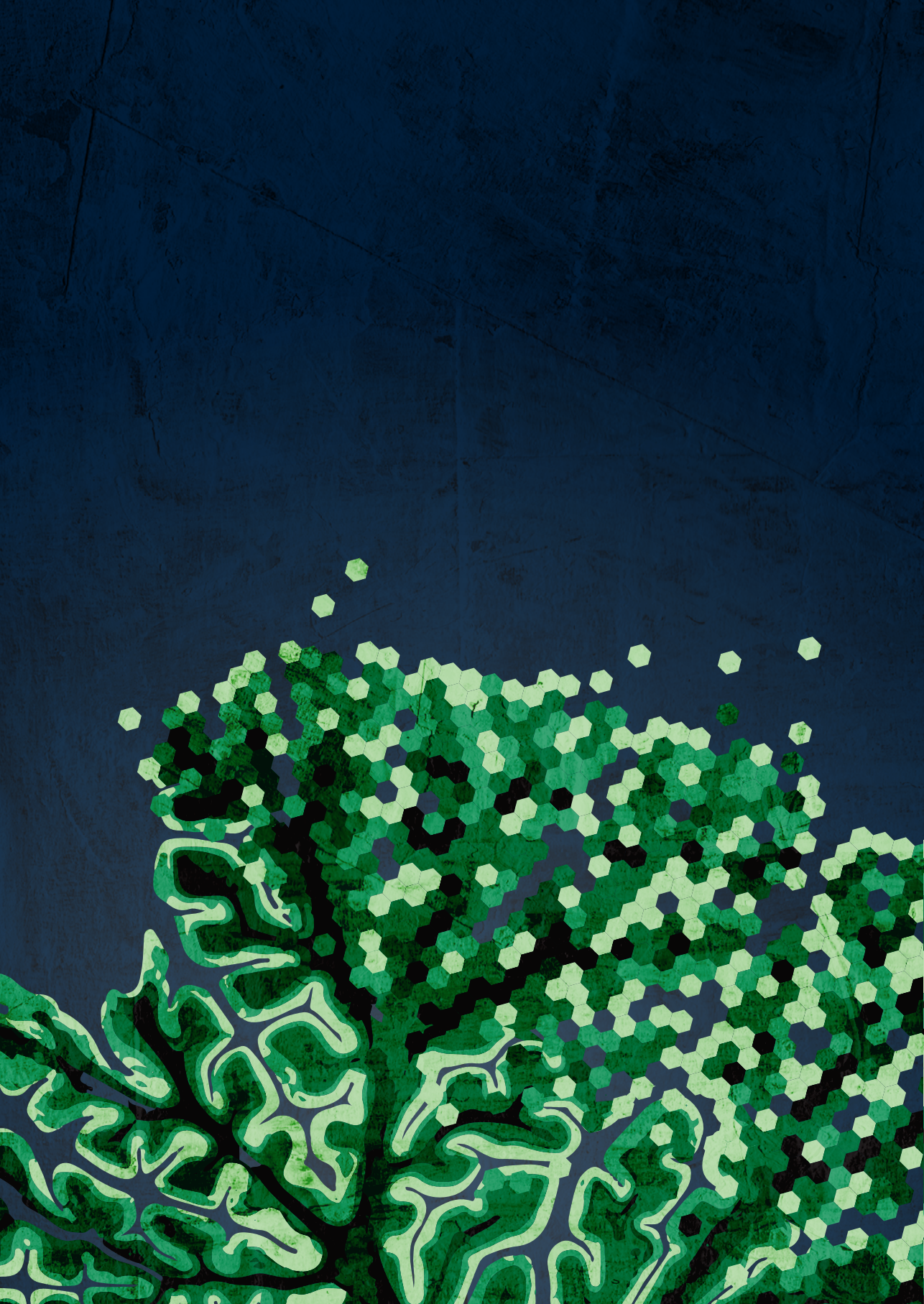
CONCLUSION

No effects of cerebellar or M1 anodal tDCS were observed on grip force control in cerebellar patients. Further studies are needed to explore different stimulation parameters including online stimulation and/or optimized electrode placements. At present tDCS cannot be recommended in the neurorehabilitation of disordered grip force control in cerebellar disease.

Author contributions
Thomas Hulst drafted manuscript; edited and revised manuscript; approved the final version of the manuscript.

7

No effects of cerebellar transcranial direct current stimulation (tDCS) on force field and visuomotor reach adaptation in young and healthy subjects

Mamlins A.[1], Hulst T. [1,2], Donchin O. [3], Timmann D. [1], Claassen J. [1]

[1] Department of Neurology, University Hospital Essen, University of Duisburg-Essen, Germany
[2] Department of Neuroscience, Erasmus MC, 3000 CA Rotterdam, The Netherlands;
Erasmus University College, Rotterdam, The Netherlands.
[3] Ben-Gurion University of the Negev, Department of Biomedical Engineering
and Zlotowski Center for Neuroscience, Beer Sheva, Israel
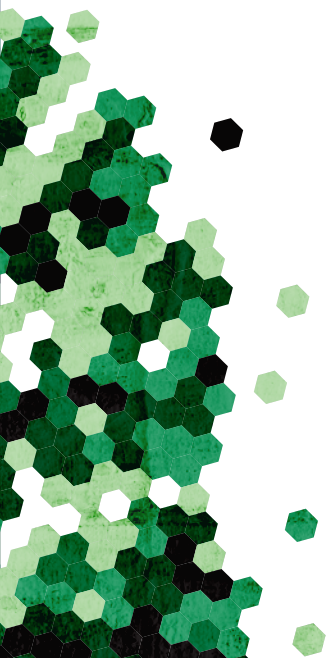
ABSTRACT

Previous studies have shown that cerebellar transcranial direct current stimulation (tDCS) leads to faster adaptation of arm reaching movements to visuomotor rotation and force field perturbations in healthy subjects. The first aim of the present study was to confirm a stimulation-dependent effect on motor adaptation. Secondly, we investigated whether tDCS effects differ depending on onset, that is prior to or at the beginning of the adaptation phase.

A total of 120 healthy and right-handed subjects (60 females, mean age 23.2 ± 2.7 years, range 18-31 years) were tested. Subjects moved a cursor with a manipulandum to one of eight targets presented on a vertically orientated screen. Three baseline blocks were followed by one adaptation block and three washout blocks. 60 subjects did a force field adaptation task (FF), and 60 subjects a visuomotor adaptation task (VM). Equal numbers of subjects received anodal, cathodal or sham cerebellar tDCS beginning either in the third baseline block or at the start of the adaptation block. In FF and VM, tDCS and the onset of tDCS did not show a significant effect on motor adaptation (all p values > 0.05). We were unable to support previous findings of modulatory cerebellar tDCS effects in reaching adaptation tasks in healthy subjects. Prior possible application in patients with cerebellar disease, future experiments are needed to determine which tDCS and task parameters lead to robust tDCS effects.

Keywords: tDCS, cerebellum, force field, visuomotor, adaptation

INTRODUCTION

Cerebellar transcranial direct current stimulation (tDCS) has been described to improve motor learning (Celnik, 2015) and is regarded as a promising tool to treat ataxias (Benussi et al., 2015, 2017) and other neurological disorders (Ferrucci et al., 2016). Recently, however, there have been multiple studies reporting negative results of direct current stimulation (Beyer et al., 2017; Hulst et al., 2017; Jalali et al., 2017; Steiner et al., 2016; van der Vliet et al., 2017), which contrasts with affirmative findings (Galea et al., 2010a; Herzfeld et al., 2014a; Leow et al., 2014).

For instance, cerebellar direct current stimulation in arm reaching movements has shown clear-cut effects on adaptation with anodal stimulation increasing and cathodal stimulation reducing error-dependent learning in healthy subjects to visuomotor transformations and force field perturbations in two influential studies (Galea et al., 2010 [anodal tDCS]; Herzfeld et al., 2014 [anodal and cathodal tDCS]), but much subtler effects of tDCS in one recent study (Jalali et al., 2017) and no pronounced effects in another study of tDCS during reaching adaptation (Hulst et al., 2017). While the experimental conditions in the aforementioned studies were largely similar, subtle differences can be found in the task parameters of each study, which may have affected tDCS efficacy. In particular Jalali et al. (2017) make a conscientious effort to investigate tDCS effects under different task-parameters.

Besides optimizing task parameters, finding the appropriate stimulation parameters might also reinforce tDCS effects. That is, stimulation duration and the time point of stimulation onset might also influence stimulation effects, e.g. direct current stimulation can be started before task onset (i.e. in baseline) (Galea et al., 2010a; Herzfeld et al., 2014a; Hulst et al., 2017) and continued throughout the task, or it can be started simultaneously with the beginning of the task (Ehsani et al., 2016; Wessel et al., 2016). The majority of previous arm reaching adaptation studies (Galea et al., 2010a; Herzfeld et al., 2014a; Hulst et al., 2017; Jalali et al., 2017) started stimulation in baseline and continued stimulation throughout adaptation. Starting tDCS in baseline allows to control for possible tDCS effects on motor performance in unperturbed trials. tDCS, however, has both online and offline effects (e.g. Yavari et al. 2018 for recent review). Online tDCS effects may be hampered by a homeostatic effect on plasticity after exposure to electrical stimulation. The response to non-invasive brain stimulation seems to depend on the previous state of the neurons (Ridding and Ziemann, 2010). Abraham and Bear (1996) coined the term "metaplasticity" referring to synaptic plasticity that has been modulated by prior synaptic activity. This mechanism seems to affect LTP and LTD processes (Abraham and Bear, 1996) which is particularly important for our study because especially LTD has been described to be crucial for cerebellar dependent

learning (Albus, 1971; Ekerot and Kano, 1985; Ito and Kano, 1982; Ito et al., 1982; Marr, 1969; Sakurai, 1987). Various non-invasive stimulation methods have been shown to be capable of influencing the LTP and LTD response in a metaplastic matter (for a review: Ridding and Ziemann, 2010). In terms of tDCS, preconditioning with anodal tDCS led to a reduced corticospinal excitability, whereas preconditioning with cathodal tDCS caused an increased corticospinal excitability (Lang et al., 2004; Siebner et al., 2004). This is why many previous motor sequence learning studies avoid to start in the baseline phase (Prichard et al., 2014; Reis and Fritsch, 2011; Reis et al., 2015).

We conducted a force field reaching adaptation experiment and a visuomotor reaching adaptation experiment. First, we wanted to confirm previous modulatory effects of cerebellar tDCS in a force field and a visuomotor arm reaching adaptation paradigm. Our second aim was to test whether these effects differed depending on the onset of stimulation. We hypothesized that stimulation starting in baseline would act like a preconditioning stimulus leading to homeostatic metaplasticity resulting in reduced effectivity of anodal stimulation. Hence, we expected that anodal stimulation starting at the beginning of the adaptation phase would cause faster adaptation than in other groups. Furthermore, we supposed that stimulation onset in adaptation leads to more robust effects due to a lack of homeostatic mechanisms that may take place during baseline stimulation.

METHODS

Subjects

One hundred and twenty right-handed subjects (60 females, mean age 23.2 ± SD 2.7 years) participated in this study. None of the subjects presented any abnormalities in a standard neurological examination, had a history of neurologic or psychiatric disorders, or was taking centrally acting medication. Additional exclusion criteria included: metallic or electronic implants, former attendance in a transcranial brain stimulation or motor adaptation study, pregnancy or breastfeeding and damaged skin on head and face. The subjects were asked to avoid both smoking and consuming drinks containing alcohol and/or caffeine on the day of the experiment. The study was approved by the local Ethics Committee. All subjects gave their written informed consent.

Experimental set-up and procedure

The subjects were seated in front of a vertical monitor (screen length: 30 cm, screen width: 48 cm) at a distance of approximately 60 cm grasping the handle of a two-joint manipulandum with their dominant right hand (**Figure 1A**). This set-up was similar to a previous study

from our lab (Rabe et al., 2009). The vision of the hand was blocked by a black cloth. Subjects' arm movements were registered by an encoder placed on each of the two motors that were connected to the manipulandum using the analog inputs of a motor controller card, with a sampling rate of 500 Hz (DMC-1826; Galil Motion Control). The position of the handle was represented by a black cursor (diameter: 3 mm) on the white screen. At the beginning of each movement a green dot (diameter: 7 mm) appeared in the middle of the screen, which represented the starting position. Whenever the cursor passed the starting position, a grey target dot (diameter: 7 mm) appeared on one of the eight possible positions. The targets were oriented with an angle of 45° to each other and had a distance of 10 cm to the starting point. All subjects were told to make a fast 'shooting' movement through the target without stopping at the end. When the required radius of 10 cm was passed, the forces of the manipulandum stopped the movement, similar like hitting against a cushion. The manipulandum was then brought back to the starting position by the motors. The cursor reappeared when coming within a distance of 2 cm to the starting position. To avoid a high variability in velocity and thus performance differences, the subjects got a velocity feedback (i.e. change of target color) after passing the radius of 10 cm at the end of each movement (blue = too slow, yellow = required velocity, red = too fast). The optimal time window for the first trial was between 250 ms and 750 ms. The required time window for the subsequent movements was adapted to the subject's speed. The lower (250 ms) and the upper (750 ms) border were reduced by 10% if the movement was within these boundaries or were increased by 10% if the movement was too fast or too slow. A rewarding sound was played together with a yellow colored feedback when the target was hit with the required velocity. We have chosen this range of movement durations (velocity) because two former force field studies used the same/a similar range (Herzfeld et al. 2014: 400-500ms; Hulst et al. 2017: 250-750ms). Although Galea et al. (2009) applied another range of movement durations (275-375 ms) in a visuomotor task, we kept to the same range as in the force field task because when thinking of a potential clinical application of tDCS, for example in cerebellar patients, one has to take into account that patients might perform an adaptation task with lower velocities. Former studies showed slower velocities (Hulst et al., 2017) and longer movement times (Rabe et al., 2009) in upper limb tasks in cerebellar patients.

The experiment consisted of three baseline blocks, one adaptation block and three washout blocks (**Figure 1C**). Each baseline block contained 64 trials. The inter-trial-interval was set to 500 ms. In the adaptation block, either a force field or a visuomotor perturbation was applied to the manipulandum. In this block, 128 trials with an inter-trial-interval of 1500 ms had to be performed. The experiment was completed with three washout blocks of 64 trials respectively and an inter-trial-interval of 500 ms. In washout blocks the perturbation was removed. Furthermore, no vision of the cursor was provided during the movement. Velocity feedback remained. With the washout phase, we wanted to test the

subjects' retention of the acquired adaptation. To prevent subjects from anticipating where the targets should appear, eight sets of eight targets each were pseudorandomized (www. randomizer.org). For the adaptation block, the eight different target orders were doubled. The target order was counterbalanced across the subjects so that half of the subjects had a different target order than the other half.
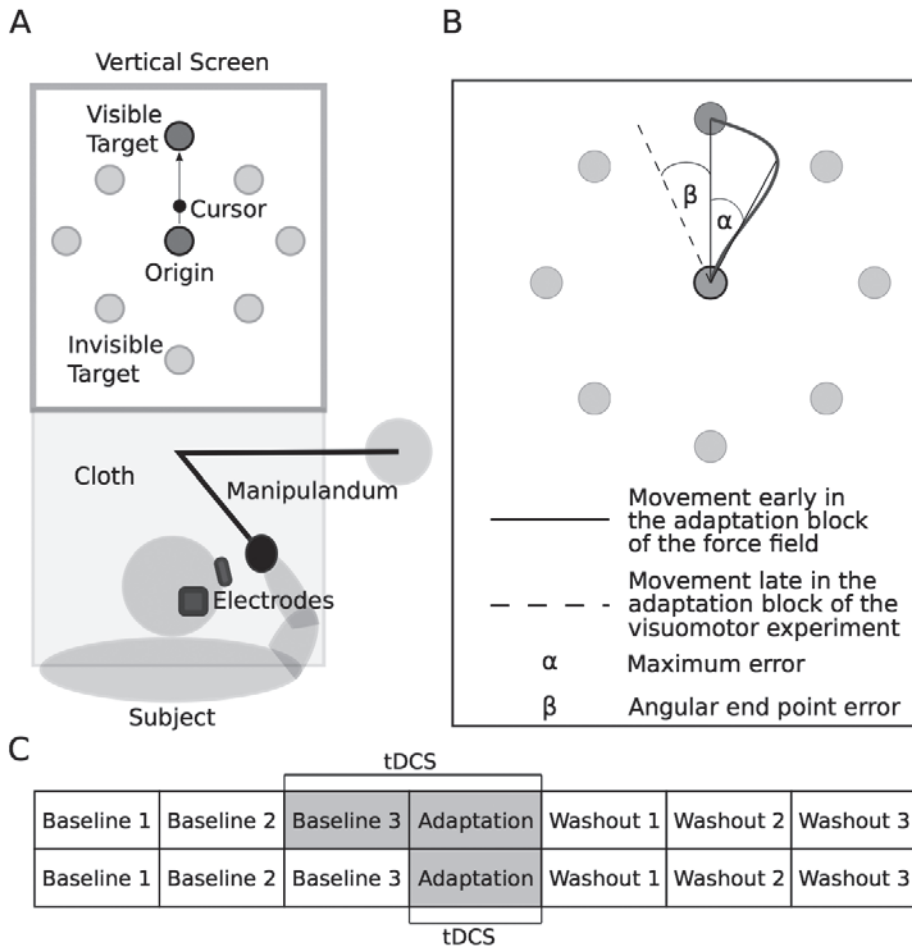

Figure 1. (A) Experimental set-up. The subject is sitting in front of a monitor holding the handle of a two-joint manipulandum with the right hand. Vision of the hand is blocked by a cloth. The active tDCS electrode is centered 3 cm lateral to the inion on the right. The reference electrode is located on the ipsilateral buccinator muscle. The electrodes are connected to the stimulator. (B) Outcome measures. Maximum Error (α) during early adaptation and Angular End point Error (β) during late adaptation. (C) Sequence of blocks in each experiment. Each experiment consisted of seven blocks, three baseline blocks followed by one adaptation block and three washout blocks. TDCS was administered either during baseline 3 and adaptation or only during adaptation.

Experiment 1 – Force field task

Sixty subjects performed experiment 1 (30 females, mean age 24.1 ± SD 2.3, range 20-31). In the force field block, a velocity-dependent clockwise perpendicular force (23 Ns/m) was applied to the manipulandum resulting in a clockwise perturbation of participants' movements.

Experiment 2 – Visuomotor task

Sixty subjects participated in experiment 2 (30 females, mean age 22.3 ± SD 3.1, range 18-31). In the visuomotor task, a 30° clockwise rotation of the cursor was applied. Thus, performing a straight hand movement towards the target, the subject would miss the target by 30°.

Cerebellar transcranial direct current stimulation (cerebellar tDCS)

Cerebellar tDCS was applied using a neuroConn® DC stimulator (model-no: 0021). The active electrode was placed 3 cm lateral to the inion with its center on the same level as the inion. The return electrode was positioned on the ipsilateral buccinator muscle (**Figure 1A**). The placement of the electrodes was based on former force field and visuomotor adaptation studies (Galea et al., 2009; Herzfeld et al., 2014a). An important reason for the placement of the return electrode, is the avoidance of interference with brachial plexus in case of placement on the deltoid muscle (Galea et al., 2009). Additionally, the current flow is likely well-adjusted to the cerebellar axis and electrodes can be fixed easily and reliably. We used two rubber electrodes (neuroConn®) with a commonly used size of 5x5 cm^2 (current density: 0.08mA/ cm^2) (Galea et al., 2009; Herzfeld et al., 2014a). Electrodes were covered with Ten20® conductive paste (Neurodiagnostic Electrode Paste, Weaver and Company, USA) to lower impedance and to prevent skin damage. Rubber electrodes were used instead of sponge electrodes soaked in saline to avoid differences in the distribution of current because of over- or undersaturation of the sponge electrodes (Woods et al., 2015). Current strength was set at 2 mA. This intensity has been shown in former studies to be efficient and safe (Galea et al., 2009; Herzfeld et al., 2014a). The intensity was reached after a 10-second ramp-up period. Ramping up the current was supposed to minimize discomfort and to avoid occurrence of phosphenes (Dun et al., 2016; Kessler et al., 2012; Nitsche et al., 2003). In the sham mode, the current was also ramped up for ten seconds until 2mA, but it was ramped down after 60 seconds of stimulation. The time for ramping down the current was set to 10 seconds. The stimulation period of 60 seconds in the sham mode was supposed to blind the subject by inducing a tingling sensation. A sham stimulation of only 30 seconds, as applied in many other tDCS studies, has been shown to be ineffective for blinding at a current intensity of 2 mA (for review: Dun et al., 2016; O'Connell et al., 2012). There were

six different stimulation conditions in both experiments respectively (with ten subjects per subgroup; see also **Table 1**). Anodal, cathodal or sham stimulation started either at the beginning of the last baseline block or at the beginning of the adaptation block (**Figure 1C**). In the force field task, stimulation was applied for 13.81 min ± SD 0.19 when starting in the last baseline block and for 10.36 min ± SD 0.12 when starting at the beginning of the adaptation block. In the visuomotor task, tDCS was applied for 10.20 min ± SD 0.16 and 7.61 min ± SD 0.17, respectively. The stimulation was finished when the subject had completed the adaptation block. Importantly, each subject was double-blind randomized to one of the six stimulation conditions. Blinding and deblinding was conducted by a lab member not directly involved in data acquisition.

Table 1. Age and sex ratio of subjects in each of the 12 subgroups tested (ten subjects per subgroup).

Stimulation onset	Stimulation	Sex ratio	Age (years)
	Forcefield experiment		
Baseline	Anodal	1:1	24.60 ± 2.99
	Cathodal	1:1	22.30 ± 1.77
	Sham	1:1	24.10 ± 1.60
Adaptation	Anodal	1:1	24.50 ± 2.12
	Cathodal	1:1	24.60 ± 2.27
	Sham	1:1	24.40 ± 2.59
	Visuomotor experiment		
Baseline	Anodal	1:1	23.30 ± 2.83
	Cathodal	1:1	22.70 ± 4.24
	Sham	1:1	22.40 ± 2.22
Adaptation	Anodal	1:1	20.50 ± 1.43
	Cathodal	1:1	23.60 ± 4.27
	Sham	1:1	21.10 ± 2.03

Age in years ± SD.

Data analysis and statistics

Data analysis was performed by means of MATLAB with Statistics Toolbox (MATLAB 8.5; Mathworks). Movements that did not exceed a velocity of 0.12 m/s were removed from further analysis. On basis of this definition, 0.82 (range: 0-6) movements per subject were excluded in the in the force field task and 0.68 (range: 0-3) movements per subject in the visuomotor task.

To measure performance of the subjects, the following outcome measures were calculated (**Figure 1B**): the Maximum Error (ME) and the Perpendicular Velocity at 60 ms after movement onset (PV) in the in force field experiment, and the Angular End point Error (AEE) in the visuomotor experiment. Movement onset was defined as the first time in a trial, where hand velocity exceeded 0.05 m/s.

The ME is calculated as the angle between a straight line from the starting position to target and a straight line from the starting position to the point of the largest error during a movement (Rabe et al., 2009). The AEE represents the error of the hand position at the end of a movement, i.e. the angle between a line from the starting position to the target and a line from the starting position to the final position of the hand in a movement (Galea et al., 2010a; Jalali et al., 2017). Finally, the PV was calculated in force field trials to assess the amount of overcompensation early-on in movements. Early overcompensation is an effective adaptation method in the force field task because it enables a smooth curved movement with minimum effort, as the arm is being moved towards the target by the motors of the manipulandum if the size of overcompensation was chosen correctly (Herzfeld et al., 2014a; Izawa et al., 2008; Joiner and Smith, 2008; Smith et al., 2006).

A correction for movement biases was made by taking the errors from the second baseline block averaged per target direction and subtracting them from the errors in the adaptation and the washout block. A moving median with a sliding window of 16 trials was calculated and errors exceeding 3 absolute deviations from the median in the sliding window were excluded from further analysis. In force field, on average 4.06% of the trials were filtered with an interquartile range of 1,86% (Q1: 2.93; Q3: 4.79). In the visuomotor experiment, on average 3.98% of the trials were filtered with an interquartile range of 2.05% (Q1: 2.34; Q3: 4.39).

To evaluate the extent of learning, we performed two-way ANOVAs (IBM SPSS Statistics 23) to analyze group effects and interactions (Galea et al., 2010a). Averaged ME, AEE and PV were calculated by first binning eight consecutive trials. Secondly, in baseline and washout blocks bin 2-6 and in adaptation block bin 2-11 were averaged. For each block, a two-way ANOVA was performed with mean ME, AEE and PV as dependent variable and stimulation (i.e. anodal, cathodal or sham) and onset of stimulation (i.e. onset in baseline or adaptation) as factors. Mean PV was compared in the adaptation block only. For post-hoc testing, we conducted a Tukey test if indicated.

Null results were analyzed with the TOST-procedure to test for equivalence (Schuirmann, 1987). To verify that we could detect practically relevant effects of tDCS given the experimental design, we conducted sensitivity analyses in G*Power (Faul et al., 2007).

To evaluate the learning rate, we performed a permutation test, in which we first fitted an exponential to the mean aiming errors of the anodal, cathodal and sham groups in the force field condition. Note, in the visuomotor task we converted the reaching directions to aiming errors (reaching direction + perturbation) to enable fitting of the data. The exponential was of the form $y = ae^{bx}$ and fitted using the fit function of the curve fitting toolbox in MATLAB (MATLAB 8.5; Mathworks). Next, we permuted the original dataset 10.000 times and fitted an exponential to each permutation to generate a null distribution of learning rates. The learning rates of the anodal, cathodal and sham groups appeared not to be different from this null distribution. To determine whether there was a difference in learning rates between the stimulation conditions and the generated null distribution, we calculated the root-mean-square error (RMSE = $\sqrt{(\Sigma(r_i - \bar{r})^2)}$ where r is the learning rate $-\frac{1}{b}$) for the permutations and stimulation conditions. A p-value was determined by calculating the proportion of RMSE's of the null distribution larger than the RMSE of the stimulation conditions. To asses equivalency between the groups, we bootstrapped the original data 10.000 times (i.e. each group was resampled with replacement 10.000 times) and fitted an exponential to each stimulation condition in the bootstrapped dataset. Then, the difference in learning rate between stimulation conditions was calculated. This resulted in three distributions of differences in learning rates: anodal – cathodal, anodal – sham and cathodal – sham. Next, we used the two one-sided tests procedure (TOST) to test for equivalence between stimulation conditions. We calculated the proportion of the bootstrapped distribution outside the smallest effect size of interest (SESOI). The SESOI was set at a difference of 10 trials in average learning rate and the maximum of the proportion to the left and right of the SESOI was taken.

RESULTS

Demographics, movement time, movement velocity and reaction time

Age did not differ significantly between the subgroups in both experiments (all: $p < 0.05$). Additionally, the sex ratio was 1:1 in all subgroups (see **Table 1**). In the force field task, average movement times (anodal: 243.84 ms ± SD 63.82 ms, cathodal: 261.95 ms ± SD 86.37 ms, sham: 222.31 ms ± SD 51.34 ms) and average movement velocities (anodal: 0.45 m/s ± SD 0.11 m/s, cathodal: 0.43 m/s ± SD 0.12 m/s, sham: 0.47 m/s ± SD 0.08 m/s) were not significantly different between stimulation groups. Likewise, there was no significant difference considering the visuomotor task (average movement time: anodal: 266.23 ms ± SD 42.90 ms, cathodal: 248.95 ms ± SD 60.97 ms, sham: 248.67 ms ± SD 56.42 ms; movement velocity: anodal: 0.42 m/s ± SD 0.07 m/s, cathodal: 0.47 m/s ± SD 0.13 m/s,

sham: 0.46 m/s ± SD 0.09 m/s). In both tasks, average movement time and velocity did not show a significant difference between subgroups (all p values > 0.05). Reaction times are presented in **Table 2**. Stimulation did not show a significant effect on reaction time (all p values > 0.05).

Table 2. Mean reaction times in the baseline, adaptation, washout phase in the force field and visuomotor experiments.

Experiment	Blocks	Reaction time (ms)
Force field	Baseline	303.60 ± 40.30
	Adaptation	355.01 ± 54.81
	Washout	310.62 ± 47.43
Visuomotor	Baseline	285.92 ± 51.76
	Adaptation	359.88 ± 74.86
	Washout	275.25 ± 60.48

Reaction times in milliseconds ± SD.

Experiment 1 – Force field task

Hand paths of a single subject during adaptation are depicted in **Figure 2A**. An unexpected velocity-dependent clockwise perpendicular force led to a high maximum error at the beginning of the adaptation block. The initial trajectories show an online correction late in the movement so that the Angular End point Error would be lower than the Maximum Error and which could mask the adaptation process. Therefore, Maximum Error was analyzed in the force field experiment. In the course of the adaptation block, subjects learned to efficiently compensate for the force by overcompensating early in the movement. This early overcompensation enables a smooth movement without online correction.

Maximum Error – extent of learning

Mean group Maximum Error (ME) is shown over the course of the experiment in **Figure 3A**. In baseline, subjects had initially a counterclockwise movement bias. The ME in the first bin was -8.01° +/- SD 4.07°. Throughout the baseline phase, the ME decreased until it reached -1.19° +/- SD 2.37° at the end of baseline. At the beginning of the adaptation block, movements had a high ME (23.24° +/- SD 4.45 in the first bin). But all subjects learned to compensate the perturbing force so that the mean ME across all groups reached 2.15° +/- SD 4.83. In the washout block, negative values for ME represent a deviation to the opposite

direction than the force that used to be applied in the adaptation block indicating a subject's retention. In the course of the washout phase, ME decreased from -12.64° +/- SD 2.60° in the first bin to -1.12 +/- SD 5.10° at the last bin.
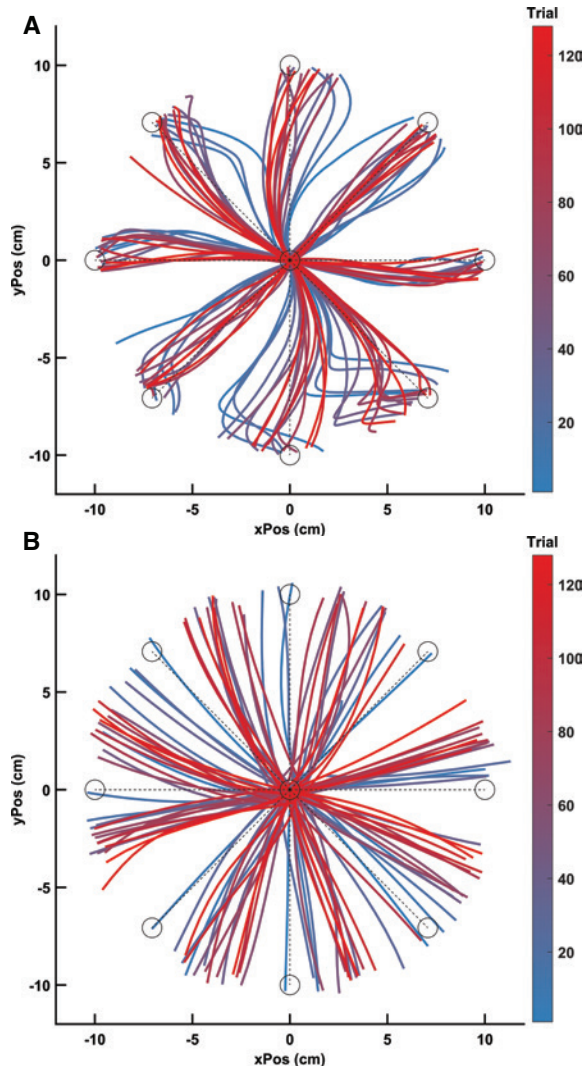

Figure 2. Single subject trajectories during the adaptation block. Movements were performed from the center point to one of the eight targets. The dashed lines show hypothetical straight movements. (A) In the experiment 1 (force field adaptation task), movements show a late compensation for the applied forces early in the block (blue) and an early overcompensation late in the block (red). (B) During experiment 2 (visuomotor adaptation task), movements show only a small deviation indicating an insufficient adaptation to the 30° clockwise rotation of the cursor early in the block (blue) and a counterclockwise compensation late in the block (red).
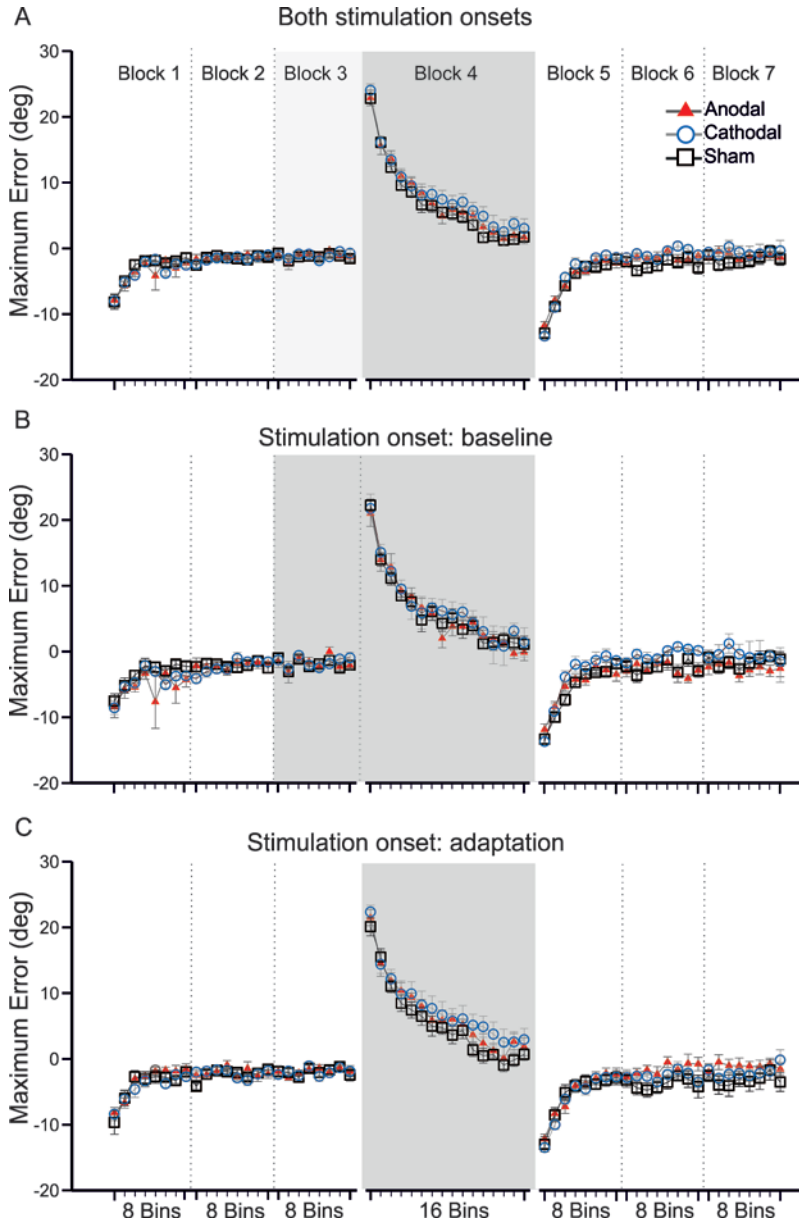
Figure 3. Mean Maximum Error (+/- SEM) in each stimulation group during baseline (Block1-3), adaptation (Block 4) and washout (Block 5-7) of experiment 1 (force field task) (A-C). The ME was calculated as the angle between a straight line from the starting position to target and a straight line from the starting position to the point of the largest error during a movement (Rabe et al., 2009). There were no significant differences between groups (all p values > 0.05). (A) Group data irrespective of stimulation onset. Light shading represents stimulation onset in baseline, dark shading stimulation onset in adaptation. (B) Stimulation onset in baseline. Shading shows the blocks with stimulation. (C) Stimulation onset in adaptation. Shading shows the block with stimulation.

In the baseline blocks, the adaptation block as well as in the first and third washout blocks, there were no significant effects of the factors stimulation and stimulation onset and no significant stimulation x stimulation onset interaction (all p > 0.05, **Table 3**).

Table 3. Statistical results of the force field task.

	Maximum error	F Statistics	P Value
Baseline 1	Stimulation	$F_{(2,54)} = 0.75$	0.48
	Stimulation Onset	$F_{(1,54)} = 1.14$	0.29
	Stimulation x Stimulation Onset	$F_{(2,54)} = 1.30$	0.28
Baseline 2	Stimulation	$F_{(2,54)} = 0.08$	0.93
	Stimulation Onset	$F_{(1,54)} = 0.01$	0.92
	Stimulation x Stimulation Onset	$F_{(2,54)} = 0.15$	0.86
Baseline 3	Stimulation	$F_{(2,54)} = 0.24$	0.76
	Stimulation Onset	$F_{(1,54)} = 0.81$	0.37
	Stimulation x Stimulation Onset	$F_{(2,54)} = 0.20$	0.82
Adaptation	Stimulation	$F_{(2,54)} = 0.70$	0.50
	Stimulation Onset	$F_{(1,54)} = 0.32$	0.58
	Stimulation x Stimulation Onset	$F_{(2,54)} = 0.12$	0.89
Washout 1	Stimulation	$F_{(2,54)} = 0.67$	0.51
	Stimulation Onset	$F_{(1,54)} = 1.02$	0.32
	Stimulation x Stimulation Onset	$F_{(2,54)} = 1.94$	0.15
Washout 2	Stimulation	$F_{(2,54)} = 3.24$	0.047
	Stimulation Onset	$F_{(1,54)} = 2.76$	0.10
	Stimulation x Stimulation Onset	$F_{(2,54)} = 2.04$	0.14
Washout 3	Stimulation	$F_{(2,54)} = 0.15$	0.86
	Stimulation Onset	$F_{(1,54)} = 0.50$	0.49
	Stimulation x Stimulation Onset	$F_{(2,54)} = 0.66$	0.53
	Perpendicular velocity at 60 ms		
Adaptation	Stimulation	$F_{(2,54)} = 0.49$	0.61
	Stimulation Onset	$F_{(1,54)} = 0.01$	0.92
	Stimulation x Stimulation Onset	$F_{(2,54)} = 0.71$	0.50

When comparing each bin of different stimulation groups in the adaptation block, cathodal stimulation tended to show higher ME towards the end of adaptation especially with stimulation onset in adaptation block. These differences, however, were not significant (see p values of t-tests in **Table 4**).

Table 4. P-values of t-tests for each bin of the adaptation block (A1-A16) in the force field and visuomotor experiments.

Onset	t-test	A1	A2	A3	A4	A5	A6	A7	A8	A9	A10	A11	A12	A13	A14	A15	A16
Force field experiment																	
Baseline	Anodal vs Cathodal	0.48	0.94	0.90	0.55	0.69	0.32	0.57	0.42	0.68	0.38	0.34	0.29	0.63	0.82	0.56	0.87
	Anodal vs Sham	0.56	0.89	0.56	0.27	0.18	0.60	0.97	0.60	0.34	0.41	0.91	0.47	0.66	0.75	0.59	0.58
	Cathodal vs Sham	0.86	0.95	0.66	0.08	0.27	0.25	0.56	0.88	0.47	0.91	0.23	0.74	0.41	0.64	0.32	0.75
Adaptation	Anodal vs Cathodal	0.99	0.39	0.56	0.37	0.23	0.91	0.50	0.70	0.95	0.13	0.95	0.45	0.55	0.92	0.51	0.82
	Anodal vs Sham	0.16	0.70	0.93	0.53	0.82	0.94	0.56	0.43	0.42	0.81	0.46	0.43	0.28	0.42	0.66	0.69
	Cathodal vs Sham	0.16	0.56	0.64	0.15	0.10	0.81	0.07	0.12	0.23	0.11	0.10	0.88	0.37	0.34	0.78	0.76
Visuomotor experiment																	
Baseline	Anodal vs Cathodal	0.60	0.60	0.79	0.88	0.55	0.74	0.66	0.84	0.42	0.23	0.91	0.80	0.76	0.88	0.02	0.56
	Anodal vs Sham	0.58	0.99	0.47	0.53	0.68	0.41	0.90	0.24	0.53	0.80	0.74	0.31	0.74	0.65	0.23	0.50
	Cathodal vs Sham	0.94	0.50	0.53	0.52	0.76	0.72	0.76	0.39	0.83	0.17	0.85	0.45	0.90	0.76	0.25	0.92
Adaptation	Anodal vs Cathodal	0.59	0.96	0.87	0.83	0.77	0.92	0.40	0.77	0.87	0.70	0.46	0.26	0.25	0.38	0.98	0.62
	Anodal vs Sham	0.46	0.68	0.60	0.28	0.18	0.41	0.63	0.54	0.13	0.55	0.13	0.32	0.66	0.62	0.09	0.94
	Cathodal vs Sham	0.20	0.57	0.51	0.56	0.26	0.50	0.28	0.42	0.37	0.47	0.07	0.04	0.14	0.13	0.15	0.25

In the second washout block, stimulation showed a significant effect on mean ME ($F_{2,54}$ = 3.24; p = 0.047) with no significant effect of stimulation onset ($F_{2,54}$ = 2.75; p = 0.10) and no significant stimulation x stimulation onset interaction ($F_{2,54}$ = 2.04; p = 0.15). The post-hoc test (Tukey-Test) of the second washout block revealed a significant lower value of mean ME in the cathodal stimulation group in comparison to the sham stimulation group (in the second washout block). Because there was neither a difference in the first nor in the third washout block, this finding may be false positive and needs to be confirmed in future studies.

When carefully looking at hand paths of a single subject during adaptation in **Figure 2A**, deviations of movements and adaptation seem to be less pronounced for targets in the x-axis (i.e. 0° and 180°). We looked at mean errors of all subjects in the course of adaptation for each target separately and saw the same trend. This may be caused by the inertial matrix of the limb. Therefore, we additionally analyzed averaged mean error in the adaptation block without those two targets mentioned above. Again, there was no significant effect neither of the factor stimulation nor of stimulation onset nor a significant stimulation x stimulation onset (all p > 0.05).

Maximum Error – rate of learning

The mean learning rate ($-\frac{1}{b}$) was 44.6 trials 95% CI(36.6, 57.2) for the anodal, 52.8 trials 95% CI(43.8, 66.6) for the cathodal and 38 trials 95% CI(31.5, 47.8) for the sham group. To assess goodness of fit, we calculated R^2 for each of the fits. R^2 for the anodal, cathodal and sham group was 0.51, 0.50 and 0.57 respectively. There was no significant difference between the null distribution and the stimulation conditions (p = 0.30). All differences in learning rates were not equivalent (anodal – cathodal, p = 0.44, anodal – sham, p = 0.28, cathodal – sham p = 0.66). Thus, while we did not find evidence for a difference between stimulation conditions, the learning rates between stimulation conditions cannot be considered as equivalent.

Perpendicular Velocity at 60 ms

The PV was calculated for the adaptation block only. PV has been used to analyze overcompensation early in the movement, which has been described to be typical of force field learning (Herzfeld et al., 2014a; Izawa et al., 2008; Joiner and Smith, 2008; Smith et al., 2006). We analyzed PV at 60 ms after movement onset because of a pronounced overcompensation at this point of time (**Figure 4**).
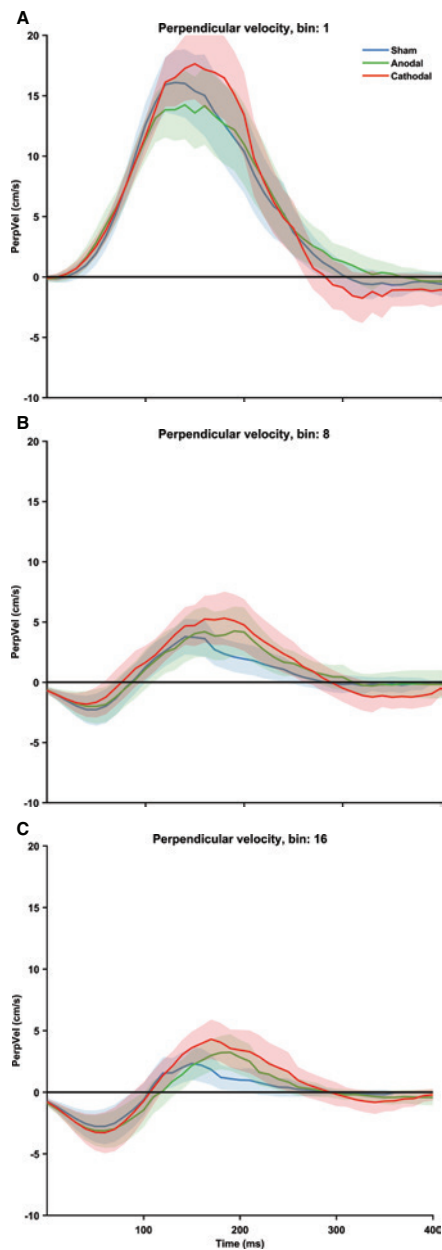
Figure 4. Mean Perpendicular Velocity (+/- SEM) in the first bin (A), the eighth bin (B) and the last bin (C) of the adaptation block in experiment 1 (force field task). Clockwise deviation, i.e. the direction of the force applied by the robot motors, results in positive values. Counterclockwise deviation, i.e. overcompensation to the force, results in negative values. At the beginning of adaptation, there is a strong clockwise deviation and a late overcompensation during a movement. At the end of adaptation, an early overcompensation with its maximum at about 60 ms is followed by a late clockwise deviation during a movement.

Positive values represent a clockwise deviation, negative values an overcompensation. **Figure 4A** shows the mean Perpendicular Velocity in the first bin of the adaptation block. After an early clockwise deviation corresponding to the direction of the force generated by the robot motors, the subjects corrected for the error by performing a late online correction. In the course of the adaptation block, subjects showed earlier overcompensation (**Figure 4B**). In **Figure 4C**, the PV at the end of the adaptation block is depicted. Here, an early overcompensation at about 60 ms after movement onset is followed by a later clockwise deviation resulting in a smooth s-shaped curve. This kind of adaptation is consistent with force field learning reported in previous studies (Herzfeld et al., 2014a; Izawa et al., 2008; Joiner and Smith, 2008; Smith et al., 2006). During adaptation, stimulation ($F_{2,54}$ = 0.49; p = 0.61) and stimulation onset ($F_{2,54}$ = 0.01; p = 0.92) did not have a significant influence on averaged PV. Furthermore, there was no significant stimulation x stimulation onset interaction ($F_{2,54}$ = 0.71; p = 0.50; **Figure 5, Table 3**)

Experiment 2 – Visuomotor task

Figure 2B shows the hand paths during the adaptation phase. At the beginning of the block, the trajectory is directed towards the target indicating a lack of compensation for the 30° clockwise rotation of the cursor. By the end of adaptation, the trajectories show a clear counterclockwise deviation indicating a good compensation for the clockwise rotation of the cursor.

Angular End point Error – extent of learning

The development of AEE during the experiment is depicted in **Figure 6**. At the beginning of the baseline phase, subjects tended to move with a counterclockwise movement bias. The AEE in the first bin was -2.14° +/- SD 3.26° and decreased throughout the baseline to -0.10° +/- SD 1.61°. At the beginning of the adaptation block, the subjects showed only a small correction for the 30° clockwise rotation of the cursor. The AEE was -4.11° +/- SD 3.87 in the first bin. In the course of the block, all subjects showed learning. At the end of adaptation, the AEE reached -25.29° +/- SD 2.61 so that the hand movement has almost equalized the 30° cursor rotation. In the washout block, a good retention was represented by high negative values of AEE. In the course of the washout phase, AEE changed from -19.45° +/- SD 2.83° in the first bin to -12.69 +/- SD 6.04° in the last bin.
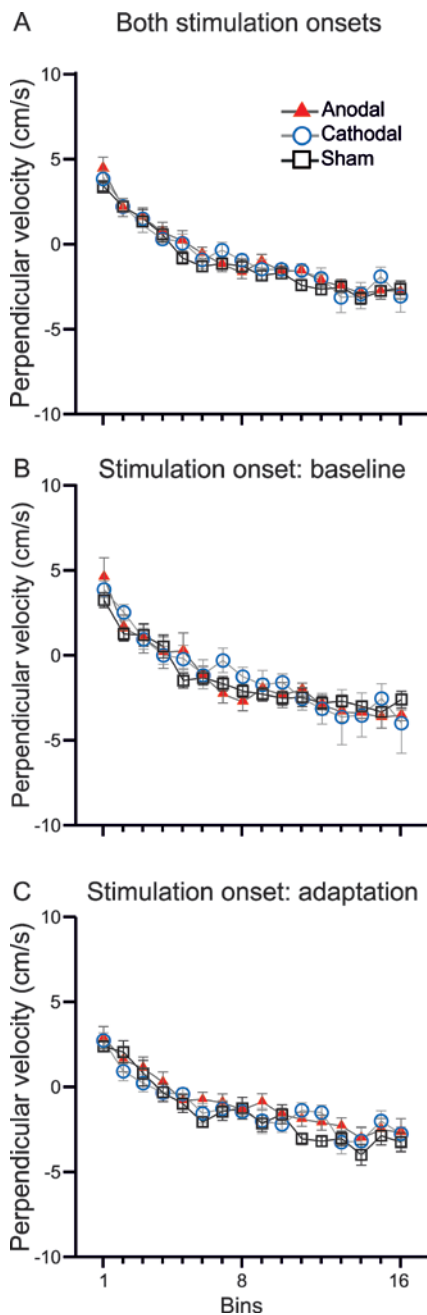
Figure 5. Perpendicular Velocity at 60 ms (+/- SEM) in each stimulation group during baseline, adaptation and washout in experiment 1 (force field task). There were no significant differences between groups (p > 0.05). (A) Stimulation onset in baseline and adaptation is shown together. (B) Stimulation onset in baseline. (C) Stimulation onset in adaptation.
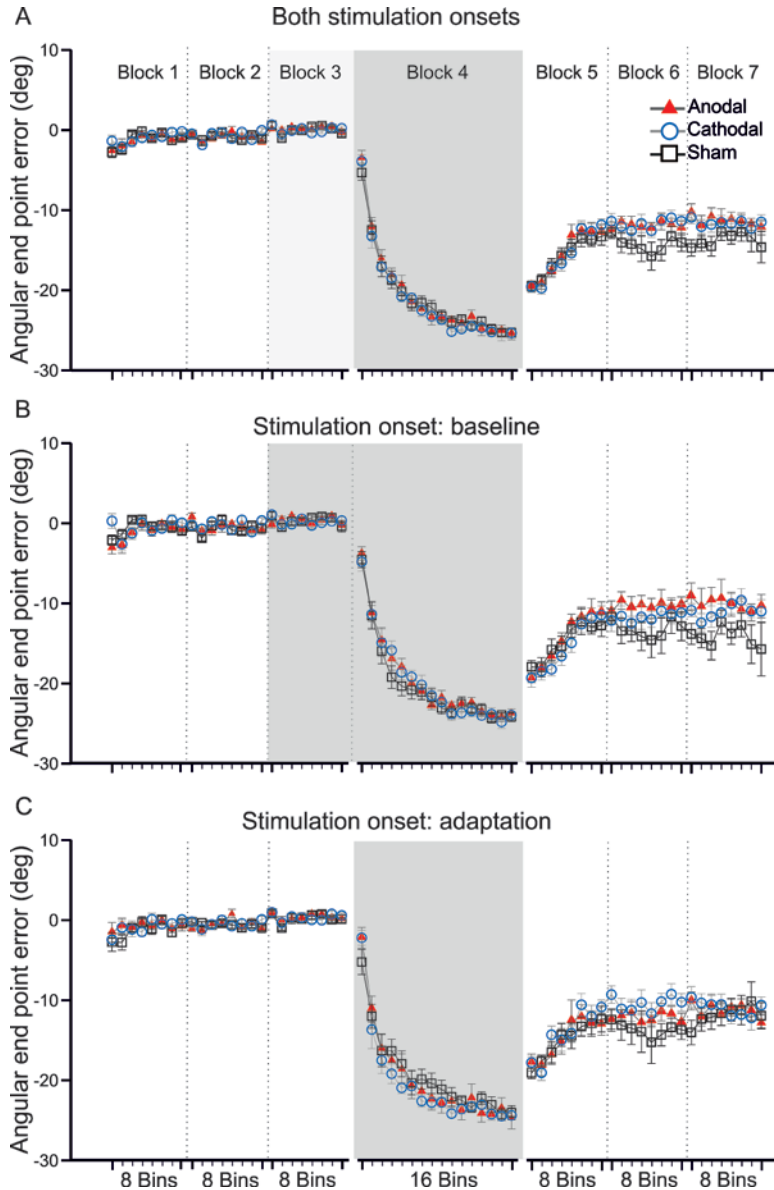
Figure 6. Angular End point Error (+/- SEM) in each stimulation group during baseline (Block 1-3), adaptation (Block 4) and washout (Block 5-7) in experiment 2 (visuomotor task). The AEE represents the error of the hand position at the end of a movement, i.e. the angle between a line from the starting position to the target and a line from the starting position to the final position of the hand in a movement (Jalali et al., 2017). There were no significant differences between groups (all p values > 0.05). (A) Stimulation onset in baseline and adaptation is shown together. Light shading represents stimulation onset in baseline, dark shading stimulation onset in adaptation. (B) Stimulation onset in baseline. Shading shows the blocks with stimulation. (C) Stimulation onset in adaptation. Shading shows the block with stimulation.

In all blocks of experiment 2, there was no significant effect of the factors stimulation and stimulation onset and no significant stimulation x stimulation onset interaction (all p > 0.05, **Table 5**). Also, when comparing each bin of different stimulation groups in the adaptation block, no significant differences could be detected (**Table 4**).

Table 5. Statistical results of the visuomotor task.

	Angular end point errors	F Statistics	P Value
Baseline 1	Stimulation	$F_{(2,54)} = 0.25$	0.78
	Stimulation Onset	$F_{(1,54)} = 0.01$	0.92
	Stimulation x Stimulation Onset	$F_{(2,54)} = 1.17$	0.32
Baseline 2	Stimulation	$F_{(2,54)} = 0.88$	0.42
	Stimulation Onset	$F_{(1,54)} = 0.02$	0.87
	Stimulation x Stimulation Onset	$F_{(2,54)} = 0.93$	0.40
Baseline 3	Stimulation	$F_{(2,54)} = 0.93$	0.40
	Stimulation Onset	$F_{(1,54)} = 0.01$	0.93
	Stimulation x Stimulation Onset	$F_{(2,54)} = 0.12$	0.88
Adaptation	Stimulation	$F_{(2,54)} = 0.22$	0.81
	Stimulation Onset	$F_{(1,54)} = 0.09$	0.76
	Stimulation x Stimulation Onset	$F_{(2,54)} = 0.97$	0.38
Washout 1	Stimulation	$F_{(2,54)} = 0.11$	0.89
	Stimulation Onset	$F_{(1,54)} = 0.21$	0.65
	Stimulation x Stimulation Onset	$F_{(2,54)} = 0.47$	0.63
Washout 2	Stimulation	$F_{(2,54)} = 2.53$	0.09
	Stimulation Onset	$F_{(1,54)} = 0.07$	0.79
	Stimulation x Stimulation Onset	$F_{(2,54)} = 0.48$	0.62
Washout 3	Stimulation	$F_{(2,54)} = 1.42$	0.25
	Stimulation Onset	$F_{(1,54)} = 0.09$	0.76
	Stimulation x Stimulation Onset	$F_{(2,54)} = 0.75$	0.48

AEE = Angular End point Error

Angular End point Error – rate of learning

The mean learning rate ($-\frac{1}{b}$) was 54.9 trials 95% CI(49.5, 61.8) for the anodal, 52.1 trials 95% CI(46.8, 58.6) for the cathodal and 61.6 trials 95% CI(55.3, 69.5) for the sham group. R^2 for the anodal, cathodal and sham group was 0.51, 0.50 and 0.74 respectively. There was no significant difference between the null distribution and the stimulation conditions (p = 0.42). All differences in learning rates were not equivalent (anodal – cathodal, p = 0.16,

anodal – sham, p = 0.32, cathodal – sham p = 0.45). Thus, similar to the force field task, while we did not find evidence for a difference between stimulation conditions, the learning rates between stimulation conditions cannot be considered as equivalent.

Power analysis

To test whether non-significant effects were due to a lack in statistical power, we estimated the minimum detectable effect size for stimulation type and separately for stimulation onset. With three groups of 20 subjects (anodal/cathodal/sham, total n = 60), α = 0.05 and $1 - \beta$ = 0.80, we could reliably reject the null hypothesis if the true effect size of stimulation was f ≥ 0.30 (d ≥ 0.6). This means that, given a pooled standard deviation of approximately 3.1° (in force field and visuomotor perturbations), we could reliably reject differences in aiming errors of 1.9° and larger. For stimulation onset, with six groups of ten subjects (total n = 60), α = 0.05 and $1 - \beta$ = 0.80, we could reliably reject the null hypothesis with true effect sizes of f ≥ 0.35 (d ≥ 0.7) or aiming errors of 2.2° and larger. Recent studies suggest a true effect size of tDCS around d = 0.5, depending on the task (Hashemirad et al., 2016; Minarik et al., 2016). Jalali et al. (2017) report an effect size of d = 0.7 (2.6° in aiming errors) of pooled experimental data in a similar task, while Galea et al. (2010) report an effect of approximately 5 degrees between sham and anodal stimulation in a visuomotor task. Thus, we conclude our experiments were powerful enough to detect practically relevant effects of stimulation type and stimulation onset.

Equivalency test – forcefield task

During baseline, we could establish equivalency between stimulation types with the smallest effect size of interest (SESOI) set at -1 and +1 degrees, for both anodal vs sham stimulation (p = 0.02) and cathodal vs sham stimulation (p = 0.01). Furthermore, we calculated the mean group differences (MD) and the 95% Confidence Interval (CI) with a Bonferroni adjustment for multiple comparisons. There was no significant difference between sham and anodal stimulation (p = 1.00; mean difference 0.17, 95%-CI[-0.74, 1.08]), no significant difference between sham and cathodal stimulation (p = 1.00); MD 0.16, 95%-CI[-0.76, 1.07]) and no significant difference between anodal and cathodal stimulation (p = 1.00; MD -0.01, 95%-CI[-0.93, 0.90]).

In the adaptation block, there was no significant difference between the sham and the anodal group (p = 1.00; MD -0.69, 95%-CI[-3.51, 2.14]), no significant difference between the sham and the cathodal group (p = 0.52; MD -1.58, 95%-CI[-4.40, 1.25]) and no significant difference between the anodal and the cathodal group (p = 1.00; MD -0.89, 95%-CI[-3.72, 1.94]). Equivalency between anodal vs sham stimulation and cathodal vs sham stimulation could not be established during adaptation (p = 0.35 and p = 0.67 respectively). The mean

maximum aiming error of sham stimulation (6.85° ± SE 0.81°) was on average slightly lower than of anodal stimulation (7.53° ± SE 0.81°) which is against the prediction of improved learning with anodal tDCS. The mean maximum aiming error of the cathodal group was on average slightly higher than the sham group (8.42° ± SE 0.81°), but, as mentioned before, failed to reach significance.

In washout, equivalency between anodal vs sham stimulation (p = 0.28) and cathodal vs sham stimulation, could not be established (p = 0.57). There was no significant difference between the sham and the anodal group (p = 1.00; MD -0.61, 95%-CI[-2.33, 1.11]), no significant difference between the sham and the cathodal group (p = 0.34; MD -1.12, 95%-CI[-2.84, 0.60]) and no significant difference between the anodal and the cathodal group (p = 1.00; MD -0.51, 95%-CI[-2.23, 1.21]).

Equivalency test – visuomotor task

During baseline, we could establish equivalency between stimulation types with the smallest effect size of interest (SESOI) set at -1 and +1 degrees, for both anodal vs sham stimulation (p < 0.001) and cathodal vs sham stimulation (p < 0.001). The comparison of the mean group differences (MD) and the 95% Confidence Interval (CI) delivered no significant differences between sham and anodal stimulation (p = 1.00; MD -0.02, 95%-CI[-0.43, 0.39]) between sham and cathodal stimulation (p = 1.00; MD -0.15, 95%-CI[-0.55, 0.26]) as well as anodal and cathodal stimulation (p = 1.00; MD -0.13, 95%-CI[-0.54, 0.28]).

In the adaptation block, there was no significant difference between the sham and the anodal group (p = 1.00; MD -0.14, 95%-CI[-2.23, 1.95]), no significant difference between the sham and the cathodal group (p = 1.00; MD 0.38, 95%-CI[-1.72, 2.47]) and no significant difference between the anodal and the cathodal group (p = 1.00; MD 0.52, 95%-CI[-1.58, 2.61]). Equivalency between anodal vs sham stimulation and cathodal vs sham stimulation could not be established during adaptation (p = 0.18 and p = 0.20 respectively). The mean aiming error of sham stimulation (-20.77° ± SE 0.60°) was on average slightly more negative than of anodal stimulation (-20.63° ± SE 0.60°) which is against the prediction of improved learning with anodal tDCS. The mean aiming error of the cathodal group was on average even more negative than of the sham group (-21.14° ± SE 0.60°), but, as mentioned before, failed to reach significance.

In washout, equivalency between anodal vs sham stimulation (p = 0.72) and cathodal vs sham stimulation, could not be established (p = 0.71). There was no significant difference between the sham and the anodal group (p = 0.38; MD -1.65, 95%-CI[-4.28, 0.98]), no

significant difference between the sham and the cathodal group (p =0.43; MD -1.58, 95%-CI[-4.20, 1.05]) and no significant difference between the anodal and the cathodal group (p = 1.00; MD 0.07, 95%-CI[-2.56, 2.70]).

DISCUSSION

In the present study, no significant stimulation effects of cerebellar tDCS were observed in reaching adaptation neither during force field nor during visuomotor perturbations. Furthermore, the onset of tDCS had no effect on adaptation.

Inconsistent effects of cerebellar tDCS

We could not confirm previous findings of effects of cerebellar tDCS on visuomotor adaptation (Galea et al., 2010a; Jalali et al., 2017). As Jalali et al. (2017) already highlighted, differences in task parameters are important which can lead to a lack of replication even for slight changes in paradigm (cf. lack of replication of Galea et al. (2010) in Jalali et al. (2017)). Jalali et al. (2017) tested the effect of cerebellar tDCS (anodal vs. sham) on visuomotor adaptation with various parameters. Only under the condition where subjects were sitting in front of a vertically oriented screen and were performing goal directed movements with their right index finger they did see a better adaptation in the anodal group. This contrasts with the study by (Galea et al., 2010a) where subjects moved a digitizing pen. However, when Jalali et al. (2017) tried an even closer replication of the study by (Galea et al., 2010a), by having the subjects move a pen-shaped tool, they failed to show any effects of cerebellar tDCS. Neither were there effects when cerebellar tDCS was applied offline, when the visual rotation was applied stepwise or gradually, nor when a horizontally oriented screen was used. Importantly, the only experiment where tDCS effects were observed could not be replicated in a further experiment in the same study (Jalali et al., 2017). In our study, subjects were sitting in front of a vertically oriented screen and were moving the handle of a manipulandum. Although the parameters were close to those in the study by (Galea et al., 2010a)and the tool-use experiment in the study by Jalali et al. (2017), the tool used to move the cursor on the screen was not the same (manipulandum vs. digitizing pen). Another possible reason of inconsistent tDCS effects in visuomotor reach adaptation studies might be the lack of dissociation of implicit and explicit processes during adaptation. Leow et al. (2014) showed that visuomotor adaptation is influenced by anodal tDCS when explicit re-aiming is suppressed. They used different preparation times (presentation of target before movement) in their paradigm (i.e. 250 or 1000 ms). Stimulation effects could only be detected in the short preparation time group representing implicit processes. In our study,

subjects were told to initiate the movement immediately after target presentation. So, we think that our paradigm mainly represents implicit processes and that the findings by Leow et al. (2014) cannot explain our negative results.

In force field adaptation, we could not confirm previous findings of stimulation effects on adaptation either (Herzfeld et al., 2014a). Again, one reason may be the differences in task parameters (point-to-point reaching movements, number of targets, less trials, error clamps, horizontal screen, different type of manipulandum used in the Herzfeld study). A previous study of our group did not reveal any stimulation effects on force field reach adaptation in cerebellar patients and in healthy subjects as well (Hulst et al., 2017). In that study we applied anodal tDCS either over the cerebellum or over M1 or sham tDCS. None of the conditions led to improvements in adaptation or retention. As in the study by Herzfeld et al. (2014), stimulation started in baseline and continued throughout adaptation and the targets were presented on a horizontally oriented screen (Hulst et al., 2017).

It is possible that tDCS studies require much higher group sizes because the effects are smaller than previously assumed (Hulst et al., 2017; Jalali et al., 2017). In the aforementioned studies, group sizes of eight to thirty subjects were used (Herzfeld et al., 2014a; Hulst et al., 2017; Jalali et al., 2017, 2017). Thus, the group sizes of our study, ten subjects per group with consideration of movement onset or twenty subjects per group without consideration of movement onset, correspond to the number of subjects previously used in comparable studies. A post-hoc power analysis also revealed that our experiments were sufficiently powered, based on the effect sizes of tDCS previously reported. We could not, however, establish equivalency between sham stimulation and anodal or cathodal stimulation. Both in the force field and in the visuomotor experiment, equivalency was not established during adaptation or washout.

The difficulty in replicating previous tDCS experiments should be considered when planning future experiments. Ideally, future studies should use much higher sample sizes as the real tDCS effect is possibly smaller than previously assumed, but, this could lead to problems in planning tDCS studies in patients with a rare disease like cerebellar degeneration where it is difficult to recruit enough subjects for a sufficiently powered study. Another approach to combat publication bias could be preregistration of experimental studies, but this approach has not permeated to the domain of neurosciences yet.

When we shift our focus to other experimental paradigms, we also find that tDCS effects are often difficult to replicate. For example, in eyeblink conditioning, a simple motor learning task that is driven by the cerebellum, (Zuchowski et al. (2014) demonstrated

anodal cerebellar tDCS to enhance the acquisition of the conditioned eyeblink response and cathodal cerebellar tDCS to inhibit this process, but a following study of our lab could not replicate these findings (Beyer et al., 2017).

Also outside of the cerebellum, difficulties replicating tDCS results are present. Lefebvre et al. (2013, 2015) applied dual-tDCS bilaterally over the primary motor cortices in chronic stroke patients while they performed a motor skill learning task. Patients receiving tDCS showed enhanced learning compared to sham. This work could not be replicated by van der Vliet et al. (2017) who used an identical design of the motor skill learning task.

It is possible that the lack of replication originates from a high individual variability in response to tDCS. Several studies have shown large inter- as well as intra-individual variability in response to tDCS (López-Alonso et al., 2014; Wiethoff et al., 2014). Similar results have also been observed for other non-invasive brain stimulation techniques as theta burst stimulation (Hamada et al., 2013), repetitive transcranial magnetic stimulation (Maeda et al., 2000) and paired associative stimulation (Müller-Dahlhaus et al., 2008).

An explanation for the individual variability in response to non-invasive brain stimulation could lie in anatomical differences among subjects (Datta et al., 2012; Kim et al., 2014a; Opitz et al., 2015; Parazzini et al., 2015; Russell et al., 2013). Furthermore, it has been shown that the orientation of the neurons relative to the current flow is crucial (Chan and Nicholson, 1986; Chan et al., 1988; Rahman et al., 2013, 2014). Current flow along the somato-dendritic axis of a neuron leads to a depolarization of membrane compartments near the cathode, whereas compartments near the anode are being hyperpolarized (Rahman et al., 2013, 2014). Since the cerebellar cortex is highly convoluted, different polarization profiles can result along the cerebellar gyri (Rahman et al., 2014). Considering the complex cerebellar architecture, its multitude of afferents and efferents and likely differences in learning mechanisms used by zebrin positive and negative zones, further analysis is needed to better predict the functional effects of cerebellar tDCS (Rahman et al., 2014).

Besides the anatomical level, former studies showed tDCS to alter the concentration of certain neurotransmitters measured by magnetic resonance spectroscopy (MRS). Stagg et al. (2011) demonstrated a positive correlation between the anodal tDCS-induced GABA decrease in M1 and the degree of motor learning. In a force field reach task, similar to the first experiment of the present study, Kim et al. (2014) demonstrated that faster adaptation and a longer retention were associated with a large decrease in GABA after anodal tDCS over M1. Regarding cerebellar tDCS and its influence on the concentration of neurotransmitters, a recent visuomotor adaptation study by Jalali et al. (2018) demonstrated that anodal cerebellar tDCS resulted in an increased motor memory retention which was strongly

correlated with a decrease in cerebellar glutamate levels. Interestingly, Galea et al. (2010) showed in a previous visuomotor adaptation study that tDCS over M1, but not cerebellar tDCS, improved retention. Conversely, anodal cerebellar tDCS led to faster adaptation (Galea et al., 2010a). Comparing the change of neurotransmitter levels caused by tDCS with the performance in a certain task is a promising tool to get a better understanding under which conditions subjects can benefit from a tDCS application.

Stimulation onset of tDCS

We supposed that a possible reason for the inconsistent results could be that stimulation effects differ depending on the onset of stimulation. TDCS studies, mostly targeting the motor cortex, but also the cerebellum have shown that stimulation effects are related to the time course of stimulation (Cabral et al., 2015; Fricke et al., 2011; Prichard et al., 2014; Sriraman et al., 2014; Stagg et al., 2011b). Galea et al. (2010) as well as Herzfeld et al. (2014) started tDCS before adaptation and continued throughout the adaptation phase. So did Jalali et al. (2017) as well as Hulst et al. (2017). However, they could not replicate previous results. Several studies reported that tDCS has mainly online effects (Ehsani et al., 2016; Galea et al., 2010a; Prichard et al., 2014). Stagg et al. (2011) demonstrated that anodal tDCS applied before the task may even inverse the effects compared to an application during the task. Hence, our hypothesis was that stimulation starting in baseline could lead to homeostatic mechanisms resulting in altered tDCS effects like a reduced effectivity of anodal stimulation. At the same time, we thought that stimulation starting with the adaptation phase would result in more robust effects. Due to a lack of tDCS effects in general this hypothesis could not be confirmed.

Limitations

We did not assess the fluctuations of the intra-individual performance level concerning motor adaptation and we did not evaluate the individual response to tDCS. TDCS effects could have been masked by a large inter-individual variability in personal adaptation skills. Thus, we suggest a cross-over design for future studies that allows an analysis of both inter-individual and intra-individual differences in (motor) performance on the one hand and of tDCS response on the other hand. A drawback of cross-over designed studies, however, are carry-over effects. Taking individual predispositions into account, it may imply that tDCS parameters should be adjusted on individual basis, which in turn requires specific biomarkers that are supposed to show what tDCS parameter is appropriate for what subject. Similar to primary motor cortex tDCS effects, which have been found to correlate with the sensitivity to TMS effects (Jamil et al., 2017; Labruna et al., 2016), sensitivity to cerebellar brain inhibition (CBI) may be a useful tool to predict effects of cerebellar tDCS effects in individual subjects.

Furthermore, it cannot be excluded that the change of ITI between the habituation and acquisition phase could have had an effect on the results. We used an ITI of 500 ms in the habituation phase and an ITI of 1500 ms in the acquisition phase. Cerebellar tDCS effects may be more obvious using shorter ITIs because trial-over-trial learning effects are more prominent (Yang and Lisberger, 2014).

Finally, in the first baseline block in force field adaptation, there was an initial movement bias of up to about 10 degrees, which was in the opposite direction to the force applied in the adaptation block. Adaptation to this initial "perturbation" could have lowered learning in the adaptation block (Sing and Smith, 2010). This interference may have reduced possible tDCS effects.
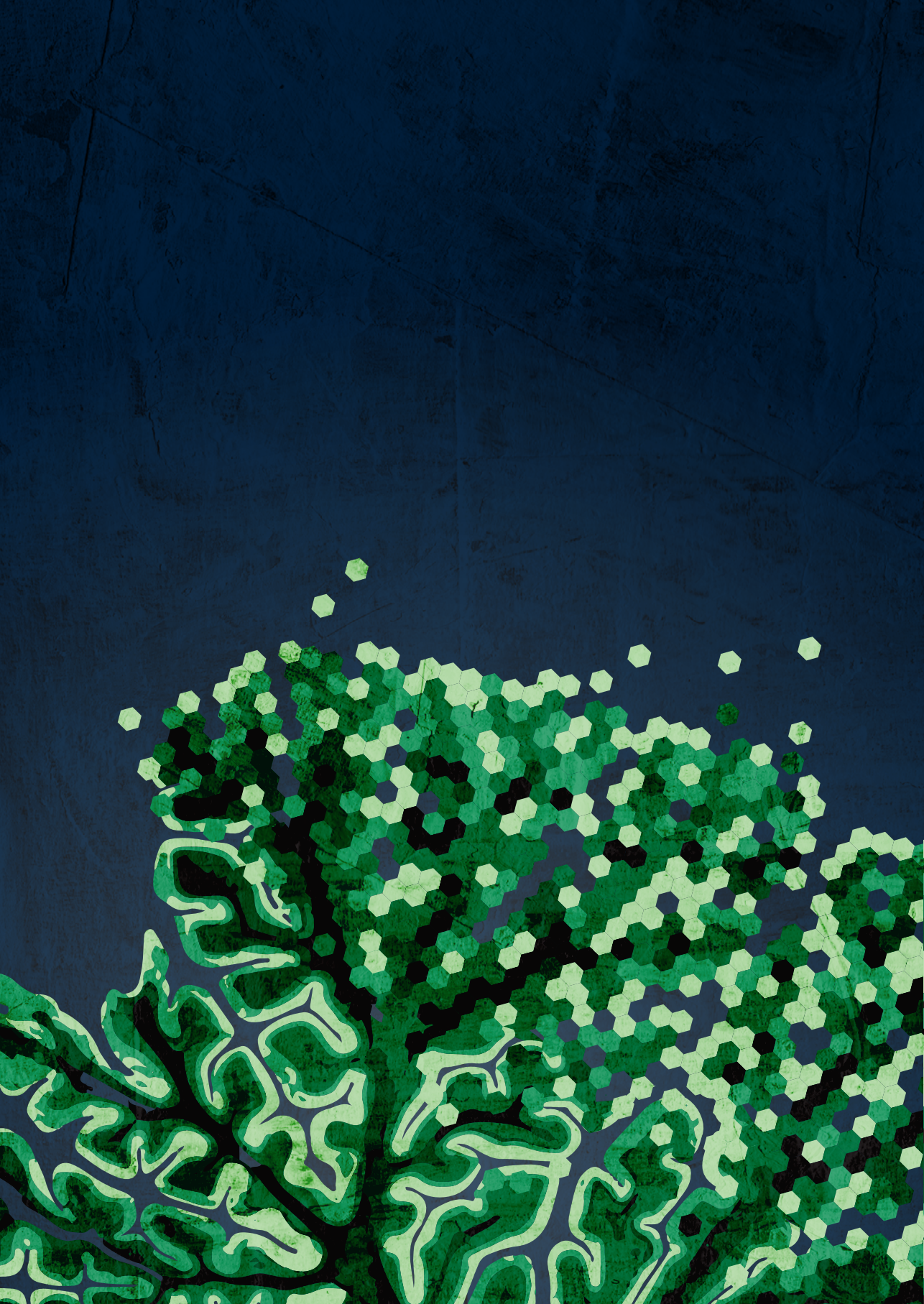
CONCLUSIONS

In the present study, we did not find cerebellar tDCS effects in two different cerebellar-dependent learning tasks independently of the polarity and onset of stimulation. In the context of heterogeneous findings in former studies, a great variability in anatomy, inner- and inter-individual performance with various cofactors like the concentration of certain neurotransmitters, especially GABA and glutamate as well as various task and set-up specific parameters, seem to affect the outcome of cerebellar tDCS. Prior to a possible clinical application, tDCS parameters that lead to robust stimulation effects have to be identified.

Author contributions

Thomas Hulst analyzed data; interpreted results; prepared figures; drafted manuscript; edited and revised manuscript; approved the final version of the manuscript.

8

Awareness of sensorimotor adaptation to visual rotations of different size

Susen Werner[1], Bernice C. van Aken[2], Thomas Hulst[2], Maarten A. Frens[2, 3], Jos N. van der Geest[2], Heiko K. Strüder[1], Opher Donchin[2, 4]

[1] Institute of Movement and Neurosciences, German Sport University, Cologne, Germany
[2] Department of Neuroscience, Erasmus MC, Rotterdam, The Netherlands
[3] Erasmus University College, Rotterdam, The Netherlands
[4] Department of Biomedical Engineering, Ben-Gurion University of the Negev, Beer-Sheva, Israel

ABSTRACT

Previous studies on sensorimotor adaptation revealed no awareness of the nature of the perturbation after adaptation to an abrupt 30° rotation of visual feedback or after adaptation to gradually introduced perturbations. Whether the degree of awareness depends on the magnitude of the perturbation, though, has as yet not been tested. Instead of using questionnaires, as was often done in previous work, the present study used a process dissociation procedure to measure awareness and unawareness. A naïve, implicit group and a group of subjects using explicit strategies adapted to 20°, 40° and 60° cursor rotations in different adaptation blocks that were each followed by determination of awareness and unawareness indices. The awareness index differed between groups and increased from 20° to 60° adaptation. In contrast, there was no group difference for the unawareness index, but it also depended on the size of the rotation. Early adaptation varied between groups and correlated with awareness: The more awareness a participant had developed the more the person adapted in the beginning of the adaptation block. In addition, there was a significant group difference for savings but it did not correlate with awareness. Our findings suggest that awareness depends on perturbation size and that aware and strategic processes are differentially involved during adaptation and savings. Moreover, the use of the process dissociation procedure opens the opportunity to determine awareness and unawareness indices in future sensorimotor adaptation research.

Keywords: Sensorimotor adaptation, Motor learning, Awareness, Process dissociation procedure

INTRODUCTION

The involvement of cognitive components such as explicit strategies and explicit knowledge, i.e. awareness, in motor learning has been intensively investigated since their manipulation is thought to lead to beneficial effects on various types of motor learning (Benson et al., 2011; Taylor et al., 2011; Willingham et al., 2002), and could thus be used in rehabilitation programs or athletes training schedules. In sensorimotor adaptation, learning was found to be increased in participants with explicit knowledge compared to those without (Hwang et al., 2006). In that study, participants performed reaching movements to visual targets while either adapting to a clockwise (CW) or a counter-clockwise (CCW) force field acting on the moving arm. Those participants, who were aware of the specific pattern of perturbation, showed a larger learning index. However, the calculation of this learning index did not allow a distinction between improvements during adaptation phase and adaptive recalibration of the sensorimotor system, which is commonly measured by reaches made without visual feedback during (catch trials) or after training (aftereffects) (Benson et al., 2011; Bock and Girgenrath, 2005). More specifically, explicit knowledge has a positive effect on the adaptation phase but not on recalibration, as indicated by the transfer to a new motor task in a further study (Werner and Bock, 2007). In addition, numerous studies showed an age-related impairment of sensorimotor adaptation during adaptation phase but not during aftereffect tests (Bock, 2005; Bock and Girgenrath, 2005; Buch et al., 2003; Fernández-Ruiz et al., 2000; McNay and Willingham, 1998) and this impairment of adaptation correlated with age-related reduction of explicit knowledge (Bock, 2005; Hegele and Heuer, 2010; Heuer and Hegele, 2008). To sum up, these results indicate a beneficial effect of explicit knowledge on performance during adaptation phase, but not on recalibration.

In the aforementioned studies, sensorimotor perturbations were induced suddenly leading to large movement errors at the beginning of adaptation. When perturbations are introduced gradually in a stepwise fashion, only small movement errors occur. Compared to sudden adaptation, performance in aftereffect tests was improved after gradual prism (Michel et al., 2007) and saccade adaptation (Wong and Shelhamer, 2011), after gradual adaptation to a visual gain (Ingram et al., 2000) and to a 90° rotation (Kagerer et al., 1997). Adaptation to smaller visual rotations (30° and 60°), however, did not lead to a difference of aftereffects between sudden or gradual adaptation (Klassen et al., 2005; Werner et al., 2014). The difference of recalibration between both conditions is usually associated with a difference in awareness of the knowledge acquired through adaptation (Benson et al., 2011; Criscimagna-Hemminger et al., 2010; Galea et al., 2010b; Ingram et al., 2000; Taylor and Ivry, 2011).

Thus, there is a contradiction between studies showing enhanced explicit knowledge not effecting recalibration as shown in the first section and others claiming that unawareness, i.e. absent explicit knowledge, results in an increase of recalibration as shown in the second section. One explanation of this inconsistency could be an intermingling effect of explicit strategies, which might have been applied independently by some participants. Explanations of the nature of the perturbation or strategies like deliberate past pointing were shown to lead to a faster reduction of errors (Benson et al., 2011; Mazzoni, 2006; Sülzenbrück and Heuer, 2009; Taylor and Ivry, 2011), but also to lessened aftereffects (Benson et al., 2011; Mazzoni, 2006) compared to adaptation without explicit knowledge. Another explanation could be the dependence of explicit knowledge on the size of the perturbation, as previous results suggest: Hegele and Heuer showed that elderly participants made less use of explicit instructions than younger participants during adaptation to a large visual rotation of 75° (Hegele and Heuer, 2013), whereas cerebellar patients were able to successfully apply an explicit strategy of reaching to aiming targets, which counteracted a smaller visual rotation of 45° (Taylor et al., 2010). While cerebellar patients clearly suffer from cerebellar atrophy, anatomical evidence also reveals an age-related atrophy of the cerebellum (Andersen et al., 2003; Dimitrova et al., 2008; Torvik et al., 1986; Woodruff-Pak et al., 2001). The different results could, thus, be related to a difference of affected anatomical regions, but also to a difference of rotation sizes. Furthermore, different generalization patterns to untrained targets were found after adaptation to a 75° (Heuer and Hegele, 2008, 2011) and to a 30° rotation (Krakauer et al., 2000). To our knowledge, awareness has as yet not been measured after different perturbation sizes.

Two further drawbacks of previous research on awareness or explicit knowledge during motor adaptation can be identified. The first drawback is the irregular use of the term awareness. Some authors refer to awareness of a perturbation, i.e. the notion that something has changed (Galea et al., 2010b; Taylor and Ivry, 2011). Others more specifically mean the awareness of the nature of the perturbation (Benson et al., 2011; Wang et al., 2011), as we relate to in the present study. The second drawback is the widespread use of questionnaires as a means of measuring awareness (Benson et al., 2011; Hwang et al., 2006; Slachevsky et al., 2001; Werner and Bock, 2007). In some studies using the gradual adaptation paradigm, even a formal questionnaire was not used. As discussed below, these methodologies have several disadvantages.

The domain of cognitive psychology has a strong tradition of analyzing awareness and there is an enduring debate about the acquisition of knowledge and whether or not it is available to conscious access (Cleeremans, 1993; Destrebecqz and Peigneux, 2005; Fu et al., 2008; Reingold and Merikle, 1990; Shanks and St. John, 1994). Questionnaires were soon the target of criticism in this field since verbal responses may fail to exhaustively

reveal all of a subjects' unconscious knowledge because the knowledge is weak or held with low confidence, on the one hand, or because of the sharp difference of retrieval contexts (motor response vs. verbal response), on the other hand (Eriksen, 1960; Nisbett and Wilson, 1977; Reingold and Merikle, 1990; Shanks and St. John, 1994; Shanks et al., 2005). Alternative methods largely abandoned in cognitive research are prediction tasks during which participants are asked to make predictions during the same sort of task, to generate the same task freely or to recognize the trained task after an adaptation phase (Frensch et al., 1994; Reber and Squire, 1994; Willingham et al., 1989). Those methods have recently been implemented in sensorimotor adaptation research (Hegele and Heuer, 2010; Heuer and Hegele, 2008; Heuer and Rapp, 2011; Taylor and Ivry, 2011) but they suffer from the disadvantage that performance might be based on feelings of familiarity (Jacoby, 1991; Jiménez et al., 1996; Johnston et al., 1991; Mandler, 1980) and might, therefore, lead to an overestimation of awareness (Cleeremans, 1993; Shanks and St. John, 1994). Consequently, cognitive psychologists developed a method called the process dissociation procedure (PDP). First used by Jacoby (1991), PDP is widely accepted and used today in the cognitive domain (Bergerbest and Goshen-Gottstein, 2002; Destrebecqz et al., 2003; Fu et al., 2008; Kane et al., 2000; Karabanov and Ullen, 2008; Norman et al., 2006; Wilkinson and Shanks, 2004). Based on the assumption that conscious knowledge is controllable, aware and unaware learning can be estimated by comparing performance when subjects attempt to either express or repress the learned behavior.

The present project pursued the idea of incorporating the current best methodology for measuring awareness and unawareness into the study of sensorimotor adaptation. We decided to test whether the degree of awareness depends on the magnitude of the perturbation applied to the subjects´ movements and whether it can be manipulated by providing the participants with an explicit strategy before adaptation.

METHODS

Participants

Twenty-four right-handed subjects participated in the study in exchange for course credit and were randomly assigned to an implicit (n=16; age: 20.2 ± 3.4; 14 female) or an explicit group (n=8; age 21.0 ± 3.2; 8 female). Participants' ages ranged from 18 to 32 years, thus all reaching majority in the country of testing. The participants of the first group were told that there would be a perturbation, but remained uninformed about its nature. The participants of the latter group, however, received detailed explanations with the help of a clock face as in Benson et al. (2011). None of the subjects had any experience in visuomotor adaptation

research or exhibited overt sensorimotor deficits besides corrected vision. The experimental protocol was pre-approved by the Erasmus MC Medical Ethical committee, was conducted according to the principles expressed in the Declaration of Helsinki, and all subjects gave written informed consent.

Task

Participants watched a horizontal screen and held the handle of a robot that was placed underneath the screen, while a cloth prevented the sight of their arm (**Figure 1A**). The position of the robot-handle was registered with a sampling frequency of 200 Hz and a resolution of 0.3 x 10-3 degrees on each joint of the shoulder which translates into a resolution in Cartesian coordinates of less than 0.2 mm. The registered signal was used to display a green cursor (diameter 6 mm) representing the handle position onto the screen with the help of a projector. Furthermore, a black origin and one of three possible red targets were alternately projected. The origin was positioned approximately 45 cm away from the eyes of the participant and the targets were positioned 10 cm away from the origin, either straight ahead or 45° to the left or the right. The origin as well as the targets had a diameter of 14 mm and the cursor one of 6 mm. The subjects were instructed to move the cursor accurately and quickly from the origin to the target and back. To control for the speed of the movements target color changed to green for actual trail times of 850 ms ± 100 ms and turned to blue or yellow when movements were too slow (>950 ms) or too fast (> 750 ms), respectively. Intertrial intervals lasted for 1500 ms.
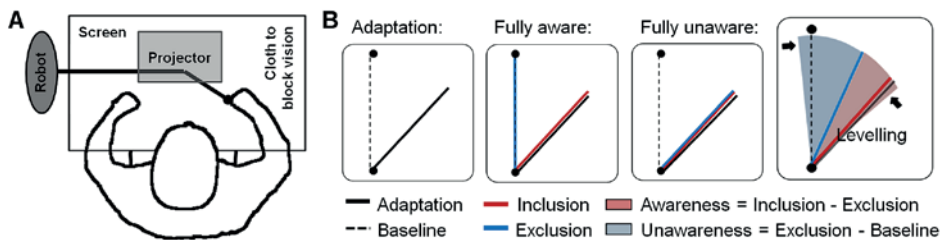

Figure 1. Scheme of experimental apparatus (A). Shown are robot, display screen and projector. Measuring awareness and unawareness (B). Exemplary adaptation, inclusion and exclusion movement directions indicating fully aware or unaware behavior. Schematic and simplified presentation of awareness and unawareness. Note that for calculation of an awareness and unawareness index normalized mean movement directions of inclusion and exclusion were used in order to allow comparison between rotation angles (see Methods). Movement directions were levelled between baseline direction -10% and size of perturbation +10% as indicated by the arrows.

After *familiarization* with veridical and *baseline without visual feedback*, i.e. no cursor visible, all participants conducted six sets, each containing a *baseline/washout* block with veridical visual feedback, an *adaptation* block with rotated visual feedback (20° CW, 40° CW or 60° CW) and an *inclusion* and *exclusion* block without feedback. During each adaptation block, six clamp trials were inserted to test for the progression of recalibration (trial number 6, 19, 30, 39, 47 and 58). In those trials a perfect movement of the cursor from the starting to the target dot was displayed independent of the subjects´ movement. Each participant performed two consecutive sets for each rotation size with alternating order of inclusion and exclusion blocks. Before inclusion subjects were instructed to 'use what was learned during adaptation' and before exclusion subjects were asked to 'refrain from using what was learned, perform movements as during baseline'. This order as well as rotation size order was randomized between participants. Between the third and fourth set there was a rest break of 5 min. **Table 1** shows an overview of the experimental protocol.

After completion of the experiment all participants filled out a questionnaire as in Benson et al. (2011). Those participants who characterized the perturbation as a rotation or reported the use of a rotational strategy were considered to be explicitly aware of the distortion.

Table 1. Experimental protocol.

	Block name	# of Trials	Visual FB
Intro	Familiarization	6	0°
	Baseline no FB	6	-
Set 20	Baseline/Washout	60	0°
	Adaptation	60	-20°
	Exclusion/Inclusion	9	-
	Inclusion/Exclusion	9	-
Set 40	Baseline/Washout	60	0°
	Adaptation	60	-40°
	Exclusion/Inclusion	9	-
	Inclusion/Exclusion	9	-
Set 60	Baseline/Washout	60	0°
	Adaptation	60	-60°
	Exclusion/Inclusion	9	-
	Inclusion/Exclusion	9	-

Visual feedback (FB) was either not present (-), veridical (0°) or rotated (20°, 40° or 60°). Each set was performed twice with alternating order of exclusion and inclusion.

Data processing

After the conclusion of the experiment, movement direction (MD) was determined as the angle between a line connecting starting and target dot and a line between movement onset and movement position at 150 ms after movement onset. Movement onset was defined as the movement position at which velocity exceeded 0.03 mm/ms for the first time. The trial was omitted if the distance between movement onset and movement position at 150 ms after movement onset was smaller than 10 mm; 4.59% of trials were thus excluded.

From the movement directions of each subject and in order to compare the three rotation sizes, we calculated normalized indices for the different parameters. Adaptation index (AI) and the clamp trial index (CI) were determined as:

$$AI = \frac{MD_{adaptation\ trials} - MD_{baseline\ trials}}{Rotation\ size - MD_{baseline\ trials}} \qquad \text{(Eq. 1)}$$

and

$$CI = \frac{MD_{clamp\ trials} - MD_{baseline\ trials}}{Rotation\ size - MD_{baseline\ trials}} \qquad \text{(Eq. 2)}$$

Where $MD_{clamp\ trials}$ and $MD_{adaptation\ trials}$ were calculated as the mean of the MD for the trials in a specific bin of trials. We used bins of 9 trials for adaptation trials and bins of 3 trials for clamp trials. We calculated $MD_{baseline\ trials}$ as the mean MD of all baseline trails. Both indices range from -1 to 1 with 1 indicating full adaptation and 0 (or a negative number) indicating no adaptation. If a subject produced an AI of ≤ 0.2 during the last two bins of an adaptation block, data for that set was dropped from further analysis. Thus, for each rotation size the data of three participants was excluded (20°: two implicit subjects and one explicit; 40° and 60°: three implicit subjects each). This resulted in a total amount of 12 implicit and 7 explicit subjects.

During the inclusion condition awareness and unawareness both contribute to performance. In the exclusion condition, however, aware and unaware learning are set in opposition. If all knowledge acquired through adaptation is conscious, i.e. a person is fully aware, performance during the exclusion task (E) should not be different from performance during baseline (B). Or, inversely, E > B can be seen as evidence for unaware knowledge. If, in addition, performance during the inclusion task equals that during exclusion, the person

is fully unaware (**Figure 1B**). Within the PDP, an estimate of awareness can therefore be derived from the difference between exclusion and inclusion performance and an estimate of unawareness can be obtained from the difference between exclusion performance and baseline as shown schematically in **Figure 1B** (Destrebecqz and Peigneux, 2005). Thus, we first calculated exclusion and inclusion indices (EI and II) as:

$$EI = \frac{MD_{exclusion\ trials} - MD_{baseline\ no\ FB\ trials}}{MD_{last\ adaptation\ trials} - MD_{baseline\ trials}} \qquad\qquad \text{(Eq. 3)}$$

and

$$II = \frac{MD_{inclusion\ trials} - MD_{baseline\ no\ FB\ trials}}{MD_{last\ adaptation\ trials} - MD_{baseline\ trials}} \qquad\qquad \text{(Eq. 4)}$$

Again, we chose a bin size of nine consecutive trials for exclusion, inclusion and the last adaptation trials and mean values of all trials were used for both baseline blocks. In the original publication introducing the PDP the inclusion and exclusion tests asked for a classification of words into 'new' or 'old' depending on its appearance in previous phases of reading, hearing or solving of anagrams of words (Mandler, 1980). Thus, answers were dichotomous. In contrast, the present inclusion and exclusion conditions allow for an answer, i.e. movement direction, continuously ranging from reproducing the learned movement to reproducing baseline movements. And, because of the circular nature of possible movement directions, even movement directions beyond the learned movement direction or beyond baseline direction could occur. In order to retain as much information as possible without allowing outliner movements to weight results, we decided to level all movement directions of exclusion and inclusion blocks between the rotation size of the previous adaptation block plus 10% and mean baseline movement direction minus 10% (**Figure 1B**). For example, movement directions in an exclusion or inclusion block that followed adaptation to 20° CW rotation should ideally range from -20° to 0°. During levelling all smaller or larger movement directions (cut off value 180°) were levelled to -22° or 2°, respectively. Finally, awareness and unawareness were calculated from EI and II with the awareness index equaling II minus EI and the unawareness index equaling EI.

For statistical analysis we submitted the different indices to several analyses of variance (ANOVAs) with the between-factor Group (implicit, explicit) and the within-factors Rotation Size (20°, 40°, 60°), Block Order of inclusion and exclusion (first, second) and Bin.

Type III sums of squares were used in all analyses unless stated otherwise. Normality within each Bin, Rotation Size and Block Order in each group separately was explored by Shapiro-Wilk test and variance stability of the pairs of levels across the factor Group was explored by Levene´s test. In case of violation, a Kruskal-Wallis-Test with the factor Group (explicit, implicit) was performed with the respective data point. Greenhouse-Geisser-adjustments were applied when necessary to compensate for heterogeneity of variances and significant effects were further explored with Turkeys HSD post-hoc tests for unequal sample sizes. Furthermore, Pearson product-moment correlation coefficients (PCC) between awareness and adaptation indices were calculated in case of normality and variance stability of the respective data. Otherwise Spearman's rank correlation coefficients (SCC) were used. All analyses were done with STATISTICA 7.1.

RESULTS

Figure 2 depicts the mean movement directions of all trials of the implicit and explicit group. Note that the shown order of 20°, 40°, and 60° is only exemplary, since rotation size order was randomized between participants. Due to randomizations of inclusion and exclusion block order each rotation size was consecutively performed twice. Clearly from this presentation, the performance of both groups was very similar during all baseline phases. Absolute movement direction angles gradually increased during each adaptation block with larger movement direction angles at the end of adaptation to 40° than to 20° rotation and during adaptation to 60° rotation movement direction angles were larger still. This was consistent across groups. During the beginning of each adaptation phase, however, the figure shows slightly larger movement direction angles for the explicit group. Movement directions of exclusion blocks abruptly return close to baseline level in both groups, whereas during inclusion blocks movement directions approach adaptation level more so in the explicit group.

The above observations of behavior during adaptation blocks are confirmed by statistical analysis of the adaptation index AI, which is shown in **Figure 3A**. An ANOVA with the factors Group (explicit, implicit), Rotation Size (20, 40, 60), Bin (1:6) and Block Order (I, II) yielded several significant effects. The adaptation index of the explicit group was larger than that of the implicit group (effect of Group [$F_{(1,16)} = 11.58$; $p < 0.01$]) and it increased during the course of adaptation (effect of Bin [$F_{corrected(3,43)} = 32.52$; $p < 0.001$)]. We further found effects of Block Order [$F_{(1,16)} = 4.73$; $p < 0.05$], Bin × Group [$F_{corrected(3,43)} = 12.81$; $p < 0.001$] and Bin × Block Order [$F_{corrected(4,60)} = 3.80$; $p < 0.01$]. Post-hoc decomposition of Bin × Group showed no significant difference of AI between both groups for each respective bin. However, AI of the first bin of the implicit group is different from all following bins of

both groups and the second bin is different from the last three bins, whereas in the explicit group the first bin is only different from the second and third bin of this group. Hence, there was a larger AI during the beginning of adaptation in the explicit group (**Figure 3A**). In addition, post-hoc analyses of Bin × Block Order revealed that AI of the first bin is significantly different between the first and second run. Due to the counterbalanced order of inclusion and exclusion blocks this savings effect should have no effect on the analysis of those blocks. Seven data points out of 72 did not show a normal distribution (6x $p < 0.05$, 1x $p < 0.01$). Levene´s test revealed no homogeneity of variance for six out of 36 data points (5x $p < 0.05$, 1x $p < 0.001$). For all those data points we performed Kruskal-Wallis-Tests with the factor Group (explicit, implicit) and 7 out of 13 revealed a significant difference between the implicit and explicit group according to the results of the analysis of variances (3x $p < 0.05$, 4x $p < 0.01$).
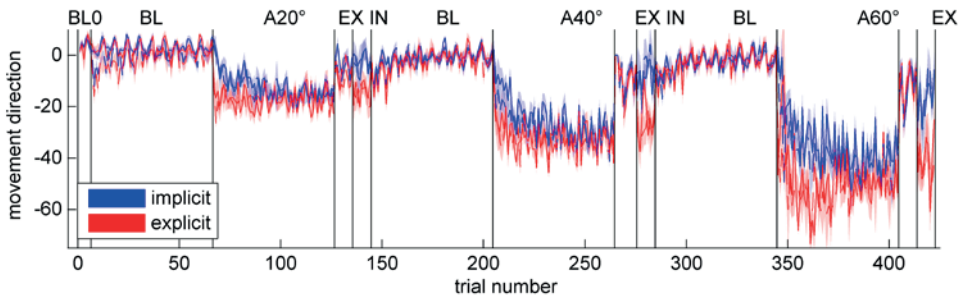

Figure 2. Movement directions of all trials. Shown are movement directions with respect to target direction of implicit (blue) and explicit (red) participants for all experimental phases. Symbols indicate across-subject means, and the shaded area display standard errors. Note that rotation size order was randomized between participants.

Figure 3B shows the mean group values of all clamp trial indices. An analysis of variances of the clamp trial index with bin size 3 yielded a significant effect of Group [$F_{(1,17)} = 6.42$; $p < 0.05$] with a higher clamp trial index in the explicit than the implicit group. It also revealed significant effects of Block Order [$F_{(1,17)} = 5.75$; $p < 0.05$], Bin [$F_{(1,17)} = 15.38$; $p < 0.01$] and Bin × Group [$F_{(1,17)} = 8.82$; $p < 0.01$] with a significant difference between first and second bin in the implicit but not in the explicit group. Levene´s test revealed no homogeneity of variance for two out of twelve data points (both $p < 0.05$). Kruskal-Wallis-Tests with the factor Group (explicit, implicit) confirmed a significant difference between groups for one of the two data points ($p < 0.01$).
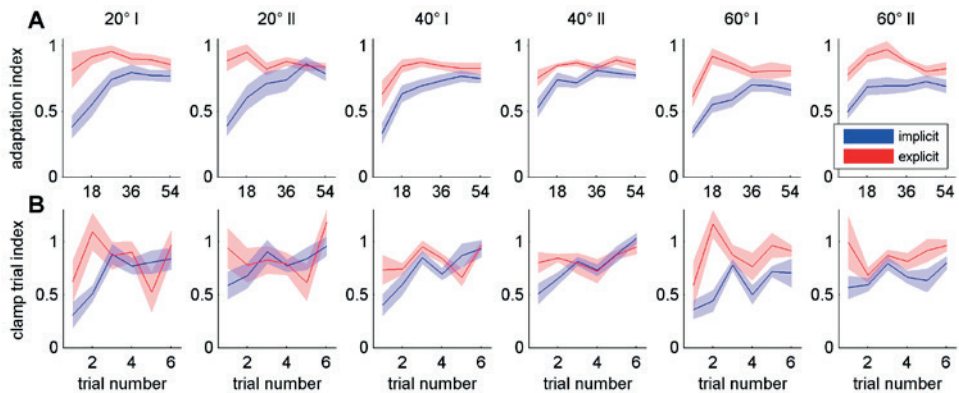
Figure 3. Mean adaptation (A) and clamp trial indices (B) of implicit (blue) and explicit (red) participants. The shaded area indicates standard errors. Note that a bin size of nine trials was used for calculation of the adaptation index. For the clamp trial index bin size of one trial was used in this figure for illustrative purposes, but bin size of three trials was used for statistical analysis. For the adaptation index statistical analysis revealed significant effects of Group ($p < 0.01$), Bin ($p < 0.001$), Block Order ($p < 0.05$), Bin × Group ($p < 0.001$) and Bin × Block Order ($p < 0.01$). For the clamp trial index the analysis yielded significant effects of Group ($p < 0.05$), Bin ($p < 0.01$), Block Order ($p < 0.05$) and Bin × Group ($p < 0.01$). Both analyses revealed no significant effects of Rotation Size or any other interaction (all $p > 0.05$).

Figure 4 illustrates the inclusion and exclusion indices of both groups. The first and second block of each rotation size and group are shown for both conditions. Note that the first block directly succeeded an adaptation block but could be second in the order of the experimental protocol due to randomization of inclusion and exclusion blocks. While inclusion and exclusion indices show similar extents in the implicit group, a clear dissociation can be observed in the explicit group. **Figure 4** further shows a decrease of the exclusion index from 20° to 40° to 60° adaptation. In addition, the inclusion index tended to be larger during the second block than during the first one, however, this was not consistent over rotation sizes or groups. Statistical analysis for the inclusion index revealed a significant effect of Group [$F_{(1,17)} = 6.35$; $p < 0.05$], whereas the analysis of the exclusion index only yielded an effect of Rotation Size [$F_{(2,34)} = 19.30$; $p < 0.001$]. Here the exclusion index after adaptation to 20° rotation differed significantly from that after 40° and 60°, but there was no difference of the exclusion indices after 40° and 60° adaptation. No block order effects were revealed for both conditions supporting our earlier visual observation. The mean values of both blocks are thus used in the following analyses.
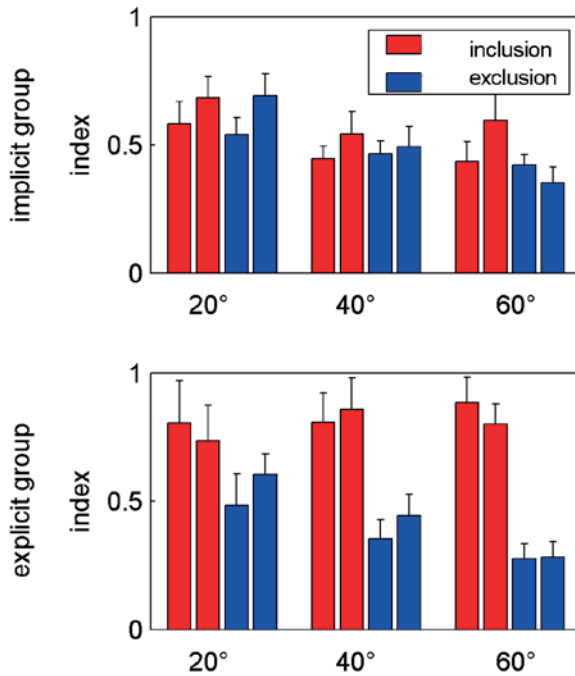
Figure 4. Mean inclusion (red) and exclusion (blue) indices for all three perturbation sizes (20°, 40° and 60°) separately for the implicit (A) and explicit (B) group. Error bars indicate standard errors. For the inclusion index statistical analysis yielded a significant effect of Group ($p < 0.05$), but no effects of Rotation Size, Block Order or any interaction (all $p > 0.05$). For the exclusion index the analysis revealed a significant effect of Rotation Size ($p < 0.001$). No significant effects of Group, Block Order or any interaction was found here (all $p > 0.05$).

The main results of the present study are shown in **Figure 5**. Awareness index is very low within the implicit group with only some awareness after adaptation to a 60° rotation. In the explicit group, however, **Figure 5** reveals an increase of the awareness index with increasing rotation size and with an equal amount of awareness and unawareness index after adaptation to a 40° rotation. We performed two ANOVAs for aware and unaware each with the factors Group (explicit, implicit) and Rotation Size (20, 40, 60). The analysis of the awareness index revealed significant effects of Group [$F_{(1,17)} = 8.66$; $p < 0.01$] and Rotation Size [$F_{corrected(1,24)} = 6.20$; $p < 0.05$] with a difference of awareness of adaptation to 20° and 60°. The mean awareness index after 20° and 60° adaptation increased from 0.02 to 0.13 in the implicit and from 0.23 to 0.56 in the explicit group. Even though this increase was larger in the explicit group, we found no significant interaction of Group × Rotation Size. The unawareness index did not differ between both groups, but also did depend on the size of the rotation (Rotation Size: [$F_{(2,34)} = 19.30$; $p < 0.001$]) with post-hoc tests revealing a significant difference between 20° and both 40° and 60° but not between 40° and 60°.
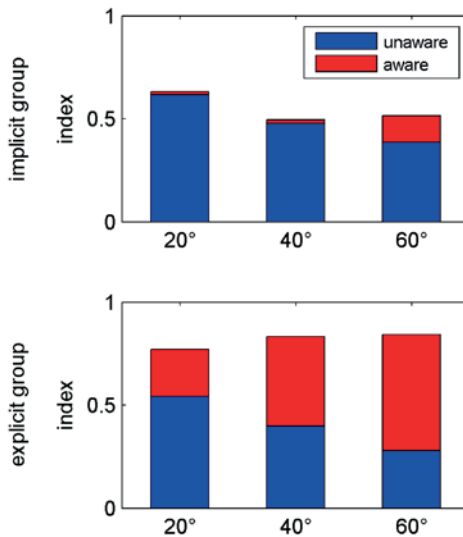
Figure 5. Mean awareness (red) and unawareness (blue) indices for all three perturbation sizes (20°, 40° and 60°) separately for the implicit (A) and explicit (B) group. For the awareness index statistical analysis revealed significant effects of Group ($p < 0.01$) and Rotation Size ($p < 0.05$), but no significant interaction ($p > 0.05$). For the unawareness index the analysis yielded a significant effect of Rotation Size ($p < 0.001$), but no significant effects of Group or Group × Rotation Size (both $p > 0.05$).

It is possible that awareness could benefit from previous training with another rotation. Therefore, the analysis of the awareness index was repeated with the additional factor Rotation Size Order (20-40-60, 20-60-40, 40-60-20, 40-20-60, 60-20-40, 60-40-20). Type VI or *Effective Hypothesis* sums of squares were used in this ANOVA since not all individual groups were included due to missing data. We found no significant effects either of Rotation Size Order or of any interaction including this factor (all $p > 0.05$). However, groups were not all normally distributed and group sizes were very small. To increase group sizes, we, thus, omitted the factor Group and calculated another analysis using only the factors Rotation Size and Rotation Size Order. This analysis also did not reveal a significant effect of Rotation Size Order or its interaction with Rotation Size (both $p > 0.05$). Since two data points out of 18 did not show a normal distribution we calculated a Kruskal-Wallis-Test for each rotation size using the factor Rotation Size Order. None of them revealed a significant effect (all $p > 0.05$).

To compare the extent of awareness to the amount of adaptation for the different rotation sizes, we first calculated correlations between the awareness index and the mean adaptation and clamp trial index of the first bin of both blocks, respectively (**Figure 6**).
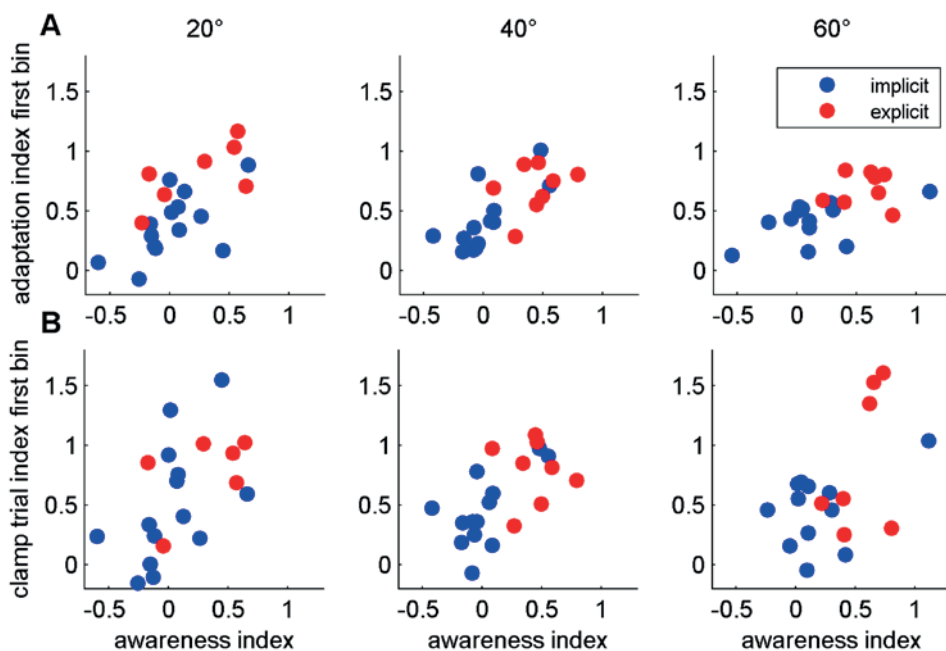
Figure 6. Correlations between the awareness indices for each rotation size and the respective adaptation (A) or clamp trial index (B). Red dots indicate explicit and blue ones implicit participants. Larger awareness of the learned perturbation was related to larger adaptation and clamp trial indices of the first bin. Second, we calculated correlations between the awareness index and the mean adaptation index of the last bin of both blocks. Here, we found a significant correlation for 40° rotation only. All results are presented in **Table 2**.

Table 2. Pearson product-moment correlation coefficients of the correlations between awareness and adaptation (first and last bin) or clamp trial indices (first bin) are shown, respectively.

		Awareness index		
		20°	40°	60°
Adaptation index	first bin	0.76***	0.73***	0.51*
	last bin	0.32	0.60**	0.3
Clamp trial index	first bin	0.51*	0.70***	0.59**

*Symbols ***, **, and * indicate p<0.001, p<0.01, and p<0.05, respectively, and the absence of a symbol indicates p>0.05.*

Measuring savings, i.e. faster relearning during a second exposure to the same perturbation, is a tool for determining whether a long-term memory of the adaptation has been established. We calculated savings as the initial learning difference score that is the difference of the

adaptation index of the first bin of the first and the second block of adaptation to the same rotation size (Morehead et al., 2015). For both groups there were almost no savings in the 20° rotation and up to about 20% savings in the 40° and 60° rotation condition as shown in **Figure 7A**. ANOVA with the factors Group (explicit, implicit) and Rotation Size (20, 40, 60) further revealed no significant effects but a trend in Rotation Size (p = 0.06). Two data points out of six did not show a normal distribution (1x p < 0.05, 1x p < 0.01) and we, therefore, performed Kruskal-Wallis-Tests with the factor Group (explicit, implicit). According to the results of the analysis of variances no group effect was revealed (both p > 0.05). We further found no correlation between the savings and awareness indices (20°: PCC = -0.22, p > 0.05; 40°: PCC = 0.02, p > 0.05; 60°: PCC = 0.39, p > 0.05).

We were further interested whether savings also transferred across rotation sizes. Hence, naïve savings was determined using only the first rotation size of the experimental protocol and experienced savings was additionally calculated using the second and third rotation sizes. Note that this differed between participants; the first rotation size was 20°, 40° or 60° for eight participants each. While naïve savings was larger in the explicit than in the implicit group the reverse holds for experienced savings as can be observed in **Figure 7B**. The statistical analysis with the factors Group (explicit, implicit) and Condition (naïve, experienced) yielded significant effects of Group [$F_{(1,17)}$ = 4.79; p < 0.05], Condition [$F_{(1,17)}$ = 8.23; p < 0.05] and Group × Condition [$F_{(1,17)}$ = 9.14; p < 0.01]. Here, naïve savings of the explicit group was different from all other savings values as confirmed by post hoc analysis of the interaction. A normal distribution was not given for naïve savings of the implicit group (p < 0.05). Kruskal-Wallis-Tests with the factor Group (explicit, implicit) confirmed the difference of naïve savings between groups (p < 0.05). No Spearman correlations were found between naïve or experienced savings on the one hand and awareness indices of respective rotation sizes on the other (naïve: SCC = 0.24, p > 0.05; experienced: SCC = -0.33, p > 0.05).

Finally, we compared the present measurement of awareness by the PDP to that of a questionnaire. Therefore, the results of the verbal assessment were used to classify all subjects into aware or unaware according to the approach used by Benson et al. (2011). Within this procedure explicit awareness was attributed to those participants who described the feedback or disturbance as rotated or claimed the application of a rotational strategy. Nine out of 16 subjects in the implicit group were considered not to have awareness, and, interestingly, two out of eight explicitly instructed subjects were also classified as unaware. For the statistical analyses we used the same data as for the correlations, i.e. the first bin of the mean adaptation and clamp trail indices of both blocks and entered them into two ANOVAS with the factors Group (aware, unaware) and Rotation Size (20, 40, 60). Neither the analysis of adaptation index (effect of Group: p = 0.32) nor that of clamp trial index

(effect of Group: p = 0.59) yielded any significant effects, showing that awareness measured by means of a questionnaire, in contrast to that measured by PDP, was not related to adaptation.
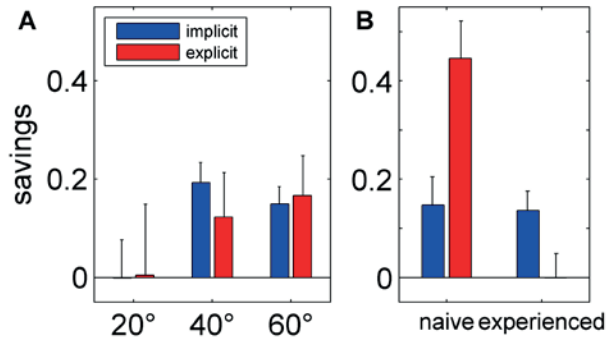

Figure 7. Mean savings for the implicit (blue) and explicit (red) group for all three perturbation sizes (20°, 40° and 60°) (A) as well as for naïve adaptation, i.e. the first rotation size of the experimental protocol, and experienced adaptation, i.e. the second and third rotation sizes (B). For the three rotation sizes statistical analysis revealed no significant effects (all p > 0.05). An analysis of the naïve and experienced condition yielded significant effects of Group (p < 0.05), Condition (p < 0.05) and Group × Condition (p < 0.01).

DISCUSSION

The aim of the present study was to find out whether the degree of awareness of the nature of the perturbation depends on its magnitude. An implicit group and a group of subjects using explicit strategies adapted to 20°, 40° and 60° cursor rotations, and we measured awareness and unawareness indices after each adaptation block with a process dissociation procedure. The analyses revealed a larger awareness index in the explicit than in the implicit group and a larger awareness index after adaptation to 60° than to 20° rotation for both groups. This did not depend on the order in which rotation sizes were presented to the subjects. Adaptation and clamp trial indices were also larger in the explicit than in the implicit group. Furthermore, initial adaptation measures – adaptation and clamp trial indices of the first bin – correlated to the size of awareness indices. Savings did not differ between groups and only showed a trend of being larger for larger rotation sizes. The explicit but not the implicit participants transferred savings from the first to the following rotation sizes. Finally, the analyses revealed that awareness measured by means of a questionnaire, in contrast to that measured by PDP, was not related to adaptation.

Awareness

The degree of awareness of the nature of the perturbation did clearly depend on the perturbations´ magnitude in both groups. Naïve participants developed a negligible awareness index of 0.02 after adaptation to 20° and 40° and an awareness index of 0.13 after 60° rotation of visual feedback. This result is consistent with previous work showing awareness only in three out of 27 participants when a 30° rotation was introduced (Benson et al., 2011). We can further conclude that awareness does not arise when visual rotations are introduced gradually in steps of 0.25° to 10° (Galea et al., 2010b; Kagerer et al., 1997; Klassen et al., 2005; Werner et al., 2014). Our results more generally suggest that the development of awareness depends on the size of target error, i.e. the perceived error between cursor and target. Since in gradual adaptation paradigms the size of perturbation steps are deliberately chosen to induce only small target errors, there should also be no awareness after gradual adaptation to optical shifts using prisms (Hatada et al., 2005; Jakobson and Goodale, 1989; Michel et al., 2007), to visuomotor gains (Ingram et al., 2000), viscous force-fields (Criscimagna-Hemminger et al., 2010; Klassen et al., 2005; Malfait and Ostry, 2004; Orban de Xivry et al., 2010), or after gradual saccade adaptation (Wong and Shelhamer, 2011). The present findings thus confirm the notion that participants adapting to gradually introduced perturbations with very small increases of perturbation size are usually not aware (Criscimagna-Hemminger et al., 2010).

Moreover, the outcome of the present study can help explaining the actual disagreement on whether the gradual adaptation paradigm can improve the amount of recalibration (Wong and Shelhamer, 2011) as shown in several studies (Huang and Shadmehr, 2009; Ingram et al., 2000; Kagerer et al., 1997; Michel et al., 2007; Wong and Shelhamer, 2011), but not in others (Hussain and Morton, 2014; Klassen et al., 2005; Werner et al., 2014). Also, intermanual transfer was revealed after sudden but not after gradual adaptation by Malfait and Ostry (2004), whereas this difference was not reported in other studies (Taylor et al., 2011; Wang et al., 2011). This could be due to the chosen perturbation size that left participants adapting to the sudden introduced distortion equally unaware as the ones in the gradual group. For example, rotation sizes of 22.5° to 32° were used in those studies that did not find a difference in retention or intermanual transfer (Klassen et al., 2005; Taylor et al., 2011; Wang et al., 2011). To finally solve this disagreement, further studies should be performed that identify the actual size of perturbation leading to awareness on the one hand and test awareness and retention or intermanual transfer at the same time on the other hand. Of course, gradual and sudden adaptation differ not only with respect to awareness and have consequently been shown to be based on distinct neural correlates (Orban de Xivry et al., 2010; Venkatakrishnan et al., 2011; Werner et al., 2014).

It can be argued, that the group difference in awareness is due to the group difference of the inclusion index, that is the lack of the implicit group of reproducing what was learned compared to the explicit group. However, underestimation of awareness in the implicit group is unlikely, because those factors that might have contributed to the increased loss between the end of adaptation and inclusion are rather implicit or unaware: the passage of time, reaching without visual feedback or the observed decrease of errors during ongoing reaching during no feedback trials (Hinder et al., 2008; Kitago and Krakauer, 2013; Peled and Karniel, 2012; Shabbott and Sainburg, 2010).

We found no effect of the order of rotation sizes on the amount of awareness. However, we cannot rule out that a possible beneficial effect of previous adaptation to different rotation sizes was cancelled out by a detrimental effect due to fatigue or to forgetting the instructions in the explicit group. Future studies should be conducted with a between-subject design in which each group gets exposed to a single rotation size only.

Unawareness

As expected the unawareness index was smaller in the explicit compared to the implicit group but with mean indices of approx. 0.55, 0.4 and 0.3 after adaptation to 20°, 40° and 60°, respectively, unawareness was still surprisingly large in explicitly instructed participants. On the one hand, this large proportion of unawareness might be consistent with the results of a study by Mazzoni (2006) in which participants used an explicit strategy to quickly reduce errors during adaptation to a visual rotation. Later on during learning, reaching errors increased again, representing a simultaneous implicit adaptation process driven by sensory prediction errors. Our unawareness index could reflect this implicit process. On the other hand, we could also be seeing a modulation of strategies over the time course of adaptation with different strategies being differently accessible to consciousness as has been suggested earlier (Taylor and Ivry, 2014).

Explicit and implicit group

Comparison of adaptation of both groups revealed a larger initial adaptation index in the explicitly instructed group. The magnitude of early adaptation clearly correlated to awareness across groups and for all rotation sizes, whereas we found no correlation between late adaptation and awareness for 20° and 60° rotations. This pattern of findings is in line with the results of a previous study showing explicit instructions leading to increased early but not late adaptation (Benson et al., 2011). Since the explicit group in the present study was a priori instructed and, thus, aware of the nature of the perturbation it can be assumed that awareness leads to increased initial adaptation and not vice versa increased initial adaptation leads to awareness. It should be noted that the increased AI of the first

bin could be due to a greater reduction of errors during those first nine trials or to a larger initial AI as a result of instructions or savings. We do not have sufficient data to distinguish these possibilities. Contrary to our findings of increased clamp trial indices in explicitly instructed participants, reduced catch trial performance in an explicit compared to an implicit group was reported earlier (Benson et al., 2011). While the explicit subjects were instructed to turn off their strategy during catch trials in that study, our clamp trials came without notice or instructions and, therefore, we probably measured the sum of multiple learning mechanisms. Instead of isolating recalibration, the same processes as during perturbed trials might have been present in the explicit group. Hence, it is not surprising that clamp trial indices, equivalent to adaptation indices, correlated to awareness for all rotation sizes.

Even though we found no significant effects of savings, there was a marked increase from almost no savings in the 20° adaptation to savings in 40° and 60° adaptation. This is in line with previous work showing savings after 45° but not after 30° rotation of visual feedback (Morehead et al., 2015). In the current study, explicitly instructed participants further transferred savings from the first to the following rotation sizes in contrast to the implicit group. To our knowledge, no study has yet tested savings after participants had used an explicit strategy. But the result of the implicit group is in agreement with uninformed subjects showing faster relearning of an unexperienced perturbation only when rotation sizes differed by 75° and not 45° (Morehead et al., 2015) or when they differed in essence like the difference from left-right reversal to a 180° rotation (Bock et al., 2001). Interestingly, awareness did not correlate with any of our savings measures.

Multiple learning processes have been suggested to facilitate motor behavior during adaptation. A distinction has been drawn between slow and fast adaptation (Smith et al., 2006), error-based and reinforcement learning (Izawa and Shadmehr, 2011) or implicit and explicit processes (Heuer and Hegele, 2011; Sülzenbrück and Heuer, 2009; Taylor and Ivry, 2011, 2014). The present data does not allow any judgement on the overlap of different theoretical frameworks. But it can help disentangling awareness and explicit strategies, which have both been attributed to explicit processes (Heuer and Hegele, 2011). Awareness or explicit knowledge of the nature of the perturbation is thought to be a prerequisite for explicit strategies (Hegele and Heuer, 2010; Heuer and Hegele, 2011; Schween et al., 2014). The latter can either be evoked by instructions (Benson et al., 2011; Mazzoni, 2006; Sülzenbrück and Heuer, 2009; Taylor and Ivry, 2011; Taylor et al., 2010) or by color cueing (Morehead et al., 2015). Explicitly instructed participants showed increased initial adaptation and increased savings compared to the implicit group in the present study. But awareness only correlated to adaptation and not to measures of savings. This dissociation of

results is supported by the notion that savings are reflected by model-free reinforcement of previously successful behavior (Huang and Shadmehr, 2009) and are thus linked to action selection or re-aiming strategies (Morehead et al., 2015; Taylor and Ivry, 2014).

Measuring awareness

The possibility to measure awareness as well as unawareness as an index is an evident advantage of using PDP over the use of a questionnaire that only allows the classification of aware or unaware. Moreover, questionnaires may underestimate awareness due to the difference of retrieval contexts or because knowledge is held with low confidence (Eriksen, 1960; Nisbett and Wilson, 1977; Reingold and Merikle, 1990; Shanks and St. John, 1994; Shanks et al., 2005). Unlike the awareness index measured by PDP, the results of the questionnaire in the present study were neither related to adaptation nor to clamp trial behavior. These results suggest that awareness of the nature of the perturbation can be more closely captured using PDP.

Heuer and Hegele measured explicit knowledge by providing the participants with a line which they moved through verbally instructing the experimenter until they found it to match the direction of a successful hand movement (Hegele and Heuer, 2010; Heuer and Hegele, 2008; Heuer and Rapp, 2011). Yet another task was used by Taylor et al. (2014) to measure explicit learning. Here, participants reported their aiming direction with the help of a circular array of landmarks encircling the target. Both methods use predictions during the same sort of task and might therefore, as outlined in the introduction, be based on feelings of familiarity (Jacoby, 1991) and lead to an overestimation of awareness (Cleeremans, 2007). Further research is required to compare the results of those prediction task methods to those of the PDP.

CONCLUSION

In conclusion, the results of this study suggest that the development of awareness of the nature of the perturbation depends on its size and confirm the idea that participants adapting to gradually introduced perturbations are usually not aware. Moreover, our findings can help explain the disagreement regarding the effects of the gradual adaptation paradigm by proposing that some studies chose perturbation sizes which left participants adapting to the suddenly introduced distortion just as unaware as those in the gradual group. Furthermore, the present results emphasize the importance of controlling or monitoring awareness in future studies comparing gradual and sudden adaptation. The awareness index of the current study measured by PDP correlated to the size of early adaptation, whereas the results

of a questionnaire were not related to adaptation. To sum up, our results can thus explain the contradiction of previous studies analyzing the effect of cognitive components such as explicit strategies and explicit knowledge, i.e. awareness, on sensorimotor adaptation.

Acknowledgements

Author contributions

Thomas Hulst analyzed data; interpreted results; edited and revised manuscript; approved the final version of the manuscript.

9

Cerebellar degeneration reduces memory resilience after extended training

Thomas Hulst[1,2,3], Ariels Mamlins[1], Maarten Frens[3], Dae-In Chang[1],
Sophia L. Göricke[4], Dagmar Timmann[1#], Opher Donchin[5#]

[1] Department of Neurology, Essen University Hospital, University of Duisburg-Essen, 45122 Essen, Germany
[2] Erasmus University College, Rotterdam, The Netherlands
[3] Department of Neuroscience, Erasmus MC, 3000 CA Rotterdam, The Netherlands
[4] Department of Diagnostic and Interventional Radiology and Neuroradiology, Essen University Hospital, University of Duisburg-Essen, 45122 Essen, Germany
[5] Department of Biomedical Engineering, Zlotowski Center for Neuroscience, Ben-Gurion University of the Negev, Beer-Sheva 8410501, Israel
[#] Authors contributed equally
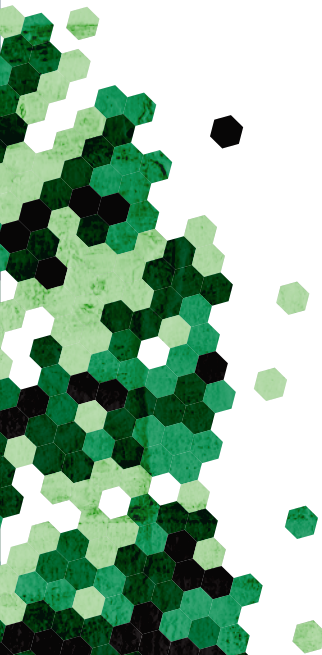
ABSTRACT

Patients with cerebellar ataxia suffer from various motor learning deficits hampering their ability to adapt movements to perturbations. Motor adaptation is hypothesized to be the result of two subsystems: a fast learning mechanism and a slow learning mechanism. We tested whether training paradigms that emphasize slow learning could alleviate motor learning deficits of cerebellar patients. Twenty patients with cerebellar degeneration and twenty age-matched controls were trained on a visuomotor task under four different paradigms: a standard paradigm, gradual learning, overlearning and long intertrial interval learning. Expectedly, cerebellar participants performed worse compared to control participants. However, both groups demonstrated elevated levels of spontaneous recovery in the overlearning paradigm, which we saw as evidence for enhanced motor memory retention after extended training. Behavioral differences were only found between the overlearning paradigm and standard learning paradigm in both groups.

Modelling suggested that, in control participants, additional spontaneous recovery was the result of higher retention rates of the slow system, as well as reduced learning rates of the slow system. In cerebellar participants, additional spontaneous recovery appeared only to be the result of higher retention rates of the slow system and not reduced learning rates of the slow system. Thus, memory resilience (our term) was reduced in cerebellar participants resulting in elevated levels of slow learning which were less resilient against washing out. To our knowledge, this is the first time this specific deficit has been described in cerebellar patients. Our results suggest that cerebellar patients might still benefit from extended training through use-dependent learning, which could be leveraged to develop more effective therapeutic strategies.

Keywords: cerebellar degeneration; motor adaptation; rehabilitation; memory resilience; overlearning

INTRODUCTION

The cerebellar ataxias are a heterogeneous group of disorders clinically identified by cerebellar dysfunction. Patients exhibit a range of impairments in motor control, including incoordination of eye movements, dysarthria, limb incoordination, and gait disturbances (Mariotti et al., 2005), as well as impairments in the cognitive domain (Schmahmann and Sherman, 1998). While the genetic and pathophysiological underpinnings of many of the cerebellar ataxias are increasingly well understood (Jayadev and Bird, 2013; Matilla-Dueñas et al., 2014; Paulson, 2009), treatment remains a major challenge with genetic therapies being at the horizon for only a subset of genetically defined ataxias (Scoles et al., 2017). Contemporary cerebellar therapy is aimed at alleviating motor symptoms to maintain activities of daily living (ADL), as no curative therapy currently exists (Ilg et al., 2014). Although the consensus is that cerebellar patients benefit from supportive therapy, i.e. physical therapy, speech therapy and occupational therapy, little is known about the mechanisms underlying the improvements and how patients can benefit most (Fonteyn et al., 2014; Ilg et al., 2014). Providing effective care for ataxia patients can be especially challenging, since cerebellar patients suffer from various motor learning deficits (Maschke et al., 2004a; Sanes et al., 1990; Tseng et al., 2007) and initial studies suggest a relationship between motor learning deficits and the efficacy of neurorehabilitation programs (Hatakenaka et al., 2012). An intervention which can lessen these motor learning deficits might therefore augment the effects of cerebellar therapy.

Previous work has found that motor learning deficits of cerebellar patients can partially be ameliorated when trained with an explicit strategy (Taylor et al., 2010) or by altering the type of feedback (Therrien et al., 2016). There is also limited evidence that training paradigms that emphasize slow learning processes might alleviate motor learning deficits (Criscimagna-Hemminger et al., 2010), but, as of yet, few studies have examined this notion. Early evidence pointed to beneficial effects of the gradual introduction of reaching movement perturbations in cerebellar patients (Criscimagna-Hemminger et al., 2010), but this was not replicated in cerebellar patients in subsequent work (Gibo et al., 2013; Schlerf et al., 2013). On the other hand, in studies with healthy individuals, training paradigms which emphasize slow learning have shown robust effects on motor performance. For instance, when healthy individuals keep training after attaining asymptotic performance on a motor learning task, so-called overlearning, retention increases with the number of trials trained at the asymptote (Joiner and Smith, 2008). The amount with which retention increases can be predicted by a two-state model that incorporates a fast and slow learning mechanism and is thought to be the result of increased engagement of the slow state of motor learning (Joiner and Smith, 2008; Smith et al., 2006). Similarly, when healthy individuals train

with long intertrial intervals (ITI) between movements, the rate of learning decreases, but retention increases due to more trial-to-trial forgetting of the fast state of motor learning and more activation of the slow state of motor learning (Kim et al., 2015; Sing et al., 2009).

The aim of the present study was to study slow learning processes in more detail, in particular in patients with cerebellar degeneration, and to assess whether paradigms that emphasize slow learning affect behavioral measures of motor learning. We tested twenty patients with degenerative ataxia and twenty healthy age- and sex-matched controls on a visuomotor reaching adaptation task under four different training paradigms (a standard learning paradigm, gradual learning, overlearning and long intertrial interval (ITI) learning). The paradigms, other than the standard learning paradigm, were specifically chosen to stimulate slow learning in individuals.

We expected to find impaired motor learning in cerebellar participants under a standard training paradigm, characterized by incomplete adaptation to visuomotor perturbations and decreased retention. Training cerebellar participants with paradigms that emphasize slow learning might enable them to compensate for these motor learning deficits. Any behavioural improvements will be modelled to determine if they are the result of additional build-up of the slow system or changes to the underlying learning and retention parameters. We expect that increased retention rates of the slow system could result in higher levels of motor retention, while reduced learning rates of the slow system could result in motor memories that are more resilient against washing out. If slow learning paradigms allow cerebellar participants to compensate motor learning deficits, it could facilitate the design of new strategies in supportive therapy.

METHODS

Participants

Twenty participants with cerebellar degeneration (9 females, 54.9 years ± 10.8 (SD), range 18 – 70 years) and twenty age- and sex-matched participants (9 females, 55.2 years ± 11.2 (SD), range 18 – 71 years), took part in the study. Cerebellar participants were recruited from the patients attending our ataxia clinic and matched controls were recruited via print advertisements distributed on the hospital campus. Only right-handed individuals were included, as assessed by the Edinburgh Handedness Inventory (Oldfield, 1971). The severity of cerebellar symptoms in the group of cerebellar participants was assessed by one experienced neurologist (DT) and healthy age- and sex-matched controls were examined by AM. Cerebellar symptoms were scored on the International Cooperative Ataxia Rating

Scale (ICARS; Trouillas et al., 1997), as well as the Scale for the Assessment and Rating of Ataxia (SARA; Schmitz-Hübsch et al., 2006). The group of cerebellar participants was diagnosed with diseases known to primarily affect the cerebellar cortex (Gomez et al., 1997; Timmann et al., 2009). Three age-matched controls were excluded and replaced due to neurological symptoms on their examination or minor extracerebellar pathology on their MRI. All participants gave informed oral and written consent. The experiment was approved by the ethics committee of the medical faculty of the University of Duisburg-Essen and conducted in accordance with the Declaration of Helsinki. The characteristics of the recruited cerebellar participants and matched controls can be found in **Table 1**.

Table 1. Cerebellar participants were age- and sex-matched with the controls on the right side of the table.

Cerebellar participants							Control participants		
ID	Age	Sex	Diagnosis	Disease duration	ICARS (total/100)	SARA (total/40)	ID	Age	Sex
P01	18	M	ADCAIII	18 years	10.5	5	C01	18	M
P02	47	M	ADCAIII	25+ years	40	17.5	C02	43	M
P03	50	F	ADCAIII	25+ years	31	11.5	C03	50	F
P04	51	M	SCA14	25+ years	31	11.5	C04	50	M
P05	51	F	ADCAIII	19 years	29	12.5	C05	51	F
P06	52	F	SCA14	22 years	26.5	12	C06	53	F
P07	53	F	SCA6	2 years	23	9.5	C07	54	F
P08	53	M	SAOA	17 years	40	15	C08	53	M
P09	53	M	ADCAIII	17 years	36	11	C09	51	M
P10	54	F	SCA6	4 years	30.5	10	C10	56	F
P11	56	F	SCA14	25+ years	28	12	C11	58	F
P12	57	M	SCA6	11 years	38	11	C12	53	M
P13	57	M	SCA6	15 years	28	8	C13	59	M
P14	58	M	SAOA	25+ years	63.5	22	C14	61	M
P15	59	M	SCA6	5 years	23	9.5	C15	63	M
P16	60	F	SCA6	11 years	36.5	14	C16	60	F
P17	63	F	ADCAIII	23 years	33	13.5	C17	66	F
P18	66	M	SAOA	13 years	24.5	11	C18	66	M
P19	70	F	SAOA	7 years	32.5	12.5	C19	71	F
P20	70	M	SAOA	16 years	38	15	C20	67	M

SCA6 = spinocerebellar ataxia type 6; SCA14 = spinocerebellar ataxia type 14; SAOA = sporadic adult onset ataxia; ADCA III = autosomal dominant ataxia type III; ICARS = International Cooperative Ataxia Rating Scale (Trouillas et al., 1997); SARA = Scale for the Assessment and Rating of Ataxia (Schmitz-Hübsch et al., 2006). Disease duration is years since presentation of the first symptoms.

Task

All participants completed a standard reaching task with visuomotor perturbations. The experimental setup and task have been described previously in other studies from our group (Rabe et al., 2009). In short, participants were seated in front of an upright monitor and could, with their right hand, move a two-jointed manipulandum freely in the horizontal plane (**Figure 1A**). Vision of the participant's arm was obstructed by a black cloth. Hand position and velocities were measured in a resolution of 10^6 counts per revolution and a sampling rate of 200 Hz (DMC-1826; Galil Motion Control). The location of the participant's hand was represented on the monitor by a green dot with a diameter of 5 mm. The origin and target locations were represented by a circle with a diameter of 10 mm, colored red and white respectively. At the start of each trial, the participant's hand was moved towards the origin location by the servomotors connected to the manipulandum. Then, after a delay of 2000ms, a target circle appeared at one of three possible target locations, located 10 centimeters away from the origin at an angle of 66°, 90° or 114° (**Figure 1B**). Participants were instructed to move the green dot from the origin towards the target with a "quick and accurate movement" as soon as the target appeared. When participants moved the cursor through an invisible boundary located 10 centimeters from the origin, their hand was gently brought to a stop by a simulated cushion, indicating the end of the movement. Following each movement, participants received feedback on whether they hit the target and moved with the correct velocity. The target turned yellow when moving too fast, blue when moving too slow, and green when moving with the correct velocity. Participants moved with the correct velocity when their movement and reaction time fell within a 250ms window centered around 500ms. The 250ms window shrunk by 10% every time a movement had the correct velocity and increased by 10% when moving too fast or slow, adapting to a participant's individual capabilities. When participants also managed to hit the target, in addition to moving with the correct velocity, a "yahoo" sound was played.

The experimental task consisted of 4 different training paradigms. Each paradigm consisted of a baseline set, an adaptation set, and a washout set. All participants completed each of the training paradigms. The order of paradigms was counterbalanced with a Latin-squares design against first-order carryover effects (Williams, 1949). Every paradigm order was completed by 10 participants each (five cerebellar participants and five control participants) (**Figure 2A**). Furthermore, perturbation direction in the adaptation sets was balanced by flipping the direction of the perturbation (clockwise or counterclockwise) in every successive adaptation set. Participants were allowed to take 5- to 10-minute breaks between paradigms, but not after sets within a paradigm. Each baseline set consisted of 135 null trials, in which participants received veridical feedback on hand position, and 15 pseudo-randomly interspersed clamp trials, in which participants received perfect feedback

regardless of movement error. Then, depending on the training paradigm, one of four adaptation sets followed. In the standard training paradigm, the adaptation set consisted of 108 adaptation trials, in which a visuomotor perturbation of 30° was introduced abruptly, and 12 pseudo-randomly interspersed clamp trials (**Figure 2B**). The gradual paradigm contained 108 adaptation trials in the adaptation set, where the visuomotor perturbation of 30° was introduced gradually over the course of the set, increasing linearly each trial. The final 6 trials of the gradual adaptation set were at 30° of visuomotor perturbation. In addition, 12 clamp trials were pseudo-randomly interspersed (**Figure 2C**). The overlearning adaptation set consisted of 324 trials with a visuomotor perturbation of 30° (three times the amount of the standard paradigm) and 36 interspersed clamp trials (**Figure 2D**). The long intertrial interval (ITI) adaptation set included 120 adaptation trials with visuomotor perturbations of 30°, where instead of delay of 2 seconds between each movement, the delay was increased to 15 seconds (**Figure 2E**). The adaptation set of the long ITI paradigm did not include any clamp trials, thus trial-to-trial forgetting was only dependent on the passage of time. Finally, all adaptation sets were followed by a washout set. The first 12 trials of the washout set consisted of counterperturbation trials, where the direction of the perturbation was flipped from the direction in the adaptation set. Then, 60 clamp trials and 60 null trials followed.
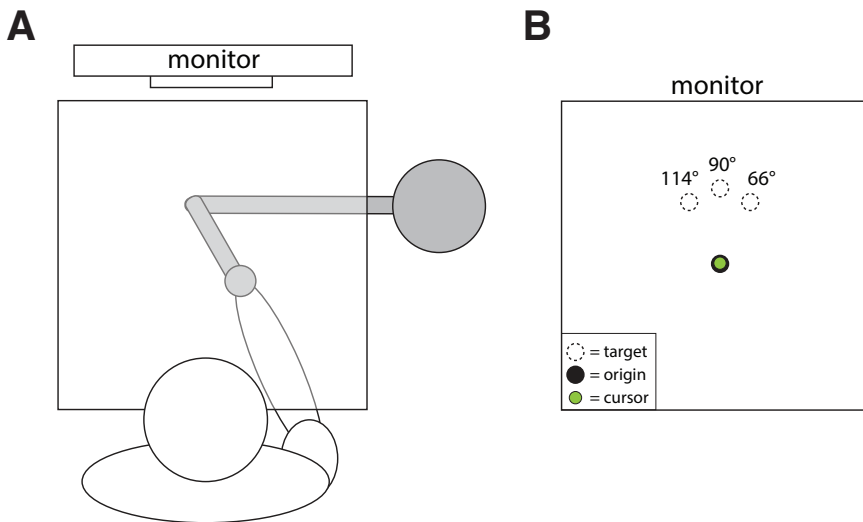
Figure 1. A) Experimental setup. For illustrative purposes the tabletop is pictured here as transparent. In reality the tabletop was opaque to obstruct the view of the hand and robot arm. Additionally, a black cloth was draped over the shoulders of the participant and attached to the table to obstruct vision of the arm. B) Localization of origin and target circles on the monitor. One of the three target circles would pseudo-randomly appear at the start of a movement trial.
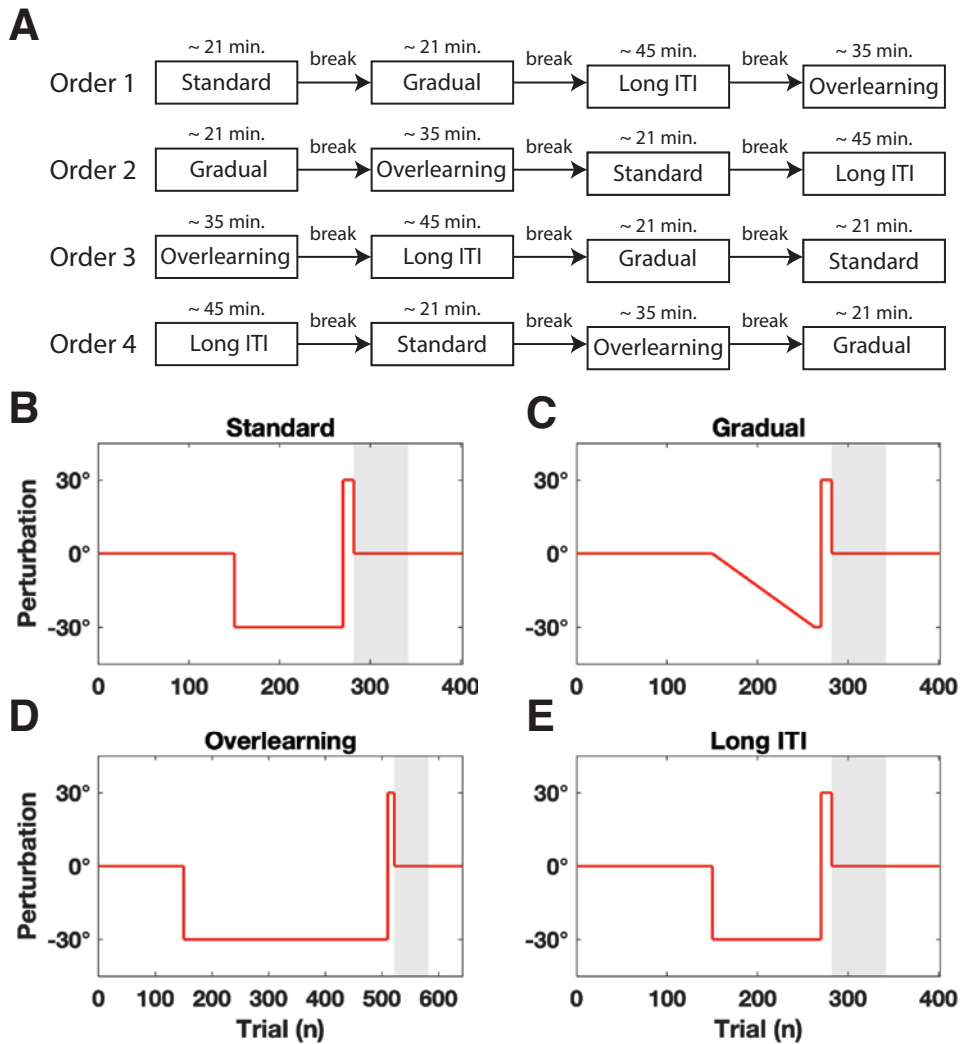
Figure 2. A) Overview of the paradigm orders. B–E) Trial structure of the experimental paradigms. Red line indicates the size and direction of the visuomotor perturbation. Direction of the perturbation is pictured here as clockwise for all paradigms, in reality perturbation direction was counterbalanced within participants. Grey area indicates the block of 60 clamp trials in the washout set. Not pictured are pseudo-randomly interspersed clamp trials during the baseline and adaptation set.

MR imaging

Cerebellar participants and age-matched controls were examined in a 3T combined MRI-PET system (Siemens Healthcare, Erlangen, Germany) with a 16-channel head coil (Siemens Healthcare) [TR, 2530 ms; TE = 3.26 ms, TI = 1100 ms; flip angle 7 deg; voxel size $0.5 \times 0.5 \times 1.0 \text{ mm}^3$]. All MR scans were evaluated by an experienced neuroradiologist (SLG). A voxel-based morphometry analysis was applied to the cerebellum of each participant as described previously (Hulst et al., 2015; Taig et al., 2012). The analysis was automated with an in-house program written for MATLAB 9.4 using the SUIT toolbox (version 3.2) (Diedrichsen et al., 2009), implemented in SPM12 (http://www.fil.ion.ucl.ac.uk/spm/software/spm12).

Analysis of behavioral data

Behavioral data was analyzed in MATLAB 9.4 (Mathworks, Natick, USA). Our primary outcome measure was the reaching direction (in degrees) at the end of the movement (i.e. when participants hit the simulated cushion). The reaching direction was calculated by taking the angle between a straight line from the position of movement onset to the target and a straight line from the position of movement onset to hand position at the end of the movement. Movement onset was defined as the first moment when movement velocity exceeded 5cm/s. Reaching directions were corrected for movement biases by calculating the average reaching direction in each baseline set and subtracting this from the subsequent adaptation and washout sets of a training paradigm. For ease of interpretation, reaching directions were flipped towards the same direction, regardless of perturbation direction, in all figures and analyses. Furthermore, paradigms were reordered to a canonical order for each participant, starting with the standard learning paradigm, then gradual learning, overlearning and finally the long ITI paradigm, regardless of the order the participant encountered the paradigms. Statistical analyses were conducted using Markov Chain Monte Carlo (MCMC) methods in MATLAB and JAGS 4.3.0 (Plummer, 2003). A mixed-design model (ANOVA-like) was used to estimate the difference in reaching directions between factors. Participant group (cerebellar participant or control participant) was included as a between-subject factor. Movement phase (baseline, early adaptation, late adaptation and recovery) and training paradigm were included as within-subject factors. A random intercept for each participant and phase was included as well. The model ran on four separate chains with an adaptation phase of 5,000 samples and burn-in phase of 25,000 samples, after which we collected 50,000 samples per chain. Each parameter was visually and quantitatively checked to assure proper sampling of the posterior distribution using common MCMC diagnostics (Kruschke, 2010). First, trace plots were visually inspected for chain convergence. Next, the effective sample size (ESS), the potential scale reduction factor (PSRF) and the Monte Carlo Standard Error (MCSE) were calculated for all parameters (**Supplementary Table 1**). The PSRF was close to 1 for each parameter (max: 1.0002),

MCSE was close to 0 for each parameter (max: 0.0001), and median ESS was generally large (>> 5000), indicating convergence of the model run. The model code is available as supplementary material (**Supplementary Data 1**).

State-space modeling

A two-state model was fit to the reaching directions of all trials in each individual participant. The equations for the state-space model are given in Equations 1-6:

$$e_t = x_t + p_t \qquad \text{(Eq. 1)}$$

$$x_{t+1}^F = A^F x_t^F - B^F e_t + \epsilon_{state} \qquad \text{(Eq. 2)}$$

$$x_{t+1}^S = A^S x_t^S - B^S e_t + \epsilon_{state} \qquad \text{(Eq. 3)}$$

$$x_t = x_t^F + x_t^S \qquad \text{(Eq. 4)}$$

$$y_t = x_t + \epsilon_{output} \qquad \text{(Eq. 5)}$$

$$\epsilon_{output} \sim N\left(0, \sigma_{\epsilon_o}^2\right), \epsilon_{state} \sim N(\sigma_{\epsilon_s}^2) \qquad \text{(Eq. 6)}$$

Where $A^S > A^F$ and $B^S < B^F$.

This state-space model, as posited by Smith and colleagues (Smith et al., 2006), consists of a fast state (x_t^F) and slow state (x_t^S). The fast state learns quickly and forgets quickly, while the slow state learns slowly and forgets slowly. Both states have an independent learning rate (B) and retention rate (A). Each movement, the fast and slow state are updated based on the error (e) in the previous movement. In visuomotor experiments, the amount of error is given by addition of the actual movement (x_t) and perturbation (p_t). The model has previously been able to predict various behavioral phenomena in reaching adaptation experiments like savings, anterograde interference and spontaneous recovery (Smith et al., 2006).

To estimate the parameters and hidden state variables for a given participant from reaching directions, we implemented a hierarchical model based on Equations 1-6 in JAGS (**Figure 3**). A hierarchical model improves fits by sharing information across participants. The

parameters and state variables were estimated by MCMC methods, separately for each of the four training paradigms (standard, gradual, overlearning and long ITI) and two participant groups (cerebellar participants or control participants). In the hierarchical model, a participants' learning rate (B^S and B^F) and retention rate (A^S and A^F) came from a normal distribution centered around μ with precision τ. The learning and retention rates were sampled in logistic space and then transformed to the range from 0 to more realistically reflect changes in the parameters and provide better sampling behavior. Precision for the states and execution noise came from a very broad gamma distribution (A = 10^{-3}, B = 10^{-3}).
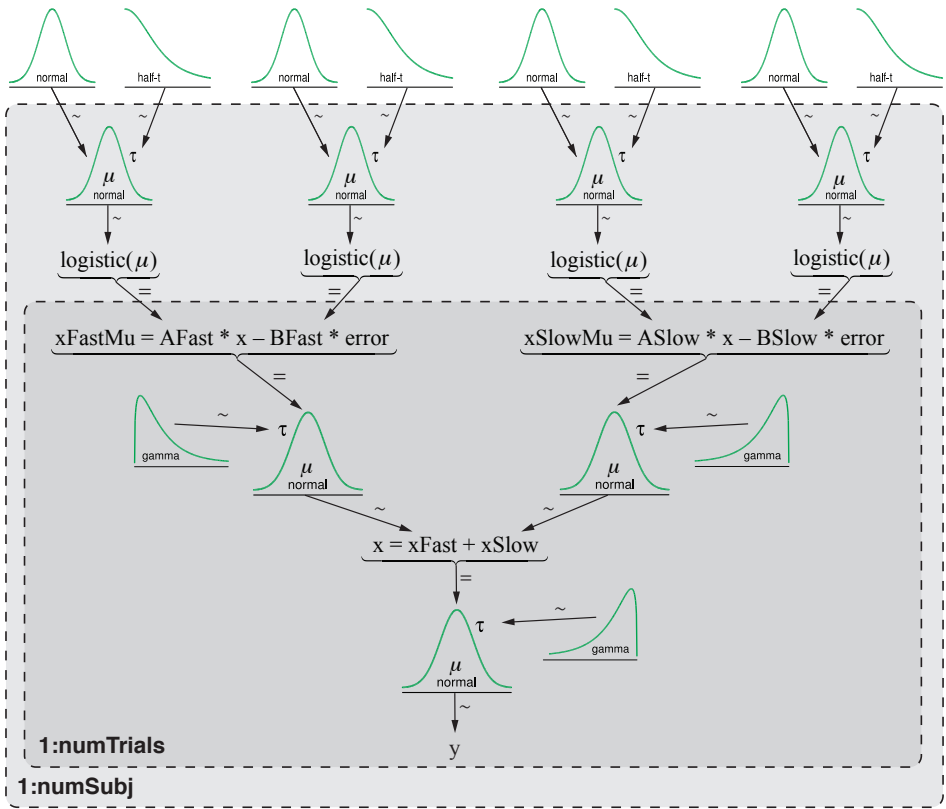

Figure 3. Diagram of the hierarchical model implemented in JAGS. The equals sign (=) denotes deterministic relationships, while tildes (~) denote stochastic relationships. The distributions on the white background indicate the hyperpriors. The light grey background indicates the subject loop, while the dark grey background indicates the trial loop.

Only the shape of the learning- and retention rate distributions was specified (normal in logistic space), the actual priors for each participant were sampled from a hyperprior. The hyperparameter for μ came from an uninformative normal distribution ($M = 0$, $S = 1000$) and τ from a weakly informed half-t distribution ($M' = 0$, $S' = 2.5$, $N = 7$) so each posterior distribution was mainly informed by the data. Reasonable initial values for M and S were estimated by running the model first without hyperpriors and weakly informed priors for the learning and retention rates of a participant (4 chains, adaptation and burn-in of 10,000 samples, 30,000 samples collected). Model runs for the model with hyperparameters started with an adaptation phase of 20,000 samples and burn-in phase of 80,000 samples, after which we collected 250,000 samples on four separate chains. Samples were thinned by a factor of 5 to decrease the memory footprint and autocorrelation of samples. For every parameter we first visually inspected the trace plots for chain convergence. Next, several MCMC diagnostics were calculated: the ESS, PSRF and MCSE (**Supplementary Table 2**). Generally, sampling of the posterior distributions was considered adequate. No large differences in ESS, PSRF and MCSE were found between the paradigms. A small number of parameters had low ESS due to high autocorrelations in specific paradigms, mainly on the participant level, but longer model runs were deemed impractical. The model code is available as supplementary material (**Supplementary Data 2**).

RESULTS

Voxel-based morphometry (VBM)

First, the results of the structural MRI data were analyzed using VBM. **Figure 4** displays the difference in gray matter volume per voxel (in t-scores) between healthy participants and cerebellar participants. A resampling procedure (permutation test) was conducted to control the family-wise error rate. The significance threshold was determined to be 3.95, meaning that voxels with an absolute t-score higher than 3.95 were considered significant. No significant positive differences were found, thus the figure displays negative t-scores only. The VBM analysis revealed a pattern of cerebellar degeneration in patients largely consistent with prior work (Hulst et al., 2015). The volume loss was largest in the anterior lobe of the cerebellum and the superior part of the posterior lobe (i.e. lobule VI). Cerebellar degeneration of the anterior cerebellum and lobule VI (i.e. the anterior hand area) are associated with motor learning deficits (Donchin et al., 2012; Rabe et al., 2009). Cerebellar degeneration was less pronounced in the inferior parts of the posterior lobe compared to earlier work (Hulst et al., 2015), which could be explained by younger cerebellar participants in the current study, with less severe ataxia scores.
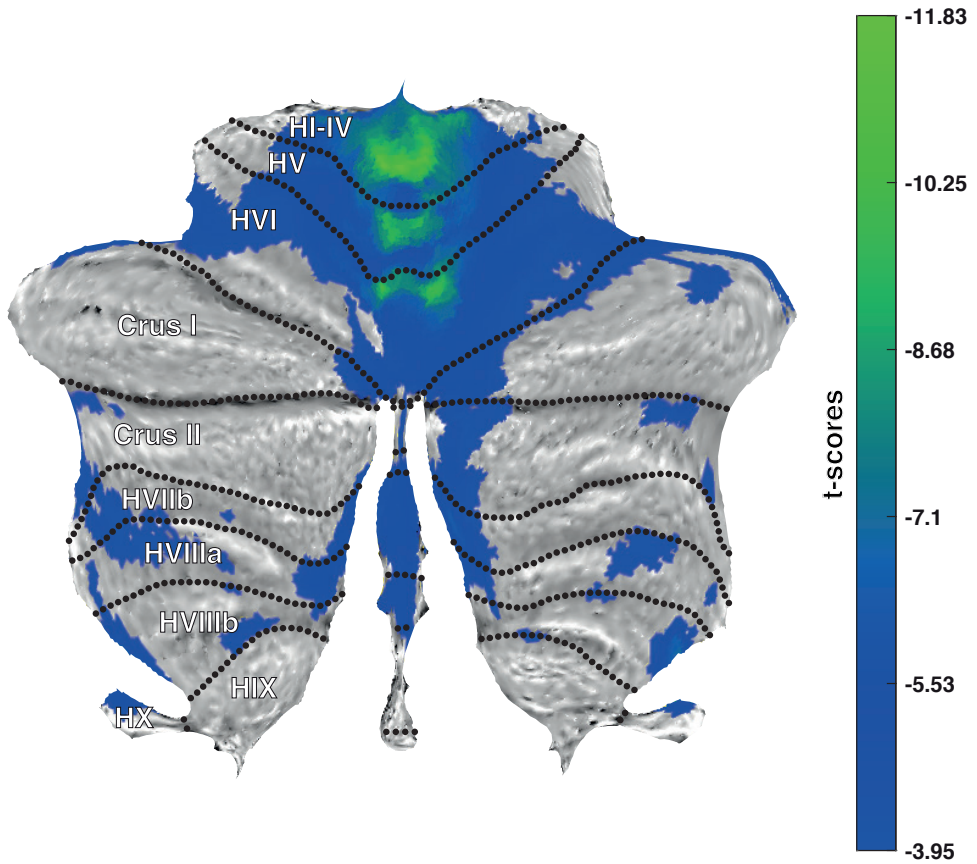
Figure 4. Flatmap of the cerebellum. Colors indicate the gray matter volume difference per voxel between healthy participants and cerebellar participants in t-scores. Voxels that do not exceed the threshold (-3.95) are not colored, low significant t-scores are colored blue, and high significant t-scores are colored green. Flatmap template from Diedrichsen and Zotow, 2015.

Average reaching directions

Next, the reaching directions were analyzed. The average reaching directions for each paradigm in control participants and cerebellar participants are plotted in **Figure 5**.
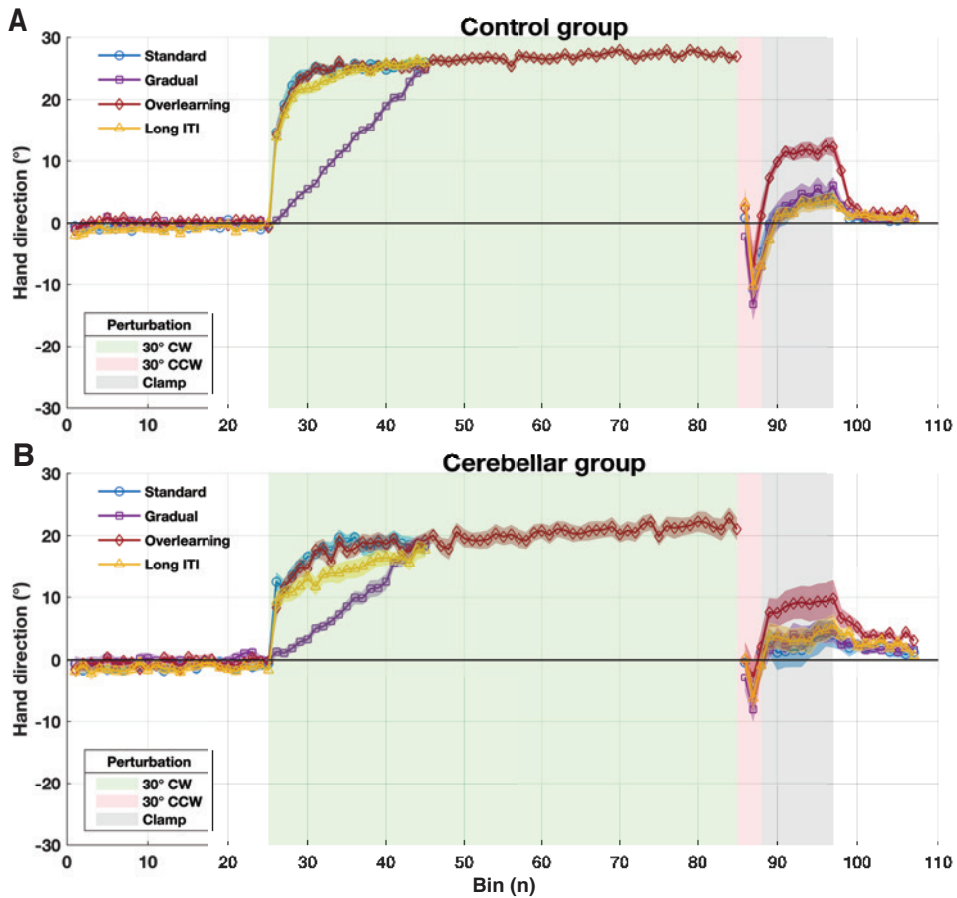
Figure 5. Reaching directions of control participants and cerebellar participants, averaged over bins. A) Control participants. B) Cerebellar participants. Trials were binned per 6 trials. Shaded error bars are mean ± SEM.

As expected, reaching directions of controls participants and cerebellar participants are almost completely straight during the baseline set in all training paradigms. When movements are perturbed by a visuomotor rotation, control participants learn the perturbation quickly, almost completely counteracting the rotation early in the adaptation set (barring the gradual paradigm). Cerebellar participants adapt much more slowly, counteracting about half of the rotation compared to healthy controls during the early phases of learning in the standard and overlearning paradigm. Furthermore, the long intertrial interval condition appears to be lagging behind in the amount of early learning compared with the standard and overlearning conditions.

Late in the adaptation set, control participants reach very similar reaching directions in all paradigms. Control participants learn only slightly more after plateauing early in the adaptation set, apart from the obvious difference in the gradual learning condition. Cerebellar participants, on the other hand, learn more after initial adaptation, albeit slowly, which is especially evident in the overlearning paradigm. In general, control participants counteract more of the perturbation both early and late in the adaptation set than cerebellar participants.

After twelve counterperturbation trials, both control participants and cerebellar participants exhibit spontaneous recovery in clamp trials immediately following the counterperturbation trials. That is, control participants and cerebellar participants move in the direction of what was previously learned in the absence of a perturbation. The amount of spontaneous recovery is largest in the overlearning paradigm in both groups. While cerebellar participants exhibit higher spontaneous recovery in the overlearning paradigm, the amount of spontaneous recovery is lower than in control participants.

Figure 6 displays individual and mean hand directions as in **Figure 5** but averaged over phases instead of bins. The baseline phase is the average movement direction of all trials in the baseline set, while the early adaptation phase is averaged over the first 30 trials (or 6 bins) of the adaptation set. Late adaptation is averaged over the last 6 trials (last bin) of the adaptation set and the recovery phase is averaged over the clamp trials in the washout set (60 trials or 10 bins). **Figure 6** corroborates the main observations of **Figure 5**. The differences in mean reaching directions per phase were tested using the mixed-design model described in the methods section. The most important findings are briefly evaluated below.

Firstly, we tested for differences between the standard, gradual, overlearning and long ITI paradigm in each phase in control participants (**Figure 7**). The MCMC procedure gives us a posterior distribution of credible parameter values, given the data. The parameter of interest in this case was the difference in reaching direction between the standard paradigm and other paradigms. The 95% highest density interval (HDI) contains 95% of the mass of credible parameter values, where each value within the HDI has a higher probability density than any value outside the HDI. When the HDI falls completely within the Region of Practical Equivalence (ROPE), we accept the null value of the parameter and when the HDI falls completely outside the ROPE, we reject the null value of the parameter. The ROPE was set at $[-3.5°; 3.5°]$. In the baseline phase of control participants, the gradual, overlearning and long ITI paradigms can be regarded as practically equivalent to the standard paradigm, with all credible values of the difference falling within the ROPE. During early learning, the gradual paradigm is obviously different from the standard paradigm, while the overlearning paradigm is practically equivalent. The long ITI paradigm cannot be regarded as equivalent
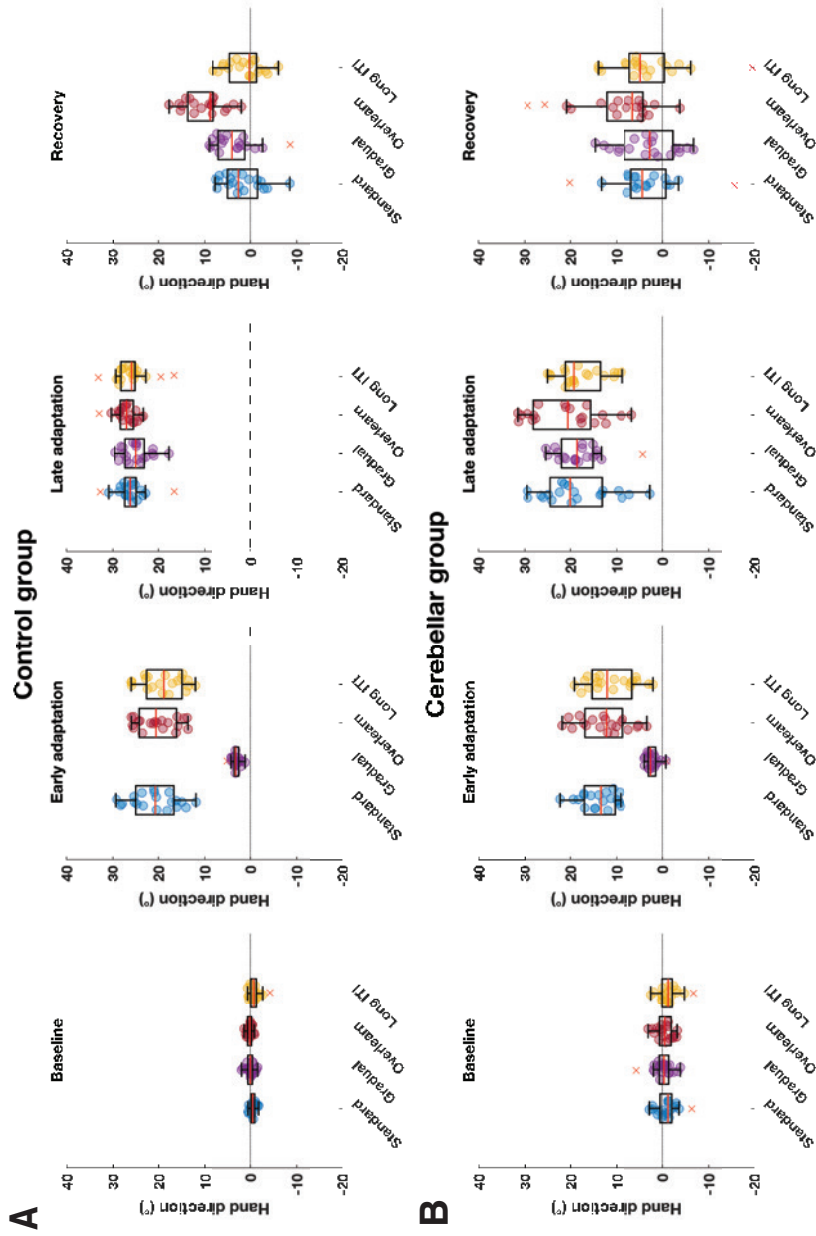
Figure 6. Boxplots of the reaching directions of control participants and cerebellar participants averaged over phases. A) Control participants. B) Cerebellar participants. The baseline phase includes all trials in the baseline set. Early adaptation includes the first 30 trials (6 bins) of the adaptation set, while late adaptation is averaged over the last 6 trials (final bin) of the adaptation set. Recovery includes all clamp trials (60 trials) in the washout set. Individual mean reaching directions are indicated with a colored circle. Individual reaching directions more than 1.5 times the interquartile range removed from the first or third quartile are indicated with a red cross.

or different from the standard paradigm during early adaptation. Late in learning, both the overlearning and long ITI paradigm are practically equivalent to the standard paradigm, while the HDI of the gradual paradigm falls just outside the ROPE. In the recovery phase, spontaneous recovery is higher in the overlearning paradigm compared to the standard paradigm, while the gradual and long ITI paradigm are practically equivalent.
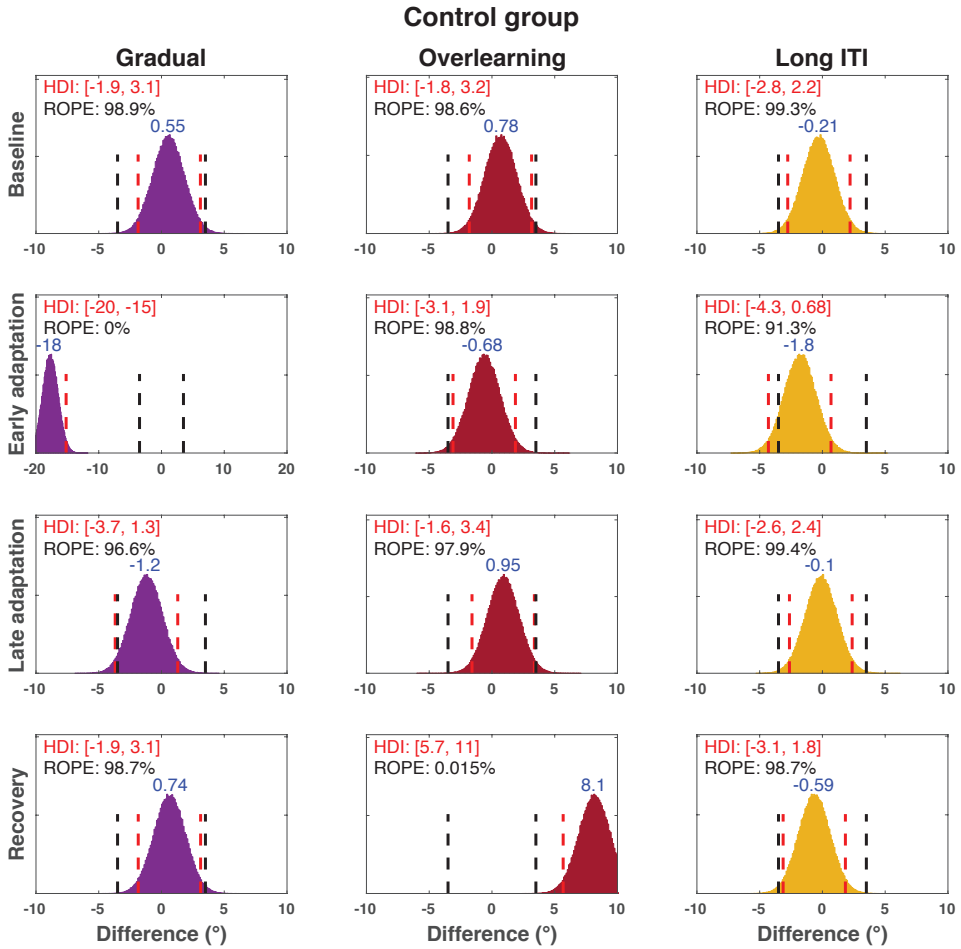

Figure 7. Posterior distributions of the difference between the standard paradigm and other paradigms in control participants. The HDI is given in red text and red bars, the ROPE in black bars, and the percentage of the HDI within the ROPE in black text. The mode of the posterior distribution is given by blue text centered around the mode.

Secondly, we tested for differences between paradigms in the cerebellar group (**Figure 8**). In the cerebellar group, similar differences and equivalencies between paradigms were established. That is, the baseline paradigms are practically equivalent, while the gradual paradigm is obviously different from the standard paradigm during the early adaptation phase. The overlearning and long ITI paradigm HDI's fall just outside the ROPE during early learning, failing to establish equivalency. Late in adaptation, the gradual paradigm and long ITI paradigm are practically equivalent to the standard learning paradigm, while no decision criterion is met for the overlearning paradigm late in adaptation. Spontaneous recovery in the gradual paradigm and long ITI paradigm is practically equivalent to the standard paradigm. Credible values for the overlearning paradigm are higher than the standard paradigm, but the HDI and ROPE overlap slightly (5.46% of credible values fall within the ROPE). In other words, while the credible values for our parameter of interest are highly suggestive for a difference between the standard paradigm and overlearning paradigm in the recovery phase in cerebellar participants, the null value cannot be fully rejected given a ROPE of [−3.5°; 3.5°].

Finally, we tested for differences between control participants and cerebellar participants (**Figure 9**). The baseline phase is practically equivalent for all paradigms between control participants and cerebellar participants. Early learning is much higher in control participants in all paradigms except the gradual paradigm, for which no decision criterion is met. The late adaptation phase is suggestive of more learning in control participants, but all HDI's overlap the ROPE. The recovery phase is suggestive of similar spontaneous recovery between control participants and cerebellar participants, but too much of the HDI falls outside the ROPE in all paradigms to establish equivalency.

To sum up, behaviorally, the most salient difference in control participants exists between the amount of spontaneous recovery in the standard paradigm versus the overlearning paradigm, i.e. there is more spontaneous recovery after overlearning than standard learning. Similarly, the difference between the overlearning paradigm and the standard paradigm in cerebellar participants is highly suggestive for more spontaneous recovery after overlearning as well, though the difference is smaller than in control participants. We hypothesized that the additional amount of spontaneous recovery in both groups could either be due to prolonged activation of the slow learning system, thereby increasing buildup of the slow state, or due to changes in the learning and retention parameters themselves. These hypotheses will be explored in the next section.
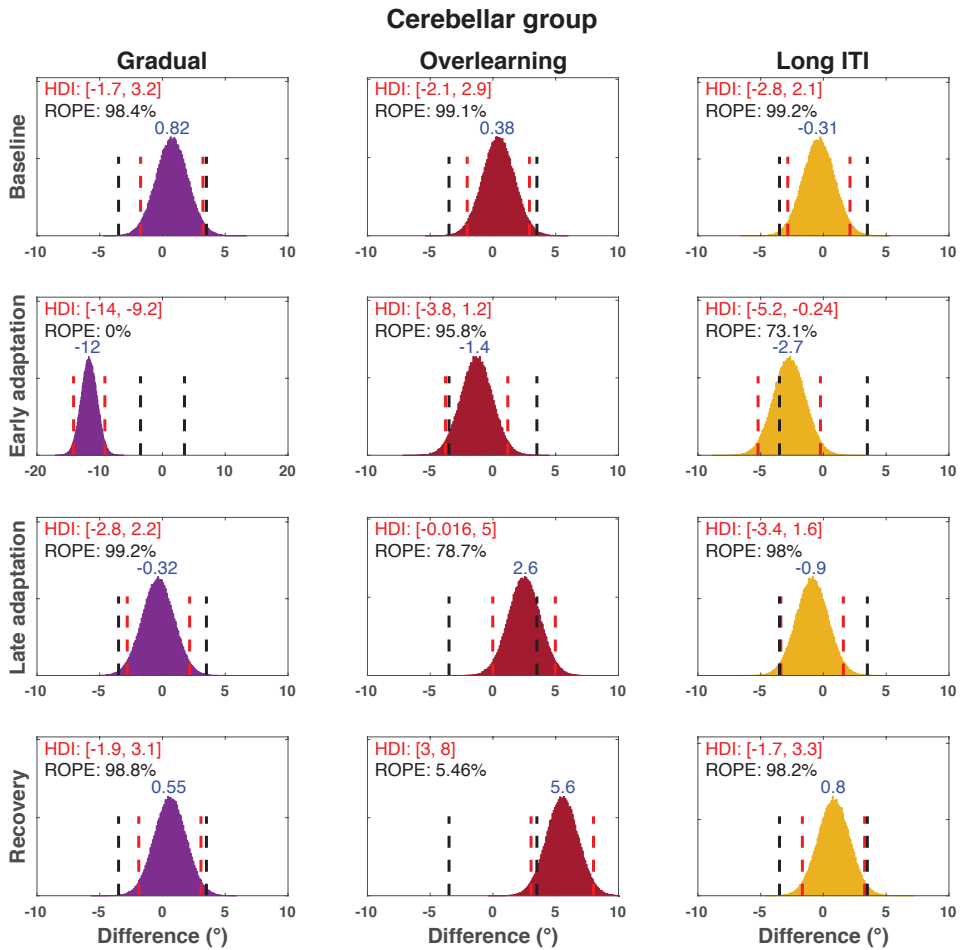
Figure 8. Posterior distributions of the difference between the standard paradigm and other paradigms in cerebellar participants. The HDI is given in red text and red bars, the ROPE in black bars, and the percentage of the HDI within the ROPE in black text. The mode of the posterior distribution is given by blue text centered around the mode.
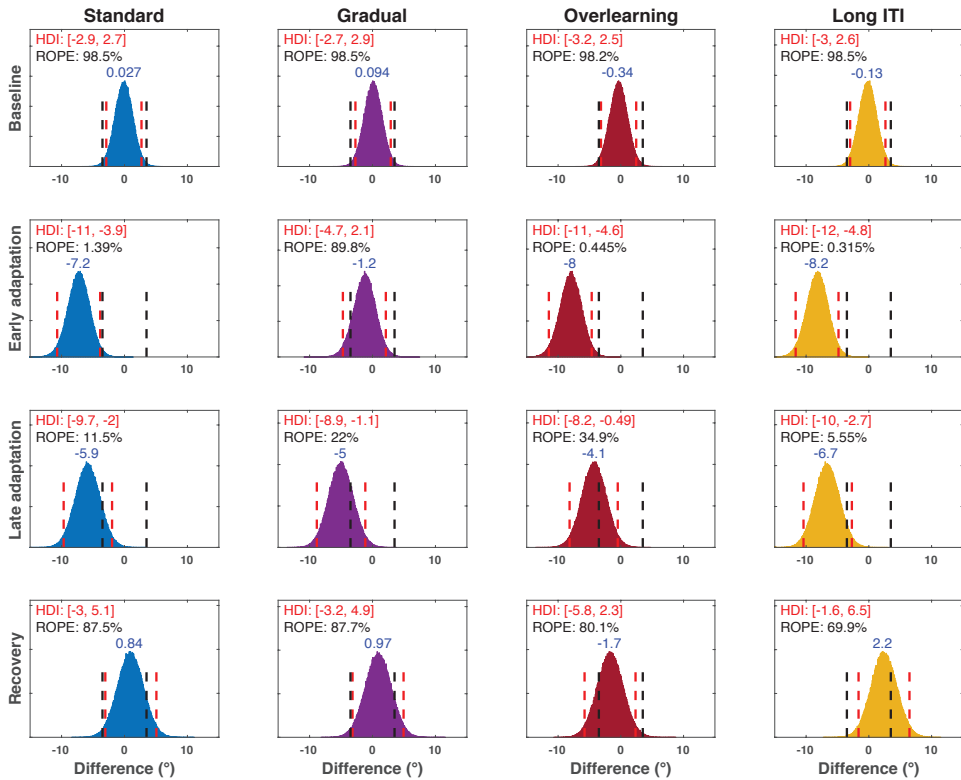
Figure 9. Posterior distributions of the difference between control participants and cerebellar participants (cerebellar participants – control participants). The HDI is given in red text and red bars, the ROPE in black bars, and the percentage of the HDI within the ROPE in black text. The mode of the posterior distribution is given by blue text centered around the mode of the posterior distribution.

Model results

Since behavioral differences between the paradigms were mainly evident in overlearning versus standard learning, the following section focusses on comparing these paradigms. The model results for the other paradigms can be found as supplementary materials (**Supplementary Table 3 and Supplementary Figure 1 - 2**).

To assess whether the estimated learning rate and retention rate of individual participants changed between paradigms, we plotted the credible values of *A* and *B* parameters of each participant in the standard paradigm versus the overlearning paradigm (**Figure 10**).
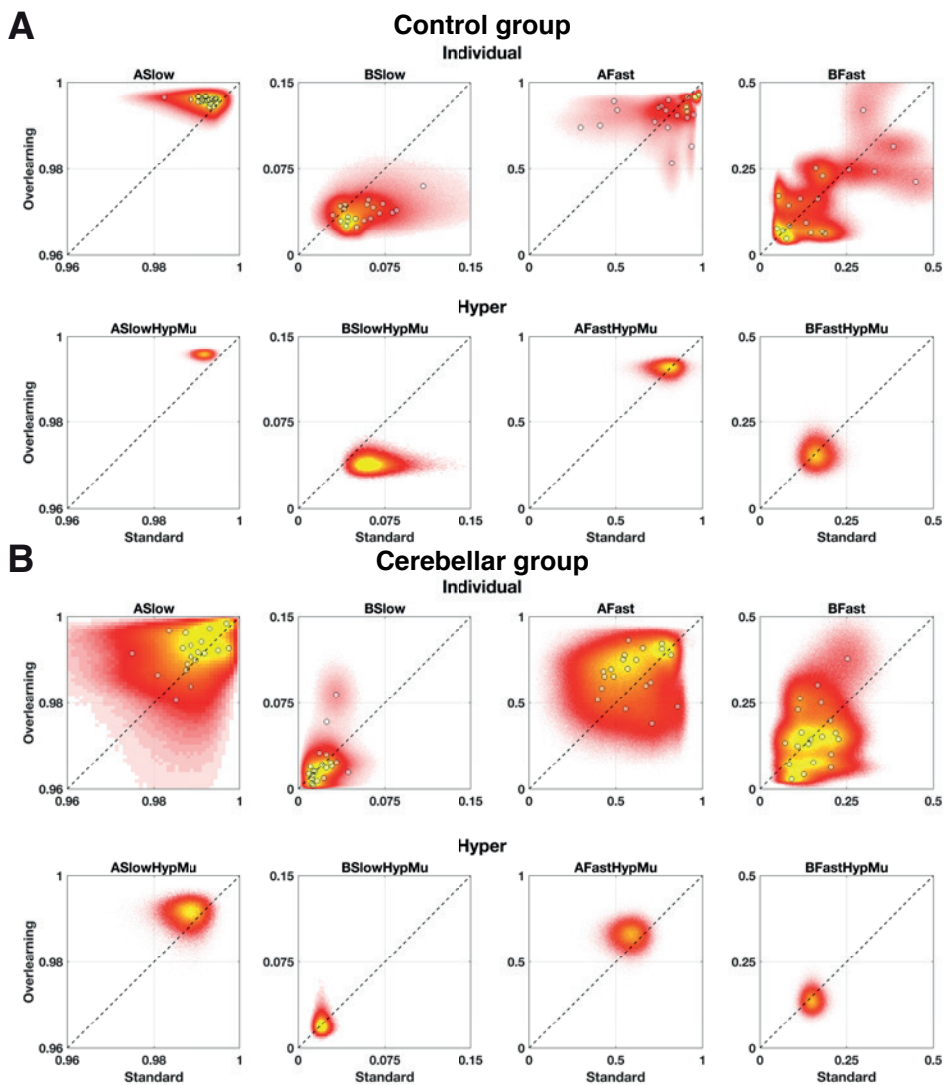
Figure 10. Bivariate histograms of the credible parameter values of individual participants and hyperparameters in the standard versus overlearning paradigm. All samples of the overlearning paradigm (y-axis) were distributed over 500 bins and plotted as a function of the standard paradigm (x-axis). Sample counts range from relatively few samples from the posterior distribution (red) to many samples from the posterior distribution (yellow). The black dashed line indicates equality between paradigms. Circles indicate the modal parameter value of individual participants. A) Control participants B) Cerebellar participants.

Two changes in the parameters between the paradigms were discernable in control participants (**Figure 10A**). Most notably, the retention rate of the slow state (A_{Slow}) was shifted towards higher values in the overlearning paradigm in control participants (i.e. more retention of the slow system). Furthermore, the learning rate of the slow state (B_{Slow}) was shifted towards lower values in the overlearning paradigm in control participants (i.e. slower learning of the slow system). Thus, the slow learning system is less sensitive to error as a result of extended training. The learning and retention rates of the fast system (A_{Fast} and B_{Fast}) appeared equivalent between the paradigms in control participants. The shifts of A_{Slow} and B_{Slow} were also reflected in the posterior distributions of the hyperparameters in control participants (second row, **Figure 10A**).

In patients, changes in parameters between the paradigms were less discernable (**Figure 10B**). Qualitatively, it appears that cerebellar participants have a slightly higher retention rate of the slow system (A_{Slow}) in the overlearning paradigm, like controls participants, but not a lower adaptation rate of the slow system (B_{Slow}). Furthermore, credible values of A_{Fast} appeared to shift towards slightly higher values in the overlearning paradigm. The modal values and HDI's of the hyperparameters of both control participants and cerebellar participants are printed in **Table 2**. Comparing the hyperparameters of control participants to cerebellar participants, we found that the values of A_{Slow}, B_{Slow}, and A_{Fast} are generally higher in control participants in both paradigms, while B_{Fast} is equivalent between participant groups. Bivariate histograms of control participants versus cerebellar participants which further illustrate these observations are found in the supplementary materials (**Supplementary Figure 3**).

Posterior predictive plots

To assess how the differences in the learning and retention rate between training paradigms affect motor output (y_t) and the states (x_t^F and x_t^s), posterior predictive plots were generated from multiple random draws (n = 10.000) of the posterior distributions of each subject (**Figure 11**). The model output ($\hat{y}_t$) generated from the posterior distributions generally fits behavior, with some notable exceptions. We will first discuss how shifts in parameters between paradigms are reflected in the posterior predictive plots. In the next section (*Exploring the lack of fit*), we will assess the ways in which the model output does not fit the behavioral data, since the amount of early learning and spontaneous recovery is generally underestimated, especially in the overlearning paradigm.

In the standard and overlearning paradigm in both groups, the model predicts large amounts of learning early in the adaptation set, driven by a quick rise of the fast state and a gradual rise of the slow state (**Figure 11**). Nearing the end of the adaptation set in both paradigms

and groups, the model output is dominated by the slow state. The fast state quickly unlearns the perturbation during counterperturbation trials in both groups and paradigms, while the slow state is more resistant to the flip in perturbation direction. The recovery phase is dominated by the slow state, but as mentioned above and further explored in the next section, the model generally underestimates the amount of spontaneous recovery.

Table 2. Mode and HDI of credible parameter values in control participants and cerebellar participants.

Control participants				
	Normal		Overlearning	
Parameter	Mode	HDI	Mode	HDI
ASlowHypMu	0.992	0.989 – 0.994	0.996	0.994 – 0.997
BSlowHypMu	0.057	0.040 – 0.103	0.039	0.029 – 0.052
AFastHypMu	0.81	0.664 – 0.903	0.82	0.750 – 0.868
BFastHypMu	0.16	0.113 – 0.221	0.154	0.106 – 0.214
Cerebellar participants				
	Normal		Overlearning	
Parameters	Mode	HDI	Mode	HDI
ASlowHypMu	0.988	0.982 – 0.994	0.992	0.986 – 0.995
BSlowHypMu	0.02	0.013 – 0.029	0.021	0.009 – 0.040
AFastHypMu	0.588	0.454 – 0.695	0.669	0.550 – 0.757
BFastHypMu	0.15	0.115 – 0.188	0.134	0.094 – 0.185

HDI is the 95% highest density interval. Parameter names correspond with nodes in JAGS model code.

In control participants, the slow state reaches similar levels of adaptation in both paradigms, about 21.1 degrees and 23.5 degrees for standard learning and overlearning respectively (**Figure 11A**). In the recovery phase of the standard paradigm the slow state is reduced to approximately 1.7 degrees, while the slow state in the overlearning paradigm retains approximately 7.8 degrees of what was learned. Thus, the difference between the slow state late in adaptation and the recovery phase is much larger in the standard paradigm than the overlearning paradigm (19.4 degrees versus 15.6 degrees respectively). This indicates that, in control participants, additional buildup of the slow state over the longer adaptation set is not the driving force behind additional spontaneous recovery as hypothesized, rather the motor memory has become more resilient, possibly due to the changes in the underlying parameters between paradigms.
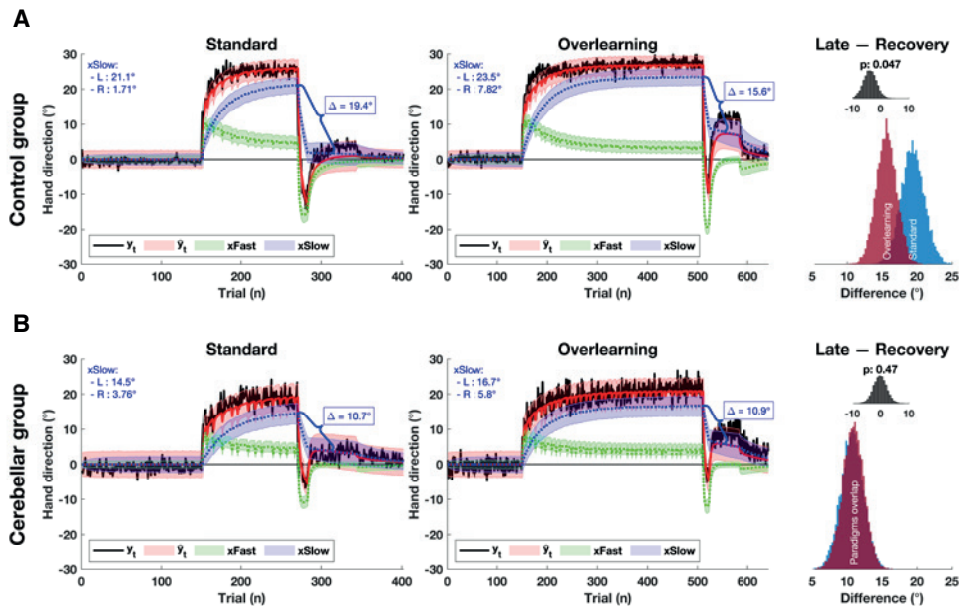
Figure 11. Posterior predictive plots of standard and overlearning paradigm. A) Control subjects. B) Cerebellar subjects. In the left and middle panels, the average behavior (y_t) is displayed with a solid black line for the standard paradigm an overlearning paradigm respectively. The average model output ($\hat{y}_t$) is displayed with a solid red line, the average fast state (x_t^F) with a dotted green line, and the average slow state (x_t^S) with a dotted blue line. The shaded errorbars indicate the variability around the average posterior predictive (2.5th percentile – 97.5th percentile of simulated data). In the top left corner of the left and middle panels, the average value of the slow state late in adaptation (L: the last 6 trials of the adaptation set) and the recovery phase (R: all 60 clamp trials in the washout set) is printed. Δ indicates the difference between the average slow state late in adaptation and the recovery phase (L - R). The distribution of Δ for all 10.000 draws is plotted in the rightmost panel. The blue histogram indicates Δ for the standard paradigm, while the red histogram indicates Δ for the overlearning paradigm. The inset histogram is the distribution of differences between Δ of the standard and overlearning paradigm (overlearning - standard) and displays the proportion (p) of draws with a difference larger than 0.

Contrastingly, in cerebellar participants, the difference between the slow state at the end of adaptation and the recovery phase is practically equivalent between the standard and overlearning paradigm, 10.7 degrees versus 10.9 degrees respectively (**Figure 11B**). Thus, while behaviorally there is more spontaneous recovery in the overlearning paradigm in cerebellar participants, this can largely be attributed by extended buildup of the slow state.

By generating posterior predictive plots from the learning and retention parameters of the standard paradigm applied to the experimental structure of the overlearning paradigm (and vice versa), we could assess how much of the amount of slow learning in the recovery phase was explained by differences in parameters between the paradigms (**Figure 12**).
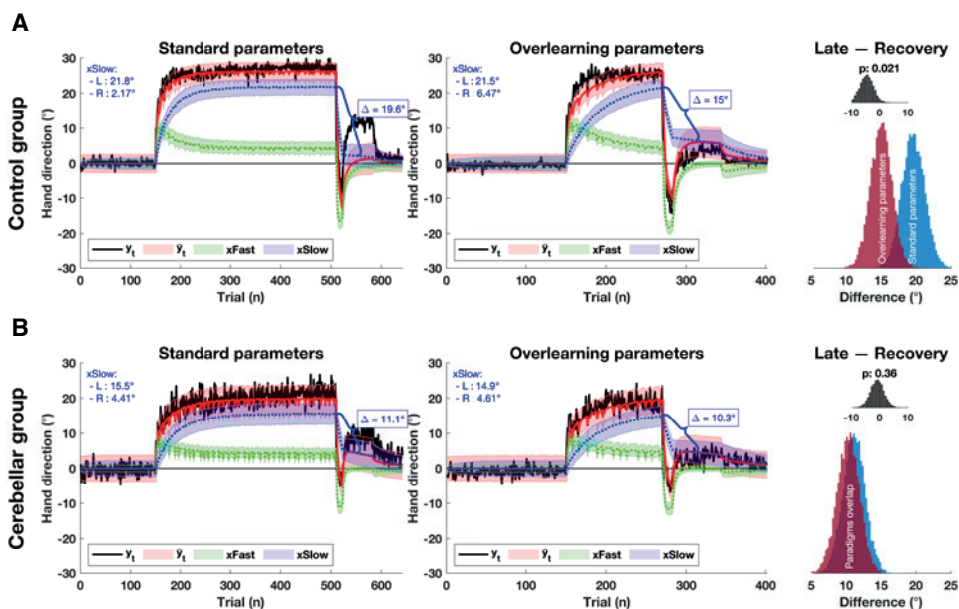
Figure 12. Posterior predictive plots of the standard and overlearning paradigm generated from parameter sets of the other paradigm. A) Control subjects. B) Cerebellar subjects. In the left and middle panels, the average behavior (y_t) is displayed with a solid black line for the overlearning and standard paradigm respectively. The average model output ($\hat{y}_t$) is displayed with a solid red line, the average fast state (x_t^F) with a dotted green line, and the average slow state (x_t^S) with a dotted blue line. The shaded errorbars indicate the variability around the average posterior predictive (2.5th percentile – 97.5th percentile of simulated data). In the top left corner of the left and middle panels, the average value of the slow state late in adaptation (L: the last 6 trials of the adaptation set) and the recovery phase (R: all 60 clamp trials in the washout set) is printed. Δ indicates the difference between the average slow state late in adaptation and the recovery phase (L - R). The distribution of Δ for all 10.000 draws is plotted in the rightmost panel. The blue histogram indicates Δ for standard parameters in the overlearning structure, while the red histogram indicates Δ for overlearning parameters in the standard structure. The inset histogram is the distribution of differences between Δ of the standard parameters and overlearning parameters (overlearning - standard) and displays the proportion (p) of draws with a difference larger than 0.

Notably, using incongruent parameter sets, the slow state reaches similar levels at the end of adaptation in the standard and overlearning experimental structure, both in control participants (**Figure 12A**) and cerebellar participants (**Figure 12B**). However, motor memory is only more resilient in the experimental structure with overlearning parameters in control participants, but not in cerebellar participants. This observation further establishes the idea that a shift in model rates between paradigms is what drives most of the additional spontaneous recovery during overlearning, and that cerebellar participants have reduced motor memory resilience since their parameters change less as a function of overlearning.

Finally, we wanted to assess whether the additional memory resilience after overlearning in control participants was driven largely by the changes in the retention parameter of the slow system (A_{Slow}) or by changes in the learning parameter of the slow system (B_{Slow}). Therefore, posterior predictive plots were generated from the original posterior distributions, but either A_{Slow} or B_{Slow} was drawn from the posterior distribution of the other paradigm (**Figure 13**). Posterior predictive plots are only shown for control participants, plots for cerebellar participants can be found in the supplementary materials (**Supplementary Figure 4**).
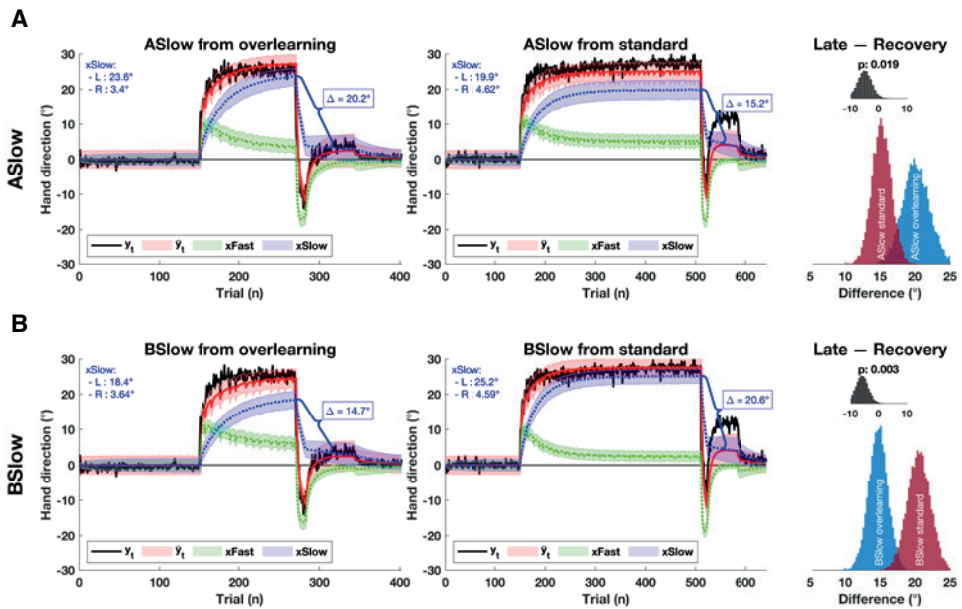

Figure 13. Posterior predictive plots of the standard and overlearning paradigm, but with ASlow or BSlow from the other paradigm. Only the posterior predictive plots of control subjects are shown. A) ASlow drawn from the other paradigm. B) BSlow drawn from the other paradigm. In the left and middle panels, the average behavior (y_t) is displayed with a solid black line for the standard paradigm an overlearning paradigm respectively. The average model output ($\hat{y}_t$) is displayed with a solid red line, the average fast state (x_t^F) with a dotted green line, and the average slow state (x_t^S) with a dotted blue line. The shaded errorbars indicate the variability around the average posterior predictive (2.5th percentile – 97.5th percentile of simulated data). In the top left corner of the left and middle panels, the average value of the slow state late in adaptation (L: the last 6 trials of the adaptation set) and the recovery phase (R: all 60 clamp trials in the washout set) is printed. Δ indicates the difference between the average slow state late in adaptation and the recovery phase (L - R). The distribution of Δ for all 10.000 draws is plotted in the rightmost panel. The blue histogram indicates Δ for the standard paradigm with one parameter from overlearning, while the red histogram indicates Δ for the overlearning paradigm with one parameter from standard learning. The inset histogram is the distribution of differences between Δ of the standard and overlearning paradigm. The paradigm with the larger amount of spontaneous recovery was subtracted from the smaller amount. The proportion (p) of draws with a difference larger than 0 is printed on top.

For the posterior predictive plots with A_{Slow} drawn from the other paradigm, the general pattern of learning and retention is similar to the original posterior predictive plots (**Figure 11A**). There is slightly more buildup of the slow state during adaptation in the standard paradigm with A_{Slow} drawn from the overlearning posterior (cf. **Figure 11A**), which suggests that A_{Slow} determines the extent of the slow state at the end of learning. However, the motor memory is still less resilient than the overlearning paradigm, given the relatively large difference between the slow state late in adaptation and the recovery phase (20.2 degrees, **Figure 13A**). In the overlearning paradigm, with A_{Slow} drawn from the standard posterior, we see slightly less buildup of the slow state during adaptation (cf. **Figure 11A**), but the motor memory remains relatively resilient (a difference of 15.2 degrees between late adaptation and the recovery phase, **Figure 13A**).

However, when B_{Slow} is drawn from the posterior of the other paradigm, we see a complete reversal of the pattern of memory resilience (**Figure 13B**). Now, the paradigm with the most resilient motor memory is the standard paradigm, instead of the overlearning paradigm. During the overlearning paradigm (middle panel, **Figure 13B**), the slow state reaches higher levels during adaptation than the slow state in the original posterior predictive plot of the overlearning paradigm (middle panel, **Figure 11A**). However, the difference of the slow state late in adaptation and the recovery phase is much larger than the posterior predictive with congruent parameters, revealing that motor memory resilience is mainly driven by a reduction in the learning rate of the slow system (B_{Slow}). This also illustrates why cerebellar participants exhibit less spontaneous recovery than control participants. Since B_{Slow} in cerebellar participants remains relatively constant between the standard paradigm and overlearning paradigm (**Figure 10B**), motor memory resilience of cerebellar participants is not increased by overlearning.

Exploring the lack of fit

As briefly alluded to in the prior section, the amount of early learning and spontaneous recovery is underestimated compared to the actual behavioral response, especially in the overlearning paradigm. We hypothesized that this could be due to the fact that the model identifies a fixed set of parameters for all trials, while in reality learning and retention rates change dynamically in response to task demands. As the learning and retention rates are considered fixed in the model, any changes due to developing task demands might be 'averaged out'. That is, because the parameters are considered constant, the model has a hard time accounting for both the large amount of quick early learning in the adaptation set, as well as the increase in memory resilience due to overlearning.

A

Control group

Standard

Overlearning

B

Cerebellar group

Standard

Overlearning
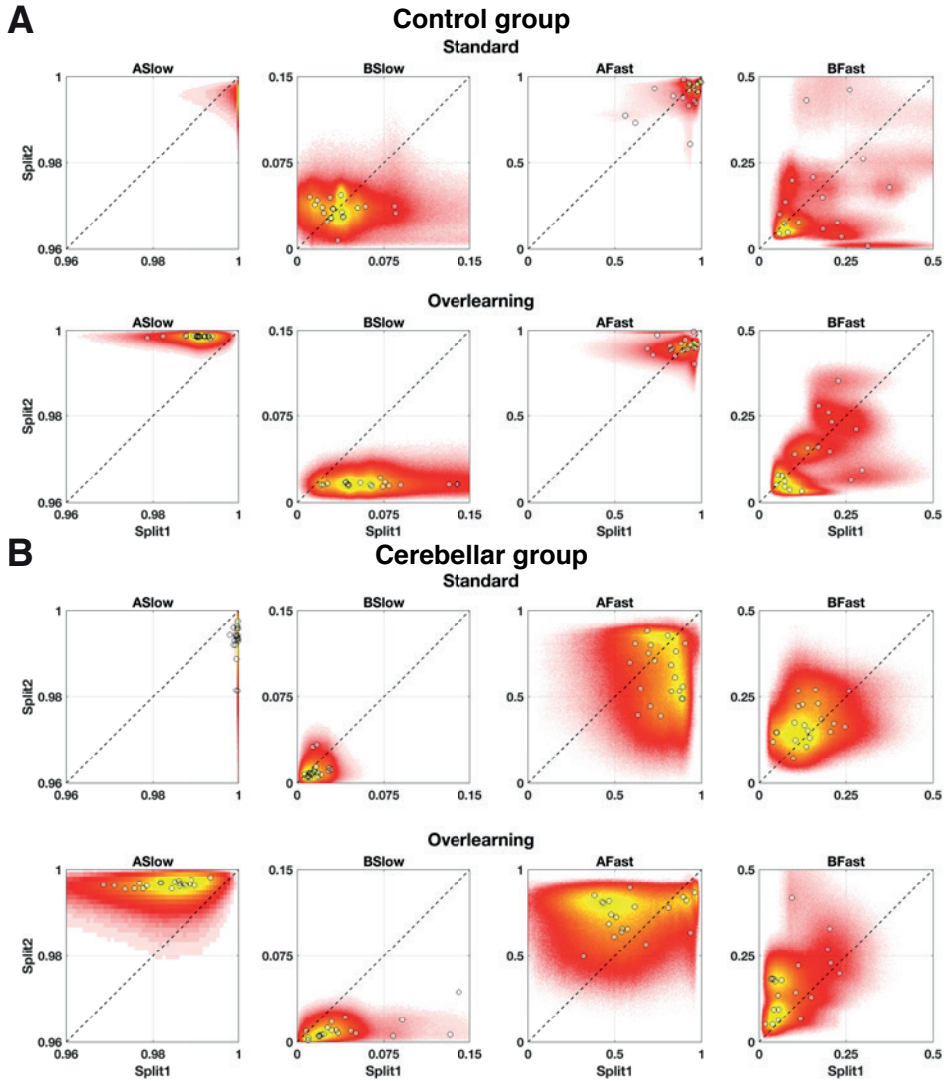
Figure 14. Bivariate histograms of the credible parameter values of individual participants in the first split (Split1) versus the second split (Split 2). A) Control participants. B) Cerebellar participants. Both the standard learning paradigm and overlearning paradigm are pictured. All samples of the second split (y-axis) were distributed over 500 bins and plotted as a function of the first split (x-axis). Sample counts range from relatively few samples from the posterior distribution (red) to many samples from the posterior distribution (yellow). The black dashed line indicates equality between paradigms. Circles indicate the modal parameter value of individual participants.

This hypothesis was explored by splitting the behavioral data in half and performing a model run for each part separately. The first split of behavioral data contained the trials of the baseline set and the early learning of the adaptation set, while the second split consisted of the trials late in adaptation, the counterperturbation trials, the recovery phase, and the washout phase. Thus, practically, an independent set of parameters was identified for each split of a paradigm.

First, we assessed whether the parameters actually changed between the two splits of behavioral data. For this purpose, the learning and retention rate of the first split were plotted versus the rates of the second split (**Figure 14**).

This suggested that the parameters of control participants are relatively stable in the standard learning paradigm, with the exception of A_{Slow}. A_{Slow} is close to 1 during the first split in all participants, likely since adaptation has not plateaued in the early trials of the standard learning paradigm. In contrast, the learning and retention rates of control participants in the overlearning paradigm change quite dramatically between splits. Specifically, the parameters of the slow state (A_{Slow} and B_{Slow}) are shifted in the second half of the paradigm versus the first half. A_{Slow} is generally higher in the second split, while B_{Slow} is generally lower in the second split.

In cerebellar participants, the shifts in parameters between the splits in the standard paradigm are mostly equivalent to control participants, though B_{Slow} also appears to be slightly lower in the second split than the first split in the standard paradigm. In the overlearning paradigm, however, not only are there similar shifts to the parameters of the slow state as seen in control participants (A_{Slow} and B_{Slow}), there is also a shift in the parameters of the fast state between splits. Namely, both A_{Fast} and B_{Fast} are higher in the second split than the first split.

To explore whether 'averaging out' the changes in parameters was actually the reason of the poor fit early in the adaptation set and recovery phase, multiple random draws (n = 10.000) were taken from the posteriors of each participant in both splits of the model data. Then, posterior predictive plots were generated from these draws and fitted to the respective split of behavioral data (**Figure 15**). The earlier observation that motor memory becomes more resilient with overlearning in control participants, but not cerebellar participants, also holds in the split model posterior predictive plots. The additional spontaneous recovery in cerebellar participants is fully explained by additional buildup of the slow state during adaptation, and not increased memory resilience. Importantly, in both paradigms and participant groups, the output of the split models clearly fits the behavioral data better than the unsplit model runs. Both the amount of early learning and the spontaneous recovery

is estimated more accurately in the split model than the unsplit model, further indicating that model parameters change dynamically in response to task demands, rather than being constant across all movements.
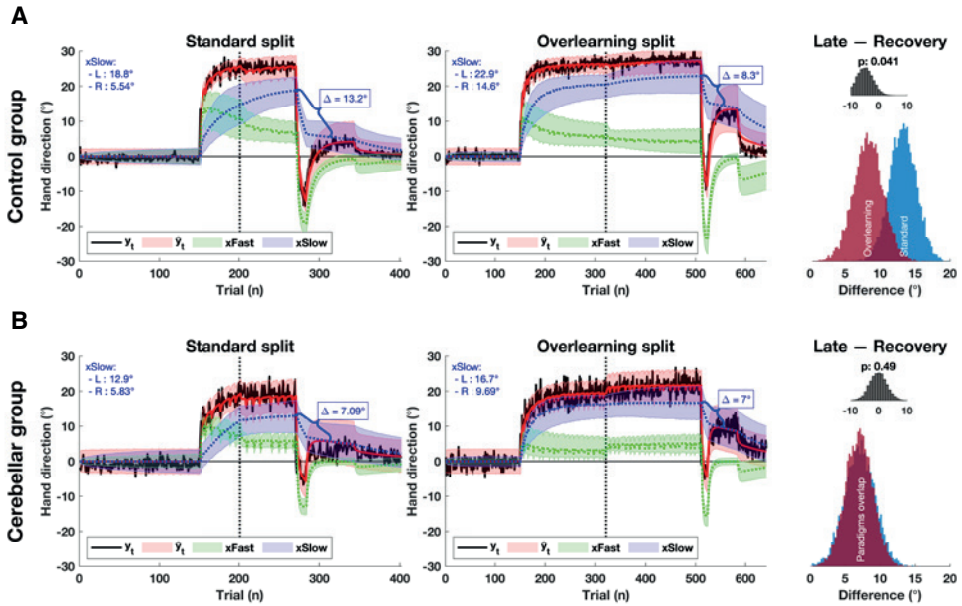
Figure 15. Posterior predictive plots of the standard and overlearning paradigm using split model parameters. A) Control subjects. B) Cerebellar subjects. In the left and middle panels, the average behavior (y_t) is displayed with a solid black line for the overlearning and standard paradigm respectively. The average model output ($\hat{y}_t$) is displayed with a solid red line, the average fast state (x_t^F) with a dotted green line, and the average slow state (x_t^S) with a dotted blue line. The shaded errorbars indicate the variability around the average posterior predictive (2.5th percentile – 97.5th percentile of simulated data). In the top left corner of the left and middle panels, the average value of the slow state late in adaptation (L: the last 6 trials of the adaptation set) and the recovery phase (R: all 60 clamp trials in the washout set) is printed. Δ indicates the difference between the average slow state late in adaptation and the recovery phase (L - R). The distribution of Δ for all 10.000 draws is plotted in the rightmost panel. The blue histogram indicates Δ for the standard paradigm, while the red histogram indicates Δ for the overlearning paradigm. The inset histogram is the distribution of differences between Δ of the standard and overlearning paradigm (overlearning - standard) and displays the proportion (p) of draws with a difference larger than 0.

DISCUSSION

The aim of the present study was to study slow learning processes in more detail, in particular in patients with cerebellar degeneration, and to assess whether paradigms that emphasize slow learning affect behavioral measures of motor learning. Three slow learning paradigms were studied: gradual learning, overlearning and long ITI learning. Our results indicate that, behaviorally, gradual and long ITI learning are practically equivalent to standard learning in healthy controls and cerebellar participants, while the overlearning paradigm resulted in elevated levels of spontaneous recovery in both groups. In other words, both participant groups exhibited a stronger reemergence of learned motor behavior in an error-free environment, which is evidence for enhanced motor memory retention after extended training.

Modelling the behavioral results of the overlearning paradigm suggested that, in control participants, additional spontaneous recovery was the result of higher retention rates of the slow system (A_{Slow}), as well as reduced learning rates of the slow system (B_{Slow}). Thus, overlearning in control participants appeared to induce higher levels of slow learning that was more resilient against washing out. In cerebellar participants however, additional spontaneous recovery appeared to be the result of higher retention rates of the slow system and not reduced learning rates of the slow system. Therefore, increased levels of slow learning in cerebellar participants were less resilient against washing out. In the following paragraphs we will discuss these observations in more detail, the possible implications for cerebellar therapy, but also several limitations of the present study.

What drives memory resilience?

Essentially, in control participants, extended training reduces sensitivity to new movement errors. Error sensitivity depends on several factors, like the size of the movement error (Marko et al., 2012), planning and execution noise (van der Vliet et al., 2018), the history of movement errors (Herzfeld et al., 2014b) and the uncertainty of movement errors (Wei, 2010). We suggest that the reduction in error sensitivity in the overlearning paradigm is the result of reduced state estimation uncertainty (Kording et al., 2007; Wei, 2010). Assuming motor learning is a process of optimally combining feedforward estimates and sensory feedback, the motor learning system should adapt slower to new movement errors given reduced state estimation uncertainty. Thus, after extended training, counterperturbation trials are slower to washout the slow state, resulting in increased levels of spontaneous recovery in control participants.

The reduction in error sensitivity appears to contrast with earlier work, which suggests that error sensitivity increases in response to more consistent error environments (Herzfeld et al., 2014b). Herzfeld et al. found that participants learned more from movement errors when an error environment was likely to persist, while learning from movement errors was suppressed in rapidly switching environments. However, in that study, error sensitivity was measured on a trial-by-trial basis, which likely captured error sensitivity of the fast process to a much greater extent than the slow process. Furthermore, the authors did not consider how extended exposure to a particular environment affected the resilience (or lack of resilience) of that environment. Therefore, our findings are likely congruent with these earlier results, as increasing error sensitivity of the fast process and reducing error sensitivity of the slow process might work in parallel.

Why is motor memory resilience attenuated in cerebellar participants?

Some researchers have suggested that the properties of the fast learning system are associated with the cerebellar cortex, while the properties of the slow system are associated with the deep cerebellar nuclei (DCN) (Antonietti et al., 2017; Casellato et al., 2015; Medina et al., 2001). We observed degeneration of the anterior hand area of the cerebellum in the patient group, predicting a deficit of the fast learning system. This would explain why the cerebellar group was much slower to adapt and did not adapt to the extent of control participants, in line with previous work on visuomotor adaptation in cerebellar patients (Donchin et al., 2012; Rabe et al., 2009). In contrast to control participants, error sensitivity of the slow system was not reduced in cerebellar participants after extended training, which made the slow state less resilient against washing out. Given the hypothesized association between the slow learning system and the DCN, reduced memory resilience could be the result of reduced DCN integrity. The cerebellar group in this study may have been affected by reduced DCN integrity, since structure and function abnormalities of the DCN are common in patients with hereditary cerebellar ataxia (Stefanescu et al., 2015). Interestingly, lesions of the DCN have been linked to impaired long-term recovery and upper limb function after stroke and surgery (Konczak et al., 2005; Küper et al., 2013; Schoch et al., 2006), which we suggest could be due to reduced memory resilience. However, since the DCN were not imaged in this study, we cannot make conclusive statements about the relationship between memory resilience and DCN integrity.

What underlies increased retention rates?

While memory resilience was reduced in cerebellar participants, spontaneous recovery was still amplified after extended training. The modelling results suggest this was due to a shift towards more retention of the slow system (A_{Slow}) and not increased memory resilience.

A similar shift towards higher retention rates of the slow system was also observed in control participants. Since this property of motor learning is still preserved in cerebellar participants, the mechanism underlying increased retention rates could be extra-cerebellar.

A possible candidate for such an extra-cerebellar mechanism is use-dependent plasticity. Use-dependent plasticity is a form of unsupervised learning (Doya, 1999) and considered to be the result of Hebbian changes in the motor cortex (Orban de Xivry et al., 2010). When movements are repeatedly made towards the same area of the workspace, directional movement biases are formed that shape consecutive movements (Diedrichsen et al., 2010; Verstynen and Sabes, 2011). Extended training towards the same target directions can therefore induce stronger movement biases and result in additional spontaneous recovery. In our experiment, targets were spread over a relatively limited area of the workspace (48°), so use-dependent movement biases were likely to build. This has been observed in previous work, where healthy participants that made movements in a limited target spread (90°) showed more spontaneous recovery than when they made the same amount of movements in a full target spread (360°) (McDougle et al., 2015). Thus, we suggest that elevated spontaneous recovery after extended training in healthy subjects is the result of two separate effects: use-dependent learning, resulting in higher retention rates of the slow system, and increased memory resilience, resulting in lower learning rates in the slow system. In contrast, we suggest that the elevated spontaneous recovery in cerebellar patients reflects only one of these effects: use-dependent learning, potentially an extra-cerebellar process.

Could use-dependent plasticity be leveraged for cerebellar therapy?

If use-dependent learning is spared in cerebellar participants, and extended training leads to higher retention of learned motor behavior, could this be leveraged to develop more effective therapy strategies?

Prior work has found that intensive physio- and occupational therapy programs are effective in reducing ataxia symptoms in cerebellar participants (Ilg et al., 2009, 2010; Miyai et al., 2012). These therapy programs were considered intensive, because patients were trained multiple times a week during the intervention period. Interestingly, long-term gains of therapy were correlated with the training intensity after the intervention period, as cerebellar patients that trained more at home retained a larger functional improvement after 1-year follow-up (Ilg et al., 2010). In that sense, continued high intensity therapy is a form of overlearning, since cerebellar patients continue training already learned behavior. The gains after high intensity therapy could therefore be the result of use-dependent learning as

well. It should be noted however that the benefit of use-dependent learning during therapy might be limited by disease progression (Donchin and Timmann, 2019). That is, impaired learning from sensory-prediction errors due to cerebellar degeneration might also disrupt other motor learning mechanisms when cerebellar disease is sufficiently far progressed, as is the case for strategic learning in cerebellar patients (Wong et al., 2018). Thus, while extended training increases short-term retention in cerebellar patients in our experiment, it remains to be seen whether it will also induce long-term therapy gains.

Another possible application of our results in cerebellar therapy is to see whether motor memory resilience can predict response to neurorehabilitation. Although evidence is still limited, there appears to be a link between motor learning deficits and the success of neurorehabilitation (Hatakenaka et al., 2012). Our modeling results suggest that healthy subjects successfully reduce error sensitivity of the slow system while cerebellar patients do not. Thus, reduced memory resilience could be a sign of disease progression and patients with reduced memory resilience might benefit less from extended training than patients with relatively intact memory resilience. As such, motor memory resilience might help in identifying which cerebellar patients will respond best to intensive therapy.

Limitations

In addition to the limitations described in the preceding paragraphs, several other limitations have to be taken into account while interpreting the results of this study. Firstly, the two-state model with fixed learning and retention rates could not account for the full amount of early learning and the extent of spontaneous recovery. Only when two independent models were fit to the early and late phase of the training, allowing the parameters to vary between phases of learning, did the model output accurately match behavior. Others have described rate changes of the two-state model as well, but mainly in the context of faster relearning (Coltman et al., 2019; Mawase et al., 2014; Zarahn et al., 2008). Our results further indicate that model parameters are likely to vary between different phases of motor learning and a model with fixed parameters cannot account for these variations.

Secondly, motor learning during reach adaptation experiments depends on several learning mechanisms (Haith and Krakauer, 2013), including learning from sensory prediction errors (Shadmehr et al., 2010), processes like use-dependent learning (Diedrichsen et al., 2010), reinforcement learning (Galea et al., 2015) and strategic learning (Taylor et al., 2014). We only considered the effects of error-based learning and use-dependent learning on motor behaviors. While our training paradigms were not developed to selectively engage reinforcement learning or strategic learning, a differential effect of these learning mechanisms between paradigms cannot be excluded. Furthermore, we only considered

that error sensitivity of the slow state changed due to reduced state estimation uncertainty, but it could be the result of other factors as well. For instance, planning and execution noise correlate with learning rates (van der Vliet et al., 2018), and the fast system might be temporally labile, while the slow system is temporally stable (Sing et al., 2009).

Finally, though the modelling results of the gradual and long ITI paradigm are not discussed in the present manuscript, the supplementary materials reveal that the learning and retention parameters shift in these paradigms as well. However, since behaviorally the gradual and long ITI paradigms are equivalent to the standard paradigm, it is difficult to infer the exact implications of these parameter shifts in the current study.

CONCLUSIONS

The present study investigated the effect of slow learning paradigms on motor behavior. Of the training paradigms tested, only overlearning elicited higher levels of spontaneous recovery compared to standard learning, which we take as evidence for enhanced motor memory retention after extended training. We suggest that enhanced motor retention was the result of changes to memory resilience and use-dependent plasticity in control participants. Memory resilience in cerebellar participants was diminished, which we suggest could be caused by reduced DCN integrity. To our knowledge, this is the first time this deficit has been described in cerebellar patients. We suggest that cerebellar patients might still benefit from extended training through use-dependent learning, which could explain the efficacy of intensive therapy programs.

Several questions are still unanswered and require follow-up research. Firstly, is there a causal link between reduced DCN integrity and diminished memory resilience? Secondly, is diminished memory resilience an indicator of cerebellar disease progression and could it be used to predict response to therapy? And finally, will overlearning induce long-term therapy gains in cerebellar patients?

Acknowledgements

Author contributions

Thomas Hulst conceived and designed the research; performed experiments; analyzed data; interpreted results; prepared figures; drafted manuscript; edited and revised manuscript; approved the final version of the manuscript.

SUPPLEMENTARY MATERIALS

Supplementary table 1. MCMC diagnostics of the ANOVA-like model. Parameter names correspond with nodes in JAGS model code. Numbers in brackets indicate the levels per effect. For an effect with multiple levels the median ESS, mean R̂ and mean MCSE are given. The interquartile range (Q1 – Q3) of the ESS is given between parentheses.

| Parameter	ESS (Q1 – Q3)		MCSE
Intercept	177,106	<1.0001	<0.0001
Phase [4]	187,582 (164,659 – 193,617)	<1.0001	<0.0001
Paradigm [4]	200,231 (198,480 – 202,158)	<1.0001	<0.0001
Group [2]	186,407	<1.0001	<0.0001
Phase * Paradigm [4,4]	198,787 (196,058 – 200,616)	<1.0001	<0.0001
Phase * Paradigm * Group [4,4,2]	197,905 (171,018 – 200,503)	<1.0001	<0.0001
BetaS [2,20]	147,074 (77,661 – 175,838)	<1.0001	<0.0001
TauY	75,781	<1.0001	<0.0001
TauS [4,2]	16,463 (9,726 – 31,007)	1.0002	0.0001

Supplementary table 2. Parameter names correspond with nodes in JAGS model code. For brevity, the median ESS, mean PSRF and mean MCSE taken over the four different paradigms are displayed. Numbers in brackets indicate the levels per parameter. Note that the model was run separately for each of the paradigms, i.e. the first level relates to the four different model runs. The interquartile range (Q1 – Q3) of the ESS is given between parentheses.

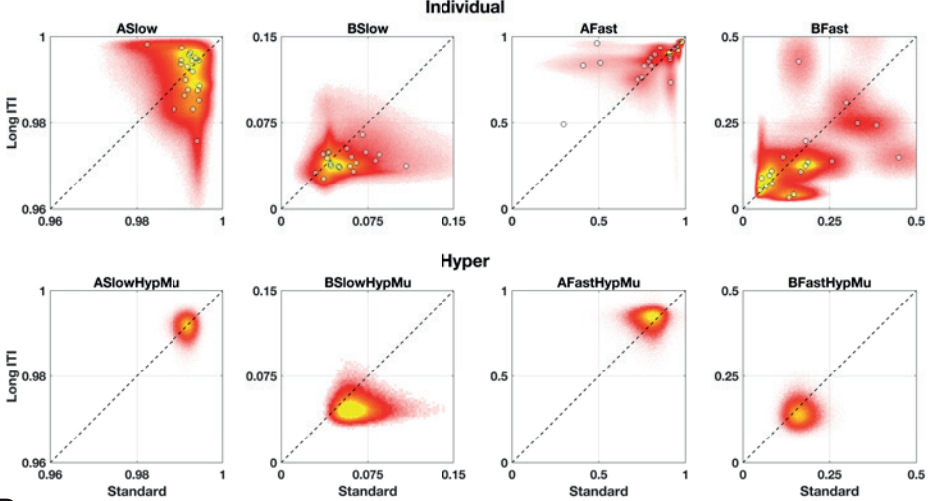| Parameters	Cerebellar participants			Control participants		
	ESS (Q1 – Q3)		MCSE	ESS (Q1 – Q3)		MCSE
ASlowHypMu [4]	4,296 (3,213 – 5,297)	1.0010	<0.0001	2,789 (1,178 – 4,972)	1.0098	0.0003
AFastHypMu [4]	1,149 (829 – 1,487)	1.0017	0.0002	957 (422 – 1,685)	1.0053	0.0006
BFastHypMu [4]	8,581 (6,536 – 12,557)	1.0004	<0.0001	39,094 (11,205 – 74,919)	1.0001	<0.0001
BSlowHypMu [4]	2,231 (1,692 – 2,558)	1.0039	0.0004	1,181 (561 – 1,487)	1.0051	0.0004
ASlowHypPrec [4]	3,490 (2,970 – 4,440)	1.0013	0.0002	3,697 (1,459 – 41,582)	1.0023	0.0005
AFastHypPrec [4]	1,371 (9,49 – 1,484)	1.0008	0.0010	1,266 (709 – 1,764)	1.0028	0.0010
BFastHypPrec [4]	4,750 (2,649 – 7,278)	1.0007	0.0003	19,099 (7,516 – 37,255)	1.0005	<0.0001
BSlowHypPrec [4]	3,911 (2,150 – 5,198)	1.0015	0.0004	2,332 (1,102 – 2,954)	1.0049	0.0023
ASlow [4,20]	7,684 (2,990 – 14,159)	1.0011	<0.0001	6,119 (2,340 – 12,758)	1.0024	<0.0001
AFast [4,20]	1,430 (894 – 2,259)	1.0024	0.0001	803 (386 – 1,249)	1.0055	0.0003
BSlow [4,20]	3,317 (1,365 – 8,521)	1.0018	<0.0001	1,001 (484 – 2,089)	1.0059	<0.0001
BFast [4,20]	2,493 (1,572 – 4,009)	1.0012	<0.0001	2,217 (943 – 4,339)	1.0021	<0.0001
outputPrec [4,20]	12,867 (6,543 – 24,204)	1.0004	0.0001	33,614 (19,436 – 50,775)	1.0003	<0.0001
statePrec [4,20]	1,857 (970 – 2,998)	1.0019	0.0906	2,835 (1,420 – 5,568)	1.0019	0.0818

Supplementary table 3. Mode and HDI of credible parameter values in control participants and cerebellar participants. HDI is the 95% highest density interval. Parameter names correspond with nodes in JAGS model code.

Control participants

Parameter	Standard		Gradual		Overlearning		Long ITI	
	Mode	HDI	Mode	HDI	Mode	HDI	Mode	HDI
ASlowHypMu	0.992	0.989 – 0.994	0.998	0.994 – 1.000	0.996	0.994 – 0.997	0.992	0.988 – 0.995
AFastHypMu	0.810	0.664 – 0.903	0.851	0.783 – 0.894	0.820	0.750 – 0.868	0.848	0.725 – 0.910
BFastHypMu	0.160	0.113 – 0.221	0.187	0.116 – 0.277	0.154	0.106 – 0.214	0.137	0.095 – 0.198
BSlowHypMu	0.057	0.040 – 0.103	0.040	0.028 – 0.068	0.039	0.029 – 0.052	0.042	0.033 – 0.068

Cerebellar participants

Parameters	Standard		Gradual		Overlearning		Long ITI	
	Mode	HDI	Mode	HDI	Mode	HDI	Mode	HDI
ASlowHypMu	0.988	0.982 – 0.994	0.992	0.981 – 0.998	0.992	0.986 – 0.995	0.990	0.982 – 0.995
AFastHypMu	0.588	0.454 – 0.695	0.649	0.532 – 0.734	0.669	0.550 – 0.757	0.633	0.527 – 0.716
BFastHypMu	0.150	0.115 – 0.188	0.172	0.129 – 0.230	0.134	0.094 – 0.185	0.155	0.118 – 0.194
BSlowHypMu	0.020	0.013 – 0.029	0.020	0.009 – 0.030	0.021	0.009 – 0.040	0.010	0.005 – 0.016
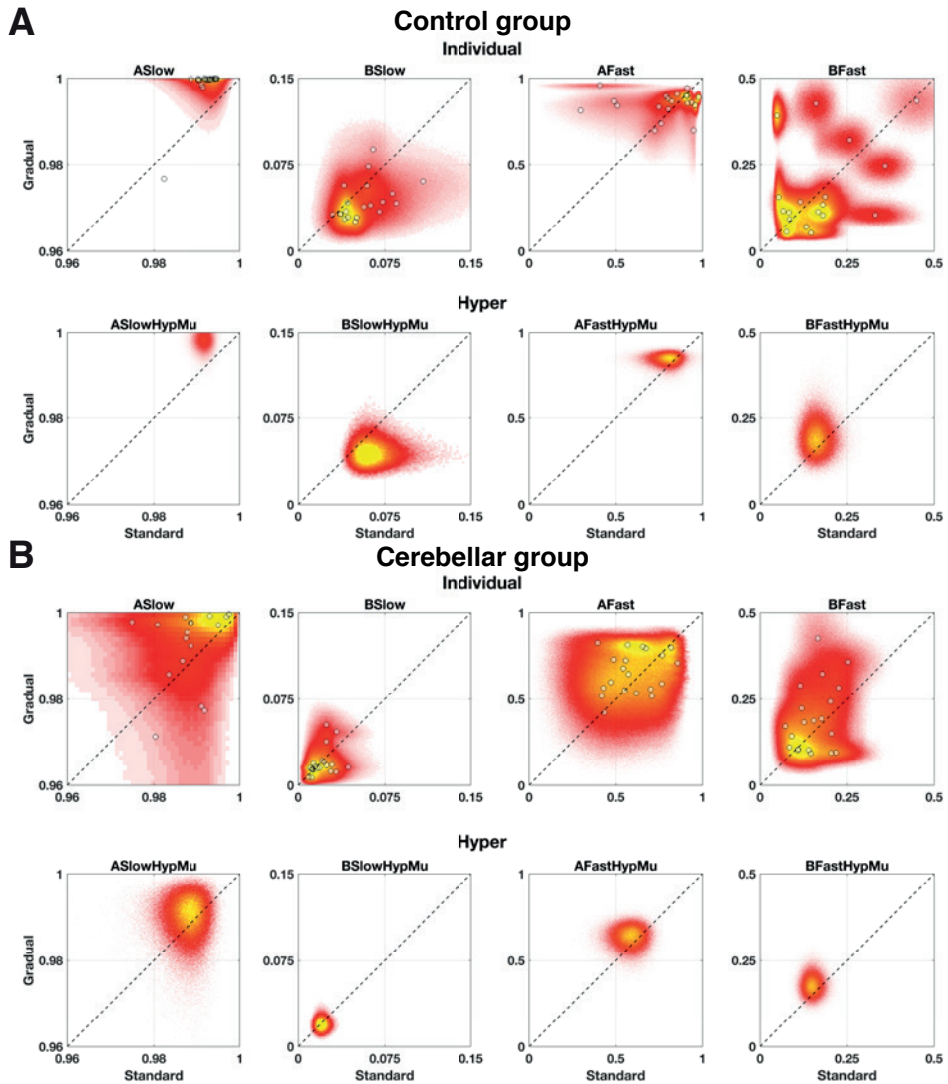
Supplementary figure 1. Bivariate histograms of the credible parameter values of individual participants and hyperparameters in the standard versus gradual paradigm. All samples of the overlearning paradigm (y-axis) were distributed over 500 bins and plotted as a function of the standard paradigm (x-axis). Sample counts range from relatively few samples from the posterior distribution (red) to many samples from the posterior distribution (yellow). The black dashed line indicates equality between paradigms. Circles indicate the modal parameter value of individual participants. A) Control participants B) Cerebellar participants.
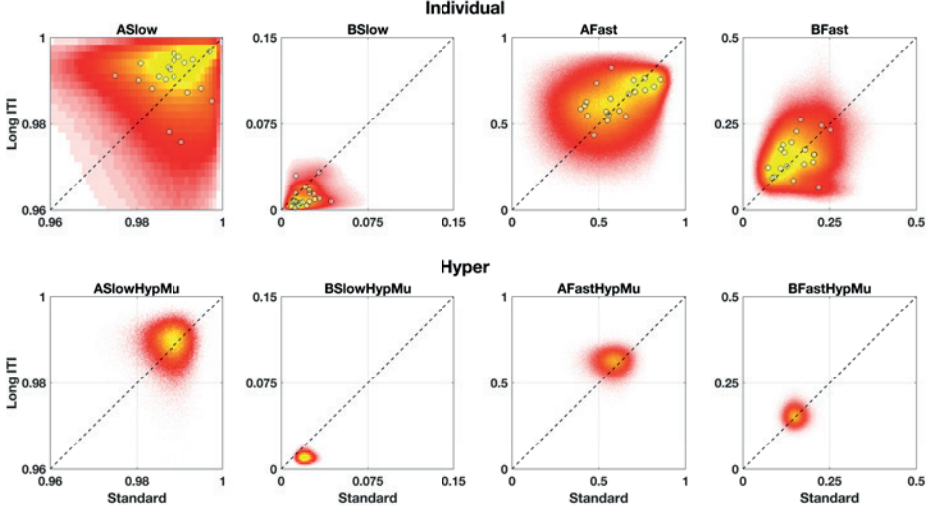
Supplementary figure 2. Bivariate histograms of the credible parameter values of individual participants and hyperparameters in the standard versus long ITI paradigm. All samples of the overlearning paradigm (y-axis) were distributed over 500 bins and plotted as a function of the standard paradigm (x-axis). Sample counts range from relatively few samples from the posterior distribution (red) to many samples from the posterior distribution (yellow). The black dashed line indicates equality between paradigms. Circles indicate the modal parameter value of individual participants. A) Control participants B) Cerebellar participants.
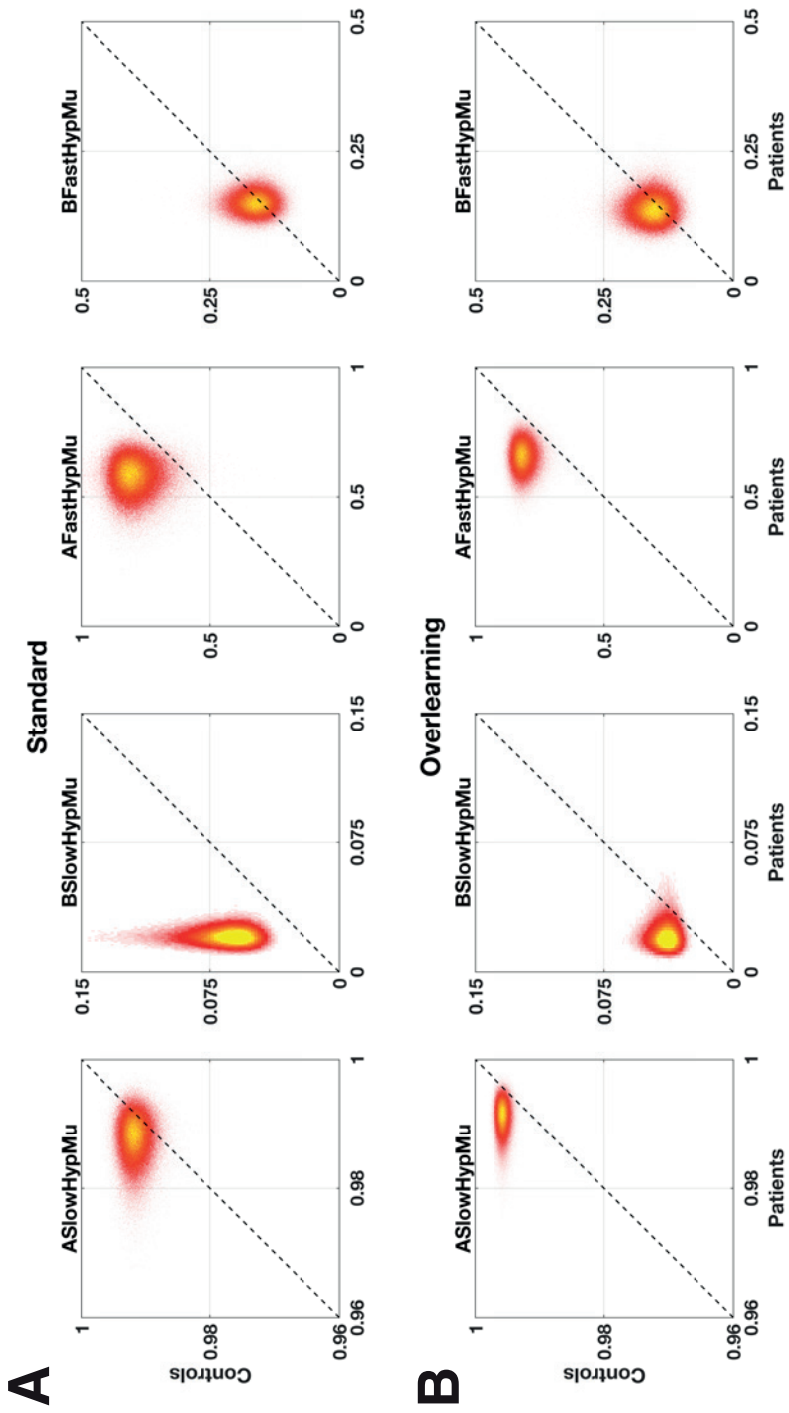
Supplementary figure 3. Bivariate histograms of the credible parameter values of hyperparameters in control participants (y-axis) versus cerebellar participants (x-axis). Sample counts range from relatively few samples from the posterior distribution (red) to many samples from the posterior distribution (yellow). The black dashed line indicates equality between groups. A) Standard paradigm B) Overlearning paradigm.
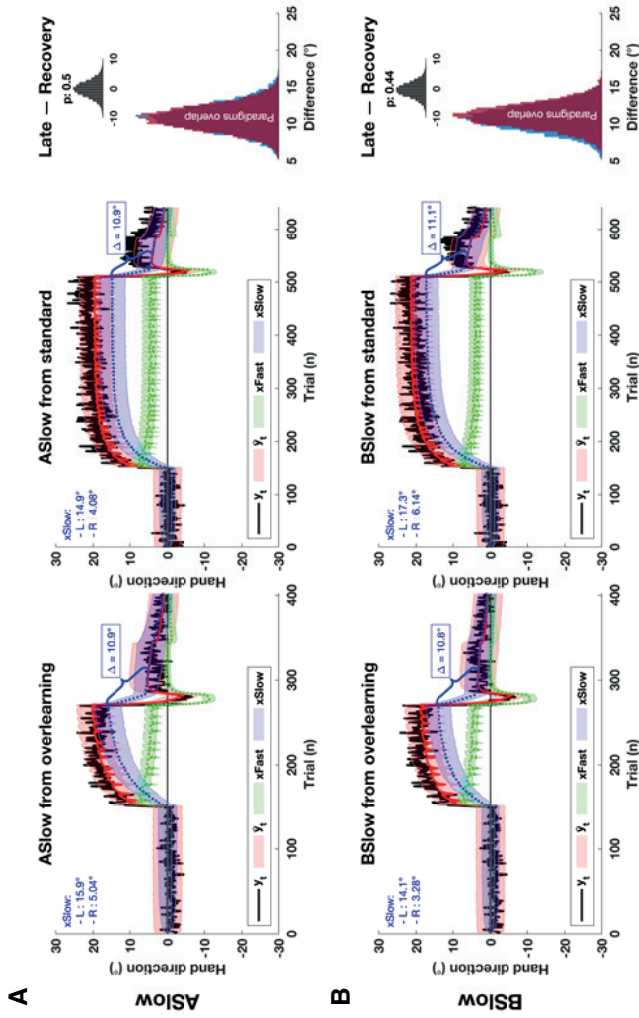
Supplementary figure 4. Posterior predictive plots of the standard and overlearning paradigm. Only the posterior predictive plots of cerebellar participants are shown. A) ASlow drawn from the other paradigm, but with ASlow or BSlow from the other paradigm. B) BSlow drawn from the other paradigm. In the left and middle panels, the average behavior (y_t) is displayed with a solid black line for the standard paradigm an overlearning paradigm respectively. The average model output ($\hat{y}_t$) is displayed with a solid red line, the average fast state (x_t^F) with a dotted green line, and the average slow state (x_t^S) with a dotted blue line. The shaded errorbars indicate the variability around the average posterior predictive (2.5^{th} percentile – 97.5^{th} percentile of simulated data). In the top left corner of the left and middle panels, the average value of the slow state late in adaptation (L: the last 6 trials of the adaptation set) and the recovery phase (R: all 60 clamp trials in the washout set) is printed. Δ indicates the difference between the average slow state late in adaptation and the recovery phase (L - R). The distribution of Δ for all 10.000 draws is plotted in the rightmost panel. The blue histogram indicates Δ for the standard paradigm with one parameter from overlearning, while the red histogram indicates Δ for the overlearning paradigm with one parameter from standard learning. The inset histogram is the distribution of differences between Δ of the standard and overlearning paradigm. The paradigm with the larger amount of spontaneous recovery was subtracted from the smaller amount. The proportion (p) of draws with a difference larger than 0 is printed on top.

Supplementary Data 1

```
1.   model{
2.   # N observations (subjects * withinX1 * withinX2 * betweenX3)
3.   for(i in 1:N){
4.       Y[i] ~ dnorm(muY[i], tauY)
5.       muY[i] <- a0 + a1[X1[i]] + a2[X2[i]] + a3[X3[i]] + a12[X1[i],X2[i]] + a123[X1[i],X2[i],X3[i]] + aS[X
     1[i],X3[i],id[i]]
6.   }
7.   # Convert effects to sum-to-zero, see 20.5.2.2 Kruschke
8.   for (j1 in 1:nX1) {
9.       for (j2 in 1:nX2) {
10.          for (j3 in 1:nX3) {
11.              for (s in 1:nS[j3]) {
12.                  m[j1,j2,j3,s] <- a0 + a1[j1] + a2[j2] + a3[j3] + a12[j1,j2] + a123[j1,j2,j3] + aS[j1,j3,
     s] # cell means
13.              }
14.          }
15.      }
16.  }
17.  # Mean for each subject
18.  for (j3 in 1:nX3) {
19.      for (s in 1:nS[j3]) {
20.          mS[j3,s] <- mean(m[1:nX1, 1:nX2, j3, s])
21.      }
22.  }
23.  # Means for each treatment condition (across subjects)
24.  for (j1 in 1:nX1) {
25.      for (j2 in 1:nX2) {
26.          for (j3 in 1:nX3) {
27.              m123[j1,j2,j3] <- mean(m[j1,j2,j3,id[1:nS[j3]]])
28.          }
29.      }
30.  }
31.  # Mean for between factor (across subjects and within factors)
32.  for (j3 in 1:nX3) {
33.      m3[j3] <- mean(m123[1:nX1,1:nX2,j3])
34.  }
35.  # Mean for within factor 1
36.  for (j1 in 1:nX1) {
37.      m1[j1] <- mean(m123[j1,1:nX2,1:nX3])
38.  }
39.  # Mean for within factor 2
40.  for (j2 in 1:nX2) {
41.      m2[j2] <- mean(m123[1:nX1,j2,1:nX3])
42.  }
43.  # Mean for 2 factor interaction
44.  for (j1 in 1:nX1) {
45.      for (j2 in 1:nX2) {
46.          m12[j1,j2] <- mean(m123[j1,j2,1:nX3])
47.      }
48.  }
49.  mTot = mean(m123[1:nX1,1:nX2,1:nX3])
50.  # Intercept
51.  intercept <- mTot
52.  # Deflection for between factor
53.  for (j3 in 1:nX3) {
54.      group[j3] <- m3[j3] - mTot
55.  }
56.  # Deflection for within factors
57.  for (j2 in 1:nX2) {
58.      paradigm[j2] <- m2[j2] - mTot
59.  }
```
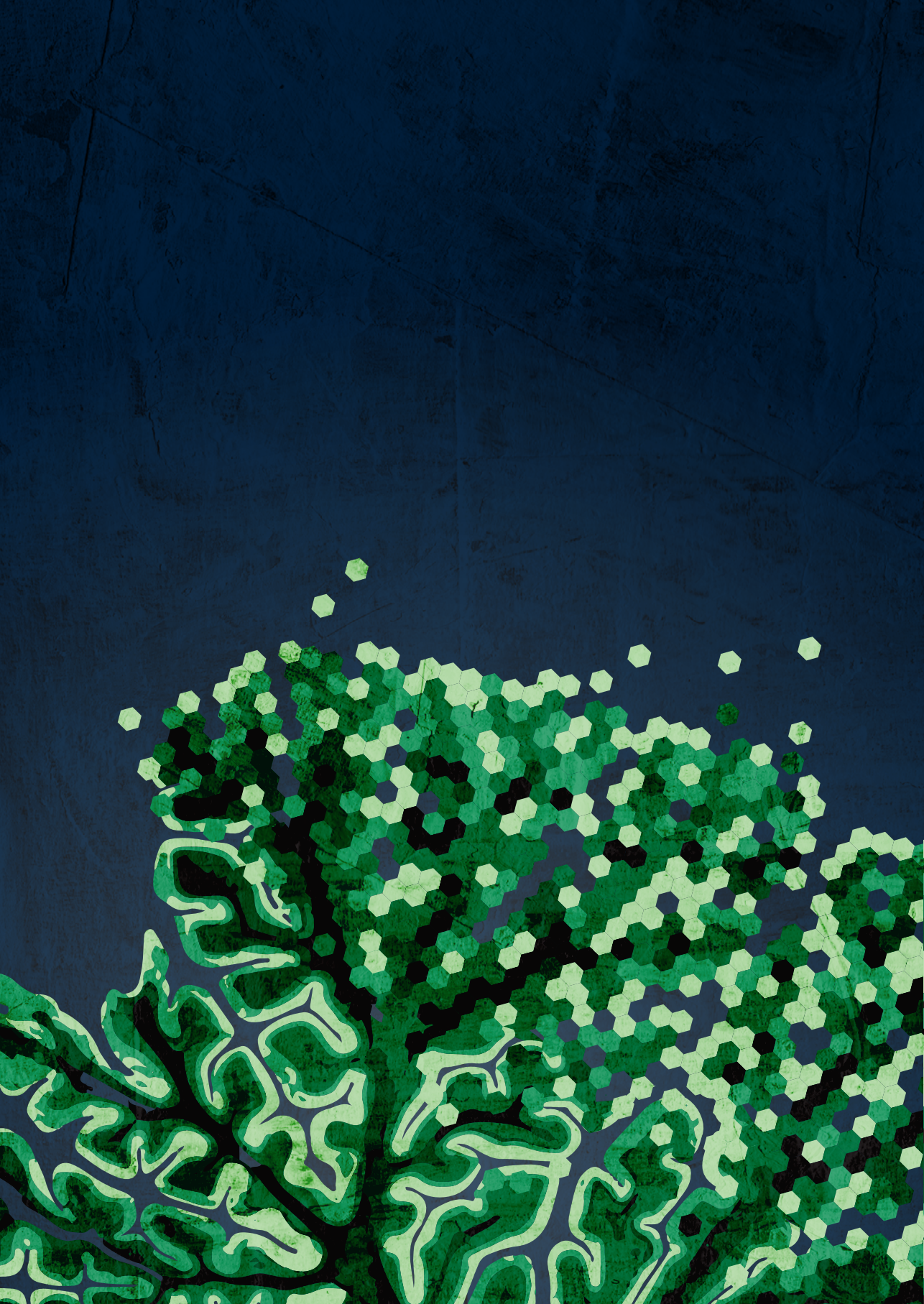
```
60.  for (j1 in 1:nX1) {
61.      phase[j1] <- m1[j1] - mTot
62.  }
63.  # Deflections for interactions
64.  for (j1 in 1:nX1) {
65.      for (j2 in 1:nX2) {
66.          phase_paradigm[j1,j2] <- m12[j1,j2] - (intercept + phase[j1] + paradigm[j2])
67.          for (j3 in 1:nX3) {
68.              phase_paradigm_group[j1,j2,j3] <- m123[j1,j2,j3] - (intercept + phase[1] + paradigm[j2] + ph
     ase_paradigm[j1, j2])
69.          }
70.      }
71.  }
72.  # Deflection for each subject
73.  for (j3 in 1:nX3) {
74.      for (s in 1:nS[j3]) {
75.          betaS[j3,s] <- mS[j3,s] - (intercept + group[j3])
76.      }
77.  }
78.  # Priors
79.  tauY ~ dgamma(0.001, 0.001)
80.  for (j1 in 1:nX1) {
81.      for (j3 in 1:nX3) {
82.      tauS[j1,j3] ~ dt(0, 1/2.5^2,7)T(0,)
83.      }
84.  }
85.
86.  a0 ~ dnorm(0, 10^-6)
87.  for (j1 in 1:nX1) {
88.      a1[j1] ~ dnorm(0, 10^-6)
89.  }
90.  for (j2 in 1:nX2) {
91.      a2[j2] ~ dnorm(0, 10^-6)
92.  }
93.  for (j3 in 1:nX3) {
94.      a3[j3] ~ dnorm(0, 10^-6)
95.  }
96.  for (j1 in 1:nX1) {
97.      for (j2 in 1:nX2) {
98.          a12[j1,j2] ~ dnorm(0, 10^-6)
99.      }
100. }
101. for (j1 in 1:nX1) {
102.     for (j2 in 1:nX2) {
103.         for(j3 in 1:nX3) {
104.             a123[j1,j2,j3] ~ dnorm(0, 10^-6)
105.         }
106.     }
107. }
108. # Random effects
109. for (j1 in 1:nX1) {
110.     for (j3 in 1:nX3) {
111.         for(s in 1:nS[j3]){
112.             aS[j1,j3,s] ~ dnorm(0, tauS[j1,j3])
113.         }
114.     }
115. }
116. }
```

Supplementary Data 2

```
1.   model{
2.       # State space model
3.       for(s in 1:numSubjects) {
4.           for(t in 1:numTrials) {
5.           # Model takes reaching angles (y) to calculate error
6.       error[s,t] <- y[s,t] + pertSize[t]
7.           xFastMu[s,t] <- (AFast[s] * xFast[s,t]) - (BFast[s] * (error[s,t]*clampTrial[t]))
8.           xSlowMu[s,t] <- (ASlow[s] * xSlow[s,t]) - (BSlow[s] * (error[s,t]*clampTrial[t]))
9.           xFast[s,t+1] ~ dnorm(xFastMu[s,t], statePrec[s])
10.          xSlow[s,t+1] ~ dnorm(xSlowMu[s,t], statePrec[s])
11.          x[s,t] <- xFast[s,t] + xSlow[s,t]
12.          y[s,t] ~ dnorm(x[s,t], outputPrec[s])
13.      }
14.
15.      # Probe states of xFast/xSlow at given intervals
16.      for(p in 1:numProbes) {
17.          xFastProbe[s,p] <- mean(xFast[s,xProbes[p,1]:xProbes[p,2]])
18.          xSlowProbe[s,p] <- mean(xSlow[s,xProbes[p,1]:xProbes[p,2]])
19.      }
20.
21.      # Draw A/B
22.      ASlow1[s] ~ dnorm(ASlowHypMu,ASlowHypPrec)
23.      AFast1[s] ~ dnorm(AFastHypMu,AFastHypPrec)T(,ASlow1[s]) # Truncate AFast so it is < ASlow
24.      BFast1[s] ~ dnorm(BFastHypMu,BFastHypPrec)
25.      BSlow1[s] ~ dnorm(BSlowHypMu,BSlowHypPrec)T(,BFast1[s]) # Truncate BSlow so it is < BFast
26.
27.      # From logspace to 0-1
28.      ASlow[s] <- ilogit(ASlow1[s])
29.      AFast[s] <- ilogit(AFast1[s])
30.      BFast[s] <- ilogit(BFast1[s])
31.      BSlow[s] <- ilogit(BSlow1[s])
32.
33.      # Draw noise
34.      statePrec[s] ~ dgamma(1.0E-3,1.0E-3)
35.      outputPrec[s] ~ dgamma(1.0E-3,1.0E-3)
36.
37.      # Initialize t = 1
38.      xFast[s,1] ~ dnorm(0, 1.0E-1)
39.      xSlow[s,1] ~ dnorm(0, 1.0E-1)
40.      }
41.
42.      # Hyperparameters
43.      ASlowHypMu ~ dnorm(0.0, 1.0E-3)
44.      AFastHypMu ~ dnorm(0.0, 1.0E-3)
45.      BFastHypMu ~ dnorm(0.0, 1.0E-3)
46.      BSlowHypMu ~ dnorm(0.0, 1.0E-3)
47.
48.      # Precs
49.      ASlowHypPrec ~ dt(0, 1/2.5^2, 7)T(0,)
50.      AFastHypPrec ~ dt(0, 1/2.5^2, 7)T(0,)
51.      BFastHypPrec ~ dt(0, 1/2.5^2, 7)T(0,)
52.      BSlowHypPrec ~ dt(0, 1/2.5^2, 7)T(0,)
53. }
```

10

Discussion
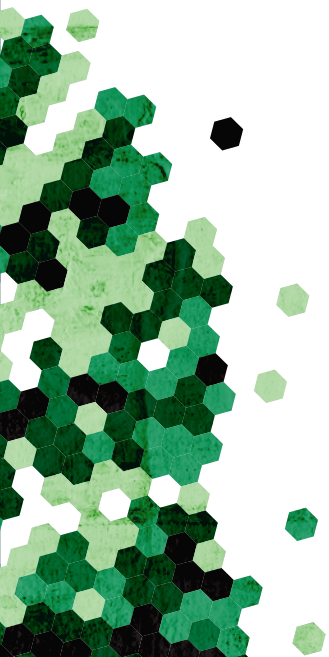
DISCUSSION

This thesis investigated the effects of cerebellar disease on cerebellar integrity, the relationship between cerebellar integrity and motor learning deficits, and two promising types of intervention to alleviate motor learning deficits of individuals with cerebellar disease. The main findings of this thesis are summarized and critically appraised below. Several directions for future research are suggested at the end of this discussion.

Cerebellar integrity in health and disease

That cerebellar disease affected cerebellar integrity which could be illustrated by neuroimaging was already well-known before this thesis (Bürk et al., 1996; Klockgether et al., 1990; Wüllner et al., 1993). Additionally, effects of ageing on cerebellar integrity have been described before (Hoogendam et al., 2012; Jernigan et al., 2001). However, the exact localization and extent of grey matter degeneration was unknown. **Chapter 2** of this thesis revealed the patterns of cerebellar degeneration during both healthy ageing as well as cerebellar disease. The pattern of cerebellar degeneration was largely analogous between healthy ageing subjects and cerebellar patients, though cerebellar patients were affected more severely. Both healthy ageing and cerebellar disease result in degeneration of the anterior lobe of the cerebellum (lobules I-V). Similarly, lobule VI and the posterior hand region (lobule VIIIb) were affected in both groups. However, large parts of the posterior lobe of the cerebellum, in particular Crus I-II and lobule VIIb, were only affected by cerebellar disease and not by healthy ageing. The patterns of degeneration fit with the specific symptomology associated with healthy ageing and cerebellar disease. That is, degeneration of the anterior cerebellum fits with impairments of motor function in both healthy ageing (Bernard and Seidler, 2013) and cerebellar disease (Donchin et al., 2012; Rabe et al., 2009), while the posterior shift of degeneration fits with impairments of higher (more abstract and complex) motor function and cognitive function in cerebellar patients (Schmahmann and Sherman, 1998; Taig et al., 2012). Thus, **Chapter 2** implicitly suggests that healthy ageing could be used as a proxy for cerebellar disease in certain motor learning experiments.

However, the methods and results of **Chapter 2** were limited to structural imaging of the cerebellar cortex, as the deep cerebellar nuclei (DCN) were not imaged in the datasets. This is particularly relevant, since cerebellar disease is known to affect DCN volume (Stefanescu et al., 2015), while less is known about the effect of ageing on the DCN (Höpker, 1951). Furthermore, increasing amounts of evidence suggest that the DCN is important in various motor learning behaviors (Habas, 2010). Therefore, **Chapter 3** explored the effects of healthy ageing and cerebellar disease on integrity of the deep cerebellar nuclei. The deep cerebellar nuclei in this study were imaged using quantitative susceptibility mapping (QSM) at clinical

field strengths of 3 Tesla. The volume of the DCN was not affected by healthy ageing, while iron load of the DCN increased with age. In cerebellar patients, the volume of the DCN *was* reduced, which we suggest is a result of a reduction in iron-containing glial cells. Being able to accurately and non-invasively map the deep cerebellar nuclei at clinical field strengths opens up the possibility to include this type of analysis in routine imaging protocols. Additionally, the results of **Chapter 3** suggest that using healthy ageing as a model system of cerebellar disease might not be appropriate, since the DCN are differentially affected by healthy ageing and cerebellar disease. Still, understanding the effect of ageing on cerebellar integrity is valuable as it provides a reference point against which cerebellar disease can be contrasted.

Motor learning deficits and cerebellar integrity

Motor learning deficits as a result of cerebellar degeneration are well-documented (Maschke et al., 2004a; Sanes et al., 1990; Tseng et al., 2007). Indeed, in this work as well, widespread motor learning deficits were observed in cerebellar patients with reduced cerebellar integrity (**Chapters 5 – 7 and Chapter 9**). This thesis further extends this knowledge by also providing evidence for a link between cerebellar integrity and motor learning deficits in children with autism spectrum disorder (**Chapter 4**). While children with ASD are not slower to adapt to visuomotor or forcefield perturbations than typically developed children per se (Gidley Larson et al., 2008), we found that error sensitivity to visual errors was reduced in children with ASD. Interestingly, in line with previous work (Haswell et al., 2009), sensitivity to proprioceptive errors was higher in children with ASD than typically developed children. As such, during motor learning, children with ASD rely more on proprioceptive errors and less on visual errors than typically developed children. Using the methods developed in **Chapter 2**, the abnormal pattern of motor learning in children with ASD was linked to a reduction in volume of the sensorimotor areas of the cerebellum. Thus, reduced cerebellar integrity is linked to abnormal motor learning in ASD as well, a disease not classically associated with the cerebellum.

tDCS and neurorehabilitation

As stated in the introduction, the initial studies using tDCS in healthy control subjects looked promising for the development of tDCS as a tool in neurorehabilitation. The idea being that tDCS might be able to speed up motor adaptation and increase motor retention in cerebellar patients compensating for cerebellar motor learning deficits. Pilot studies provided early evidence that neuromodulation was indeed beneficial for cerebellar patients, but additional research was required to establish this potential. So, in **Chapter 5**, we investigated the ability of tDCS to speed up motor adaptation and increase motor retention in a group of cerebellar patients and healthy age-matched controls. TDCS was

applied during a forcefield perturbation task (i.e. online stimulation) and subjects were stimulated anodally over the cerebellum or primary motor cortex over the course of three sessions (including one sham session). Unfortunately, no stimulation effects were observed in cerebellar patients. Surprisingly, stimulation effects in healthy controls were also absent. In **Chapter 5** we suggest several reasons for the lack of stimulation effects and the failure to reproduce earlier (positive) tDCS findings. For example, tDCS effects during motor adaptation may depend on cerebellar integrity which, as we have seen in **Chapter 2**, are reduced both in cerebellar patients as well as healthy age-matched controls. To make sure the lack of observed stimulation effects was not due to reduced cerebellar integrity, we conducted a control experiment in **Chapter 5** as well. Thirty young control subjects participated in the same forcefield task and stimulation parameters. In this between-subject experiment, no stimulation effects were observed as well, suggesting the negative results in healthy ageing subjects and cerebellar patients were not just the result of reduced cerebellar integrity, but could also be due to not fully developed task and stimulation parameters and/ or inter- and intra-subject variability.

A different experimental task with alternative stimulation parameters was tested in **Chapter 6**. As part of the study in **Chapter 5**, cerebellar subjects and healthy age-matched controls participated in a grip force experiment conducted on the same day as the reaching experiment. Measurements of grip force were compared between a session prior to tDCS stimulation (before the reaching experiment) and after tDCS stimulation (after the reaching experiment), thus tDCS stimulation was applied offline (not during the task), as opposed to the online stimulation in **Chapter 5**. In the grip force experiment as well, no stimulation effects were observed in both groups. Finally, in **Chapter 7**, we attempted to reproduce earlier tDCS results in a large group of young and healthy subjects and investigated whether stimulation onset (during baseline or during adaptation) resulted in differential stimulation effects. The subjects took part in a reaching experiment with visuomotor or forcefield perturbations, and anodal, cathodal or sham cerebellar stimulation. Again, no stimulation effects were found under any of the task and stimulation parameters.

Taken together, the initial hopeful expectations of a clinical application of tDCS in neurorehabilitation should be tempered. Several parameters of stimulation effects should first be understood before pursuing further clinical application of tDCS. Firstly, tDCS effects are possibly highly task parameter specific. For example, Jalali et al. (2017) were unable to elicit consistent stimulation effects across a range of varying task parameters and experimental paradigms. As our group was unable to reproduce earlier tDCS work (including work of Jalali and colleagues) in **Chapter 5**, we contacted Jalali and colleagues who suggested our screen orientation might have reduced tDCS efficacy. In the experiments of **Chapter 7** we made sure to use the same screen orientation and reproduce earlier

experiments as closely as possible, but we were still unable to replicate stimulation effects. Possibly there were other unaddressed differences in task parameters, but it remains to be seen whether a technique that is only effective under a very small subset of task parameters can have clinical relevance.

Secondly, stimulation parameters are still insufficiently fleshed out and understood. For instance, the effect of stimulation polarity (cathodal or anodal) is unpredictably heterogenous (Jacobson et al., 2012), stimulation during baseline (sometimes) has different behavioral effects than stimulation during learning (Stagg et al., 2011b), and neural excitability differences between offline and online stimulation are still incompletely explored (Das et al., 2016). Furthermore, electrode placement is highly variable between studies and the most commonly used electrode placements are possibly not optimally exciting the targeted brain areas (Parazzini et al., 2014; Rampersad et al., 2014). Thus, optimal stimulation parameters should first be established before tDCS is ready for clinical application.

Thirdly, intra- and inter-individual variability in stimulation efficacy is still insufficiently understood (Horvath et al., 2014b; Ridding and Ziemann, 2010). That is, tDCS effects can differ within the same subject between two identical stimulation sessions, and identical stimulation parameters can elicit different excitability effects between subjects. Several causes for these intra- and inter-individual differences have been suggested, like state dependency to explain intra-individual variability (Silvanto et al., 2008), and brain-derived neurotropic factor (BDNF) polymorphisms to explain inter-individual variability (Antal et al., 2010), but the exact causes still need to be elucidated. It should be noted that these caveats not only apply to tDCS research in healthy subjects, but especially to tDCS research in cerebellar patients. Consistent and predictable stimulation effects in cerebellar patients are likely even more difficult to elicit due to reduced cerebellar integrity.

Finally, several metascientific complexities affect the field of tDCS research. That is, the field likely suffers from a file drawer problem (publication bias) and (too) many researcher degrees of freedom, resulting in inflated statistical and practical significance and underpowered studies. For example, a recent analysis of the reported p-values of tDCS research in cognition and working memory revealed little to no evidential value of tDCS studies (Medina and Cason, 2017) and private discussions with fellow researchers lead us to believe this is no different for motor learning tDCS research. Furthermore, the current publication model places a lot of value on novel and positive findings, and possibly too little value on negative findings and replication work. The problems of publication bias and researcher degrees of freedom are larger than just the tDCS field and motor learning, and addressing it in more detail is outside scope of this thesis, but (peer-reviewed) preregistration and data sharing

could be a first important step. Although preregistration and data sharing of course come with their own set of problems and are certainly no magic bullets (Claesen et al., 2019; Gelman and Loken, 2013), it is a direction the field should consider.

To summarize, it remains to be seen whether arguably limited stimulation effects on the speed of motor adaptation or amount of motor retention will translate to actual clinical improvements in cerebellar patients and a critical reevaluation of tDCS and its clinical potential is demanded. Stimulation effects should be consistent and predictable between subjects and tasks, and should lead to behavioral improvements which are large enough to be clinically relevant, before tDCS can become a tool in the neurorehabilitation of cerebellar disease.

Training-related interventions and neurorehabilitation

The final part of this thesis focused on training-related interventions. **Chapter 8** investigated awareness and unawareness of motor learning in an implicit learning group and explicit learning group using a method called the process dissociation procedure (PDP). Awareness and unawareness of motor learning was measured in both groups under different visuomotor perturbation sizes (20°, 40° and 60°). As expected, the explicit group was more aware of sensorimotor learning than the implicit group as measured by the awareness index. Furthermore, both groups were more aware of larger visuomotor perturbations than smaller visuomotor perturbations. We did not directly test a training-related intervention in **Chapter 8**, but the results of our experiment indicate that the PDP could be used to measure awareness and unawareness in future studies testing training-related interventions based on implicit and explicit learning processes.

The final chapter, **Chapter 9,** investigated whether training paradigms that emphasize so-called slow learning could alleviate motor learning deficits of cerebellar patients. The experiment revealed that extended training enhances motor memory retention in cerebellar patients as well as healthy age-matched controls. However, motor memory retention in cerebellar patients was not enhanced to the level of control subjects. In healthy control subjects we suggest that enhanced retention was the result of two processes: use-dependent plasticity and increased memory resilience. Modelling work suggested that memory resilience was reduced in cerebellar patients. To our knowledge, this is the first time this specific motor learning deficit has been described in cerebellar patients. Possibly, use-dependent plasticity is spared in cerebellar patients, as this is hypothesized to be an extra-cerebellar process, while reduced memory resilience might be the result of reduced DCN integrity.

The fact that motor memory retention is still elevated by extended training in cerebellar patients could be helpful for the development of therapeutic strategies. Furthermore, the experiment in **Chapter 9** provides a possible mechanistic explanation why massed physiotherapy sessions are more effective in reducing ataxic symptoms than a regular therapy schedule (Ilg et al., 2009; Miyai et al., 2012). Future work can explore whether memory resilience predicts therapy response and whether massed training will improve the efficacy of other types of supportive therapy as well. Finally, quantitative susceptibility mapping (**Chapter 3**) should be used to provide more conclusive evidence that memory resilience is associated with DCN integrity.
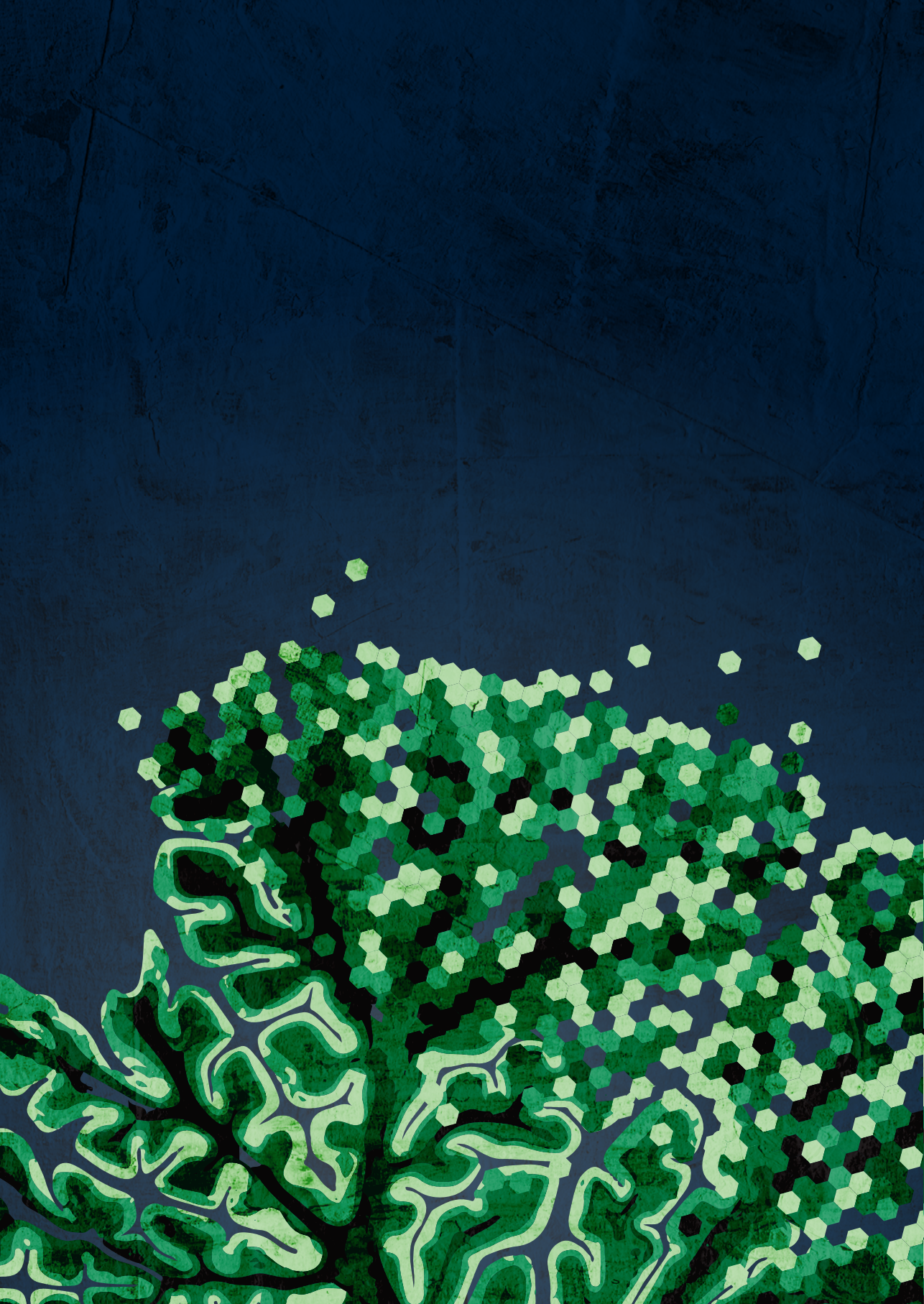
CONCLUSIONS AND FUTURE DIRECTIONS

Taken together, several recommendations and future research directions follow from this thesis. Firstly, researchers should start with routinely imaging the DCN in future motor learning research. Until now, structural imaging of the cerebellum in motor learning experiments was usually limited to the cerebellar cortex due to methodological difficulties of DCN imaging. The development of a QSM protocol at relatively low field strengths (**Chapter 3**) opens the way to routine inclusion of DCN imaging in motor learning experiments. Because the effects of cerebellar disease are usually not isolated to the cerebellar cortex, even in so-called "pure" cerebellar disorders, important information is missing when the DCN are not imaged. For example, our work on memory resilience would have benefitted from DCN imaging to solidify the relationship between memory resilience and integrity of the DCN (**Chapter 9**). Furthermore, future lesion-symptom mapping of the DCN in stroke or postoperative cerebellar patients could be used to establish deficits of DCN damage isolated from cerebellar cortical damage. Additionally, the work of **Chapter 3** should be extended to include other cerebellar diseases as well. Reduced iron content due to reduced glial cells could be unique for certain types of cerebellar disease (like SCA6), while other cerebellar disease might result in reduced volume due to lower neuronal cell counts, but not reduced glial cells.

Secondly, researchers should carefully consider whether to spend resources on the study of tDCS in cerebellar patients until the working of tDCS is further elucidated by animal and control studies. Unfortunately, we were unable to find any beneficial effects of tDCS for cerebellar patients in our experiments (**Chapters 5 and 6**). As discussed earlier in this thesis, there could be several reasons for our negative results, but it is clear that additional research is required before tDCS is ready for neurorehabilitation of cerebellar patients (if ever).

Thirdly, training-related interventions should be developed further. Extended training improved one component of motor learning behavior, but a lot is still unknown and other training-related interventions (based on reinforcement learning or strategic processes) should be further developed as well. However, from this thesis it does appear that training-related interventions are more effective in improving motor learning than neuromodulation. Thus, as of right now, resources are probably better spent on further developing training-related interventions for cerebellar patients than on neuromodulation in cerebellar patients.

Lastly, current research practices can be and should be improved. This is not limited to tDCS research or cerebellar research in general, but applies to many scientific endeavors. Current research incentives should be critically evaluated and open science initiatives like preregistration and data sharing should be considered to become the norm. Furthermore, scientists should be aware of the opportunity costs of their research. Any resources spend on one particular research project cannot be spend on another, thus problems of publication bias and researcher degrees of freedom not only affect our current understanding of natural processes, but also shape future research directions and scientific discoveries.

10

DISCUSSION

11

References
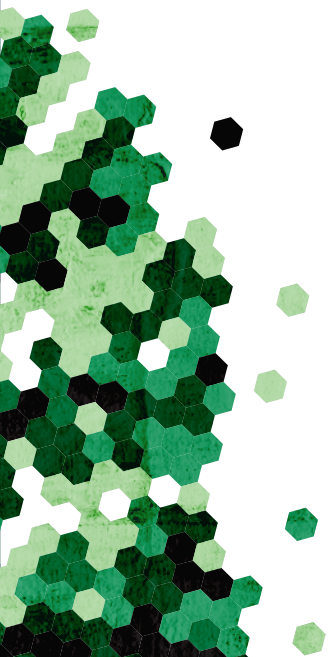
Abdul-Rahman, H.S., Gdeisat, M.A., Burton, D.R., Lalor, M.J., Lilley, F., and Moore, C.J. (2007). Fast and robust three-dimensional best path phase unwrapping algorithm. Appl. Opt. *46*, 6623–6635.

Abele, M., Minnerop, M., Urbach, H., Specht, K., and Klockgether, T. (2007). Sporadic adult onset ataxia of unknown etiology: A clinical, electrophysiological and imaging study. J. Neurol. *254*, 1384–1389.

Abraham, W.C., and Bear, M.F. (1996). Metaplasticity: the plasticity of synaptic plasticity. Trends Neurosci. *19*, 126–130.

Acosta-Cabronero, J., Betts, M.J., Cardenas-Blanco, A., Yang, S., and Nestor, P.J. (2016). In vivo MRI mapping of brain iron deposition across the adult lifespan. J. Neurosci. *36*, 364–374.

Adrian, E.D. (1943). Afferent areas in the cerebellum connected with the limbs. Brain *66*, 289–315.

Albus, J.S. (1971). A theory of cerebellar function. Math. Biosci. *10*, 25–61.

Allen, G., and Courchesne, E. (2003). Differential Effects of Developmental Cerebellar Abnormality on Cognitive and Motor Functions in the Cerebellum: An fMRI Study of Autism. Am. J. Psychiatry *160*, 262–273.

Alonso, E., Martínez-Ruano, L., De Biase, I., Mader, C., Ochoa, A., Yescas, P., Gutiérrez, R., White, M., Ruano, L., Fragoso-Benítez, M., et al. (2007). Distinct distribution of autosomal dominant spinocerebellar ataxia in the Mexican population. Mov. Disord. *22*, 1050–1053.

Andersen, B.B., Korbo, L., and Pakkenberg, B. (1992). A quantitative study of the human cerebellum with unbiased stereological techniques. J. Comp. Neurol. *326*, 549–560.

Andersen, B.B., Gundersen, H.J.G.J.G., and Pakkenberg, B. (2003). Aging of the human cerebellum: a stereological study. J. Comp. Neurol. *466*, 356–365.

Antal, A., Chaieb, L., Moliadze, V., Monte-Silva, K., Poreisz, C., Thirugnanasambandam, N., Nitsche, M.A., Shoukier, M., Ludwig, H., and Paulus, W. (2010). Brain-derived neurotrophic factor (BDNF) gene polymorphisms shape cortical plasticity in humans. Brain Stimulat. *3*, 230–237.

Antonietti, A., Casellato, C., D'Angelo, E., and Pedrocchi, A. (2017). Model-Driven Analysis of Eyeblink Classical Conditioning Reveals the Underlying Structure of Cerebellar Plasticity and Neuronal Activity. IEEE Trans. Neural Netw. Learn. Syst. *28*, 2748–2762.

Aoki, S., Okada, Y., Nishimura, K., Barkovich, A., Kjos, B., Brasch, R., and Norman, D. (1989). Normal deposition of brain iron in childhood and adolescence: MR imaging at 1.5 T. Radiology *172*, 381–385.

Apps, R., and Garwicz, M. (2005). Anatomical and physiological foundations of cerebellar information processing. Nat. Rev. Neurosci. *6*, 297–311.

Apps, R., Hawkes, R., Aoki, S., Bengtsson, F., Brown, A.M., Chen, G., Ebner, T.J., Isope, P., Jörntell, H., Lackey, E.P., et al. (2018). Cerebellar Modules and Their Role as Operational Cerebellar Processing Units. The Cerebellum.

Ashburner, J., and Friston, K.J. (2000). Voxel-Based Morphometry—The Methods. NeuroImage *11*, 805–821.

Ashburner, J., and Friston, K.J. (2005). Unified segmentation. NeuroImage *26*, 839–851.

Avila, E., Geest, J.N.V.D., Kamga, S.K., Verhage, M.C., Donchin, O., and Frens, M.A. (2015). Cerebellar Transcranial Direct Current Stimulation Effects on Saccade Adaptation. *2015*.

Bailey, A. (1998). A clinicopathological study of autism. Brain *121*, 889–905.

Barber, T.W., Brockway, J.A., and Higgins, L.S. (1970). The density of tissues in and about the head. Acta Neurol. Scand. *46*, 85–92.

Bell, C.C., Han, V., and Sawtell, N.B. (2008). Cerebellum-Like Structures and Their Implications for Cerebellar Function. Annu. Rev. Neurosci. *31*, 1–24.

Benkovic, S.A., and Connor, J.R. (1993). Ferritin, transferrin, and iron in selected regions of the adult and aged rat brain. J. Comp. Neurol. *338*, 97–113.

Benson, B.L., Anguera, J.A., and Seidler, R.D. (2011). A spatial explicit strategy reduces error but interferes with sensorimotor adaptation. J. Neurophysiol. *105*, 2843–2851.

Benussi, A., Koch, G., Cotelli, M., Padovani, A., and Borroni, B. (2015). Cerebellar transcranial direct current stimulation in patients with ataxia: A double-blind, randomized, sham-controlled study. Mov. Disord. *30*, 1701–1705.

Benussi, A., Dell'Era, V., Cotelli, M.S., Turla, M., Casali, C., Padovani, A., and Borroni, B. (2017). Long term clinical and neurophysiological effects of cerebellar transcranial direct current stimulation in patients with neurodegenerative ataxia. Brain Stimulat. *10*, 242–250.

Bergerbest, D., and Goshen-Gottstein, Y. (2002). The origins of levels-of-processing effects in a conceptual test: Evidence for automatic influences of memory from the process-dissociation procedure. Mem. Cognit. *30*, 1252–1262.

Bernard, J. a., and Seidler, R.D. (2013). Relationships between regional cerebellar volume and sensorimotor and cognitive function in young and older adults. Cerebellum *12*, 721–737.

Bernard, J. a., and Seidler, R.D. (2014). Moving forward: Age effects on the cerebellum underlie cognitive and motor declines. Neurosci. Biobehav. Rev. *42*, 193–207.

Beyer, L., Batsikadze, G., Timmann, D., and Gerwig, M. (2017). Cerebellar tDCS Effects on Conditioned Eyeblinks using Different Electrode Placements and Stimulation Protocols. Front. Hum. Neurosci. *11*.

Bilgic, B., Pfefferbaum, A., Rohlfing, T., Sullivan, E.V., and Adalsteinsson, E. (2012). MRI estimates of brain iron concentration in normal aging using quantitative susceptibility mapping. Neuroimage *59*, 2625–2635.

Bird, T.D. (2016). Hereditary ataxia overview.

Block, H., and Celnik, P. (2013). Stimulating the cerebellum affects visuomotor adaptation but not intermanual transfer of learning. Cerebellum Lond. Engl. *12*, 781–793.

Bock, O. (2005). Components of sensorimotor adaptation in young and elderly subjects. Exp. Brain Res. *160*, 259–263.

Bock, O., and Girgenrath, M. (2005). Relationship between sensorimotor adaptation and cognitive functions in younger and older subjects. Exp. Brain Res. *169*, 400–406.

Bock, O., Schneider, S., and Bloomberg, J. (2001). Conditions for interference versus facilitation during sequential sensorimotor adaptation. Exp. Brain Res. *138*, 359–365.

Brandauer, B., Hermsdörfer, J., Beck, A., Aurich, V., Gizewski, E.R., Marquardt, C., and Timmann, D. (2008). Impairments of prehension kinematics and grasping forces in patients with cerebellar degeneration and the relationship to cerebellar atrophy. Clin. Neurophysiol. *119*, 2528–2537.

Brandauer, B., Timmann, D., Häusler, A., and Hermsdörfer, J. (2010). Influences of Load Characteristics on Impaired Control of Grip Forces in Patients With Cerebellar Damage. J. Neurophysiol. *103*, 698–708.

Buch, E.R., Young, S., and Contreras-Vidal, J.L. (2003). Visuomotor Adaptation in Normal Aging. Learn. Mem. *10*, 55–63.

Buch, E.R., Santarnecchi, E., Antal, A., Born, J., Celnik, P.A., Classen, J., Gerloff, C., and Nitsche, M.A. (2016). Effects of tDCS on motor learning and memory formation : a consensus and critical position paper.

Buckner, R.L., Krienen, F.M., Castellanos, a., Diaz, J.C., and Yeo, B.T.T. (2011). The organization of the human cerebellum estimated by intrinsic functional connectivity. J. Neurophysiol. *106*, 2322–2345.

Burge, J., Ernst, M.O., and Banks, M.S. (2008). The statistical determinants of adaptation rate in human reaching. J. Vis. *8*, 20–20.

Bürk, K., Abele, M., Fetter, M., Dichgans, J., Skalej, M., Laccone, F., Didierjean, O., Brice, A., and Klockgether, T. (1996). Autosomal dominant cerebellar ataxia type I clinical features and MRI in families with SCA1, SCA2 and SCA3. Brain *119*, 1497–1505.

Butcher, P.A., Ivry, R.B., Kuo, S.-H., Rydz, D., Krakauer, J.W., and Taylor, J.A. (2017). The cerebellum does more than sensory prediction error-based learning in sensorimotor adaptation tasks. J Neurophysiol 15.

Cabral, M.E., Baltar, A., Borba, R., Galvão, S., Santos, L., Fregni, F., and Monte-Silva, K. (2015). Transcranial direct current stimulation: before, during, or after motor training? NeuroReport *26*, 618–622.

Caithness, G. (2004). Failure to Consolidate the Consolidation Theory of Learning for Sensorimotor Adaptation Tasks. J. Neurosci. *24*, 8662–8671.

Campuzano, V., Montermini, L., Moltò, M.D., Pianese, L., Cossée, M., Cavalcanti, F., Monros, E., Rodius, F., Duclos, F., Monticelli, A., et al. (1996). Friedreich's ataxia: autosomal recessive disease caused by an intronic GAA triplet repeat expansion. Science *271*, 1423–1427.

Casellato, C., Antonietti, A., Garrido, J.A., Ferrigno, G., D'Angelo, E., and Pedrocchi, A. (2015). Distributed cerebellar plasticity implements generalized multiple-scale memory components in real-robot sensorimotor tasks. Front. Comput. Neurosci. *9*.

Cattaneo, L., Fabbri-Destro, M., Boria, S., Pieraccini, C., Monti, A., Cossu, G., and Rizzolatti, G. (2007). Impairment of actions chains in autism and its possible role in intention understanding. Proc. Natl. Acad. Sci. *104*, 17825–17830.

Cavanagh, J.B., Holton, J.L., and Nolan, C.C. (1997). Selective damage to the cerebellar vermis in chronic alcoholism: a contribution from neurotoxicology to an old problem of selective vulnerability. Neuropathol. Appl. Neurobiol. *23*, 355–363.

Celnik, P. (2015). Understanding and Modulating Motor Learning with Cerebellar Stimulation. The Cerebellum *14*, 171–174.

Chan, C.Y., and Nicholson, C. (1986). Modulation by applied electric fields of Purkinje and stellate cell activity in the isolated turtle cerebellum. J. Physiol. *371*, 89–114.

Chan, C.Y., Hounsgaard, J., and Nicholson, C. (1988). Effects of electric fields on transmembrane potential and excitability of turtle cerebellar Purkinje cells in vitro. J. Physiol. *402*, 751–771.

Chung, H.D. (1985). Retrograde crossed cerebellar atrophy.

Claesen, A., Gomes, S.L.B.T., Tuerlinckx, F., and others (2019). Preregistration: Comparing Dream to Reality.

Cleeremans, A. (1993). Mechanisms of implicit learning: Connectionist models of sequence processing (MIT press).

Cleeremans, A. (2007). Consciousness: the radical plasticity thesis. Prog. Brain Res. 19–33.

Collin, L., Doretto, S., Malerba, M., Ruat, M., and Borrelli, E. (2007). Oligodendrocyte ablation affects the coordinated interaction between granule and Purkinje neurons during cerebellum development. Exp. Cell Res. *313*, 2946–2957.

Coltman, S.K., Cashaback, J.G.A., and Gribble, P.L. (2019). Both fast and slow learning processes contribute to savings following sensorimotor adaptation. J. Neurophysiol. *121*, 1575–1583.

Cook, J., Saygin, A.P., Swain, R., and Blakemore, S.-J. (2009). Reduced sensitivity to minimum-jerk biological motion in autism spectrum conditions. Neuropsychologia *47*, 3275–3278.

Courchesne, E., Karns, C.M., Davis, H.R., Ziccardi, R., Carper, R.A., Tigue, Z.D., Chisum, H.J., Moses, P., Pierce, K., and Lord, C. (2001). Unusual brain growth patterns in early life in patients with autistic disorder an MRI study. Neurology *57*, 245–254.

Criscimagna-Hemminger, S.E., Donchin, O., Gazzaniga, M.S., and Shadmehr, R. (2003). Learned dynamics of reaching movements generalize from dominant to nondominant arm. J. Neurophysiol. *89*, 168–176.

Criscimagna-Hemminger, S.E., Bastian, A.J., and Shadmehr, R. (2010). Size of error affects cerebellar contributions to motor learning. J. Neurophysiol. *103*, 2275–2284.

Cronbach, L.J. (1951). Coefficient alpha and the internal structure of tests. Psychometrika *16*, 297–334.

D'Angelo, E., and Casali, S. (2013). Seeking a unified framework for cerebellar function and dysfunction: from circuit operations to cognition. Front. Neural Circuits *6*.

Das, S., Holland, P., Frens, M.A., and Donchin, O. (2016). Impact of transcranial direct current stimulation (tDCS) on neuronal functions. Front. Neurosci. *10*, 550.

Datta, A., Truong, D., Minhas, P., Parra, L.C., and Bikson, M. (2012). Inter-Individual Variation during Transcranial Direct Current Stimulation and Normalization of Dose Using MRI-Derived Computational Models. Front. Psychiatry *3*.

De Zeeuw, C.I., Hoebeek, F.E., Bosman, L.W.J., Schonewille, M., Witter, L., and Koekkoek, S.K. (2011). Spatiotemporal firing patterns in the cerebellum. Nat. Rev. Neurosci. *12*, 327–344.

Deistung, A., Rauscher, A., Sedlacik, J., Stadler, J., Witoszynskyj, S., and Reichenbach, J.R. (2008). Susceptibility weighted imaging at ultra high magnetic field strengths: theoretical considerations and experimental results. Magn. Reson. Med. Off. J. Int. Soc. Magn. Reson. Med. *60*, 1155–1168.

Deistung, A., Schäfer, A., Schweser, F., Biedermann, U., Turner, R., and Reichenbach, J.R. (2013). Toward in vivo histology: a comparison of quantitative susceptibility mapping (QSM) with magnitude-, phase-, and R2 -imaging at ultra-high magnetic field strength. Neuroimage *65*, 299–314.

Deistung, A., Stefanescu, M.R., Ernst, T.M., Schlamann, M., Ladd, M.E., Reichenbach, J.R., and Timmann, D. (2016). Structural and Functional Magnetic Resonance Imaging of the Cerebellum: Considerations for Assessing Cerebellar Ataxias. The Cerebellum *15*, 21–25.

Deistung, A., Schweser, F., and Reichenbach, J.R. (2017). Overview of quantitative susceptibility mapping: Overview of Quantitative Susceptibility Mapping. NMR Biomed. *30*, e3569.

Destrebecqz, A., and Peigneux, P. (2005). Methods for studying unconscious learning. Prog. Brain Res. 69–80.

Destrebecqz, A., Peigneux, P., Laureys, S., Degueldre, C., Del Fiore, G., Aerts, J., Luxen, A., van der Linden, M., Cleeremans, A., and Maquet, P. (2003). Cerebral correlates of explicit sequence learning. Cogn. Brain Res. *16*, 391–398.

Destrieux, C., Fischl, B., Dale, A., and Halgren, E. (2010). Automatic parcellation of human cortical gyri and sulci using standard anatomical nomenclature. Neuroimage *53*, 1–15.

Diallo, A., Jacobi, H., Cook, A., Labrum, R., Durr, A., Brice, A., Charles, P., Marelli, C., Mariotti, C., Nanetti, L., et al. (2018). Survival in patients with spinocerebellar ataxia types 1, 2, 3, and 6 (EUROSCA): a longitudinal cohort study. Lancet Neurol. *17*, 327–334.

Diedrichsen, J. (2006). A spatially unbiased atlas template of the human cerebellum. NeuroImage *33*, 127–138.

Diedrichsen, J., and Zotow, E. (2015). Surface-Based Display of Volume-Averaged Cerebellar Imaging Data. PLOS ONE *10*, e0133402.

Diedrichsen, J., Balsters, J.H., Flavell, J., Cussans, E., and Ramnani, N. (2009). A probabilistic MR atlas of the human cerebellum. NeuroImage *46*, 39–46.

Diedrichsen, J., White, O., Newman, D., and Lally, N. (2010). Use-Dependent and Error-Based Learning of Motor Behaviors. J. Neurosci. *30*, 5159–5166.

Diedrichsen, J., Maderwald, S., Küper, M., Thürling, M., Rabe, K., Gizewski, E.R., Ladd, M.E., and Timmann, D. (2011). Imaging the deep cerebellar nuclei: A probabilistic atlas and normalization procedure. NeuroImage *54*, 1786–1794.

Dimitrova, A., Zeljko, D., Schwarze, F., Maschke, M., Gerwig, M., Frings, M., Beck, A., Aurich, V., Forsting, M., and Timmann, D. (2006). Probabilistic 3D MRI atlas of the human cerebellar dentate/interposed nuclei. Neuroimage *30*, 12–25.

Dimitrova, A., Gerwig, M., Brol, B., Gizewski, E.R., Forsting, M., Beck, A., Aurich, V., Kolb, F.P., and Timmann, D. (2008). Correlation of cerebellar volume with eyeblink conditioning in healthy subjects and in patients with cerebellar cortical degeneration. Brain Res. *1198*, 73–84.

Donchin, O., and Timmann, D. (2019). How to help cerebellar patients make the most of their remaining learning capacities. Brain *142*, 492–495.

Donchin, O., Francis, J.T., and Shadmehr, R. (2003). Quantifying generalization from trial-by-trial behavior of adaptive systems that learn with basis functions: theory and experiments in human motor control. J. Neurosci. Off. J. Soc. Neurosci. *23*, 9032–9045.

Donchin, O., Rabe, K., Diedrichsen, J., Lally, N., Schoch, B., Gizewski, E.R., and Timmann, D. (2012). Cerebellar Regions Involved in Adaptation to Force Field and Visuomotor Perturbation. J. Neurophysiol. *107*, 134–147.

Dowell, L.R., Mahone, E.M., and Mostofsky, S.H. (2009). Associations of postural knowledge and basic motor skill with dyspraxia in autism: Implication for abnormalities in distributed connectivity and motor learning. Neuropsychology *23*, 563–570.

Doya, K. (1999). What are the computations of the cerebellum, the basal ganglia and the cerebral cortex? Neural Netw. *12*, 961–974.

Doya, K., Kimura, H., and Kawato, M. (2001). Neural mechanisms of learning and control. IEEE Control Syst. *21*, 42–54.

Drayer, B., Burger, P., Darwin, R., Riederer, S., Herfkens, R., and Johnson, G. (1986). MRI of brain iron. Am. J. Roentgenol. *147*, 103–110.

Dun, K. van, Bodranghien, F.C.A.A., Mariën, P., and Manto, M.U. (2016). tDCS of the Cerebellum: Where Do We Stand in 2016? Technical Issues and Critical Review of the Literature. Front. Hum. Neurosci. *10*.

Dürr, A., Cossee, M., Agid, Y., Campuzano, V., Mignard, C., Penet, C., Mandel, J.-L., Brice, A., and Koenig, M. (1996). Clinical and Genetic Abnormalities in Patients with Friedreich's Ataxia. N. Engl. J. Med. *335*, 1169–1175.

Dziuk, M.A., Larson, J.C.G., Apostu, A., Mahone, E.M., Denckla, M.B., and Mostofsky, S.H. (2007). Dyspraxia in autism: association with motor, social, and communicative deficits. Dev. Med. Child Neurol. *49*, 734–739.

Ebner, T.J., Hewitt, A.L., and Popa, L.S. (2011). What Features of Limb Movements are Encoded in the Discharge of Cerebellar Neurons? The Cerebellum *10*, 683–693.

Eckstein, K., Dymerska, B., Bachrata, B., Bogner, W., Poljanc, K., Trattnig, S., and Robinson, S.D. (2018). Computationally efficient combination of multi-channel phase data from multi-echo acquisitions (ASPIRE). Magn. Reson. Med. *79*, 2996–3006.

Ehsani, F., Bakhtiary, A.H., Jaberzadeh, S., Talimkhani, A., and Hajihasani, A. (2016). Differential effects of primary motor cortex and cerebellar transcranial direct current stimulation on motor learning in healthy individuals: A randomized double-blind sham-controlled study. Neurosci. Res. *112*, 10–19.

Eichler, L., Bellenberg, B., Hahn, H., Köster, O., Schöls, L., and Lukas, C. (2011). Quantitative assessment of brain stem and cerebellar atrophy in spinocerebellar ataxia types 3 and 6: impact on clinical status. Am. J. Neuroradiol. *32*, 890–897.

Ekerot, C.-F., and Kano, M. (1985). Long-term depression of parallel fibre synapses following stimulation of climbing fibres. Brain Res. *342*, 357–360.

Eriksen, C.W. (1960). Discrimination and learning without awareness: A methodological survey and evaluation. Psychol. Rev. *67*, 279–300.

Falcon, M., Gomez, C., Chen, E., Shereen, A., and Solodkin, A. (2015). Early cerebellar network shifting in spinocerebellar ataxia type 6. Cereb. Cortex *26*, 3205–3218.

Faul, F., Erdfeld, E., Lang, A.G., and Buchner, A. (2007). A flexible statistical power analysis program for the social, behavioral, and biomedical sciences. Behav. Res. Methods *39*, 175–191.

Fernández-Ruiz, J., Hall, C., Vergara, P., Díaz, R., and Dı az, R. (2000). Prism adaptation in normal aging: Slower adaptation rate and larger aftereffect. Cogn. Brain Res. *9*, 223–226.

Ferrucci, R., Bocci, T., Cortese, F., Ruggiero, F., and Priori, A. (2016). Cerebellar transcranial direct current stimulation in neurological disease. Cerebellum Ataxias *3*.

Fischl, B., Salat, D.H., Busa, E., Albert, M., Dieterich, M., Haselgrove, C., Van Der Kouwe, A., Killiany, R., Kennedy, D., Klaveness, S., et al. (2002). Whole brain segmentation: automated labeling of neuroanatomical structures in the human brain. Neuron *33*, 341–355.

Flanagan, J.R., and Johansson, R.S. (2002). Hand Movements. In Encyclopedia of the Human Brain, (Elsevier), pp. 399–414.

Flanagan, J.R., and Wing, A. (1990). The stability of precision grip forces during cyclic arm movements with a hand-held load. Exp. Brain Res. *105*.

Flanagan, J.R., Bowman, M.C., and Johansson, R.S. (2006). Control strategies in object manipulation tasks. Curr. Opin. Neurobiol. *16*, 650–659.

Flourens, P. (1824). Les propriétés et les fonctions du système nerveux, dans les animaux vertébrés (Ballière).

Fonteyn, E.M.R., Keus, S.H.J., Verstappen, C.C.P., Schöls, L., de Groot, I.J.M., and van de Warrenburg, B.P.C. (2014). The effectiveness of allied health care in patients with ataxia: a systematic review. J. Neurol. *261*, 251–258.

Fregni, F., and Pascual-Leone, A. (2007). Technology Insight: noninvasive brain stimulation in neurology—perspectives on the therapeutic potential of rTMS and tDCS. Nat. Clin. Pract. Neurol. *3*, 383–393.

Frensch, P.A., Buchner, A., and Lin, J. (1994). Implicit learning of unique and ambiguous serial transitions in the presence and absence of a distractor task. J. Exp. Psychol. Learn. Mem. Cogn. *20*, 567–584.

Fricke, K., Seeber, A.A., Thirugnanasambandam, N., Paulus, W., Nitsche, M.A., and Rothwell, J.C. (2011). Time course of the induction of homeostatic plasticity generated by repeated transcranial direct current stimulation of the human motor cortex. J. Neurophysiol. *105*, 1141–1149.

Fritsch, B., Reis, J., Martinowich, K., Schambra, H.M., Ji, Y., Cohen, L.G., and Lu, B. (2010). Direct current stimulation promotes BDNF-dependent synaptic plasticity: Potential implications for motor learning. Neuron *66*, 198–204.

Fu, Q., Fu, X., and Dienes, Z. (2008). Implicit sequence learning and conscious awareness. Conscious. Cogn. *17*, 185–202.

Fuentes, C.T., Mostofsky, S.H., and Bastian, A.J. (2009). Children with autism show specific handwriting impairments. Neurology *73*, 1532–1537.

Galea, J.M., Jayaram, G., Ajagbe, L., and Celnik, P. (2009). Modulation of Cerebellar Excitability by Polarity-Specific Noninvasive Direct Current Stimulation. J. Neurosci. *29*, 9115–9122.

Galea, J.M., Vazquez, A., Pasricha, N., Xivry, J.-J.O. de, and Celnik, P. (2010a). Dissociating the Roles of the Cerebellum and Motor Cortex during Adaptive Learning: The Motor Cortex Retains What the Cerebellum Learns. Cereb. Cortex *21*, 1761–1770.

Galea, J.M., Sami, S.A., Albert, N.B., and Miall, R.C. (2010b). Secondary tasks impair adaptation to step- and gradual-visual displacements. Exp. Brain Res. *202*, 473–484.

Galea, J.M., Mallia, E., Rothwell, J., and Diedrichsen, J. (2015). The dissociable effects of punishment and reward on motor learning. Nat Neurosci *18*, 597–602.

Gallese, V., Keysers, C., and Rizzolatti, G. (2004). A unifying view of the basis of social cognition. Trends Cogn. Sci. *8*, 396–403.

Galliano, E., and De Zeeuw, C.I. (2014). Questioning the Cerebellar Doctrine. In Progress in Brain Research, (Elsevier), pp. 59–77.

Gallichan, D., Marques, J.P., and Gruetter, R. (2016). Retrospective correction of involuntary microscopic head movement using highly accelerated fat image navigators (3D FatNavs) at 7T. Magn. Reson. Med. *75*, 1030–1039.

Gandiga, P.C., Hummel, F.C., and Cohen, L.G. (2006). Transcranial DC stimulation (tDCS): a tool for double-blind sham-controlled clinical studies in brain stimulation. Clin. Neurophysiol. Off. J. Int. Fed. Clin. Neurophysiol. *117*, 845–850.

Gans, A. (1924). Beitrag zur kenntnis des aufbaus des nucleus dentatus aus zwei teilen, namentlich auf grund von untersuchungen mit der eisenreaktion. Z. Für Gesamte Neurol. Psychiatr. *93*, 750–755.

Gao, Z., van Beugen, B.J., and De Zeeuw, C.I. (2012). Distributed synergistic plasticity and cerebellar learning. Nat. Rev. Neurosci. *13*, 619–635.

Gelman, A., and Loken, E. (2013). The garden of forking paths: Why multiple comparisons can be a problem, even when there is no "fishing expedition" or "p-hacking" and the research hypothesis was posited ahead of time. Dep. Stat. Columbia Univ.

Ghassaban, K., Liu, S., Jiang, C., and Haacke, E.M. (2019). Quantifying iron content in magnetic resonance imaging. Neuroimage *187*, 77–92.

Gibo, T.L., Criscimagna-Hemminger, S.E., Okamura, A.M., and Bastian, A.J. (2013). Cerebellar motor learning: are environment dynamics more important than error size? J. Neurophysiol. *110*, 322–333.

Gidley Larson, J.C., Bastian, A.J., Donchin, O., Shadmehr, R., and Mostofsky, S.H. (2008). Acquisition of internal models of motor tasks in children with autism. Brain *131*, 2894–2903.

Gierga, K., Schelhaas, H., Brunt, E., Seidel, K., Scherzed, W., Egensperger, R., De Vos, R., Den Dunnen, W., Ippel, P., Petrasch-Parwez, E., et al. (2009). Spinocerebellar ataxia type 6 (SCA6): neurodegeneration goes beyond the known brain predilection sites. Neuropathol. Appl. Neurobiol. *35*, 515–527.

Glickstein, M. (2000). How are visual areas of the brain connected to motor areas for the sensory guidance of movement? Trends Neurosci. *23*, 613–617.

Glickstein, M., Strata, P., and Voogd, J. (2009). Cerebellum: history. Neuroscience *162*, 549–559.

Gomez, C.M., Thompson, R.M., Gammack, J.T., Perlman, S.L., Dobyns, W.B., Truwit, C.L., Zee, D.S., Clark, H.B., and Anderson, J.H. (1997). Spinocerebellar ataxia type 6: Gaze-evoked and vertical nystagmus, Purkinje cell degeneration, and variable age of onset. Ann. Neurol. *42*, 933–950.

Gonzalez Castro, L.N., Hadjiosif, A.M., Hemphill, M.A., and Smith, M.A. (2014). Environmental Consistency Determines the Rate of Motor Adaptation. Curr. Biol. *24*, 1050–1061.

Goodwill, A.M., Reynolds, J., Daly, R.M., and Kidgell, D.J. (2013). Formation of cortical plasticity in older adults following tDCS and motor training. Front. Aging Neurosci. *5*, 1–9.

Gowen, E. (2012). Imitation in autism: why action kinematics matter. Front. Integr. Neurosci. *6*.

Gray, H. (1878). Anatomy of the human body (Lea & Febiger).

Grimaldi, G., Oulad Ben Taib, N., Manto, M., and Bodranghien, F. (2014a). Marked reduction of cerebellar deficits in upper limbs following transcranial cerebello-cerebral DC stimulation: tremor reduction and re-programming of the timing of antagonist commands. Front. Syst. Neurosci. *8*, 9–9.

Grimaldi, G., Argyropoulos, G.P., Bastian, a., Cortes, M., Davis, N.J., Edwards, D.J., Ferrucci, R., Fregni, F., Galea, J.M., Hamada, M., et al. (2014b). Cerebellar Transcranial Direct Current Stimulation (ctDCS): A Novel Approach to Understanding Cerebellar Function in Health and Disease. The Neuroscientist.

Grodd, W., Hülsmann, E., Lotze, M., Wildgruber, D., and Erb, M. (2001). Sensorimotor mapping of the human cerebellum: fMRI evidence of somatotopic organization: Sensorimotor Mapping of the Cerebellum. Hum. Brain Mapp. *13*, 55–73.

Haacke, E.M., Xu, Y., Cheng, Y.-C.N., and Reichenbach, J.R. (2004). Susceptibility weighted imaging (SWI). Magn. Reson. Med. Off. J. Int. Soc. Magn. Reson. Med. *52*, 612–618.

Habas, C. (2010). Functional Imaging of the Deep Cerebellar Nuclei: A Review. The Cerebellum *9*, 22–28.

Hadipour-Niktarash, A., Lee, C.K., Desmond, J.E., and Shadmehr, R. (2007). Impairment of Retention But Not Acquisition of a Visuomotor Skill Through Time-Dependent Disruption of Primary Motor Cortex. J. Neurosci. *27*, 13413–13419.

Haith, A.M., and Krakauer, J.W. (2013). Model-Based and Model-Free Mechanisms of Human Motor Learning. In Progress in Motor Control, M.J. Richardson, M.A. Riley, and K. Shockley, eds. (New York, NY: Springer New York), pp. 1–21.

Hallgren, B., and Sourander, P. (1958). The effect of age on the non-haemin iron in the human brain. J. Neurochem. *3*, 41–51.

Hamada, M., Murase, N., Hasan, A., Balaratnam, M., and Rothwell, J.C. (2013). The Role of Interneuron Networks in Driving Human Motor Cortical Plasticity. Cereb. Cortex *23*, 1593–1605.

Hametner, S., Endmayr, V., Deistung, A., Palmrich, P., Prihoda, M., Haimburger, E., Menard, C., Feng, X., Haider, T., Leisser, M., et al. (2018). The influence of brain iron and myelin on magnetic susceptibility and effective transverse relaxation-A biochemical and histological validation study. Neuroimage *179*, 117–133.

Hardwick, R.M., and Celnik, P. a (2014). Cerebellar direct current stimulation enhances motor learning in older adults. Neurobiol. Aging *35*, 1–5.

Hashemirad, F., Zoghi, M., Fitzgerald, P.B., and Jaberzadeh, S. (2016). The effect of anodal transcranial direct current stimulation on motor sequence learning in healthy individuals: A systematic review and meta-analysis. Brain Cogn. *102*, 1–12.

Hashimoto, T., Tayama, M., Murakawa, K., Yoshimoto, T., Miyazaki, M., Harada, M., and Kuroda, Y. (1995). Development of the brainstem and cerebellum in autistic patients. J. Autism Dev. Disord. *25*, 1–18.

Haswell, C.C., Izawa, J., R Dowell, L., H Mostofsky, S., and Shadmehr, R. (2009). Representation of internal models of action in the autistic brain. Nat. Neurosci. *12*, 970–972.

Hatada, Y., Miall, R.C., and Rossetti, Y. (2005). Two waves of a long-lasting aftereffect of prism adaptation measured over 7 days. Exp. Brain Res. *169*, 417–426.

Hatakenaka, M., Miyai, I., Mihara, M., Yagura, H., and Hattori, N. (2012). Impaired Motor Learning by a Pursuit Rotor Test Reduces Functional Outcomes During Rehabilitation of Poststroke Ataxia. Neurorehabil. Neural Repair *26*, 293–300.

He, N., Langley, J., Huddleston, D.E., Ling, H., Xu, H., Liu, C., Yan, F., and Hu, X.P. (2017). Improved Neuroimaging Atlas of the Dentate Nucleus. The Cerebellum *16*, 951–956.

Heckroth, J.A. (1994). Quantitative morphological analysis of the cerebellar nuclei in normal and lurcher mutant mice. I. Morphology and cell number. J. Comp. Neurol. *343*, 173–182.

Hegele, M., and Heuer, H. (2010). Implicit and explicit components of dual adaptation to visuomotor rotations. Conscious. Cogn. *19*, 906–917.

Hegele, M., and Heuer, H. (2013). Age-related variations of visuomotor adaptation result from both the acquisition and the application of explicit knowledge. Psychol. Aging *28*, 333–339.

Herculano-Houzel (2010). Coordinated scaling of cortical and cerebellar numbers of neurons. Front. Neuroanat.

Herzfeld, D.J., Pastor, D., Haith, A.M., Rossetti, Y., Shadmehr, R., and O'Shea, J. (2014a). Contributions of the cerebellum and the motor cortex to acquisition and retention of motor memories. NeuroImage *98*, 147–158.

Herzfeld, D.J., Vaswani, P.A., Marko, M.K., and Shadmehr, R. (2014b). A memory of errors in sensorimotor learning. Science *345*, 1349–1353.

Heuer, H., and Hegele, M. (2008). Adaptation to visuomotor rotations in younger and older adults. Psychol. Aging *23*, 190–202.

Heuer, H., and Hegele, M. (2011). Generalization of implicit and explicit adjustments to visuomotor rotations across the workspace in younger and older adults. J. Neurophysiol. *106*, 2078–2085.

Heuer, H., and Rapp, K. (2011). Active error corrections enhance adaptation to a visuo-motor rotation. Exp. Brain Res. *211*, 97–108.

Hinder, M.R., Tresilian, J.R., Riek, S., and Carson, R.G. (2008). The contribution of visual feedback to visuomotor adaptation: How much and when? Brain Res. *1197*, 123–134.

Hobson, R.P., and Hobson, J.A. (2008). Dissociable aspects of imitation: A study in autism. J. Exp. Child Psychol. *101*, 170–185.

Holm, S. (1979). A simple sequentially rejective multiple test procedure. Scand. J. Stat. 65–70.

Holmes, G. (1908). A form of familial degeneration of the cerebellum. Brain *30*, 466–489.

Holmes, G. (1917). THE SYMPTOMS OF ACUTE CEREBELLAR INJURIES DUE TO GUNSHOT INJURIES. Brain *40*, 461–535.

Hoogendam, Y.Y., van der Geest, J.N., van der Lijn, F., van der Lugt, A., Niessen, W.J., Krestin, G.P., Hofman, A., Vernooij, M.W., Breteler, M.M.B., and Ikram, M.A. (2012). Determinants of cerebellar and cerebral volume in the general elderly population. Neurobiol. Aging *33*, 2774–2781.

Höpker, W. (1951). Das altern des nucleus dentatus. Z Altersforsch *5*, 256–277.

Horvath, J.C., Forte, J.D., and Carter, O. (2014a). Evidence that transcranial direct current stimulation (tDCS) Generates little-to-no reliable neurophysiologic effect beyond MEP amplitude modulation in healthy Human subjects: A systematic review. Neuropsychologia *66*, 213–236.

Horvath, J.C., Carter, O., and Forte, J.D. (2014b). Transcranial direct current stimulation: five important issues we aren't discussing (but probably should be). Front. Syst. Neurosci. *8*, 2.

Huang, V.S., and Shadmehr, R. (2007). Evolution of Motor Memory During the Seconds After Observation of Motor Error. J. Neurophysiol. *97*, 3976–3985.

Huang, V.S., and Shadmehr, R. (2009). Persistence of Motor Memories Reflects Statistics of the Learning Event. J. Neurophysiol. *102*, 931–940.

Hulst, T., van der Geest, J.N.J.N., Thürling, M., Goericke, S., Frens, M. a., Timmann, D., and Donchin, O. (2015). Ageing shows a pattern of cerebellar degeneration analogous, but not equal, to that in patients suffering from cerebellar degenerative disease. NeuroImage *116*, 196–206.

Hulst, T., John, L., Küper, M., van der Geest, J.N., Göricke, S.L., Donchin, O., and Timmann, D. (2017). Cerebellar patients do not benefit from cerebellar or M1 transcranial direct current stimulation during force field reaching adaptation. J. Neurophysiol. jn.00808.2016-jn.00808.2016.

Hummel, F.C., and Cohen, L.G. (2006). Non-invasive brain stimulation: a new strategy to improve neurorehabilitation after stroke? Lancet Neurol. *5*, 708–712.

Hunter, T., Sacco, P., Nitsche, M. a, and Turner, D.L. (2009). Modulation of internal model formation during force field-induced motor learning by anodal transcranial direct current stimulation of primary motor cortex. J. Physiol. *587*, 2949–2961.

Hussain, S.J., and Morton, S.M. (2014). Perturbation schedule does not alter retention of a locomotor adaptation across days. J. Neurophysiol. *111*, 2414–2422.

Hwang, E.J., Smith, M.A., and Shadmehr, R. (2006). Dissociable effects of the implicit and explicit memory systems on learning control of reaching. Exp. Brain Res. *173*, 425–437.

Iacoboni, M. (2009). Imitation, Empathy, and Mirror Neurons. Annu. Rev. Psychol. *60*, 653–670.

Ilg, W., Synofzik, M., Brötz, D., Burkard, S., Giese, M.A., and Schöls, L. (2009). Intensive coordinative training improves motor performance in degenerative cerebellar disease. Neurology *73*, 1823–1830.

Ilg, W., Brötz, D., Burkard, S., Giese, M.A., Schöls, L., and Synofzik, M. (2010). Long-term effects of coordinative training in degenerative cerebellar disease. Mov. Disord. *25*, 2239–2246.

Ilg, W., Bastian, A.J., Boesch, S., Burciu, R.G., Celnik, P., Claa??en, J., Feil, K., Kalla, R., Miyai, I., Nachbauer, W., et al. (2014). Consensus paper: Management of degenerative cerebellar disorders. Cerebellum *13*, 248–268.

Ingram, H.A., van Donkelaar, P., Cole, J., Vercher, J.-L., Gauthier, G.M., and Miall, R.C. (2000). The role of proprioception and attention in a visuomotor adaptation task. Exp. Brain Res. *132*, 114–126.

Ito, M. (2001). Cerebellar Long-Term Depression: Characterization, Signal Transduction, and Functional Roles. Physiol. Rev. *81*, 1143–1195.

Ito, M., and Kano, M. (1982). Long-lasting depression of parallel fiber-Purkinje cell transmission induced by conjunctive stimulation of parallel fibers and climbing fibers in the cerebellar cortex. Neurosci. Lett. *33*, 253–258.

Ito, M., Sakurai, M., and Tongroach, P. (1982). Climbing fibre induced depression of both mossy fibre responsiveness and glutamate sensitivity of cerebellar Purkinje cells. J. Physiol. *324*, 113–134.

Izawa, J., and Shadmehr, R. (2011). Learning from Sensory and Reward Prediction Errors during Motor Adaptation. PLoS Comput. Biol. *7*, e1002012–e1002012.

Izawa, J., Rane, T., Donchin, O., and Shadmehr, R. (2008). Motor Adaptation as a Process of Reoptimization. *28*, 2883–2891.

Izawa, J., Criscimagna-Hemminger, S.E., and Shadmehr, R. (2012a). Cerebellar Contributions to Reach Adaptation and Learning Sensory Consequences of Action. J. Neurosci. *32*, 4230–4239.

Izawa, J., Pekny, S.E., Marko, M.K., Haswell, C.C., Shadmehr, R., and Mostofsky, S.H. (2012b). Motor Learning Relies on Integrated Sensory Inputs in ADHD, but Over-Selectively on Proprioception in Autism Spectrum Conditions. Autism Res. *5*, 124–136.

Jacobi, H., Reetz, K., Montcel, S.T. du, Bauer, P., Mariotti, C., Nanetti, L., Rakowicz, M., Sulek, A., Durr, A., Charles, P., et al. (2013). Biological and clinical characteristics of individuals at risk for spinocerebellar ataxia types 1, 2, 3, and 6 in the longitudinal RISCA study: analysis of baseline data. Lancet Neurol. *12*, 650–658.

Jacobson, L., Koslowsky, M., and Lavidor, M. (2012). tDCS polarity effects in motor and cognitive domains: a meta-analytical review. Exp. Brain Res. *216*, 1–10.

Jacoby, L.L. (1991). A process dissociation framework: Separating automatic from intentional uses of memory. J. Mem. Lang. *30*, 513–541.

Jakobson, L.S., and Goodale, M.A. (1989). Trajectories of reaches to prismatically-displaced targets: evidence for ?automatic? visuomotor recalibration. Exp. Brain Res. *78*.

Jalali, R., Miall, R.C., and Galea, J.M. (2017). No consistent effect of cerebellar transcranial direct current stimulation (tDCS) on visuomotor adaptation. J. Neurophysiol. jn.00896.2016-jn.00896.2016.

Jalali, R., Chowdhury, A., Wilson, M., Miall, R.C., and Galea, J.M. (2018). Neural changes associated with cerebellar tDCS studied using MR spectroscopy. Exp. Brain Res. *236*, 997–1006.

Jamil, A., Batsikadze, G., Kuo, H.-I., Labruna, L., Hasan, A., Paulus, W., and Nitsche, M.A. (2017). Systematic evaluation of the impact of stimulation intensity on neuroplastic after-effects induced by transcranial direct current stimulation: Effects of DC intensity on cortical excitability. J. Physiol. *595*, 1273–1288.

Jansen, J., and Brodal, A. (1958). Das Kleinhirn. Handbuch der Mikroskopischen Anatomie des Menschen. Springer-Verl. *91*, 162.

Jansiewicz, E.M., Goldberg, M.C., Newschaffer, C.J., Denckla, M.B., Landa, R., and Mostofsky, S.H. (2006). Motor Signs Distinguish Children with High Functioning Autism and Asperger's Syndrome from Controls. J. Autism Dev. Disord. *36*, 613–621.

Jayadev, S., and Bird, T.D. (2013). Hereditary ataxias: Overview. Genet. Med. *15*, 673–683.

Jayaram, G., Tang, B., Pallegadda, R., Vasudevan, E.V.L., Celnik, P., and Bastian, A. (2012). Modulating locomotor adaptation with cerebellar stimulation. J. Neurophysiol. *107*, 2950–2957.

Jernigan, T.L., Archibald, S.L., Fennema-Notestine, C., Gamst, A.C., Stout, J.C., Bonner, J., and Hesselink, J.R. (2001). Effects of age on tissues and regions of the cerebrum and cerebellum. Neurobiol. Aging *22*, 581–594.

Jiménez, L., Méndez, C., and Cleeremans, A. (1996). Comparing direct and indirect measures of sequence learning. J. Exp. Psychol. Learn. Mem. Cogn. *22*, 948–969.

Johansson, R.S., and Westling, G. (1988). Programmed and triggered actions to rapid load changes during precision grip. Exp. Brain Res. *71*.

Johnson, B.P., Rinehart, N.J., White, O., Millist, L., and Fielding, J. (2013). Saccade adaptation in autism and Asperger's disorder. Neuroscience *243*, 76–87.

Johnston, W.A., Hawley, K.J., and Elliott, J.M. (1991). Contribution of perceptual fluency to recognition judgments. J. Exp. Psychol. Learn. Mem. Cogn. *17*, 210–223.

Joiner, W.M., and Smith, M.A. (2008). Long-Term Retention Explained by a Model of Short-Term Learning in the Adaptive Control of Reaching. J. Neurophysiol. *100*, 2948–2955.

Jung, B.C., Choi, S.I., Du, A.X., Cuzzocreo, J.L., Geng, Z.Z., Ying, H.S., Perlman, S.L., Toga, A.W., Prince, J.L., and Ying, S.H. (2012). Principal component analysis of cerebellar shape on MRI separates SCA types 2 and 6 into two archetypal modes of degeneration. The Cerebellum *11*, 887–895.

Kagerer, F.A., Contreras-Vidal, J.L., and Stelmach, G.E. (1997). Adaptation to gradual as compared with sudden visuo-motor distortions. Exp. Brain Res. *115*, 557–561.

Kane, K.A., Picton, T.W., Moscovitch, M., and Winocur, G. (2000). Event-related potentials during conscious and automatic memory retrieval. Cogn. Brain Res. *10*, 19–35.

Karabanov, A., and Ullen, F. (2008). Implicit and Explicit Learning of Temporal Sequences Studied With the Process Dissociation Procedure. J. Neurophysiol. *100*, 733–739.

Kemper, T.L., and Bauman, M. (1998). Neuropathology of Infantile Autism. J. Neuropathol. Exp. Neurol. *57*, 645–652.

Kessler, S.K., Turkeltaub, P.E., Benson, J.G., and Hamilton, R.H. (2012). Differences in the experience of active and sham transcranial direct current stimulation. Brain Stimulat. *5*, 155–162.

Kim, J.-H., Kim, D.-W., Chang, W.H., Kim, Y.-H., Kim, K., and Im, C.-H. (2014a). Inconsistent outcomes of transcranial direct current stimulation may originate from anatomical differences among individuals: Electric field simulation using individual MRI data. Neurosci. Lett. *564*, 6–10.

Kim, S., Stephenson, M.C., Morris, P.G., and Jackson, S.R. (2014b). tDCS-induced alterations in GABA concentration within primary motor cortex predict motor learning and motor memory: A 7T magnetic resonance spectroscopy study. NeuroImage *99*, 237–243.

Kim, S., Oh, Y., and Schweighofer, N. (2015). Between-Trial Forgetting Due to Interference and Time in Motor Adaptation. PLOS ONE *10*, e0142963.

Kitago, T., and Krakauer, J.W. (2013). Motor learning principles for neurorehabilitation. Neurol. Rehabil. 93–103.

Kitago, T., Ryan, S.L., Mazzoni, P., Krakauer, J.W., and Haith, A.M. (2013). Unlearning versus savings in visuomotor adaptation: comparing effects of washout, passage of time, and removal of errors on motor memory. Front. Hum. Neurosci. *7*, 307–307.

Klassen, J., Tong, C., and Flanagan, J.R. (2005). Learning and recall of incremental kinematic and dynamic sensorimotor transformations. Exp. Brain Res. *164*, 250–259.

Klein, A.P., Ulmer, J.L., Quinet, S.A., Mathews, V., and Mark, L.P. (2016). Nonmotor Functions of the Cerebellum: An Introduction. Am. J. Neuroradiol. *37*, 1005–1009.

Klockgether, T. (2007). Ataxias. In Textbook of Clinical Neurology, (Philadelphia: Saunders Elsevier), pp. 765–780.

Klockgether, T. (2011). Update on degenerative ataxias. Curr. Opin. Neurol. *24*, 339–345.

Klockgether, T. (2012). Sporadic adult-onset ataxia of unknown etiology. In Handbook of Clinical Neurology, (Elsevier), pp. 253–262.

Klockgether, T., Schroth, G., Diener, H., and Dichgans, J. (1990). Idiopathic cerebellar ataxia of late onset: natural history and MRI morphology. J. Neurol. Neurosurg. Psychiatry *53*, 297–305.

Koeppen, A.H. (2005). The pathogenesis of spinocerebellar ataxia. The Cerebellum *4*, 62.

Koeppen, A.H., Ramirez, R.L., Yu, D., Collins, S.E., Qian, J., Parsons, P.J., Yang, K.X., Chen, Z., Mazurkiewicz, J.E., and Feustel, P.J. (2012). Friedreich's Ataxia Causes Redistribution of Iron, Copper, and Zinc in the Dentate Nucleus. The Cerebellum *11*, 845–860.

Konczak, J., Schoch, B., Dimitrova, A., Gizewski, E., and Timmann, D. (2005). Functional recovery of children and adolescents after cerebellar tumour resection. Brain *128*, 1428–1441.

Koppelmans, V., Hirsiger, S., Mérillat, S., Jäncke, L., and Seidler, R.D. (2015). Cerebellar gray and white matter volume and their relation with age and manual motor performance in healthy older adults: Cerebellar Volume and Fine Motor Performance. Hum. Brain Mapp. *36*, 2352–2363.

Kording, K.P., Tenenbaum, J.B., and Shadmehr, R. (2007). The dynamics of memory as a consequence of optimal adaptation to a changing body. Nat. Neurosci. *10*, 779–786.

Krakauer, J.W., Pine, Z.M., Ghilardi, M.-F., and Ghez, C. (2000). Learning of visuomotor transformations for vectorial planning of reaching trajectories. J. Neurosci. *20*, 8916–8924.

Kruschke, J. (2010). Doing Bayesian Data Analysis.

Küper, M., Brandauer, B., Thürling, M., Schoch, B., Gizewski, E.R., Timmann, D., and Hermsdörfer, J. (2011a). Impaired prehension is associated with lesions of the superior and inferior hand representation within the human cerebellum. J. Neurophysiol. *105*, 2018–2029.

Küper, M., Hermsdörfer, J., Brandauer, B., Thürling, M., Schoch, B., Theysohn, N., and Timmann, D. (2011b). Lesions of the dentate and interposed nuclei are associated with impaired prehension in cerebellar patients. Neurosci. Lett. *499*, 132–136.

Küper, M., Döring, K., Spangenberg, C., Konczak, J., Gizewski, E.R., Schoch, B., and Timmann, D. (2013). Location and Restoration of Function after Cerebellar Tumor Removal—A Longitudinal Study of Children and Adolescents. The Cerebellum *12*, 48–58.

Labruna, L., Dabit, M., Vanderschelden, B., Nitsche, M., and Ivry, R.B. (2015). Individual differences in TMS sensitivity influence the effect of tDCS in a motor adaptation task. In SfN, pp. 3–3.

Labruna, L., Jamil, A., Fresnoza, S., Batsikadze, G., Kuo, M.-F., Vanderschelden, B., Ivry, R.B., and Nitsche, M.A. (2016). Efficacy of Anodal Transcranial Direct Current Stimulation is Related to Sensitivity to Transcranial Magnetic Stimulation. Brain Stimulat. *9*, 8–15.

Lang, N., Siebner, H.R., Ernst, D., Nitsche, M.A., Paulus, W., Lemon, R.N., and Rothwell, J.C. (2004). Preconditioning with transcranial direct current stimulation sensitizes the motor cortex to rapid-rate transcranial magnetic stimulation and controls the direction of after-effects. Biol. Psychiatry *56*, 634–639.

Langkammer, C., Schweser, F., Krebs, N., Deistung, A., Goessler, W., Scheurer, E., Sommer, K., Reishofer, G., Yen, K., Fazekas, F., et al. (2012). Quantitative susceptibility mapping (QSM) as a means to measure brain iron? A post mortem validation study. Neuroimage *62*, 1593–1599.

Larsell, O., and Jansen, J. (1972). The comparative anatomy and histology of the cerebellum (Univ. Minnesota Press, Minneapolis).

Lefebvre, S., Thonnard, J.-L., Laloux, P., Peeters, A., Jamart, J., and Vandermeeren, Y. (2013a). Single Session of Dual-tDCS Transiently Improves Precision Grip and Dexterity of the Paretic Hand After Stroke. Neurorehabil. Neural Repair *28*, 100–110.

Lefebvre, S., Laloux, P., Peeters, A., Desfontaines, P., Jamart, J., and Vandermeeren, Y. (2013b). Dual-tDCS Enhances Online Motor Skill Learning and Long-Term Retention in Chronic Stroke Patients. Front. Hum. Neurosci. *6*.

Lefebvre, S., Dricot, L., Laloux, P., Gradkowski, W., Desfontaines, P., Evrard, F., Peeters, A., Jamart, J., and Vandermeeren, Y. (2015). Neural substrates underlying stimulation-enhanced motor skill learning after stroke. Brain *138*, 149–163.

Leow, L.-A., Hammond, G., and de Rugy, A. (2014). Anodal motor cortex stimulation paired with movement repetition increases anterograde interference but not savings. Eur. J. Neurosci. *40*, 3243–3252.

Li, S.C., Lindenberger, U., and Sikström, S. (2001). Aging cognition: From neuromodulation to representation. Trends Cogn. Sci. *5*, 479–486.

Li, W., Wu, B., Batrachenko, A., Bancroft-Wu, V., Morey, R.A., Shashi, V., Langkammer, C., De Bellis, M.D., Ropele, S., Song, A.W., et al. (2014). Differential developmental trajectories of magnetic susceptibility in human brain gray and white matter over the lifespan. Hum. Brain Mapp. *35*, 2698–2713.

Li, W., Wang, N., Yu, F., Han, H., Cao, W., Romero, R., Tantiwongkosi, B., Duong, T.Q., and Liu, C. (2015). A method for estimating and removing streaking artifacts in quantitative susceptibility mapping. NeuroImage *108*, 111–122.

Liepert, J., Wessel, K., Schwenkreis, P., Trillenberg, P., Otto, V., Vorgerd, M., Malin, J.-P., and Tegenthoff, M. (2009). Reduced intracortical facilitation in patients with cerebellar degeneration. Acta Neurol. Scand. *98*, 318–323.

Lisberger, S., and Thach, T. (2013). The Cerebellum. In Principles of Neural Science, (McGraw-Hill Companies, Inc.), pp. 961–981.

López-Alonso, V., Cheeran, B., Río-Rodríguez, D., and Fernández-del-Olmo, M. (2014). Inter-individual Variability in Response to Non-invasive Brain Stimulation Paradigms. Brain Stimulat. *7*, 372–380.

López-Bastida, J., Perestelo-Pérez, L., Montón-álvarez, F., and Serrano-Aguilar, P. (2008). Social economic costs and health-related quality of life in patients with degenerative cerebellar ataxia in Spain: Costs and Quality of Life in Ataxias. Mov. Disord. *23*, 212–217.

Lukas, C., Schöls, L., Bellenberg, B., Rüb, U., Przuntek, H., Schmid, G., Köster, O., and Suchan, B. (2006). Dissociation of grey and white matter reduction in spinocerebellar ataxia type 3 and 6: a voxel-based morphometry study. Neurosci. Lett. *408*, 230–235.

MacLullich, A.M.J., Edmond, C.L., Ferguson, K.J., Wardlaw, J.M., Starr, J.M., Seckl, J.R., and Deary, I.J. (2004). Size of the neocerebellar vermis is associated with cognition in healthy elderly men. Brain Cogn. *56*, 344–348.

Maderwald, S., Thürling, M., Küper, M., Theysohn, N., Müller, O., Beck, A., Aurich, V., Ladd, M.E., and Timmann, D. (2012). Direct visualization of cerebellar nuclei in patients with focal cerebellar lesions and its application for lesion-symptom mapping. Neuroimage *63*, 1421–1431.

Maeda, F., Keenan, J.P., Tormos, J.M., Topka, H., and Pascual-Leone, A. (2000). Interindividual variability of the modulatory effects of repetitive transcranial magnetic stimulation on cortical excitability. Exp. Brain Res. *133*, 425–430.

Malfait, N., and Ostry, D.J. (2004). Is Interlimb Transfer of Force-Field Adaptation a Cognitive Response to the Sudden Introduction of Load? J. Neurosci. *24*, 8084–8089.

Mandler, G. (1980). Recognizing: The judgment of previous occurrence. Psychol. Rev. *87*, 252–271.

Manjón, J.V., Coupé, P., Martí-Bonmatí, L., Collins, D.L., and Robles, M. (2010). Adaptive non-local means denoising of MR images with spatially varying noise levels. J. Magn. Reson. Imaging *31*, 192–203.

Manni, E., and Petrosini, L. (2004). A century of cerebellar somatotopy: a debated representation. Nat. Rev. Neurosci. *5*, 241–249.

Manto, M.-U. (2005). The wide spectrum of spinocerebellar ataxias (SCAs). The Cerebellum *4*, 2–6.

Manto, M., and Taib, N.O.B. (2008). A novel approach for treating cerebellar ataxias. Med. Hypotheses *71*, 58–60.

Marcus, D.S., Wang, T.H., Parker, J., Csernansky, J.G., Morris, J.C., and Buckner, R.L. (2007). Open Access Series of Imaging Studies (OASIS): cross-sectional MRI data in young, middle aged, nondemented, and demented older adults. J. Cogn. Neurosci. *19*, 1498–1507.

Mariotti, C., Fancellu, R., and Donato, S. (2005). An overview of the patient with ataxia. J. Neurol. *252*, 511–518.

Marko, M.K., Haith, A.M., Harran, M.D., and Shadmehr, R. (2012). Sensitivity to prediction error in reach adaptation. J. Neurophysiol. *108*, 1752–1763.

Marr, D. (1969). A theory of cerebellar cortex. J. Physiol. *202*, 437–470.

Marsden, J., and Harris, C. (2011). Cerebellar ataxia: pathophysiology and rehabilitation. Clin. Rehabil. *25*, 195–216.

Maschke, M., Gomez, C.M., Ebner, T.J., and Konczak, J. (2004a). Hereditary cerebellar ataxia progressively impairs force adaptation during goal-directed arm movements. J. Neurophysiol. *91*, 230–238.

Maschke, M., Weber, J., Dimitrova, A., Bonnet, U., Bohrenkämper, J., Sturm, S., Kindsvater, K., Müller, B.W., Gastpar, M., Diener, H.-C., et al. (2004b). Age-related changes of the dentate nuclei in normal adults as revealed by 3D fast low angle shot (FLASH) echo sequence magnetic resonance imaging. J. Neurol. *251*, 740–746.

Mathis, C., Collin, L., and Borrelli, E. (2003). Oligodendrocyte ablation impairs cerebellum development. Development *130*, 4709–4718.

Matilla-Dueñas, A., Ashizawa, T., Brice, A., Magri, S., McFarland, K.N., Pandolfo, M., Pulst, S.M., Riess, O., Rubinsztein, D.C., Schmidt, J., et al. (2014). Consensus Paper: Pathological Mechanisms Underlying Neurodegeneration in Spinocerebellar Ataxias. The Cerebellum *13*, 269–302.

Mawase, F., Shmuelof, L., Bar-Haim, S., and Karniel, A. (2014). Savings in locomotor adaptation explained by changes in learning parameters following initial adaptation. J. Neurophysiol. *111*, 1444–1454.

Mazzoni, P. (2006). An Implicit Plan Overrides an Explicit Strategy during Visuomotor Adaptation. J. Neurosci. *26*, 3642–3645.

McDougle, S.D., Bond, K.M., and Taylor, J. a. (2015). Explicit and Implicit Processes Constitute the Fast and Slow Processes of Sensorimotor Learning. J. Neurosci. *35*, 9568–9579.

McGibney, G., and Smith, M. (1993). An unbiased signal-to-noise ratio measure for magnetic resonance images. Med. Phys. *20*, 1077–1078.

McNay, E.C., and Willingham, D.B. (1998). Deficit in learning of a motor skill requiring strategy, but not of perceptuomotor recalibration, with aging. Learn. Mem. *4*, 411–420.

Medina, J., and Cason, S. (2017). No evidential value in samples of transcranial direct current stimulation (tDCS) studies of cognition and working memory in healthy populations. Cortex *94*, 131–141.

Medina, J.F., Garcia, K.S., and Mauk, M.D. (2001). A Mechanism for Savings in the Cerebellum. J. Neurosci. *21*, 4081–4089.

Michel, C., Pisella, L., Prablanc, C., Rode, G., and Rossetti, Y. (2007). Enhancing Visuomotor Adaptation by Reducing Error Signals: Single-step (Aware) versus Multiple-step (Unaware) Exposure to Wedge Prisms. J. Cogn. Neurosci. *19*, 341–350.

Middleton, F. (2000). Basal ganglia and cerebellar loops: motor and cognitive circuits. Brain Res. Rev. *31*, 236–250.

Middleton, F.A., and Strick, P.L. (2001). Cerebellar Projections to the Prefrontal Cortex of the Primate. J. Neurosci. *21*, 700 LP – 712.

Miller, A.J., and Joseph, P.M. (1993). The use of power images to perform quantitative analysis on low SNR MR images. Magn. Reson. Imaging *11*, 1051–1056.

Minarik, T., Berger, B., Althaus, L., Bader, V., Biebl, B., Brotzeller, F., Fusban, T., Hegemann, J., Jesteadt, L., Kalweit, L., et al. (2016). The importance of sample size for reproducibility of tDCS effects. Front. Hum. Neurosci. *10*, 453–453.

Mitoma, H., and Manto, M. (2016). The physiological basis of therapies for cerebellar ataxias. Ther. Adv. Neurol. Disord. *9*, 396–413.

Miyai, I., Ito, M., Hattori, N., Mihara, M., Hatakenaka, M., Yagura, H., Sobue, G., and Nishizawa, M. (2012). Cerebellar ataxia rehabilitation trial in degenerative cerebellar diseases. Neurorehabil. Neural Repair *26*, 515–522.

Morehead, J.R., Qasim, S.E., Crossley, M.J., and Ivry, R. (2015). Savings upon Re-Aiming in Visuomotor Adaptation. J. Neurosci. *35*, 14386–14396.

Mosconi, M.W., Luna, B., Kay-Stacey, M., Nowinski, C.V., Rubin, L.H., Scudder, C., Minshew, N., and Sweeney, J.A. (2013). Saccade Adaptation Abnormalities Implicate Dysfunction of Cerebellar-Dependent Learning Mechanisms in Autism Spectrum Disorders (ASD). PLoS ONE *8*, e63709–e63709.

Mostofsky, S.H., Dubey, P.,. Jerath, V.K.,. Jansiewicz, E.M.,. Goldberg, M.C.,.&. Denckla, M.B. (2006). Developmental dyspraxia is not limited to imitation in children with autism spectrum disorders. J. Int. Neuropsychol. Soc. *12*.

Mostofsky, S.H., and Ewen, J.B. (2011). Altered Connectivity and Action Model Formation in Autism Is Autism. The Neuroscientist *17*, 437–448.

Mostofsky, S.H., Powell, S.K., Simmonds, D.J., Goldberg, M.C., Caffo, B., and Pekar, J.J. (2009). Decreased connectivity and cerebellar activity in autism during motor task performance. Brain *132*, 2413–2425.

Mottron, L. (2004). Matching Strategies in Cognitive Research with Individuals with High-Functioning Autism: Current Practices, Instrument Biases, and Recommendations. J. Autism Dev. Disord. *34*, 19–27.

Müller-Dahlhaus, J.F.M., Orekhov, Y., Liu, Y., and Ziemann, U. (2008). Interindividual variability and age-dependency of motor cortical plasticity induced by paired associative stimulation. Exp. Brain Res. *187*, 467–475.

Murakami, J.W., Courchesne, E., Press, G.A., Yeung-Courchesne, R., and Hesselink, J.R. (1989). Reduced Cerebellar Hemisphere Size and Its Relationship to Vermal Hypoplasia in Autism. Arch. Neurol. *46*, 689–694.

Nachbauer, W., Eigentler, A., and Boesch, S. (2015). Acquired ataxias: the clinical spectrum, diagnosis and management. J. Neurol. *262*, 1385–1393.

Nakano, T., Ota, H., Kato, N., and Kitazawa, S. (2009). Deficit in visual temporal integration in autism spectrum disorders. Proc. R. Soc. B Biol. Sci. *277*, 1027–1030.

Nakano, T., Kato, N., and Kitazawa, S. (2012). Superior haptic-to-visual shape matching in autism spectrum disorders. Neuropsychologia *50*, 696–703.

Nisbett, R.E., and Wilson, T.D. (1977). Telling more than we can know: Verbal reports on mental processes. Psychol. Rev. *84*, 231–259.

Nitsche, M.A., and Paulus, W. (2001). Sustained excitability elevations induced by transcranial DC motor cortex stimulation in humans. Neurology *57*, 1899–1901.

Nitsche, M. a, Cohen, L., Wassermann, E.M., Priori, A., Lang, N., Antal, A., Paulus, W., Hummel, F., Boggio, P.S., Fregni, F., et al. (2008). Transcranial direct current stimulation: State of the art 2008. Brain Stimulat. *1*, 206–223.

Nitsche, M.A., Paulus, W., Nitsche, M.A., Paulus, W., and Paulus, W. (2000). Excitability changes induced in the human motor cortex by weak transcranial direct current stimulation. J. Physiol. *527 Pt 3*, 633–639.

Nitsche, M.A., Liebetanz, D., Lang, N., Antal, A., Tergau, F., and Paulus, W. (2003). Safety criteria for transcranial direct current stimulation (tDCS) in humans. Clin. Neurophysiol. *114*, 2220–2222.

Nitschke, M., Kleinschmidt, A., Wessel, K., and Frahm, J. (1996). Somatotopic motor representation in the human anterior cerebellum: A high-resolution functional MRI study. Brain *119*, 1023–1029.

Norman, E., Price, M.C., and Duff, S.C. (2006). Fringe consciousness in sequence learning: The influence of individual differences. Conscious. Cogn. *15*, 723–760.

Nowak, D.A., and Hermsdörfer, J. (2004). Grip force behavior during object manipulation in neurological disorders: Toward an objective evaluation of manual performance deficits. Mov. Disord. *20*, 11–25.

O'Connell, N.E., Cossar, J., Marston, L., Wand, B.M., Bunce, D., Moseley, G.L., and De Souza, L.H. (2012). Rethinking Clinical Trials of Transcranial Direct Current Stimulation: Participant and Assessor Blinding Is Inadequate at Intensities of 2mA. PLoS ONE *7*, e47514.

Oldfield, R.C. (1971). The assessment and analysis of handedness: The Edinburgh inventory. Neuropsychologia *9*, 97–113.

Opitz, A., Paulus, W., Will, S., Antunes, A., and Thielscher, A. (2015). Determinants of the electric field during transcranial direct current stimulation. NeuroImage *109*, 140–150.

Orban de Xivry, J.-J., Criscimagna-Hemminger, S.E., and Shadmehr, R. (2010). Contributions of the Motor Cortex to Adaptive Control of Reaching Depend on the Perturbation Schedule. Cereb. Cortex *21*, 1475–1484.

Orban de Xivry, J.-J., Marko, M.K., Pekny, S.E., Pastor, D., Izawa, J., Celnik, P., and Shadmehr, R. (2011). Stimulation of the Human Motor Cortex Alters Generalization Patterns of Motor Learning. J. Neurosci. *31*, 7102–7110.

Özbay, P.S., Deistung, A., Feng, X., Nanz, D., Reichenbach, J.R., and Schweser, F. (2017). A comprehensive numerical analysis of background phase correction with V-SHARP. NMR Biomed. *30*, e3550.

Pandolfo, M. (2009). Friedreich ataxia: The clinical picture. J. Neurol. *256*, 3–8.

Panouillères, M., and Jenkinson, N. (2015). Reversing motor adaptation deficits in the ageing brain using non-invasive stimulation.

Parazzini, M., Rossi, E., Ferrucci, R., Liorni, I., Priori, A., and Ravazzani, P. (2014). Modelling the electric field and the current density generated by cerebellar transcranial DC stimulation in humans. Clin. Neurophysiol. *125*, 577–584.

Parazzini, M., Fiocchi, S., Liorni, I., and Ravazzani, P. (2015). Effect of the Interindividual Variability on Computational Modeling of Transcranial Direct Current Stimulation. Comput. Intell. Neurosci. *2015*, 1–9.

Parikh, P.J., and Cole, K.J. (2014). Effects of transcranial direct current stimulation in combination with motor practice on dexterous grasping and manipulation in healthy older adults. Physiol. Rep. *2*, e00255.

Parikh, P.J., and Cole, K.J. (2015). Effects of Transcranial Direct Current Stimulation on the Control of Finger Force during Dexterous Manipulation in Healthy Older Adults. PLOS ONE *10*, e0124137.

Park, D.C., and Reuter-Lorenz, P. (2009). The adaptive brain: aging and neurocognitive scaffolding. Annu. Rev. Psychol. *60*, 173–196.

Paul, R., Grieve, S.M., Chaudary, B., Gordon, N., Lawrence, J., Cooper, N., Clark, C.R., Kukla, M., Mulligan, R., and Gordon, E. (2009). Relative contributions of the cerebellar vermis and prefrontal lobe volumes on cognitive function across the adult lifespan. Neurobiol. Aging *30*, 457–465.

11

REFERENCES

Paulson, H.L. (2009). The spinocerebellar ataxias. J. Neuro-Ophthalmol. Off. J. North Am. Neuro-Ophthalmol. Soc. *29*, 227–237.

Pavone, P., Praticò, A.D., Pavone, V., Lubrano, R., Falsaperla, R., Rizzo, R., and Ruggieri, M. (2017). Ataxia in children: early recognition and clinical evaluation. Ital. J. Pediatr. *43*.

Peled, A., and Karniel, A. (2012). Knowledge of Performance is Insufficient for Implicit Visuomotor Rotation Adaptation. J. Mot. Behav. *44*, 185–194.

Perlmutter, E., and Gregory, P.C. (2003). Rehabilitation Treatment Options for a Patient with Paraneoplastic Cerebellar Degeneration: Am. J. Phys. Med. Rehabil. *82*, 158–162.

Persson, N., Wu, J., Zhang, Q., Liu, T., Shen, J., Bao, R., Ni, M., Liu, T., Wang, Y., and Spincemaille, P. (2015). Age and sex related differences in subcortical brain iron concentrations among healthy adults. Neuroimage *122*, 385–398.

Peters, A.M., Brookes, M.J., Hoogenraad, F.G., Gowland, P.A., Francis, S.T., Morris, P.G., and Bowtell, R. (2007). T2* measurements in human brain at 1.5, 3 and 7 T. Magn. Reson. Imaging *25*, 748–753.

Plummer, M. (2003). JAGS: A program for analysis of Bayesian graphical models using Gibbs sampling. Proc. 3rd Int. Workshop Distrib. Stat. Comput. DSC 2003 20–22.

Popa, L.S., Streng, M.L., Hewitt, A.L., and Ebner, T.J. (2016). The Errors of Our Ways: Understanding Error Representations in Cerebellar-Dependent Motor Learning. The Cerebellum *15*, 93–103.

Pope, P.A., and Miall, R.C. (2012). Task-specific facilitation of cognition by cathodal transcranial direct current stimulation of the cerebellum. Brain Stimulat. *5*, 84–94.

Pozzi, N.G., Minafra, B., Zangaglia, R., Marzi, R.D., Sandrini, G., Priori, A., and Pacchetti, C. (2013). Transcranial Direct Current Stimulation (tDCS) of the Cortical Motor Areas in Three Cases of Cerebellar Ataxia. The Cerebellum *13*, 109–112.

Price, M., Cardenas, V. a., and Fein, G. (2014). Automated MRI cerebellar size measurements using active appearance modeling. NeuroImage *103*, 511–521.

Prichard, G., Weiller, C., Fritsch, B., and Reis, J. (2014). Effects of Different Electrical Brain Stimulation Protocols on Subcomponents of Motor Skill Learning. Brain Stimulat. *7*, 532–540.

Provost, B., Lopez, B.R., and Heimerl, S. (2006). A Comparison of Motor Delays in Young Children: Autism Spectrum Disorder, Developmental Delay, and Developmental Concerns. J. Autism Dev. Disord. *37*, 321–328.

Pulst, S.M. (2016). Degenerative ataxias, from genes to therapies: The 2015 Cotzias Lecture. Neurology *86*, 2284–2290.

Rabe, K., Livne, O., Gizewski, E.R., Aurich, V., Beck, A., Timmann, D., and Donchin, O. (2009). Adaptation to Visuomotor Rotation and Force Field Perturbation Is Correlated to Different Brain Areas in Patients With Cerebellar Degeneration. J. Neurophysiol. *101*, 1961–1971.

Rahman, A., Reato, D., Arlotti, M., Gasca, F., Datta, A., Parra, L.C., and Bikson, M. (2013). Cellular effects of acute direct current stimulation: somatic and synaptic terminal effects. J. Physiol. *591*, 2563–2578.

Rahman, A., Toshev, P.K., and Bikson, M. (2014). Polarizing cerebellar neurons with transcranial Direct Current Stimulation. Clin. Neurophysiol. *125*, 435–438.

Ramos, P., Santos, A., Pinto, N.R., Mendes, R., Magalhães, T., and Almeida, A. (2014). Iron levels in the human brain: a post-mortem study of anatomical region differences and age-related changes. J. Trace Elem. Med. Biol. *28*, 13–17.

Rampersad, S.M., Janssen, A.M., Lucka, F., Aydin, U., Lanfer, B., Lew, S., Wolters, C.H., Stegeman, D.F., and Oostendorp, T.F. (2014). Simulating Transcranial Direct Current Stimulation With a Detailed Anisotropic Human Head Model. IEEE Trans. Neural Syst. Rehabil. Eng. *22*, 441–452.

Raz, N., Dupuis, J.H., Briggs, S.D., McGavran, C., and Acker, J.D. (1998). Differential effects of age and sex on the cerebellar hemispheres and the vermis: A prospective MR study. Am. J. Neuroradiol. *19*, 65–71.

Raz, N., Williamson, A., Gunning-Dixon, F., Head, D., and Acker, J.D. (2000). Neuroanatomical and cognitive correlates of adult age differences in acquisition of a perceptual-motor skill. Microsc. Res. Tech. *51*, 85–93.

Raz, N., Gunning-Dixon, F., Head, D., Williamson, A., and Acker, J.D. (2001). Age and Sex Differences in the Cerebellum and the Ventral Pons: A Prospective MR Study of Healthy Adults. 7.

Reber, P.J., and Squire, L.R. (1994). Parallel brain systems for learning with and without awareness. Learn. Mem. *1*, 217–229.

Reetz, K., Costa, A.S., Mirzazade, S., Lehmann, A., Juzek, A., Rakowicz, M., Boguslawska, R., Schöls, L., Linnemann, C., Mariotti, C., et al. (2013). Genotype-specific patterns of atrophy progression are more sensitive than clinical decline in SCA1, SCA3 and SCA6. Brain *136*, 905–917.

Reichenbach, J.R., and Haacke, E.M. (2001). High-resolution BOLD venographic imaging: a window into brain function. NMR Biomed. Int. J. Devoted Dev. Appl. Magn. Reson. Vivo *14*, 453–467.

Reingold, E., and Merikle, P. (1990). On the Inter-relatedness of Theory and Measurement in the Study of Unconscious Processes. Mind Lang. *5*, 9–28.

Reis, J., and Fritsch, B. (2011). Modulation of motor performance and motor learning by transcranial direct current stimulation: Curr. Opin. Neurol. *24*, 590–596.

Reis, J., Schambra, H.M., Cohen, L.G., Buch, E.R., Fritsch, B., Zarahn, E., Celnik, P. a, and Krakauer, J.W. (2009). Noninvasive cortical stimulation enhances motor skill acquisition over multiple days through an effect on consolidation. Proc. Natl. Acad. Sci. U. S. A. *106*, 1590–1595.

Reis, J., Fischer, J.T., Prichard, G., Weiller, C., Cohen, L.G., and Fritsch, B. (2015). Time- but Not Sleep-Dependent Consolidation of tDCS-Enhanced Visuomotor Skills. Cereb. Cortex *25*, 109–117.

Ridding, M., and Ziemann, U. (2010). Determinants of the induction of cortical plasticity by non-invasive brain stimulation in healthy subjects. J. Physiol. *588*, 2291–2304.

Ritvo E, F.B., Scheibel A, Duong T, Robinson H, Guthrie D. (1986). Lower Purkinje cell counts in the cerebella of four autistic subjects: initial findings of the UCLA-NSAC Autopsy Research Report. Am. J. Psychiatry *143*, 862–866.

Roemer, P.B., Edelstein, W.A., Hayes, C.E., Souza, S.P., and Mueller, O.M. (1990). The NMR phased array. Magn. Reson. Med. *16*, 192–225.

Rost, K., Nowak, D.A., Timmann, D., and Hermsdörfer, J. (2005). Preserved and impaired aspects of predictive grip force control in cerebellar patients. Clin. Neurophysiol. *116*, 1405–1414.

Ruano, L., Melo, C., Silva, M.C., and Coutinho, P. (2014). The global epidemiology of hereditary ataxia and spastic paraplegia: A systematic review of prevalence studies. Neuroepidemiology *42*, 174–183.

Ruigrok, T.J.H. (2011). Ins and Outs of Cerebellar Modules. The Cerebellum *10*, 464–474.

Russell, M.J., Goodman, T., Pierson, R., Shepherd, S., Wang, Q., Groshong, B., and Wiley, D.F. (2013). Individual differences in transcranial electrical stimulation current density. J. Biomed. Res. *27*, 495.

Sakurai, M. (1987). Synaptic modification of parallel fibre-Purkinje cell transmission in in vitro guinea-pig cerebellar slices. J. Physiol. *394*, 463–480.

Sanes, J.N., Dimitrov, B., and Hallett, M. (1990). Motor learning in patients with cerebellar dysfunction. Brain J. Neurol. *113 (Pt 1*, 103–120.

Sapir, S., Spielman, J., Ramig, L.O., Hinds, S.L., Countryman, S., Fox, C., and Story, B. (2003). Effects of Intensive Voice Treatment (the Lee Silverman Voice Treatment [LSVT]) on Ataxic Dysarthria: A Case Study. 13.

Sarva, H., and Shanker, V.L. (2014). Treatment Options in Degenerative Cerebellar Ataxia: A Systematic Review. Mov. Disord. Clin. Pract. *1*, 291–298.

Sasaki, H., Kojima, H., Yabe, I., Tashiro, K., Hamada, T., Sawa, H., Hiraga, H., and Nagashima, K. (1998). Neuropathological and molecular studies of spinocerebellar ataxia type 6 (SCA6). Acta Neuropathol. (Berl.) *95*, 199–204.

Schäfer, A., Wharton, S., Gowland, P., and Bowtell, R. (2009). Using magnetic field simulation to study susceptibility-related phase contrast in gradient echo MRI. Neuroimage *48*, 126–137.

Scheidt, R.A. (2005). Interaction of Visual and Proprioceptive Feedback During Adaptation of Human Reaching Movements. J. Neurophysiol. *93*, 3200–3213.

Schlerf, J.E., Xu, J., Klemfuss, N.M., Griffiths, T.L., and Ivry, R.B. (2013). Individuals with cerebellar degeneration show similar adaptation deficits with large and small visuomotor errors. J. Neurophysiol. *109*, 1164–1173.

Schmahmann, J.D. (1991). An Emerging Concept: The Cerebellar Contribution to Higher Function. Arch. Neurol. *48*, 1178.

Schmahmann, J.D., and Sherman, J.C. (1998). The cerebellar cognitive affective syndrome. Brain *121*, 561–579.

Schmitz-Hübsch, T., Du Montcel, S.T., Baliko, L., Berciano, J., Boesch, S., Depondt, C., Giunti, P., Globas, C., Infante, J., Kang, J.S., et al. (2006). Scale for the assessment and rating of ataxia. Neurology *66*, 1717–1720.

Schmitz-Hübsch, T., Coudert, M., Bauer, P., Giunti, P., Globas, C., Baliko, L., Filla, A., Mariotti, C., Rakowicz, M., Charles, P., et al. (2008a). Spinocerebellar ataxia types 1, 2, 3, and 6: disease severity and nonataxia symptoms. Neurology *71*, 982–989.

Schmitz-Hübsch, T., Giunti, P., Stephenson, D., Globas, C., Balikó, L., Saccà, F., Mariotti, C., Rakowicz, M., Szymanski, S., Infante, J., et al. (2008b). SCA Functional Index: a useful compound performance measure for spinocerebellar ataxia. Neurology *71*, 486–492.

Schmitz-Hübsch, T., Coudert, M., Giunti, P., Globas, C., Baliko, L., Fancellu, R., Mariotti, C., Filla, A., Rakowicz, M., Charles, P., et al. (2010). Self-rated health status in spinocerebellar ataxia-Results from a European multicenter study. Mov. Disord. *25*, 587–595.

Schoch, B., Dimitrova, A., Gizewski, E.R., and Timmann, D. (2006). Functional localization in the human cerebellum based on voxelwise statistical analysis: A study of 90 patients. NeuroImage *30*, 36–51.

Schöls, L., Amoiridis, G., Büttner, T., Przuntek, H., Epplen, J.T., and Riess, O. (1997). Autosomal dominant cerebellar ataxia: Phenotypic differences in genetically defined subtypes?: Phenotypes in Dominant Ataxias. Ann. Neurol. *42*, 924–932.

Schöls, L., Krüger, R., Amoiridis, G., Przuntek, H., Epplen, J.T., and Riess, O. (1998). Spinocerebellar ataxia type 6: genotype and phenotype in German kindreds. J. Neurol. Neurosurg. Psychiatry *64*, 67–73.

Schöls, L., Bauer, P., Schmidt, T., Schulte, T., and Riess, O. (2004). Autosomal dominant cerebellar ataxias: clinical features, genetics, and pathogenesis. Lancet Neurol. *3*, 291–304.

Schonewille, M., Gao, Z., Boele, H.-J., Vinueza Veloz, M.F., Amerika, W.E., Šimek, A.A.M., De Jeu, M.T., Steinberg, J.P., Takamiya, K., Hoebeek, F.E., et al. (2011). Reevaluating the Role of LTD in Cerebellar Motor Learning. Neuron *70*, 43–50.

Schuirmann, D.J. (1987). A comparison of the Two One-Sided Tests Procedure and the Power Approach for assessing the equivalence of average bioavailability. J. Pharmacokinet. Biopharm. *15*, 657–680.

Schulz, J.B., Borkert, J., Wolf, S., Schmitz-Hübsch, T., Rakowicz, M., Mariotti, C., Schoels, L., Timmann, D., van de Warrenburg, B., Dürr, A., et al. (2010). Visualization, quantification and correlation of brain atrophy with clinical symptoms in spinocerebellar ataxia types 1, 3 and 6. Neuroimage *49*, 158–168.

Schween, R., Taube, W., Gollhofer, A., and Leukel, C. (2014). Online and post-trial feedback differentially affect implicit adaptation to a visuomotor rotation. Exp. Brain Res. *232*, 3007–3013.

Schweser, F., Deistung, A., Lehr, B.W., and Reichenbach, J.R. (2011). Quantitative imaging of intrinsic magnetic tissue properties using MRI signal phase: an approach to in vivo brain iron metabolism? Neuroimage *54*, 2789–2807.

Schweser, F., Sommer, K., Deistung, A., and Reichenbach, J.R. (2012). Quantitative susceptibility mapping for investigating subtle susceptibility variations in the human brain. Neuroimage *62*, 2083–2100.

Schweser, F., Hagemeier, J., Dwyer, M., Bergsland, N., Dhamankar, A., Weinstock-Guttman, B., and Zivadinov, R. (2018). Assessment of the total iron mass using Quantitative Susceptibility Mapping (QSM): Deep gray matter iron depletion in multiple sclerosis? p.

Scoles, D.R., Meera, P., Schneider, M.D., Paul, S., Dansithong, W., Figueroa, K.P., Hung, G., Rigo, F., Bennett, C.F., Otis, T.S., et al. (2017). Antisense oligonucleotide therapy for spinocerebellar ataxia type 2. Nature *544*, 362–366.

Scott, J.A., Schumann, C.M., Goodlin-Jones, B.L., and Amaral, D.G. (2009). A comprehensive volumetric analysis of the cerebellum in children and adolescents with autism spectrum disorder. Autism Res. *2*, 246–257.

Seaman, M. a., and Serlin, R.C. (1998). Equivalence confidence intervals for two-group comparisons of means. Psychol. Methods *3*, 403–411.

Seidler, R.D., Bernard, J. a., Burutolu, T.B., Fling, B.W., Gordon, M.T., Gwin, J.T., Kwak, Y., and Lipps, D.B. (2010). Motor control and aging: Links to age-related brain structural, functional, and biochemical effects. Neurosci. Biobehav. Rev. *34*, 721–733.

Shabbott, B.A., and Sainburg, R.L. (2010). Learning a visuomotor rotation: simultaneous visual and proprioceptive information is crucial for visuomotor remapping. Exp. Brain Res. *203*, 75–87.

Shadmehr, R., and Krakauer, J.W. (2008). A COMPUTATIONAL NEUROANATOMY FOR MOTOR CONTROL. Exp. Brain Res. Exp. Hirnforsch. Exp. Cerebrale *185*, 359–381.

Shadmehr, R., and Mussa-Ivaldi, F.A. (1994). Adaptive Representation of Dynamics During Learning of a Motor Task. J. Neurosci. *14*, 3208–3224.

Shadmehr, R., and Wise, S.P. (2005). The computational neurobiology of reaching and pointing: a foundation for motor learning (MIT press).

Shadmehr, R., Smith, M. a, and Krakauer, J.W. (2010). Error correction, sensory prediction, and adaptation in motor control. Annu. Rev. Neurosci. *33*, 89–108.

Shanks, D.R., and St. John, M.F. (1994). Characteristics of dissociable human learning systems. Behav. Brain Sci. *17*, 367–395.

Shanks, D.R., Rowland, L.A., and Ranger, M.S. (2005). Attentional load and implicit sequence learning. Psychol. Res. Psychol. Forsch. *69*, 369–382.

Siebner, H.R., Lang, N., Rizzo, V., Nitsche, M.A., Paulus, W., Lemon, R.N., and Rothwell, J.C. (2004). Preconditioning of low-frequency repetitive transcranial magnetic stimulation with transcranial direct current stimulation: evidence for homeostatic plasticity in the human motor cortex. J. Neurosci. *24*, 3379–3385.

Silva, R.C.R., Saute, J.A.M., Silva, A.C.F., Coutinho, A.C.O., Saraiva-Pereira, M.L., and Jardim, L.B. (2010). Occupational therapy in spinocerebellar ataxia type 3: an open-label trial. Braz. J. Med. Biol. Res. *43*, 537–542.

Silvanto, J., Muggleton, N., and Walsh, V. (2008). State-dependency in brain stimulation studies of perception and cognition. Trends Cogn. Sci. *12*, 447–454.

Sing, G.C., and Smith, M.A. (2010). Reduction in learning rates associated with anterograde interference results from interactions between different timescales in motor adaptation. PLoS Comput. Biol. *6*, e1000893.

Sing, G., Najafi, B., Adewuyi, A., and Smith, M. (2009). A mechanism for the spacing effect: Competitive inhibition between adaptive processes explains the increase in motor skill retention associated with prolonged inter-trial spacing. Adv. Comput. Mot. Control Chic. IL.

Slachevsky, A., Pillon, B., Fourneret, P., Pradat-Diehl, P., Jeannerod, M., and Dubois, B. (2001). Preserved Adjustment but Impaired Awareness in a Sensory-Motor Conflict following Prefrontal Lesions. J. Cogn. Neurosci. *13*, 332–340.

Smith, M. a, and Shadmehr, R. (2005). Intact ability to learn internal models of arm dynamics in Huntington's disease but not cerebellar degeneration. J. Neurophysiol. *93*, 2809–2821.

Smith, M.A., Ghazizadeh, A., and Shadmehr, R. (2006). Interacting Adaptive Processes with Different Timescales Underlie Short-Term Motor Learning. PLoS Biol *4*, e179.

Snider, R., and Stowell, A. (1944). Receiving areas of the tactile, auditory, and visual systems in the cerebellum. J. Neurophysiol. *7*, 331–357.

Sparks, B.F., Friedman, S.D., Shaw, D.W., Aylward, E.H., Echelard, D., Artru, A.A., Maravilla, K.R., Giedd, J.N., Munson, J., Dawson, G., et al. (2002). Brain structural abnormalities in young children with autism spectrum disorder. Neurology *59*, 184–192.

Sriraman, A., Oishi, T., and Madhavan, S. (2014). Timing-dependent priming effects of tDCS on ankle motor skill learning. Brain Res. *1581*, 23–29.

Stagg, C.J., and Nitsche, M.A. (2011). Physiological basis of transcranial direct current stimulation. Neuroscientist *17*, 37–53.

Stagg, C.J., Bachtiar, V., and Johansen-Berg, H. (2011a). The Role of GABA in Human Motor Learning. Curr. Biol. *21*, 480–484.

Stagg, C.J., Jayaram, G., Pastor, D., Kincses, Z.T., Matthews, P.M., and Johansen-Berg, H. (2011b). Polarity and timing-dependent effects of transcranial direct current stimulation in explicit motor learning. Neuropsychologia *49*, 800–804.

Stanfield, A.C., McIntosh, A.M., Spencer, M.D., Philip, R., Gaur, S., and Lawrie, S.M. (2008). Towards a neuroanatomy of autism: A systematic review and meta-analysis of structural magnetic resonance imaging studies. Eur. Psychiatry *23*, 289–299.

Stefanescu, M.R., Dohnalek, M., Maderwald, S., Thürling, M., Minnerop, M., Beck, A., Schlamann, M., Diedrichsen, J., Ladd, M.E., and Timmann, D. (2015). Structural and functional MRI abnormalities of cerebellar cortex and nuclei in SCA3, SCA6 and Friedreich's ataxia. Brain *138*, 1182–1197.

Steiner, K.M., Enders, A., Thier, W., Batsikadze, G., Ludolph, N., Ilg, W., and Timmann, D. (2016). Cerebellar tDCS Does Not Improve Learning in a Complex Whole Body Dynamic Balance Task in Young Healthy Subjects. PLOS ONE *11*, e0163598.

Steinlin, M. (1998a). Non-progressive congenital ataxias. Brain Dev. *20*, 199–208.

Steinlin, M. (1998b). Non-progressive congenital ataxia with or without cerebellar hypoplasia: a review of 34 subjects. Dev. Med. Child Neurol. *40*, 148–154.

Stieglitz Ham, H., Corley, M., Rajendran, G., Carletta, J., and Swanson, S. (2007). Brief Report: Imitation of Meaningless Gestures in Individuals with Asperger Syndrome and High-functioning Autism. J. Autism Dev. Disord. *38*, 569–573.

Stoodley, C.J., and Schmahmann, J.D. (2009). Functional topography in the human cerebellum: A meta-analysis of neuroimaging studies. NeuroImage *44*, 489–501.

Stoodley, C.J., and Schmahmann, J.D. (2010). Evidence for topographic organization in the cerebellum of motor control versus cognitive and affective processing. Cortex *46*, 831–844.

Strick, P.L., Dum, R.P., and Fiez, J.A. (2009). Cerebellum and Nonmotor Function. Annu. Rev. Neurosci. *32*, 413–434.

Strupp, M., Kalla, R., Claassen, J., Adrion, C., Mansmann, U., Klopstock, T., Freilinger, T., Neugebauer, H., Spiegel, R., Dichgans, M., et al. (2011). A randomized trial of 4-aminopyridine in EA2 and related familial episodic ataxias. 7.

Sullivan, E.V., and Pfefferbaum, A. (2006). Diffusion tensor imaging and aging. Neurosci. Biobehav. Rev. *30*, 749–761.
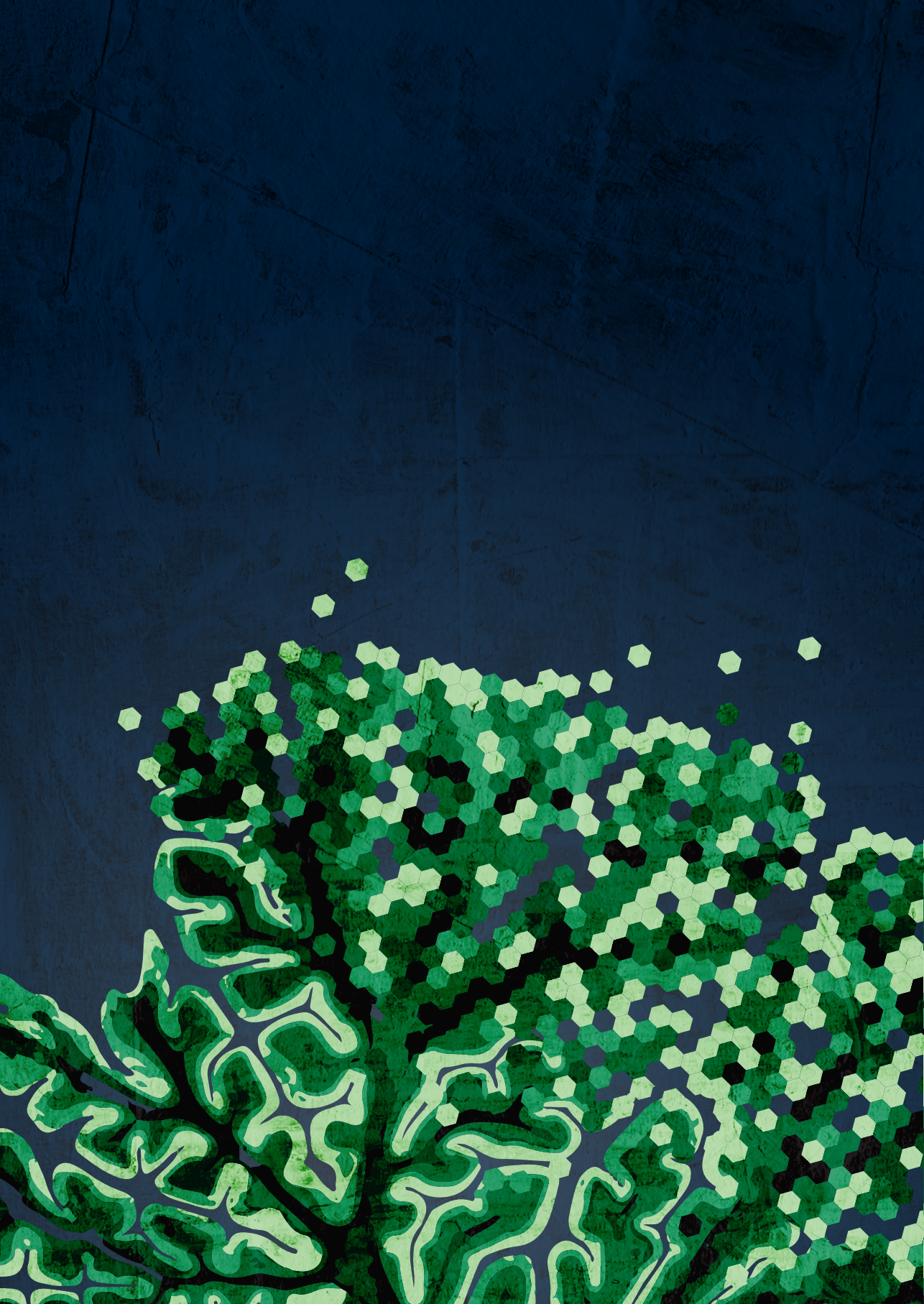
Sultan, F., König, T., Möck, M., and Thier, P. (2002). Quantitative organization of neurotransmitters in the deep cerebellar nuclei of the Lurcher mutant. J. Comp. Neurol. *452*, 311–323.

Sülzenbrück, S., and Heuer, H. (2009). Functional independence of explicit and implicit motor adjustments. Conscious. Cogn. *18*, 145–159.

Taig, E., Küper, M., Theysohn, N., Timmann, D., and Donchin, O. (2012). Deficient use of visual information in estimating hand position in cerebellar patients. J. Neurosci. Off. J. Soc. Neurosci. *32*, 16274–16284.

Tavano, A., Grasso, R., Gagliardi, C., Triulzi, F., Bresolin, N., Fabbro, F., and Borgatti, R. (2007). Disorders of cognitive and affective development in cerebellar malformations. Brain *130*, 2646–2660.

Taylor, J.A., and Ivry, R.B. (2011). Flexible Cognitive Strategies during Motor Learning. PLoS Comput. Biol. *7*, e1001096–e1001096.

Taylor, J.A., and Ivry, R.B. (2014). Cerebellar and Prefrontal Cortex Contributions to Adaptation, Strategies, and Reinforcement Learning. Prog. Brain Res. 217–253.

Taylor, J.A., Klemfuss, N.M., and Ivry, R.B. (2010). An Explicit Strategy Prevails When the Cerebellum Fails to Compute Movement Errors. The Cerebellum *9*, 580–586.

Taylor, J.A., Wojaczynski, G.J., and Ivry, R.B. (2011). Trial-by-trial analysis of intermanual transfer during visuomotor adaptation. J. Neurophysiol. *106*, 3157–3172.

Taylor, J.A., Krakauer, J.W., and Ivry, R.B. (2014). Explicit and Implicit Contributions to Learning in a Sensorimotor Adaptation Task. J. Neurosci. *34*, 3023–3032.

Tellmann, S., Bludau, S., Eickhoff, S., Mohlberg, H., Minnerop, M., and Amunts, K. (2015). Cytoarchitectonic mapping of the human brain cerebellar nuclei in stereotaxic space and delineation of their co-activation patterns. Front. Neuroanat. *9*, 54.

Tezenas du Montcel, S., Durr, A., Rakowicz, M., Nanetti, L., Charles, P., Sulek, A., Mariotti, C., Rola, R., Schols, L., Bauer, P., et al. (2014). Prediction of the age at onset in spinocerebellar ataxia type 1, 2, 3 and 6. J. Med. Genet. *51*, 479–486.

Therrien, A.S., Wolpert, D.M., and Bastian, A.J. (2016). Effective reinforcement learning following cerebellar damage requires a balance between exploration and motor noise. Brain *139*, 101–114.

Thieme, A., Thürling, M., Galuba, J., Burciu, R.G., Göricke, S., Beck, A., Aurich, V., Wondzinski, E., Siebler, M., Gerwig, M., et al. (2013). Storage of a naturally acquired conditioned response is impaired in patients with cerebellar degeneration. Brain *136*, 2063–2076.

Thomas Yeo, B.T., Krienen, F.M., Sepulcre, J., Sabuncu, M.R., Lashkari, D., Hollinshead, M., Roffman, J.L., Smoller, J.W., Zöllei, L., Polimeni, J.R., et al. (2011). The organization of the human cerebral cortex estimated by intrinsic functional connectivity. J. Neurophysiol. *106*, 1125–1165.

Thoroughman, K.A., and Shadmehr, R. (2000). Learning of action through adaptative combination of motor primitives. Nature *407*, 742–747.

Tiemeier, H., Lenroot, R.K., Greenstein, D.K., Tran, L., Pierson, R., and Giedd, J.N. (2010). Cerebellum development during childhood and adolescence: A longitudinal morphometric MRI study. NeuroImage *49*, 63–70.

Timmann, D., and Daum, I. (2007). Cerebellar contributions to cognitive functions: a progress report after two decades of research. Cerebellum Lond. Engl. *6*, 159–162.

Timmann, D., and Daum, I. (2010). How consistent are cognitive impairments in patients with cerebellar disorders? Behav. Neurol. *23*, 81–100.

Timmann, D., and Diener, H. (2007). Coordination and Ataxia. In Textbook of Clinical Neurology, (Philadelphia: Saunders Elsevier), pp. 307–325.

Timmann, D., Konczak, J., Ilg, W., Donchin, O., Hermsdörfer, J., Gizewski, E.R., and Schoch, B. (2009). Current advances in lesion-symptom mapping of the human cerebellum. Neuroscience *162*, 836–851.

Todorov, E., and Jordan, M.I. (2002). Optimal feedback control as a theory of motor coordination. Nat. Neurosci. *5*, 1226–1235.

Toonen, L.J.A., Rigo, F., van Attikum, H., and van Roon-Mom, W.M.C. (2017). Antisense Oligonucleotide-Mediated Removal of the Polyglutamine Repeat in Spinocerebellar Ataxia Type 3 Mice. Mol. Ther. - Nucleic Acids *8*, 232–242.

Torvik, A., Torp, S., and Lindboe, C.F. (1986). Atrophy of the cerebellar vermis in ageing. J. Neurol. Sci. *76*, 283–294.

Trewartha, K.M., Garcia, a., Wolpert, D.M., and Flanagan, J.R. (2014). Fast But Fleeting: Adaptive Motor Learning Processes Associated with Aging and Cognitive Decline. J. Neurosci. *34*, 13411–13421.

Triarhou, L., Norton, J., and Ghetti, B. (1987). Anterograde transsynaptic degeneration in the deep cerebellar nuclei of Purkinje cell degeneration (pcd) mutant mice. Exp. Brain Res. *66*, 577–588.

Trouillas, P, Takayanagi, T., Hallett, M., Currier, R.D., Subramony, S.H., Wessel, K., Bryer, A., Diener, H.C., Massaquoi, S., Gomez, C.M., et al. (1997). International Cooperative Ataxia Rating Scale for pharmacological assessment of the cerebellar syndrome. J. Neurol. Sci. *145*, 205–211.

Tseng, Y.-W., Diedrichsen, J., Krakauer, J.W., Shadmehr, R., and Bastian, A.J. (2007). Sensory Prediction Errors Drive Cerebellum-Dependent Adaptation of Reaching. J. Neurophysiol. *98*, 54–62.

Tsou, A.Y., Paulsen, E.K., Lagedrost, S.J., Perlman, S.L., Mathews, K.D., Wilmot, G.R., Ravina, B., Koeppen, A.H., and Lynch, D.R. (2011). Mortality in Friedreich Ataxia. J. Neurol. Sci. *307*, 46–49.

Ugawa, Y., Genba-Shimizu, K., Rothwell, J.C., Iwata, M., and Kanazawa, I. (1994). Suppression of motor cortical excitability by electrical stimulation over the cerebellum in ataxia. Ann. Neurol. *36*, 90–96.

Van Essen, D.C., Smith, S.M., Barch, D.M., Behrens, T.E.J., Yacoub, E., and Ugurbil, K. (2013). The WU-Minn Human Connectome Project: An overview. NeuroImage *80*, 62–79.

Vanvuchelen, M., Roeyers, H., and De Weerdt, W. (2007). Nature of motor imitation problems in school-aged boys with autism. Autism *11*, 225–240.

Velázquez-Pérez, L., Rodríguez-Labrada, R., García-Rodríguez, J.C., Almaguer-Mederos, L.E., Cruz-Mariño, T., and Laffita-Mesa, J.M. (2011). A Comprehensive Review of Spinocerebellar Ataxia Type 2 in Cuba. The Cerebellum *10*, 184–198.

Venkatakrishnan, A., Banquet, J.P., Burnod, Y., and Contreras-vidal, J.L. (2011). Parkinson's disease differentially affects adaptation to gradual as compared to sudden visuomotor distortions. Hum. Mov. Sci. *30*, 760–769.

Verstynen, T., and Sabes, P.N. (2011). How Each Movement Changes the Next: An Experimental and Theoretical Study of Fast Adaptive Priors in Reaching. J. Neurosci. *31*, 10050–10059.

van der Vliet, R., Ribbers, G.M., Vandermeeren, Y., Frens, M.A., and Selles, R.W. (2017). BDNF Val66Met but not transcranial direct current stimulation affects motor learning after stroke. Brain Stimulat. *10*, 882–892.

van der Vliet, R., Frens, M.A., de Vreede, L., Jonker, Z.D., Ribbers, G.M., Selles, R.W., van der Geest, J.N., and Donchin, O. (2018). Individual Differences in Motor Noise and Adaptation Rate Are Optimally Related. Eneuro *5*, ENEURO.0170-18.2018.

Voogd, J., and Ruigrok, T.J.H. (2012). Chapter 15 - Cerebellum and Precerebellar Nuclei. In The Human Nervous System (Third Edition), J.K. Mai, and G. Paxinos, eds. (San Diego: Academic Press), pp. 471–545.

Wang, J., Joshi, M., and Lei, Y. (2011). The extent of interlimb transfer following adaptation to a novel visuomotor condition does not depend on awareness of the condition. J. Neurophysiol. *106*, 259–264.

Wang, X., Wang, H., Xia, Y., Jiang, H., Shen, L., Wang, S., Shen, R., Huang, L., Wang, J., Xu, Q., et al. (2010). A neuropathological study at autopsy of early onset spinocerebellar ataxia 6. J. Clin. Neurosci. *17*, 751–755.

van de Warrenburg, B.P.C., Sinke, R.J., Verschuuren-Bemelmans, C.C., Scheffer, H., Brunt, E.R., Ippel, P.F., Maat-Kievit, J.A., Dooijes, D., Notermans, N.C., Lindhout, D., et al. (2002). Spinocerebellar ataxias in the Netherlands: Prevalence and age at onset variance analysis. Neurology *58*, 702–708.

Wei, K. (2010). Uncertainty of feedback and state estimation determines the speed of motor adaptation. Front. Comput. Neurosci.

Wei, K., and Kording, K. (2008). Relevance of Error: What Drives Motor Adaptation? J. Neurophysiol. *101*, 655–664.

Werner, S., and Bock, O. (2007). Effects of variable practice and declarative knowledge on sensorimotor adaptation to rotated visual feedback. Exp. Brain Res. *178*, 554–559.

Werner, S., Schorn, C.F., Bock, O., Theysohn, N., and Timmann, D. (2014). Neural correlates of adaptation to gradual and to sudden visuomotor distortions in humans. Exp. Brain Res. *232*, 1145–1156.

Wessel, M.J., Zimerman, M., Timmermann, J.E., Heise, K.F., Gerloff, C., and Hummel, F.C. (2016). Enhancing Consolidation of a New Temporal Motor Skill by Cerebellar Noninvasive Stimulation. Cereb. Cortex *26*, 1660–1667.

Whitney, E.R., Kemper, T.L., Bauman, M.L., Rosene, D.L., and Blatt, G.J. (2008). Cerebellar Purkinje Cells are Reduced in a Subpopulation of Autistic Brains: A Stereological Experiment Using Calbindin-D28k. The Cerebellum *7*, 406–416.

Wiethoff, S., Hamada, M., and Rothwell, J.C. (2014). Variability in Response to Transcranial Direct Current Stimulation of the Motor Cortex. Brain Stimulat. *7*, 468–475.

Wild, K.S., Poliakoff, E., Jerrison, A., and Gowen, E. (2011). Goal-Directed and Goal-Less Imitation in Autism Spectrum Disorder. J. Autism Dev. Disord. *42*, 1739–1749.
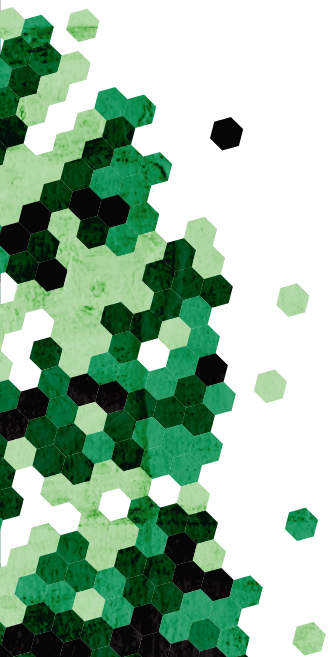
Wilkinson, L., and Shanks, D.R. (2004). Intentional Control and Implicit Sequence Learning. J. Exp. Psychol. Learn. Mem. Cogn. *30*, 354–369.

Williams, E. (1949). Experimental designs balanced for the estimation of residual effects of treatments. Aust. J. Chem. *2*, 149–168.

Williams, J.H.G., Whiten, A., and Singh, T. (2004). A Systematic Review of Action Imitation in Autistic Spectrum Disorder. J. Autism Dev. Disord. *34*, 285–299.

Willingham, D.B., Nissen, M.J., and Bullemer, P. (1989). On the development of procedural knowledge. J. Exp. Psychol. Learn. Mem. Cogn. *15*, 1047–1060.

Willingham, D.B., Salidis, J., and Gabrieli, J.D.E. (2002). Direct comparison of neural systems mediating conscious and unconscious skill learning. J. Neurophysiol. *88*, 1451–1460.

Wong, A.L., and Shelhamer, M. (2011). Saccade adaptation improves in response to a gradually introduced stimulus perturbation. Neurosci. Lett. *500*, 207–211.

Wong, A.L., Marvel, C.L., Taylor, J.A., and Krakauer, J.W. (2018). Can patients with cerebellar disease switch learning mechanisms to reduce their adaptation deficits? (Neuroscience).

Woodruff-Pak, D.S., Vogel, R.W., Ewers, M., Coffey, J., Boyko, O.B., and Lemieux, S.K. (2001). MRI-assessed volume of cerebellum correlates with associative learning. Neurobiol. Learn. Mem. *76*, 342–357.

Woods, A.J., Antal, A., Bikson, M., Boggio, P.S., Brunoni, A.R., Celnik, P, Cohen, L.G., Fregni, F., Herrmann, C.S., Kappenman, E.S., et al. (2015). A technical guide to tDCS, and related non-invasive brain stimulation tools. Clin. Neurophysiol. *127*, 1031–1048.

Wu, B., Li, W., Avram, A.V., Gho, S.-M., and Liu, C. (2012a). Fast and tissue-optimized mapping of magnetic susceptibility and T2* with multi-echo and multi-shot spirals. Neuroimage *59*, 297–305.

Wu, B., Li, W., Guidon, A., and Liu, C. (2012b). Whole brain susceptibility mapping using compressed sensing. Magn. Reson. Med. *67*, 137–147.

Wüllner, U., Klockgether, T., Petersen, D., Naegele, T., and Dichgans, J. (1993). Magnetic resonance imaging in hereditary and idiopathic ataxia. Neurology *43*, 318.

Xu-Wilson, M., Chen-Harris, H., Zee, D.S., and Shadmehr, R. (2009). Cerebellar Contributions to Adaptive Control of Saccades in Humans. J. Neurosci. *29*, 12930–12939.

Yang, Y., and Lisberger, S.G. (2014). Role of plasticity at different sites across the time course of cerebellar motor learning. J. Neurosci. *34*, 7077–7090.

Yang, Q., Hashizume, Y., Yoshida, M., Wang, Y., Goto, Y., Mitsuma, N., Ishikawa, K., and Mizusawa, H. (2000). Morphological Purkinje cell changes in spinocerebellar ataxia type 6. Acta Neuropathol. (Berl.) *100*, 371–376.

Yang, Z., Ye, C., Bogovic, J.A., Carass, A., Jedynak, B.M., Ying, S.H., and Prince, J.L. (2016). Automated cerebellar lobule segmentation with application to cerebellar structural analysis in cerebellar disease. NeuroImage *127*, 435–444.

Yao, B., Li, T.-Q., van Gelderen, P., Shmueli, K., de Zwart, J.A., and Duyn, J.H. (2009). Susceptibility contrast in high field MRI of human brain as a function of tissue iron content. Neuroimage *44*, 1259–1266.

Yavari, F., Jamil, A., Mosayebi Samani, M., Vidor, L.P., and Nitsche, M.A. (2018). Basic and functional effects of transcranial Electrical Stimulation (tES)—An introduction. Neurosci. Biobehav. Rev. *85*, 81–92.

Zarahn, E., Weston, G.D., Liang, J., Mazzoni, P., and Krakauer, J.W. (2008). Explaining savings for visuomotor adaptation: linear time-invariant state-space models are not sufficient. J. Neurophysiol. *100*, 2537–2548.

Zheng, W., Nichol, H., Liu, S., Cheng, Y.-C.N., and Haacke, E.M. (2013). Measuring iron in the brain using quantitative susceptibility mapping and X-ray fluorescence imaging. Neuroimage *78*, 68–74.

Zhou, H., Lin, Z., Voges, K., Ju, C., Gao, Z., Bosman, L.W.J., Ruigrok, T.J., Hoebeek, F.E., De Zeeuw, C.I., and Schonewille, M. (2014). Cerebellar modules operate at different frequencies. ELife *2014*, e02536–e02536.

Zimerman, M., Nitsch, M., Giraux, P., Gerloff, C., Cohen, L.G., and Hummel, F.C. (2013). Neuroenhancement of the aging brain: Restoring skill acquisition in old subjects. Ann. Neurol. *73*, 10–15.

Zuchowski, M.L., Timmann, D., and Gerwig, M. (2014). Acquisition of Conditioned Eyeblink Responses is Modulated by Cerebellar tDCS. Brain Stimulat. *7*, 525–531.

12

English summary

Movement allows us to interact with our direct environment, manipulate objects and communicate with each other. Moreover, we can adjust our movements to fit a remarkable range of situations and circumstances. The ability to adjust movements in response to changes in the environment and task demands is referred to as motor learning. The cerebellum is a key neural structure for motor learning. As such, disease of the cerebellum, in addition to the clinical symptom of ataxia, results in various motor learning deficits. There is a consensus that supportive therapy (e.g. physiotherapy, occupational therapy or speech therapy) can reduce ataxia symptoms of cerebellar patients, but little is known about the mechanisms underlying the improvements, and how patients can benefit most. Additionally, motor learning deficits are associated with reduced efficacy of supportive therapy. With the work described in this thesis, we sought to unravel the structural components of cerebellar disease and the relationship between cerebellar integrity and motor learning. Furthermore, we investigated whether motor learning deficits in cerebellar patients could be ameliorated with neuromodulation or training-related interventions, under experimental conditions, hoping to support the development of interventions relevant for application in a clinical setting.

Chapter 2 describes the pattern of cortical cerebellar degeneration due to healthy ageing and cerebellar disease. The pattern of degeneration was found to be largely analogous between healthy ageing and cerebellar disease. However, the most strongly degenerated regions in cerebellar disease were shifted posteriorly compared to healthy ageing. As such, the degeneration patterns fit with the specific symptomology associated with healthy ageing and cerebellar disease. The work in this chapter provides new insights in the specific localization and extent of cortical cerebellar degeneration in healthy ageing and cerebellar disease, and suggests a possible role for healthy ageing as a model system for cerebellar disease.

Chapter 3 further explores the degenerative effects of a healthy ageing and cerebellar disease, but focuses on the deep cerebellar nuclei (DCN) instead of the cerebellar cortex. Using a method called quantitative susceptibility mapping (QSM), we were able to image the DCN at clinical field strengths (3 Tesla). We found that the volume of the DCN was not affected by healthy ageing, but was reduced as a result of cerebellar disease. Being able to accurately and non-invasively map the deep cerebellar nuclei at clinical field strengths opens up the possibility to include this type of analysis in routine imaging protocols. Additionally, the results of **Chapter 3** suggest that the DCN are affected differentially by healthy ageing and cerebellar disease, which might limit the viability of using healthy ageing as a model system for cerebellar disease.

Chapter 4 employed the imaging method developed in **Chapter 2** to study motor learning deficits in children with autism spectrum disorder (ASD). In **Chapter 4**, children with ASD were found to rely more on proprioceptive errors and less on visual errors than typically developed children. The abnormal pattern of motor learning in children with ASD was linked to a reduction in volume of the sensorimotor areas of the cerebellum.

Chapters 5, 6 and 7 investigated the effects of transcranial direct current stimulation (tDCS), a type of neuromodulation, on motor learning in cerebellar patients and control subjects. We were unable to elicit any behavioral effects of tDCS in cerebellar patients and control subjects under any of the task and stimulation parameters described. Several possible reasons for the lack of effects are given in **Chapters 5 – 7**, but our results indicate that additional research is required before tDCS is ready for the neurorehabilitation of cerebellar patients.

Chapter 8 investigated awareness and unawareness of motor learning in an implicit learning group and explicit learning group using a method called the process dissociation procedure (PDP). The results of this chapter indicate that the PDP could be used to measure awareness and unawareness in future studies testing training-related interventions based on implicit and explicit learning processes.

Finally, in **Chapter 9**, we investigated whether training-related interventions could alleviate motor learning deficits of cerebellar patients. We found that extended training enhances motor memory retention in cerebellar patients as well as healthy age-matched controls. However, motor memory retention in cerebellar patients was not enhanced to the level of control subjects. In healthy control subjects we suggest that enhanced retention was the result of two processes: use-dependent plasticity and increased memory resilience. Modelling work suggested that memory resilience was reduced in cerebellar patients. To our knowledge, this is the first time this specific motor learning deficit has been described in cerebellar patients. The fact that motor memory retention is still elevated by extended training in cerebellar patients could be helpful for the development of therapeutic strategies.

Taken together, this thesis has further unraveled the structural components of cerebellar disease and the relationship between cerebellar integrity and motor learning. The work in this thesis also suggests that tDCS is not ready for application in a clinical setting, at least until the working of tDCS is further elucidated by animal and control studies. As of right now, resources are probably better spent on further developing training-related interventions for cerebellar patients than on neuromodulation in cerebellar patients.

NEDERLANDSE SAMENVATTING

Door te bewegen kunnen wij objecten verplaatsen, onze directe omgeving manipuleren en met elkaar communiceren. Wij zijn ook in staat onze bewegingen aan te passen naar gelang de situatie en omstandigheden. Het vermogen om onze bewegingen aan te passen als reactie op veranderingen wordt ook wel motorisch leren genoemd. Het cerebellum is een belangrijke neurale structuur voor motorisch leren. Daarom zorgt ziekte van het cerebellum, naast het klinisch symptoom ataxie, ook voor diverse deficiënties in het motorisch leren. Ondersteunende therapie (bijvoorbeeld fysiotherapie, ergotherapie of spraaktherapie) kan ataxie symptomen verminderen in cerebellaire patiënten, maar men weet nog niet hoe deze verbeteringen tot stand komen, of hoe patiënten het meest voordeel kunnen doen met therapie. Daarnaast zijn deficiënties in het motorisch leren geassocieerd met verminderde effectiviteit van ondersteunende therapie. Met het werk beschreven in dit proefschrift hebben wij getracht de onderliggende structuren van cerebellaire ziekte verder te ontrafelen, alsmede de verbinding tussen cerebellaire integriteit en motorisch leren. Verder hebben wij onderzocht of deficiënties in het motorisch leren van cerebellaire patiënten kunnen worden verminderd, onder experimentele omstandigheden, met behulp van neuromodulatie dan wel training-gerelateerde interventies hopende dat dit kan bijdragen aan de ontwikkeling van interventies relevant voor de kliniek.

In **Hoofdstuk 2** worden de patronen van corticale cerebellaire degeneratie beschreven als gevolg van veroudering en ziekte van het cerebellum. Het degeneratie patroon blijkt grotendeels gelijkwaardig tussen veroudering en cerebellaire ziekte. Echter, de sterkst gedegenereerde gebieden in cerebellaire ziekte zijn meer naar de achterzijde van het cerebellum verplaatst vergeleken met veroudering. De symptomen geassocieerd met veroudering en cerebellaire ziekte passen dus bij het specifieke patroon van cerebellaire degeneratie. Het werk beschreven in **Hoofdstuk 2** biedt nieuwe inzichten over de specifieke lokalisatie en sterkte van corticale cerebellaire degeneratie als gevolg van veroudering en cerebellaire ziekte, en geeft aan dat er een mogelijke rol is weggelegd voor veroudering als een modelsysteem van cerebellaire ziekte.

In **Hoofdstuk 3** zijn de degeneratieve effecten van veroudering en cerebellaire ziekte verder onderzocht, maar met een focus op de diepe cerebellaire kernen in plaats van de cerebellaire cortex. Door gebruik te maken van "quantitative susceptibility mapping" (QSM), waren wij in staat om de diepe kernen in beeld te brengen onder klinische veldsterktes (3 Tesla). Het volume van de diepe kernen blijkt niet te veranderen door veroudering, maar verminderd wel als gevolg van cerebellaire ziekte. Het feit dat wij de diepe kernen accuraat en non-invasief kunnen opmeten onder klinische veldsterktes geeft aan dat deze techniek mogelijk kan worden gebruikt als onderdeel van routine beeldvorming. Bovendien geven de resultaten

van **Hoofdstuk 3** aan dat de diepe kernen anders zijn aangedaan door veroudering dan door cerebellaire ziekte, wat de mogelijkheid om veroudering als modelsysteem van cerebellaire ziekte te gebruiken beperkt.
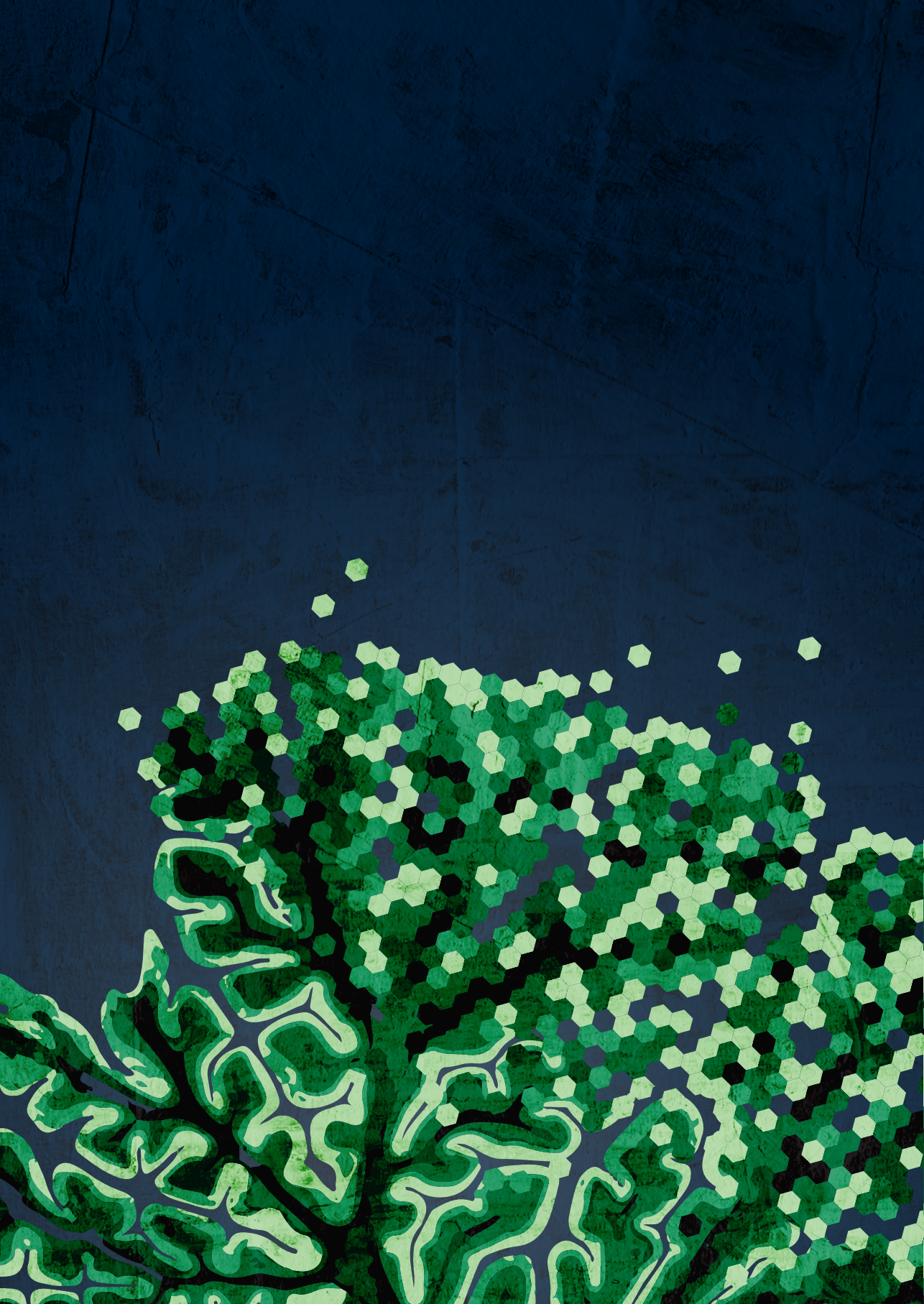
In **Hoofdstuk 4** is gebruik gemaakt van de methode ontwikkeld in **Hoofdstuk 2** om motorisch leren deficiënties van kinderen met autisme spectrum stoornis (ASS) te onderzoeken. Uit dit hoofdstuk blijkt dat kinderen met ASS meer leren van proprioceptieve fouten en minder van visuele fouten dan typisch ontwikkelde kinderen. Het atypisch motorisch leren in kinderen met ASS is geassocieerd met het volume van de sensomotorische gebieden van het cerebellum.

In **Hoofdstuk 5, 6 en 7** zijn de effecten van "transcranial direct current stimulation" (tDCS), een vorm van neuromodulatie, onderzocht op het motorisch leren van cerebellaire patiënten en gezonde proefpersonen. Wij hebben geen gedragseffecten door tDCS kunnen opwekken in cerebellaire patiënten en gezonde proefpersonen onder alle verschillende stimulatie- en taakparameters beschreven. Verschillende redenen voor het gebrek aan gedragseffecten worden gegeven in **Hoofdstukken 5 – 7**, maar onze resultaten geven in ieder geval aan dat aanvullend onderzoek nodig is voordat tDCS kan worden toegepast in de neurorehabilitatie van cerebellaire patiënten.

In **Hoofdstuk 8** is bewust en onbewust motorisch leren onderzocht in een impliciete leergroep en een expliciete leergroep, gebruikmakende van de "process dissociation procedure" (PDP). De resultaten van dit hoofdstuk suggereren dat de PDP gebruikt kan worden om bewust en onbewust motorisch leren te meten in toekomstige studies met training-gerelateerde interventies gebaseerd op impliciete en expliciete leer processen.
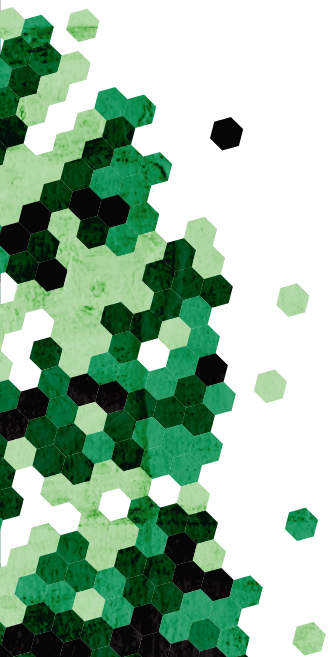
Afsluitend is in **Hoofdstuk 9** onderzocht of training-gerelateerde interventies de motorisch leren deficiënties van cerebellaire patiënten kunnen verminderen. Onze resultaten geven aan dat verlengd trainen het vermogen tot onthouden van motorisch leren verbeterd in cerebellaire patiënten en gezonde proefpersonen van dezelfde leeftijd. Echter, retentie van het motorisch leren was niet verbeterd tot hetzelfde niveau in cerebellaire patiënten vergeleken met gezonde proefpersonen. Wij veronderstellen dat verhoogde retentie het gevolg is van twee processen in gezonde proefpersonen: gebruiksafhankelijke plasticiteit en zogenaamde "geheugentaaiheid". Modelwerk suggereert dat de geheugentaaiheid in verminderd in cerebellaire patiënten. Voor zover wij weten is dit de eerste keer dat deze specifieke motorisch leren deficiëntie is beschreven in cerebellaire patiënten. Het feit dat retentie van motorisch leren nog steeds verhoogd wordt in cerebellaire patiënten door verlengd trainen kan behulpzaam zijn voor het ontwikkelen van therapeutische strategieën.

Tezamen heeft dit proefschrift de structurele componenten van cerebellaire ziekte en de associatie tussen cerebellaire integriteit en motorisch leren verder ontrafelt. Het werk beschreven in dit proefschrift geeft ook aan dat tDCS als techniek nog niet klaar is voor toepassing in een klinische omgeving, in ieder geval tot de werking van tDCS beter begrepen is met behulp van diermodellen of controle studies. Op dit moment is het waarschijnlijk beter om middelen in te zetten om training-gerelateerde interventies door te ontwikkelen, dan voor neuromodulatie in cerebellaire patiënten.

12

SUMMARY

A

Appendix

CURRICULUM VITAE

Thomas Jan Hulst was born in Rotterdam on the 6th of June 1988. After graduating from the Libanon Lyceum in Rotterdam, Thomas applied to medical school at the Erasmus University Rotterdam. He obtained a BSc. in Medicine in 2011 but decided to pursue a career in research and education instead. Thomas obtained a MSc. in Neuroscience in 2014 under the supervision of prof. dr. Opher Donchin. In parallel to his research master, he was active as a problem-based learning tutor for the academic core courses at the Erasmus University College. Following his research master, Thomas engaged in a fruitful collaboration with prof. dr. Dagmar Timmann from the University Hospital in Essen, Germany. Thomas worked for three years in Essen as a PhD candidate. Upon his return to Rotterdam he finished his PhD under the supervision of prof.dr. Maarten Frens. In 2018, Thomas started in his current position as lecturer in Methods and Statistics at the Erasmus University College.

Thomas is married to Imke and they live in Delfshaven, Rotterdam.

PHD PORTFOLIO

Personalia

Name	Thomas Jan Hulst
Date of birth	6 June 1988
Place of birth	Rotterdam, The Netherlands
E-mail	thomashulst@gmail.com

Education

2014 – 2020	**PhD candidate Neuroscience**
	Erasmus University Rotterdam, The Netherlands
	Supervisor: Prof. dr. Maarten A. Frens
2011 – 2014	**Master of Neuroscience** (research master)
	Erasmus University Rotterdam, The Netherlands
	Supervisor: Dr. Opher Donchin
2007 – 2011	**Bachelor of Medicine**
	Erasmus University Rotterdam, The Netherlands

Teaching experience

2018 – present	**Lecturer Methods and Statistics**
	Erasmus University College, The Netherlands
2013 – 2015	**PBL Tutor** (academic core courses)
	Erasmus University College, The Netherlands

Conferences and presentations

2017	**Gordon Research Conference Cerebellum** (poster presentation)
	Lewiston, USA
	1.5 ECTS
2017	**Gordon Research Seminar Cerebellum** (poster presentation)
	Lewiston, USA
	1 ECTS

2017	**NIN Summer school** (poster presentation)
	Amsterdam, The Netherlands
	1 ECTS
2016	**Helmholtz Retreat** (oral presentation)
	Schoorl, The Netherlands
	1.5 ECTS
2015	**Computational Motor Control Workshop** (poster presentation)
	Beer Sheeva, Israel
	1.5 ECTS
2014	**Computational Motor Control Workshop** (conference)
	Beer Sheeva, Israel
	1 ECTS

Courses, skills and seminars

2014 – present	**Labmeetings System Physiology**
	Erasmus MC, The Netherlands
	5 ECTS
2014 – present	**Department of Neuroscience Labtalks and Seminars**
	Erasmus MC, The Netherlands
	5 ECTS
2015 – 2018	**Journal Club Experimentelle Neurologie**
	Universitätsklinikum Essen, Germany
	5 ECTS
2017	**Organization Summer Seminar Experimentelle Neurologie**
	Universitätsklinikum Essen, Germany
	3 ECTS
2016	**MRI Safety Course and MRI Training**
	Universitätsklinikum Essen, Germany
	3 ECTS
2014	**Python Programming**
	Medgen Centre Leiden, The Netherlands
	1.5 ECTS

LIST OF PUBLICATIONS

Ariels Mamlins, **Thomas Hulst**, Opher Donchin, Dagmar Timmann, Jens Claaßen. No effects of cerebellar transcranial direct current stimulation (tDCS) on force field and visuomotor reach adaptation in young and healthy subjects (2019). Journal of Neurophysiology. doi: 10.1152/jn.00352.2018

Liane John, Michael Küper, **Thomas Hulst**, Dagmar Timmann, Joachim Hermsdörfer. Effects of transcranial direct current stimulation on grip force control in patients with cerebellar degeneration (2017). Cerebellum & Ataxias. doi: 10.1186/s40673-017-0072-8

Thomas Hulst, Liane John, Michael Küper, Jos van der Geest, Sophia Göricke, Opher Donchin, Dagmar Timmann. Cerebellar patients do not benefit from cerebellar or M1 transcranial direct current stimulation during force field reaching adaptation (2017). Journal of Neurophysiology. doi: 10.1152/jn.00808.2016

Susen Werner, Bernice van Aken, **Thomas Hulst**, Maarten Frens, Jos van der Geest, Heiko Strüder, Opher Donchin. Awareness of Sensorimotor Adaptation to Visual Rotations of Different Size (2015). PLoS ONE. doi: 10.1371/journal.pone.0123321

Thomas Hulst, Jos van der Geest, Thurling, M., Sophia Göricke, Maarten Frens, Dagmar Timmann, Opher Donchin. Ageing shows a pattern of cerebellar degeneration analogous, but not equal, to that in patients suffering from cerebellar degenerative disease (2015). NeuroImage. doi: 10.1016/j.neuroimage.2015.03.084

Mollie Marko, Deana Crocetti, **Thomas Hulst**, Opher Donchin, Reza Shadmehr, Stewart Mostofsky. Behavioural and neural basis of anomalous motor learning in children with autism (2015). Brain. doi: 10.1093/brain/awu394

Articles in preparation

Thomas Hulst, Ariels Mamlins, Maarten Frens, Dae-In Chang, Sophia Göricke, Dagmar Timmann, Opher Donchin. Cerebellar degeneration reduces memory resilience after extended training. *In preparation.*

Dominik Jäschke, Katharina M. Steiner, Dae-In Chang, Jens Claaßen, Ellen Uslar, Andreas Thieme, Marcus Gerwig, Viktor Pfaffenrot, **Thomas Hulst**, Stefan Maderwald, Sophia L. Göricke, Martina Minnerop, Mark E. Ladd, Jürgen R. Reichenbach, Dagmar Timmann,

Andreas Deistung. Age-Related Changes of Cerebellar Cortex and Nuclei: MRI findings in Healthy Controls and its Application to Spinocerebellar Ataxia (SCA6) Patients. *Under review – NeuroImage*

Katharina M. Steiner, Sarah Jansen, Nino Adeishvili, **Thomas Hulst**, Thomas M. Ernst, Oliver Müller, Elke Wondzinski, Sophia Göricke, Mario Siebler, Metin Uengoer, Dagmar Timmann. Extinction of cognitive associations is preserved in patients with cerebellar disease. *Under review – Neurobiology of Learning and Memory*

Posters, presentations and conference papers

Thomas Hulst, Arik Mamlins, Sophia Göricke, Dagmar Timmann, Opher Donchin. Cerebellar degeneration reduces memory resilience after extended training (poster). 75th Fujihara Seminar, Tokyo, Japan (2018).

Thomas Hulst, Arik Mamlins, Opher Donchin, Dagmar Timmann. The effect of training paradigm on learning rate and retention in cerebellar ataxia patients (poster). Gordon Research Conference Cerebellum, Lewiston, United States (2017).

Thomas Hulst, Arik Mamlins, Opher Donchin, Dagmar Timmann. The effect of training paradigm on learning rate and retention in cerebellar ataxia patients (poster). NIN Summer School, Amsterdam, The Netherlands (2017).

Arik Mamlins, **Thomas Hulst**, Opher Donchin, Dagmar Timmann, Jens Claaßen. Cerebellar tDCS effects on the adaptation of arm reaching movements to force-field and visuomotor perturbations (poster and conference paper). 6th International Conference on Transcranial Brain Stimulation, Göttingen, Germany (2017).

Arik Mamlins, **Thomas Hulst**, Opher Donchin, Dagmar Timmann, Jens Claaßen. Cerebellar tDCS effects on the adaptation of arm reaching movements to force-field perturbations (poster and conference paper). 60th Scientific Annual Meeting of the German Society for Clinical Neurophysiology and Functional Imaging, Düsseldorf, Germany (2016).

Thomas Hulst, Liane John, Küper, M., Jos van der Geest, Sophia Göricke, Opher Donchin, Dagmar Timmann. Cerebellar patients do not benefit from cerebellar or M1 transcranial direct current stimulation during force field reaching adaptation (oral presentation). Helmholtz Retraite, Schoorl, The Netherlands (2016).

Thomas Hulst, Jos van der Geest, Thurling, M., Sophia Göricke, Maarten Frens, Dagmar Timmann, Opher Donchin. Ageing shows a pattern of cerebellar degeneration analogous, but not equal, to that in patients suffering from cerebellar degenerative disease (poster, 2nd place poster prize). Computational Motor Control Workshop, Beer Sheeva, Israel (2015).

Liane John, Küper M, **Thomas Hulst**, Hermsdörfer J, Opher Donchin & Dagmar Timmann. Modulation of reach adaptation through transcranial direct current stimulation (tDCS) in patients with cerebellar degeneration (poster). Cerebellar Contribution to brain function: from molecules to behavior, SRC, Rome, Italy (2014).

MK Marko, D Crocetti, **Thomas Hulst**, Opher Donchin, Reza Shadmehr, SH Mostofsky. Neural basis of anomalous motor learning in children with autism (poster, SfN Hot Topic). Society for Neuroscience Meeting, Washington DC, USA (2014).

Susen Werner, van Aken BC, **Thomas Hulst**, Maarten Frens, Jos van der Geest, Strüder HK, Opher Donchin. Awareness of Sensorimotor Adaptation to Visual Rotations of Different Sizes (poster). Society for the Neural Control of Movement Meeting, Amsterdam, The Netherlands (2014).